Evaluation of local fields and effective behavior of viscoelastic heterogeneous materials

A DISSERTATION
SUBMITTED TO THE FACULTY OF THE GRADUATE SCHOOL
OF THE UNIVERSITY OF MINNESOTA
BY

Andrey V. Pyatigorets

IN PARTIAL FULFILLMENT OF THE REQUIREMENTS
FOR THE DEGREE OF
DOCTOR OF PHILOSOPHY

Sofia G. Mogilevskaya, Mihai O. Marasteanu, Advisers

July, 2010

Acknowledgements

I would like to express my deep gratitude to my academic advisers, Professor Mihai O. Marasteanu and Dr. Sofia G. Mogilevskaya, for their valuable advices, inspiration, and consistent encouragement during the course of this research. Their fruitful criticism and advocacy for new studies, broad knowledge and experience helped me to accomplish all that is shaped in this dissertation. I am very grateful to Professors Henryk K. Stolarski, Joseph F. Labuz, and Lev Khazanovich for numerous interesting and fruitful discussions.

I would also like to thank the members of my examination committee, Professors Perry H. Leo, Henryk K. Stolarski, Mihai O. Marasteanu, and Dr. Sofia G. Mogilevskaya, for their valuable comments and suggestions.

The continuous financial support provided by Professors Steven L. Crouch, Mihai O. Marasteanu, Joseph F. Labuz, and by the Department of Civil Engineering of the University of Minnesota is gratefully acknowledged.

I deeply appreciate the time spent with my friend and office mate Jim Hambleton. Having always interesting conversations with him, sharing laughs, joy, and sometimes sadness, all of this was a truly enjoyable experience for me. Though life separates most of my workmates and university friends, among which are Raul Velasquez, Kairat Tuleubekov, Gregory Wachman, Keith Palmer, years spent with these great people are not to be forgotten.

Last, but not least, I am very grateful to Elisey Yagodkin and Jason Furtney for being my best friends.

Dedication

I dedicate this dissertation to my loving mother, who helped and supported me in the times of hardship and prosperity, throughout all the ups and downs in my life.

Contents

List of Tables

List of Figures

Chapter 1

Introduction

1.1 Preamble

Composite materials (or composites) are materials made from at least two discrete substances. Principal advantage of composites resides in the possibility of combining physical properties of the constituents to obtain new structural or functional characteristics. Due to the possibility of designing specific properties, the composites have been widely used in those areas where high stiffness/weight and strength/weight ratios, ability to tailor structural performances and thermal expansion, as well as corrosion or fatigue resistance are required.

Many industries, including biomedical, aerospace, automotive and other, heavily rely on the use of composites [48]. As for 2000, the leading role in consuming the composite materials belonged to the automotive industry that used roughly 25% of the world market of composites [1]. Figure 1.1 presents data for the European market of composite materials; some information about the US market is available in [6]. During the last two decades, the market for composites has been growing at an annual rate over 10%, reaching tens of billions of US dollars [1].

Composites are often made of an organic matrix (e.g. from thermoset and thermoplastic polymers)[1] and reinforced by particles, laminates, or fibers. An example

[1] Thermoset polymers are polymers that are heat processed. They exhibit irreversible transformations during processing. Thermoplastic polymers harden during a cooling process, which is a reversible

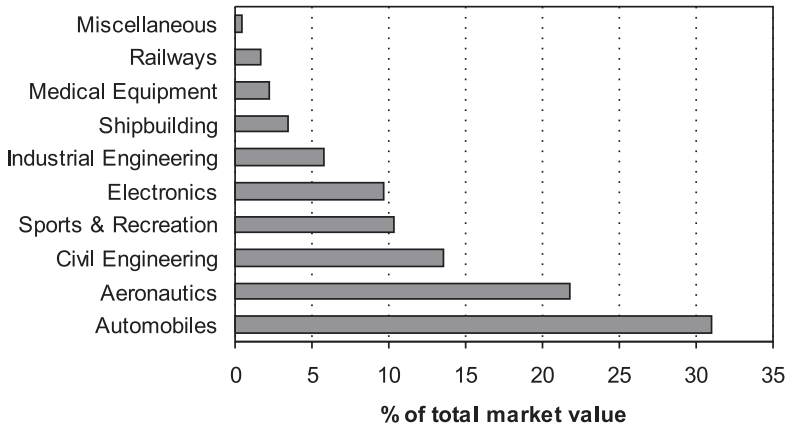

Figure 1.1: The use of composite materials in different industries in 2000 in Europe. The horizontal scale represents the Europian market shares. Data source: *Les 4 pages de la DGCIS* [1].

of thermoset polymers are epoxy and phenolic resins, which are used in the majority of the composites with polymeric matrix [1], [136]. Thermoplastic polymers include polypropylene and polyamides. All these types of polymers exhibit both viscous and elastic characteristics, i.e. they are considered to be viscoelastic. The mechanical properties of such materials depend on a number of parameters, among which are time, rate of loading, temperature, and age [135]. Thus, if the composite's matrix is made of viscoelastic material, the latter usually has profound influence on the overall time-depending behavior of the composite.

The most commonly used reinforcements in the composite materials are the fibers, which are usually made of glass, carbon, or aramid. The fibers can be distributed in the matrix in periodic or random manner, which determines the directional characteristics of the composite (such as overall isotropy or orthotropy).

chemical process.

Viscoelastic porous materials are often considered as a particular example of composite materials (voids can be treated as a phase with zero mechanical properties). Porous materials made from polymers are used as different filters, membranes, insulation and damping devices, liquid or gas storage devices, etc. (e.g. [39], [50], [64]). In many engineering applications (e.g. for fuel cells, membranes, various coatings) it is important to have the ability to tailor the mechanical properties and predict the behavior of viscoelastic porous materials in order to achieve better performance.

The study of micro- and macro-mechanical behavior of viscoelastic composites and porous media is often a challenging task. This is related to the fact that the analysis of such materials should not only take into account their complex structure, but also the time-varying properties of one or more constituents.

1.2 Motivation

The information about the micro-mechanical behavior (about the local values of time-dependent stresses and strains) of viscoelastic composite materials is necessary in understanding their failure mechanisms and necessary in designing new materials with specified physical properties. From the other hand, the information about the macro-mechanical behavior of composites (at the scale where they can be perceived as homogeneous materials) is critical in determining their overall stiffness, strength, and other macroscopic mechanical parameters.

Physical experiments are capable of providing only limited information (e.g. composite's behavior in certain range of times, frequencies, temperatures, etc.). Numerical simulations of micro-and macro-mechanical behavior with standard methods (e.g. the finite element method) are often very involved and require large computational resources.

This research is concerned with the analytical and numerical analysis of the viscoelastic composites and porous materials. It is motivated by the need to develop

computational tools for more efficient and accurate modeling of the micro- and macro-mechanical behavior of such heterogeneous media. These new tools should be capable of dealing with the large number of inhomogeneities, solving viscoelastic problems in reasonable time on a standard PC, and taking into account various mechanical loading conditions and temperature variations.

1.3 Present state of knowledge

This section provides a general overview of the literature concerned with the study of the micro- and macro-scale behavior of viscoelastic composites. A brief overview of some relevant works dealing with elastic composites is also provided. More detailed literature reviews specific to each chapter of this dissertation can be found in the introductory sections of these chapters.

The systematic study of heterogeneous (composite) materials started several decades ago. Several fundamental works on the mechanics of materials were published at that time. Among them are the works by Muskhelishvili on the mathematical theory of elasticity (e.g. [108]) and by Eshelby [44], [45], who proposed the method for the solution of the problem of a single ellipsoidal inhomogeneity embedded in an infinite matrix loaded at infinity. These works gave a significant push to the number of studies of homogeneous and heterogeneous elastic media.

The technique of elastic potentials presented in [108] was adopted by various researchers. Linkov [85] used the potentials to derive the complex boundary integral equations for the solution of problems of piece-wise homogeneous elastic media. Somewhat different approach was used by Mogilevskaya and Linkov [100], who adopted Somigliana's identities [120] and Kolosov-Muskhelishvili's potentials to derive the complex boundary integral equations for elastic homogeneous media. Following this work, Mogilevskaya and Crouch presented the technique for the solution of piece-wise homogeneous problems involving multiple cracks [101] or multiple inhomogeneities with

circular boundaries [102], [103]. To solve the latter problem, the authors proposed using the Fourier series decomposition of the unknown displacements or tractions on the circular boundaries. This technique was used by Wang et al. [132], who considered the problem of an elastic plane subjected to far-field stress and containing pores subjected to internal pressure.

A comprehensive review of the literature related to the elastic semi-infinite porous media is given in [38]. Two relevant papers that are not mentioned in the review by Dejoie et al. [38] are papers by Spencer and Sinclair [122] and Pobedonostsev [110]. The first paper considers the case of one or two pores and assumes that the boundary of the half-plane is traction free. Pobedonostsev [110] assumed more general conditions at the boundary of the half-plane; nevertheless, he studied a single hole problem only. Dejoie et al. [38] gave the solution for the problem with multiple circular holes, however, the surface of the half-plane was considered traction free. A similar approach as in Dejoie et al. [38] was used by Legros et al. [81] to solve the problem of an elastic half-plane containing multiple inhomogeneities. Again, the boundary of the half-plane was assumed to be traction free. Additional references related to the elastic problem with multiple inhomogeneities can be found in [77].

Huang et al. [65] extended the semi-analytical method proposed by Mogilevskaya and Crouch [102] to the case of a linearly viscoelastic porous plane. Using the elastic-viscoelastic correspondence principle based on the Laplace transform, the authors of [65] obtained the solution for the time-varying fields in the porous plane. The work of Huang et al. [65] provides a brief overview of some other methods that are used for the solution of the viscoelastic heterogeneous problems. Among these methods are the Finite Element (FEM) and Boundary Element (BEM) methods, which usually employ time-stepping algorithms or the finite difference approach to treat the time integrals and derivatives (see e.g. [18], [99], [140], and references in [65]). The major difficulty in using these methods is the necessity to deal with very fine meshes and large number of finite elements/segments to obtain an accurate solution. Besides the works that employ FEM

or BEM, the literature devoted to the calculation of time-varying fields in viscoelastic composites is rather limited. Few additional references are provided in Chapter 4.

Despite the fact that the information about the micro-scale behavior is often necessary for the accurate analysis of the macroscopic (overall) characteristics of composite materials, the first studies were devoted to the investigation of their overall behavior. This is related to the fact that the micro-scale simulations require large computational resources that were not available several decades ago. At the same time, several models were developed to approximate the overall behavior of elastic and viscoelastic composites. In works [55], [56], Hashin extended the composite cylinder assemblage model to the case of viscoelastic matrix. Wang and Weng [134], Chen et al. [24], and Brinson and Lin [19] adopted the Mori-Tanaka scheme [106] to the evaluation of the effective properties of viscoelastic composites. The Self-Consistent method was used by Laws and McLaughlin [79] to estimate viscoelastic creep compliances of certain composite materials. The mentioned approaches usually employ the correspondence principle based on the Laplace transform or the half-sided Fourier transform (see Section 2.1.6). Several authors adopted the Volterra correspondence principle (see Section 2.1.6) and method of fractional-exponential operators to obtain the viscoelastic effective properties (e.g. [71], [84]). This approach, however, is much more involved than the methods based on the use of the Laplace or Fourier transforms. Besides, its accuracy greatly depends on a number of terms used in the discrete representation of Volterra-type operators. The review of several other works concerned with the study of the effective properties of viscoelastic fiber-reinforced composites is provided in Chapter 5.

Many researchers have been concerned with the thermal analysis of viscoelastic composite structures (for instance, such structures that contain the elastic and viscoelastic parts). One of the first works on this topic is by Schwarzl and Staverman [117], who established the equivalence between time and temperature (time-temperature superposition) for certain class of viscoelastic materials. The number of experimental works were published in support of this superposition principle (e.g. [14], [23], [125]). The

time-temperature superposition was later adopted by various authors (e.g. [27], [43], [124]) to solve the problem of thermo-mechanical deformation of viscoelastic solids or composite structures. However, one of the most challenging problems that remains poorly studied is the problem of thermal cracking of viscoelastic asphalt binders and mixes. This is due to the complex viscoelastic behavior of the asphalt binders [93] and complex microstructure of the mixes. Chapter 6 provides a deeper insight into the problem and more detailed literature review.

1.4 Objectives and significance of research

The objective of this research is to develop a mathematical basis and computational tools for modeling the micro- and macro-mechanical behavior of viscoelastic composites and structures. The research has three major aspects:

- The development of an efficient numerical approach and computer codes for simulation of time-dependent stress, strain, and displacement fields in porous materials and fiber-reinforced composites. The approach should explicitly take into account the microstructure of the material and interactions between the inhomogeneities. The idea is to develop a technique for the solution of a problem of viscoelastic media containing randomly distributed elastic inhomogeneities (fibers) and/or holes (pores) of arbitrary sizes. The holes can be either traction free or subjected to time-varying pressure. The fibers can be idealized as long, parallel, isotropic inclusions with the circular cross-section perfectly bonded to the bulk material of the matrix. This allows for a two-dimensional formulation of the problem for the case when the loads are applied in the plane perpendicular to the axis of the fibers.

  The approach should also be able to take into account far-field stress and tractions acting on the upper boundary of the half-plane. This is necessary for the study of the problems involving indentation processes. As a consequence of this general

formulation, the approach is assumed to be capable of dealing with the cases of full viscoelastic plane and elastic half- and full planes.

- The development of an approach for the evaluation of the transverse effective properties of viscoelastic fiber-reinforced composites and porous media. It can be done after the tools for the simulation of viscoelastic fields on the micro-scale are designed. The distribution of the inhomogeneities can be considered as statistically isotropic [13]. The approach should be able to adopt different viscoelastic models describing the time-dependent behavior of the composite's matrix and provide accurate results in the whole range of volume fractions or porosities. To estimate the accuracy and efficiency of the method, the results are to be compared with the benchmark solutions.

- The investigation of the problem of thermal deformation of viscoelastic composite structures using the time-temperature superposition principle. An important case, in which the application of the correspondence principle based on the Laplace transform fails, is to be studied. A simple and accurate technique for the solution of the problem for the case of transient temperature conditions should be designed. The consideration of this problem is helpful in developing new tools for the analysis of the viscoelastic composite materials and structures in which the viscoelastic phase exhibits characteristics that can not be approximated by simple models or functions.

The research presented in this dissertation will help to enhance the understanding of mechanical behavior of viscoelastic composite and porous materials on micro- and macroscopic levels. For example, the ability to efficiently simulate time-dependent viscoelastic fields in composite media allows one to predict where and when cracking or yielding initiates. These predictions are based on the analysis of the areas with the highest principal and/or shear stresses. Such information in combination with the ability to evaluate the effective properties of composites and porous media, can potentially help

engineers to devise specialized composite materials to suit specific purposes. Finally, the development of new methods for the analysis of viscoelastic composite structures under transient temperature conditions contributes to better understanding of various thermo-mechanical processes, including low-temperature thermal cracking.

1.5 Organization of the dissertation

The dissertation is organized as follows.

Chapter 2 consists of two parts. The first part presents an overview of the linear theory of viscoelasticity. The description of the differential and integral representations of the viscoelastic constitutive equations is provided. The basics of the thermal viscoelastic analysis and the time-temperature superposition principle are outlined. This part also describes three types of elastic-viscoelastic correspondence principles: (i) the principle based on the use of the Laplace transform, (ii) the principle based on the use of integral operators of Volterra type, and (iii) the Hashin's approach (principle) that is often used for the evaluation of the effective complex moduli. The second part of the chapter provides a brief overview of the boundary integral equations for elastic and viscoelastic problems and includes an outline of the theory of the Fourier series.

Chapter 3 deals with the problem of semi-infinite viscoelastic porous medium. A semi-analytical method of solution of the problem is presented. The method is based on the use of complex direct boundary integral approach and employs the elastic-viscoelastic correspondence principle based on the Laplace transform. The solution adopts the Fourier series approximation of the unknown boundary displacements. To obtain the time-domain solution, the transformed parameters are inverted analytically from the Laplace domain. Several examples illustrate the abilities and the accuracy of the method.

Chapter 4 extends the research presented in the previous chapter to the case of viscoelastic semi-infinite medium containing multiple elastic inhomogeneities and holes.

Similar approach is adopted for the solution of the problem. The major difference is in that an algorithm of numerical inversion of the Laplace transform is used. Several examples provide useful information about the behavior of several types of viscoelastic heterogeneous materials.

Chapter 5 describes novel approach for the evaluation of the transverse effective properties of viscoelastic fiber-reinforced composite and porous materials. The approach is based on the equivalent inhomogeneity technique and requires the calculation of the time-dependent stresses using the approaches presented in two previous chapters. Numerical examples compare the results from the present approach with those obtained by using some micromechanical schemes and the finite element formulation. The advantages of the developed approach are discussed.

Chapter 6 presents a technique for the solution of thermo-viscoelastic problems for the case of transient temperature conditions. Particular attention is paid to the asphalt binders, which master relaxation modulus is described by a rather complex functional dependency. Due to the fact that the use of the correspondence principle based on the Laplace transform fails in this case, the Volterra correspondence principle is adopted. A simple numerical technique is developed for the calculation of thermal stresses in composite structures containing asphalt binders. Some practical applications of the proposed technique are discussed.

Chapter 7 concludes the dissertation and presents the summary of the key research findings.

Chapter 2

Preliminaries

2.1 Linear viscoelasticity

2.1.1 Introduction

Elastic solids and viscous fluids differ significantly in their deformational characteristics. In elastic materials stress is directly proportional to strain in accordance with the Hooke's law (e.g. [28]), and material returns to its natural or undeformed state instantaneously upon removal of applied loads. Viscous (Newtonian's) fluids possess no tendency for deformational recovery, and in accordance with Newton's viscosity law, stress is directly proportional to the rate of strain (e.g [10]). Viscoelastic materials have elements of both of these properties and, as such, exhibit time dependent behavior. Elastic solid and viscous Newtonian fluid represent opposite endpoints of a wide spectrum of viscoelastic behavior.

If both strain and rate of strain are small enough, and the time-dependent stress-strain relations can be described by linear differential equations with constant coefficients (or by linear Volterra integral equation of the second kind with the difference kernel [88]), material is called *linear viscoelastic*. In other words, a material is said to

be linearly viscoelastic if the following equalities hold:

$$\varepsilon\left(c\cdot\sigma\left(t\right)\right)=c\cdot\varepsilon\left(\sigma\left(t\right)\right) \tag{2.1}$$

$$\varepsilon\left(\sigma_1\left(t_1\right)+\sigma_2\left(t_2\right)\right)=\varepsilon\left(\sigma_1\left(t_1\right)\right)+\varepsilon\left(\sigma_2\left(t_2\right)\right) \tag{2.2}$$

where $\varepsilon\left(\sigma\right)$ is strain as a function of stress σ, c is a constant, and $t,\ t_1,\ t_2$ are some time instances. Similar relations can be written for stress as a function of strain. The second requirement is usually referred to as the *Boltzmann superposition principle* [15].

Many viscoelastic materials exhibit linear, or nearly linear, response under small strain levels (strain $\lesssim 0.005$), while they may have a non-linear behavior upon large deformations. The use of linear relations in mathematical theory of viscoelasticity yields tractable representation for stress-strain-time relations and allows for relatively simple solutions for many viscoelastic boundary value problems.

2.1.2 Creep and relaxation

Majority of viscoelastic materials exhibit two fundamental phenomena: (i) if the stress is held constant, the strain increases with time (*creep*); (ii) if the strain is held constant, the stress decreases with time (*relaxation*). These effects can be easily observed in the one-dimensional tension (or compression) test or simple shear test.

In a creep test (Fig.2.1a,b) a viscoelastic material is subjected to a step of constant stress $\sigma=\sigma_0 H(t)$, and the time-dependent strain is measured. Here $H(t)$ is the Heaviside step function defined as

$$H(t)=\begin{cases}0,\ t<0\\ 1/2,\ t=0\\ 1,\ t>0\end{cases} \tag{2.3}$$

If material behaves linearly, time-dependent strain $\varepsilon(t)$ can be related to constant stress σ_0 through *creep compliance* $J(t)$, which is independent of applied stress:

$$\varepsilon(t)=J(t)\sigma_0 \tag{2.4}$$

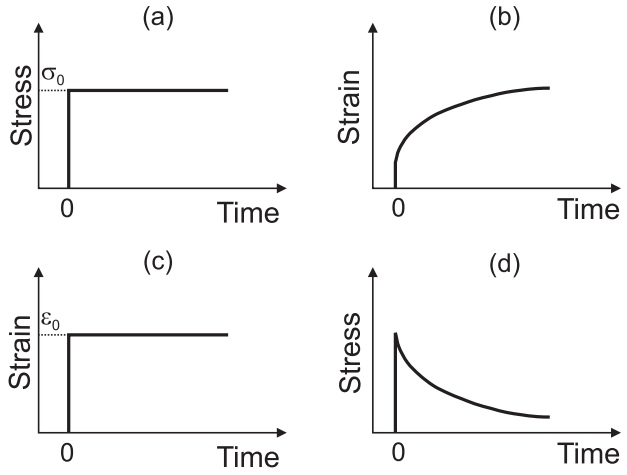

Figure 2.1: Creep and relaxation curves for viscoelastic media.

Creep compliance is a material property; it is often determined in viscoelastic tests due to the simplicity of conducting strain measurements. The vertical part on a creep curve (Fig.2.1b) is usually referred as instantaneous elasticity. Creep occurs in various materials, including metals. However, there are several significant differences between polymeric (viscoelastic) and metallic (plastic) creep (for details see [98]).

The alternative step function experiment is the stress relaxation test (Fig.2.1c,d) in which a step of constant strain $\varepsilon = \varepsilon_0 H(t)$ is applied, and stress $\sigma(t)$ is measured. Stress is found to decrease (relax) with time (Fig.2.1d), and it can be related to applied strain ε_0 through *relaxation modulus* $E(t)$:

$$\sigma(t) = E(t)\varepsilon_0 \tag{2.5}$$

Relaxation modulus is a material property and it is independent of applied strain or stress for small deformations.

2.1.3 Linear viscoelastic constitutive equations

In general there are two alternative forms of viscoelastic constitutive equations that are used to represent stress-strain-time relations. They are called the differential operator method and the integral representation. The first is widely used in viscoelastic analysis as mathematical treatment required is reasonably simple. The integral representation, however, is able to describe time dependency in more general way (for example, it can incorporate aging and temperature effects), and it is often used for the description of actual (experimentally determined) material properties.

Mechanical models analogies: differential representation

All linear viscoelastic models are made of linear springs and linear viscous dashpots. Constitutive equations for these elements are as follows

$$\sigma = E\varepsilon \tag{2.6}$$

$$\sigma = \eta\dot{\varepsilon} \tag{2.7}$$

where R is the spring's modulus (Young's modulus), η is the viscosity of the dashpot, and the dot denotes the time derivative. Viscoelastic behavior of materials can be approximated by a specific combination of linear springs and dashpots. Some of the most basic combinations (models) are presented in Figs.2.2-2.5.

The most general form of the differential representation in the case of simple state of stress such as pure shear or uniaxial tension is

$$P\sigma(t) = Q\varepsilon(t) \tag{2.8}$$

where linear differential operators P and Q are defined as

$$P = \sum_{k=0}^{N_p} p_k \frac{d^k}{dt^k}, \qquad Q = \sum_{k=0}^{N_q} q_k \frac{d^k}{dt^k} \tag{2.9}$$

in which t is time, and p_k and q_k are time-independent coefficients specific for each material. Constitutive relations for several viscoelastic models are presented below.

- **Maxwell model**

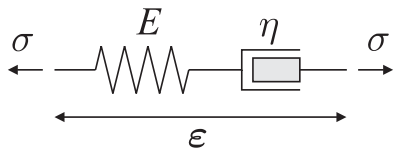

Figure 2.2: Maxwell model

The Maxwell model consists of an elastic spring and a viscous dashpot connected in series (Fig.2.2). It is straightforward to derive the constitutive relation for this model. Total strain in the model equals to the sum of strains in each element:

$$\varepsilon = \varepsilon_R + \varepsilon_\eta \tag{2.10}$$

and the rate of strain is

$$\dot{\varepsilon} = \dot{\varepsilon}_R + \dot{\varepsilon}_\eta \tag{2.11}$$

where ε_R and ε_η stand for strains in spring and dashpot respectively. Using (2.11) with (2.6)-(2.7) one arrives at the constitutive relation for the Maxwell model

$$\sigma + \frac{\eta}{E}\dot{\sigma} = \eta\dot{\varepsilon} \tag{2.12}$$

- **Kelvin model**

The Kelvin model consists of a spring and a dashpot combined in parallel (Fig.2.3). The total stress in the model is equal to the sum of stresses in each element

$$\sigma = \sigma_R + \sigma_\eta \tag{2.13}$$

Using 2.13 together with (2.6)-(2.7) the following constitutive relation is obtained:

$$\sigma = E\varepsilon + \eta\dot{\varepsilon} \tag{2.14}$$

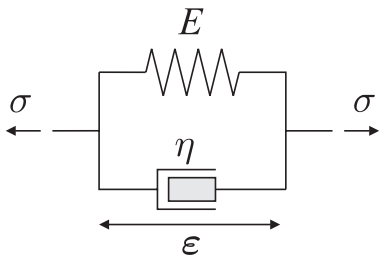

Figure 2.3: Kelvin model

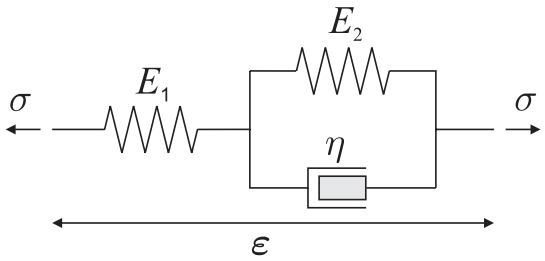

Figure 2.4: Boltzmann model

- **Boltzmann model**

The Boltzmann model (Fig.2.4) represents a combination of the Kelvin model with a spring attached to it in series. Following derivations similar to the previous two cases, it is straightforward to obtain the constitutive relation for this model:

$$\frac{E_1 + E_2}{E_1}\sigma + \frac{\eta}{E_1}\dot{\sigma} = E_2\varepsilon + \eta\dot{\varepsilon} \tag{2.15}$$

The Boltzmann model is related to the class of standard solid models, which exhibit a solid like behavior with retarded elasticity (instantaneous elastic deformation and delayed elastic deformation).

- **Burgers model**

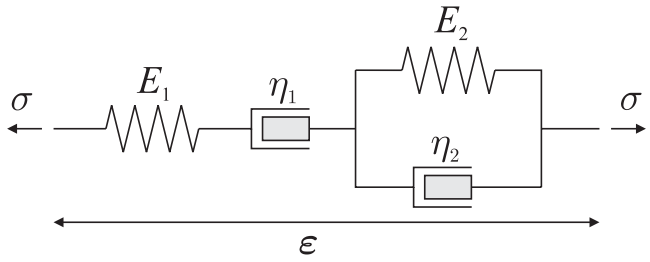

Figure 2.5: Burgers model

The Burgers model is shown in Fig.2.5 where the Maxwell and Kelvin models are connected in series. The constitutive equation for this model is as follows

$$\sigma + \left(\frac{\eta_1}{E_1} + \frac{\eta_1}{E_2} + \frac{\eta_2}{E_2}\right)\dot{\sigma} + \frac{\eta_1\eta_2}{E_1E_2}\ddot{\sigma} = \eta_1\dot{\varepsilon} + \frac{\eta_1\eta_2}{E_2}\ddot{\varepsilon} \tag{2.16}$$

The Burgers model exhibits an instantaneous elastic response followed by viscous flow and delayed elasticity.

For the case of multiaxial state of stress it is convenient to consider volumetric and deviatoric effects separately since many viscoelastic media exhibit different response to shear and dilatational stress. Thus, the constitutive equations analogous to (2.8)-(2.9) can be written for isotropic and deviatoric parts of stress and strain tensors.

Simple models, such as the Kelvin or Maxwell models, poorly describe the behavior of real viscoelastic materials. By increasing the number of elements in a model, a better material description can be obtained. Among the four cases presented above, the Burgers model provides the best description for many viscoelastic solids, and it has been used in a number of studies (e.g. [41], [89], [134]). However, it is impractical to increase infinitely the number of elements in a mechanical model, as it may not be possible to determine all the coefficients in the differential representation and it also leads to complex mathematical description. Instead, it is often more convenient to adopt the integral representation for characterizing the behavior of real viscoelastic materials.

Integral representation

The integral representation of viscoelastic constitutive relations directly follows from the Boltzmann superposition principle [15], which states that (a) the creep in a specimen is a function of the entire loading history and (b) each loading step makes an independent contribution to the final deformation, and the final deformation can be obtained by the simple addition of each contribution. Equation (2.2) represents the second part of this statement.

Considering an infinite number of infinitesimal consequent steps of loading history, the sum (superposition) of such steps can be substituted by an integral, and strain history can be represented as

$$\varepsilon(t) = \int_0^t J(t-\tau)d\sigma(\tau) = \int_0^t J(t-\tau)\frac{\partial\sigma(\tau)}{\partial\tau}d\tau \tag{2.17}$$

where $J(t)$ is creep compliance, $\sigma(\tau)$ is stress history, and τ is any arbitrary time between 0 and t, representing past time. Equation (2.17) can be used to describe the creep strain under any given stress history provided creep compliance $J(t)$ is known.

Following similar arguments, stress can be expressed through the strain history as

$$\sigma(t) = \int_0^t E(t-\tau)d\varepsilon(\tau) = \int_0^t E(t-\tau)\frac{\partial\varepsilon(\tau)}{\partial\tau}d\tau \tag{2.18}$$

where $E(t)$ is relaxation modulus. Integrals (2.17) and (2.18) are called hereditary integrals and were originally suggested by Volterra [130].

In the case of multiaxial state of stress in homogeneous isotropic materials, it is convenient to separate shear and dilatational components of stress and strain tensors. Thus, the stress history can be represented as

$$\begin{aligned}\sigma_{ii}(t) &= 3\int_0^t K(t-\tau)\frac{\partial\varepsilon_{ii}(\tau)}{\partial\tau}d\tau \\ \sigma_{ij}(t) &= 2\int_0^t G(t-\tau)\frac{\partial\varepsilon_{ij}(\tau)}{\partial\tau}d\tau, \quad i \neq j\end{aligned} \tag{2.19}$$

where $\sigma_{ii}(t)$ and $\varepsilon_{ii}(t)$ are their volumetric parts, $\sigma_{ij}(t)$ and $\varepsilon_{ij}(t)$ $(i \neq j)$ are deviatoric parts of stress and strain tensors respectively, $K(t)$ and $G(t)$ are bulk and shear relaxation moduli respectively.

It can be shown that both differential and integral representations are equivalent [47]. One form of the representation can be changed to another form by using an appropriate number of differential operators and coefficients in (2.9) or appropriately choosing creep and relaxation functions. The Laplace transform (see (2.40)) is often used for the transition from the differential to integral form of viscoelastic constitutive equations.

2.1.4 Complex moduli

Another type of representation of viscoelastic constitutive equations that is often used in practice involves the so-called complex moduli. These moduli can be obtained from an experiment with periodically varying loading F, e.g.

$$F(t) = F_0 \cos(\omega t) \tag{2.20}$$

where F_0 is the amplitude of the force and ω is the angular frequency. This steady state vibration induces a variation in stress at a given point with the same frequency,

$$\sigma(t) = \sigma_0 \cos(\omega t) \tag{2.21}$$

Equation (2.21) is equivalent to the real part of expression

$$\sigma = \sigma_0 \mathrm{e}^{i\omega t} \tag{2.22}$$

where $i = \sqrt{-1}$ is the complex unity. The latter expression is introduced due to the convenience of using complex algebra operations. For linear viscoelastic materials, strain at a point oscillates with the same frequency as stress but lags behind by angle δ,

$$\varepsilon = \varepsilon_0 \mathrm{e}^{i(\omega t - \delta)} = \varepsilon^* \mathrm{e}^{i\omega t} \tag{2.23}$$

where ε^* is the complex strain amplitude,

$$\varepsilon^* = \varepsilon_0 \mathrm{e}^{-i\delta} = \varepsilon_0 \left(\cos\delta - i\sin\delta\right) \tag{2.24}$$

The complex parameter

$$J^*(\omega) = \frac{\varepsilon^*}{\sigma_0} \tag{2.25}$$

is called complex creep compliance. The dependency of complex creep compliance on frequency can be shown [47] by substituting (2.22) and (2.23) into the differential form of viscoelastic constitutive equations (2.8).

Similar relations can be obtained if the input is an oscillatory strain,

$$\varepsilon = \varepsilon_0 \mathrm{e}^{i\omega t} \tag{2.26}$$

Then the stress response will lead the strain by a phase angle δ and it can be presented as

$$\sigma = \sigma_0 e^{i(\omega t+\delta)} = \sigma^* \mathrm{e}^{i\omega t} \tag{2.27}$$

The complex parameter $E^*(\omega)$ defined as

$$E^*(\omega) = \frac{\sigma^*}{\varepsilon_0} = \frac{\sigma_0}{\varepsilon_0}\mathrm{e}^{i\delta} = E_1 + iE_2 \tag{2.28}$$

$$E_1 = \frac{\sigma_0}{\varepsilon_0}\cos\delta = |E^*|\cos\delta \tag{2.29}$$

$$E_2 = \frac{\sigma_0}{\varepsilon_0}\sin\delta = |E^*|\sin\delta \tag{2.30}$$

is called complex relaxation modulus. Its real part E_1 is usually referred to as storage modulus, while its imaginary part E_2 is loss modulus. These names are related to the fact that storage modulus defines the energy stored in the specimen due to applied strain, while loss modulus defines its dissipation (e.g. [135]). Similarly, storage J_1 and loss J_2 compliance can be defined,

$$J = J_1 - iJ_2 \tag{2.31}$$

$$J_1 = |J^*|\cos\delta \tag{2.32}$$

$$J_2 = |J^*|\sin\delta \tag{2.33}$$

The parameter

$$\tan\delta = \frac{E_2}{E_1} = \frac{J_2}{J_1} \tag{2.34}$$

is called the loss tangent or mechanical loss. An important observation is that complex relaxation modulus and complex creep compliance are reciprocal [47]. Thus

$$J^* E^* = 1 \tag{2.35}$$

It is straightforward to derive complex moduli for different viscoelastic mechanical models and establish the relations between the relaxation modulus and creep compliance and their complex analogs (e.g. [47], [135], [138]).

2.1.5 Temperature effects: time-temperature superposition

Temperature effects in viscoelastic materials (especially in polymers) play an important role because such materials show very large changes in properties with changing temperature. It is due to the changes in the molecular structure of viscoelastic materials, which cause material to behave glass-like at low temperatures and rubber-like or even liquid-like at high temperatures. A transition point from glassy- to rubber-like state at which a significant change of viscoelastic moduli occurs is called glass-transition point [135]. In some materials this transition point is well defined (e.g. polymethyl methacrylate, [135]), while for other viscoelastic materials the transition happens over large period of time and temperature (e.g. polyethylene terephthalate, [135]).

In general, the influence of temperature effects on viscoelastic constitutive equations can be taken into account by assuming that the coefficients in front of each term in the differential representation (2.8)-(2.9), or creep compliance and relaxation modulus in the integral representation (2.17)-(2.18), are functions of time and temperature. For example, relaxation modulus is presented as

$$E = E(t, T) \tag{2.36}$$

where T is temperature. The unknown time and temperature dependent moduli could be determined from experiments conducted at different temperatures. To properly describe

material properties over large range of times and temperatures, a significant number of experiments may be required.

The problem of description of thermo-mechanical behavior of viscoelastic materials can be significantly simplified with the use of *time-temperature superposition principle*, which is applicable for a certain class of viscoelastic materials [46], [47], [135], [138]. Theoretical and experimental results indicate (e.g. [14], [46], [23], [125]) that for such materials the response to a load at a high temperature over a short duration of time is identical to that at a lower temperature but over a longer duration of time, and vice-versa. Thus, material property, such as relaxation modulus or creep compliance, at any temperature T can be expressed in terms of the material property at reference temperature T_0 and another material property known as the time-shift factor a_T, e.g.

$$E(t,T) = E(\zeta, T_0) \tag{2.37}$$

$$\zeta = t/a_T(T) \tag{2.38}$$

where t is actual time of observation measured from the first application of load and ζ is fictitious "reduced time". Expression (2.37)-(2.38) state that the effect of temperature on the time-dependent mechanical behavior is equivalent to a stretching (or shrinking) the real time for temperatures above (or below) the reference temperature. Following Schwarzl and Staverman [117], materials that exhibit such property are called thermorheologically simple.

In the case of transient temperature conditions where temperature varies in time [107], the reduced time is given by

$$\zeta = \int_0^t \frac{d\tau}{a_T\left[T(\tau)\right]} \tag{2.39}$$

Relaxation modulus $E(\zeta, T_0)$ given in the reduced time scale is called *master relaxation modulus*. To illustrate the way of obtaining the master relaxation modulus, consider plots in Fig.2.6 and Fig.2.7. Plots in Fig.2.6 illustrate the variation of the relaxation modulus of viscoelastic asphalt binder in time for three different temperatures.

Take the reference temperature $T_0 = -18°C$. The master relaxation curve at T_0 can be obtained by applying horizontal shifts (along the log-time scale) to the curves for other temperatures to make them join as smoothly as possible to the curve at T_0 (Fig.2.6, 2.7). This very simple approach was originally proposed by Ferry [46]. The shift factors a_T applied to each relaxation curve can now be plotted versus corresponding temperature, and the obtained set of points fitted to provide functional relation $a_T(T)$. Then using (2.39) one can express reduced time ζ as a function of time or temperature. Similar procedure can be applied to other viscoelastic moduli or compliances.

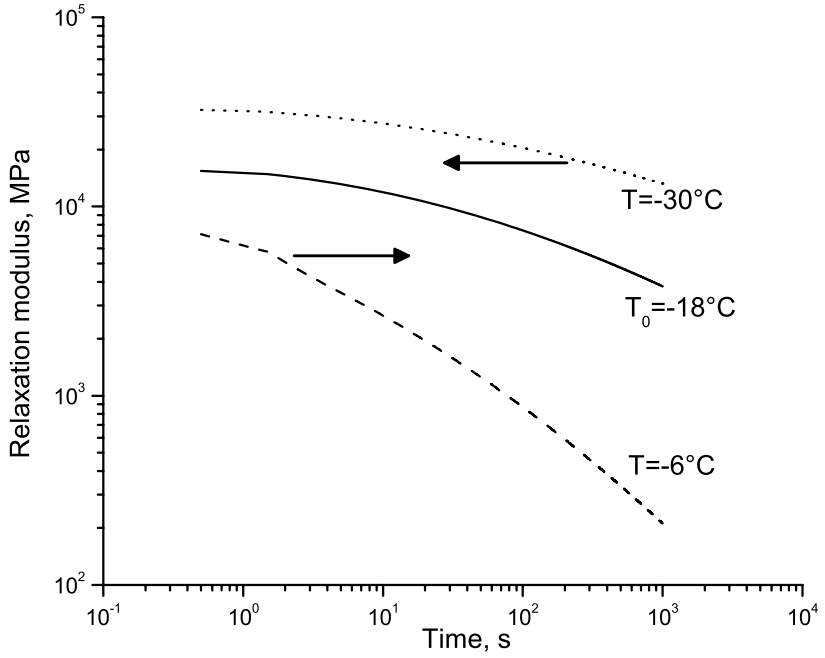

Figure 2.6: Relaxation modulus of an asphalt binder measured at three diffrerent temperatures. Data are plotted in log-log scale.

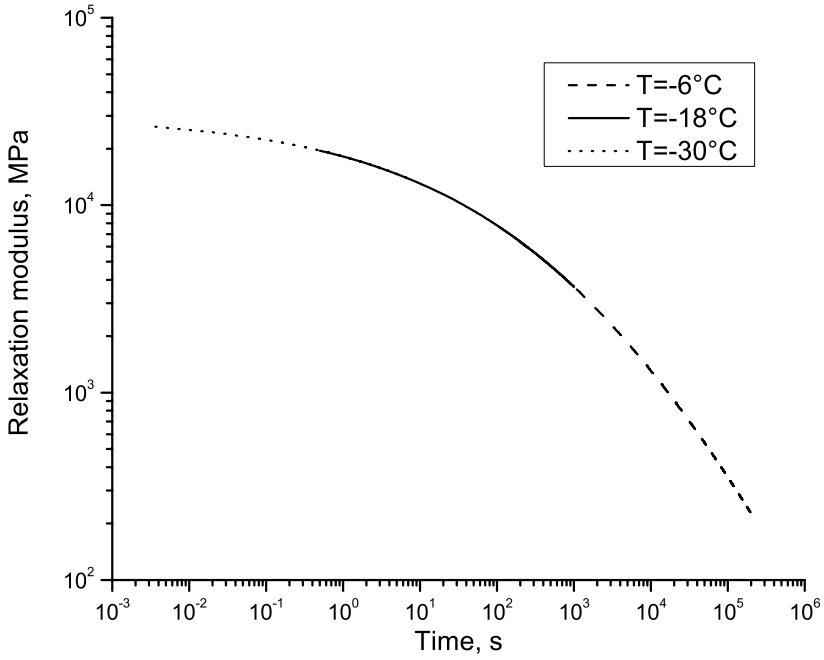

Figure 2.7: Master relaxation modulus. Data are plotted in log-log scale.

2.1.6 Elastic-Viscoelastic correspondence principles

One of the most powerful approaches to solve linear viscoelastic problems consists in the reduction of the original problem to the corresponding elastic one. Such an approach can provide an analytical solution for time-dependent problems and often is simpler in implementation than numerical algorithms of calculating time-varying fields in viscoelastic homogeneous or heterogeneous materials. Several techniques can be used to obtain the corresponding elastic problem.

Correspondence principle based on the Laplace transform

First technique is based on the application of the Laplace transform to all governing equations and boundary conditions describing a viscoelastic problem. The Laplace

transform of a real function $f(t)$ is defined as [111]

$$\hat{f}(s) = \mathcal{L}\left[f(t)\right] = \int_0^\infty f(t)e^{-st}dt \tag{2.40}$$

where s is the complex transform parameter. The inverse Laplace transform is given by the Bromwich integral:

$$f(t) = \mathcal{L}^{-1}\left[\hat{f}(s)\right] = \frac{1}{2\pi i}\int_{\gamma-i\cdot\infty}^{\gamma+i\cdot\infty} \hat{f}(s)e^{st}ds \tag{2.41}$$

where γ is a vertical contour in the complex plane chosen in such a way that all singularities of $f(s)$ are located to the left of it.

Applying the Laplace transform to the convolution integrals (2.19), expressions formally equivalent to the elastic Hooke's law are obtained,

$$\begin{aligned} \hat{\sigma}_{ii}(s) &= 3s\hat{K}(s)\hat{\varepsilon}_{ii}(s) \\ \hat{\sigma}_{ij}(s) &= 2s\hat{G}(s)\hat{\varepsilon}_{ij}(s), \quad i \neq j \end{aligned} \tag{2.42}$$

Furthermore, application of the Laplace transform to the equilibrium equations, kinematic equations, compatibility conditions, and boundary conditions allows fully formulate a problem in the Laplace domain. Due to the fact that the transformed equations resemble elastic equations [47], the obtained problem is formally equivalent to an elastic one, which is called the *corresponding elastic problem*. This problem does not include time, but all the 'elastic constants' are functions of the transform parameter s (in addition, they are multiplied[2] by s; see (2.42)), as are the transformed boundary conditions. By solving this corresponding problem and applying a procedure of Laplace inversion to s-dependent solution, the time-domain solution can be obtained [47], [116].

The use of the Laplace transform allows one to express the relaxation modulus and creep compliance through the parameters of the corresponding mechanical model.

[2] Note that when replacing elastic time-dependent parameters according to the correspondence principle, one should not multiply the transformed Poisson's ratio $\hat{\nu}(s)$ by s as compared to the rest of elastic parameters (e.g. $s\hat{G}(s)$ or $s\hat{K}(s)$). This is due to the fact that Poisson's ratio is defined as ratio of strain components measured in orthogonal directions, and it is not present explicitly in the convolution integrals in the formulation of viscoelastic constitutive equations.

For example, consider the Boltzmann model, for which the constitutive equation in differential form is given by Eq.(2.15). Assume that this equation describes the shear behavior of a material, while its dilatational behavior is time-independent (elastic). Using the the notation of expression (2.19), the constitutive equations can be written as

$$\frac{E_1+E_2}{E_1}\sigma_{ij}(t)+\frac{\eta}{E_1}\dot{\sigma}_{ij}(t)=2E_2\varepsilon_{ij}(t)+2\eta\dot{\varepsilon}_{ij}(t), \quad i\neq j \tag{2.43}$$

$$\sigma_{kk}(t)=3K\varepsilon_{kk}(t)$$

Applying the Laplace transform to (2.43), the following relations are obtained

$$\left[\frac{E_1+E_2}{E_1}+s\frac{\eta}{E_1}\right]\hat{\sigma}_{ij}(s)=2\left[E_2+s\eta\right]\hat{e}_{ij}(s) \tag{2.44}$$

$$\hat{\sigma}_{kk}(s)=3K\hat{\varepsilon}_{kk}(s) \tag{2.45}$$

Expression (2.44) can be presented in the form

$$\hat{\sigma}_{ij}=2\hat{\mu}\hat{e}_{ij} \tag{2.46}$$

which resembles the Hooke's law for shear behavior. Thus, s-dependent shear modulus is

$$\hat{\mu}(s)=\frac{E_1(E_2+\eta s)}{E_1+E_2+\eta s} \tag{2.47}$$

Note that representation (2.47) for shear modulus already includes an additional multiplication by the transform parameter s. The transformed physical shear relaxation modulus $\hat{G}(s)$ (see Eq.(2.19)) is related to $\hat{\mu}(s)$ as

$$\hat{G}(s)=\frac{\hat{\mu}(s)}{s} \tag{2.48}$$

Similar arguments can be adopted to relate other material properties obtained from the differential and integral representations (except for the Poisson's ratio).

All the relations between s-dependent 'elastic constants' in the Laplace domain are similar to those in elasticity. Thus, in the present example the s-dependent Poisson's ratio $\hat{\nu}(s)$ and relaxation (Young's) modulus $\hat{E}(s)$ can be easily expressed through

shear modulus (2.47) and constant bulk modulus K. It is useful to introduce Kolosov-Muskhelishvili's parameter κ, which is defined as

$$\kappa = \begin{cases} 3-4\nu, & \text{for plane strain} \\ \dfrac{3-\nu}{1+\nu}, & \text{for plane stress} \end{cases} \tag{2.49}$$

This parameter will be extensively used in further analysis. For the example presented above (see Eqs.(2.44)-(2.47)), the plane strain Kolosov-Muskhelishvili's parameter in the Laplace domain is found as

$$\hat{\kappa}(s) = 3 - 4\hat{\nu}(s) = 3 - 4\frac{3K - 2\hat{\mu}}{2\left(3K + \hat{\mu}\right)} = 1 + \frac{6E_1(E_2 + \eta s)}{E_1(E_2 + \eta s) + 3K(E_1 + E_2 + \eta s)} \tag{2.50}$$

Special attention should be given to the case of constant Poisson's ratio. For illustration purposes consider a case when material's relaxation (Young's) modulus E depends on time, while its Poisson's ratio ν is constant. In this case, the temporal variation of all viscoelastic moduli, except for the Poisson's ratio, is proportional to each other in isotropic linearly viscoelastic medium. Therefore, using the following expressions given in the Laplace domain,

$$\hat{K} = \frac{\hat{E}}{3\left(1-2\nu\right)}, \qquad \hat{\mu} = \frac{\hat{E}}{2\left(1+\nu\right)} \tag{2.51}$$

one can show that

$$\hat{\nu} = \nu \tag{2.52}$$

and thus

$$\hat{\kappa} = \begin{cases} 3-4\nu, & \text{for plane strain} \\ \dfrac{3-\nu}{1+\nu}, & \text{for plane stress} \end{cases} \quad \text{and time-independent } \nu \tag{2.53}$$

There are some restrictions for the application of the correspondence principle based on the Laplace transform. This method can be used when stress or deformation boundary conditions are prescribed on the whole boundary. In the case of mixed stress and deformation boundary conditions the method can be applied only when the interface between stress and deformation boundaries does not change with time [80].

In some cases the use of this approach may be limited by the fact that strain or stress histories and/or material properties may be rather complex functions of time, so the Laplace transform of these functions can not be found in a closed form. This makes obtaining the solution of the corresponding elastic problem a difficult issue.

Volterra correspondence principle

The Volterra correspondence principle [114], [131] can be used in the case when the Laplace transform is not applicable. The principle is based on the representation of hereditary integrals of type (2.17)-(2.19) as integral operators acting on time-varying functions. Such technique also leads to the reduction of a time-dependent problem to the corresponding elastic problem.

Consider the case of a simple deformation caused by uniaxial tension of a linear viscoelastic body. Evaluating integral (2.18) by parts, it can be found that

$$\sigma(t) = E(0)\varepsilon(t) - \int_0^t \varepsilon(\tau) dE(t-\tau) \equiv \tilde{E} \cdot \varepsilon(t) \tag{2.54}$$

where $\tilde{E}$ is an integral operator acting on a function of time, $E(0)$ is the value of the relaxation modulus at zero moment of time. It is seen that (2.54) is formally equivalent to the Hooke's law. Operator $\tilde{E}$ will be referred as the relaxation operator. In more general case, it can be shown [114] that other viscoelastic parameters, such as creep compliance, viscoelastic bulk and shear moduli etc., can be expressed in an operator form in such a way that the constitutive equations written with the use of these operators resemble elastic constitutive equations. This implies that in order to solve a viscoelastic problem, one has to solve a corresponding elastic problem, and substitute the elastic properties with the corresponding integral operators in the obtained elastic solution for each physical variable of interest. Since superposition holds for elasticity, viscoelastic solution for any physical variable $\gamma(t)$ can be presented as a combination of functions of one or more commutative integral operators[3] acting on known functions of time $f_i(t)$,

[3] The term "commutativity" is understood here in the sense used by Rabotnov [114] and Arutyunyan

which can be time-dependent boundary parameters, body forces, temperature, etc. In the case of an isotropic viscoelastic material, such relation can be presented as

$$\gamma(t) = \sum_i F_i \left[\tilde{E}, \tilde{\nu}\right] \cdot f_i(t) \tag{2.55}$$

where $\tilde{\nu}$ is the integral operator corresponding to viscoelastic Poisson's ratio and F_i are functions of operators. Operators corresponding to viscoelastic shear or bulk modulus can be equally used in (2.55) instead of $\tilde{\nu}$. Note that the commutativity between integral operators mentioned before holds only for the case of non-ageing viscoelasticity. Indeed, for the case of linear non-ageing viscoelasticity

$$\begin{aligned}\mathcal{L}\left(\tilde{K} \cdot \left[\tilde{E} \cdot \varepsilon(t)\right]\right) = \mathcal{L}\left(\tilde{K} \cdot \sigma(t)\right) = \mathcal{L}\left(\int_0^t K(t-\tau)\frac{\partial \sigma(\tau)}{\partial \tau} d\tau\right) = \hat{K}(s)\hat{\sigma}(s) = \\ = \hat{K}(s)\hat{E}(s)\hat{\varepsilon}(s) = \hat{E}(s)\hat{K}(s)\hat{\varepsilon}(s) = \mathcal{L}\left(\tilde{E} \cdot \left[\tilde{K} \cdot \varepsilon(t)\right]\right)\end{aligned} \tag{2.56}$$

where (2.54) was used, and $\tilde{K}$ and $\tilde{E}$ are operators of type (2.54). Due to the uniqueness of the inverse Laplace transform [118],

$$\tilde{K} \cdot \left[\tilde{E} \cdot \varepsilon(t)\right] = \tilde{E} \cdot \left[\tilde{K} \cdot \varepsilon(t)\right] \tag{2.57}$$

In the case of ageing viscoelastic material, the constitutive equations can not be presented in the form of convolution integrals (e.g. Eq.(2.17)), therefore the commutativity of integral operators is not valid.

Hashin's correspondence principle

It was shown in Section 2.1.4 that dynamic (complex) moduli can be used to describe the relations between stress and strain amplitudes in steady state vibrations induced in homogeneous viscoelastic materials. Introducing time-harmonic deformation histories

and Zevin [7]. This mutual commutativeness of operators should not be confused with the commutativeness of operations of integration with respect to time and differentiation or integration with respect to coordinates.

(2.23) into (2.19), and using the Fourier transform, one obtains

$$\sigma^*_{kk}(\omega) = 3i\omega\breve{K}(\omega)\varepsilon^*_{kk}(\omega) \tag{2.58}$$
$$\sigma^*_{ij}(\omega) = 2i\omega\breve{G}(\omega)\varepsilon^*_{ij}(\omega), \quad i \neq j$$

where $\breve{K}$ and $\breve{G}$ are half-sided Fourier transforms of the moduli, e.g.

$$\breve{K}(\omega) = \int_0^\infty K(t)\exp(-i\omega t)dt \tag{2.59}$$

Relations (2.58) can be written in terms of complex moduli if one denotes

$$K^*(\omega) = i\omega\breve{K}(\omega), \qquad G^*(\omega) = i\omega\breve{G}(\omega) \tag{2.60}$$

Note that expressions (2.58) and (2.60) resemble the correspondence principle based on the Laplace transform if one formally substitutes $i\omega$ instead of parameter s in (2.42).

For composite materials relations similar to (2.58) are obtained in terms of averages of stress and strain amplitudes. In the case of statistically isotropic composites [13], Hashin [58] showed that

$$\bar{\sigma}^*_{kk}(\omega) = 3K^*_{eff}(\omega)\bar{\varepsilon}^*_{kk}(\omega) \tag{2.61}$$
$$\bar{\sigma}^*_{ij}(\omega) = 2G^*_{eff}(\omega)\bar{\varepsilon}^*_{ij}(\omega), \quad i \neq j$$

where $\bar{\sigma}$ and $\bar{\varepsilon}$ are space averages of stress and strain respectively, $K^*_{eff}(\omega)$ and $G^*_{eff}(\omega)$ are effective complex bulk and shear moduli respectively. Eqs.(2.61) are analogous to the corresponding expressions for homogeneous media. Based on this, Hashin stated the following correspondence principle for complex moduli of composites [57]: "The effective complex moduli (compliances) of a viscoelastic composite are obtained by replacement of phase elastic moduli by corresponding phase complex moduli in the expressions for the effective elastic moduli (compliances) of a composite with identical phase geometry". For further details on the application of this principle the reader is referred to works [30], [57], [58].

2.2 Boundary integral equations

Several viscoelastic problems under the condition of plane strain or plane stress are considered in this dissertation. The solution of the these problems is found with the use of complex boundary integral equations that are written in the Laplace domain. This section provides a brief overview of the theory of complex integral equations for plane elasticity, and the transition from the elastic case to viscoelastic one is outlined.

2.2.1 Elastic case

Kolosov-Muskhelishvili's potentials

It is well known that in the absence of body forces, the solution of many plane elasticity problems can be obtained with the use of Airy stress function U that satisfies the biharmonic equation (e.g. [34])

$$\triangle^2 U(x,y) = 0 \tag{2.62}$$

Stress components can be expressed via function U as

$$\sigma_{xx} = \frac{\partial^2 U}{\partial y^2}, \qquad \sigma_{yy} = \frac{\partial^2 U}{\partial x^2}, \qquad \sigma_{xy} = -\frac{\partial^2 U}{\partial x \partial y} \tag{2.63}$$

According to Goursat's formula [108], the real stress function $U(x,y)$ can be represented as a combination of two complex analytic functions $\varphi(z)$ and $\chi(z)$,

$$U = \mathrm{Re}\left[\bar{z}\varphi(z) + \chi(z)\right] = \frac{1}{2}\left[\bar{z}\varphi(z) + z\overline{\varphi(z)} + \chi(z) + \overline{\chi(z)}\right] \tag{2.64}$$

where $z = x + iy$ is complex coordinate and the bar over a symbol denotes the complex conjugation. Then, following the derivations presented by Muskhelishvili [108], complex displacement vector $u(z) = u_x(x,y) + iu_y(x,y)$ can be expressed as

$$2\mu u(z) = \kappa\varphi(z) - z\overline{\varphi'(z)} - \overline{\psi(z)} \tag{2.65}$$

where $\psi(z) = \chi'(z)$ and the prime means the derivative over the complex coordinate z. Here μ is the shear modulus and κ is Kolosov-Muskhelishvili's parameter (Eq.(2.49)).

Using Hooke's law, the following relations between in-plane stress and strain components are obtained

$$\sigma_{xx} + \sigma_{yy} = \frac{4\mu}{\kappa - 1}\left(\varepsilon_{xx} + \varepsilon_{yy}\right) \tag{2.66}$$
$$\sigma_{yy} - \sigma_{xx} + 2i\sigma_{xy} = 2\mu\left(\varepsilon_{yy} - \varepsilon_{xx} + 2i\varepsilon_{xy}\right)$$

Employing strain-displacement relations, Muskhelishvili showed [108] that

$$\sigma_{xx}(z) + \sigma_{yy}(z) = 4\,\mathrm{Re}\left[\varphi'(z)\right] \tag{2.67}$$
$$\sigma_{yy}(z) - \sigma_{xx}(z) + 2i\sigma_{xy}(z) = 2\left[\bar{z}\varphi''(z) + \psi'(z)\right]$$

Similar expressions were derived by Kolosov [75], therefore the complex functions $\varphi(z)$ and $\psi(z)$ are called Kolosov-Muskhelishvili's potentials. Expressions (2.65) and (2.67) in addition with the formula

$$t(z) = \varphi'(z) + \overline{\varphi'(z)} + \frac{d\bar{z}}{dz}\left[z\overline{\varphi''(z)} + \overline{\psi'(z)}\right] \tag{2.68}$$

are called Kolosov-Muskhelishvili's formulae [108], [115]. Here $t(z) = t_n(z) + it_s(z)$ is complex traction at point z, $t_n(z)$ and $t_s(z)$ are the normal and shear tractions respectively, $d\bar{z}/dz = \exp(-2i\theta)$, where θ is the angle between Ox and the line on which the tractions are computed.

Potentials $\varphi(z)$ and $\psi(z)$ for a problem of a point force applied in the interior of an infinite elastic domain (the Kelvin's solution) can be found with the use of formula (2.68) and Fourier series approximations [108]. They are

$$\varphi'(z) = -\frac{F_x + iF_y}{2\pi\left(1+\kappa\right)}\frac{1}{z - z_0}$$
$$\psi'(z) = \kappa\frac{F_x - iF_y}{2\pi\left(1+\kappa\right)}\frac{1}{z - z_0} - \frac{F_x + iF_y}{2\pi\left(1+\kappa\right)}\frac{\overline{z_0}}{\left(z - z_0\right)^2} \tag{2.69}$$

where $(F_x,\ F_y)$ are the components of the point force applied at point z_0. The expressions for some other cases (e.g. a point force applied inside of a half-plane - the Melan's solution; a point force applied on the boundary of half-plane - the Flamant's solution) can be found in [100].

In the case of a problem including multiply connected domain, the potentials $\varphi(z)$ and $\psi(z)$ can be presented in the form of boundary integrals that include physical parameters given on the boundaries of the domain (e.g. displacements, displacement discontinuities, or tractions). Linkov [85] and Mogilevskaya [101] presented approaches for a wide variety of elastic problems. The potentials used in the present work can be obtained from the expressions for $\varphi(z)$ and $\psi(z)$ provided in [101].

Complex hyper-singular boundary integral equations

The solution of elastic problems based on the use of integral equations can be obtained employing two approaches that are called indirect and direct formulation of boundary integral equations[4] . The indirect method employs fictitious density functions to formulate the problem. These density functions have no physical significance, but can be integrated to obtain the actual displacements and stresses (e.g. [109]). Thus, this approach is indirect in the sense that actual displacements and stresses are not used. Besides, depending on the problem, some additional conditions are required for the solution to exist (e.g. the condition of single-valuedness of the displacements is required for a crack problem considered in [59]).

Mogilevskaya [100] presented an approach to obtain complex boundary integral equations with the use of the indirect and direct formulations. In the present work the direct approach is employed, as it is more convenient to deal with physical boundary parameters than with fictitious density functions, and no additional conditions are required for the existence of the solution.

In the direct approach the actual physical quantities such as displacements and tractions are used to formulate the integral equations. Such equations were originally obtained by Somigliana in 1885 [120] based on Betti's reciprocal theorem (e.g. [12]). The theorem links the states of displacements and tractions to two different problems for the same region. The first state is associated with the problem to be solved, and the

[4] For the history of development of boundary integral and boundary element methods see [26].

second - with a problem for which solution is known (test solution). In the case of zero body forces the theorem takes the form

$$\int_L t_i^{(a)}(\varsigma)u_i^{(b)}(\varsigma)dl(\varsigma) = \int_L t_i^{(b)}(\varsigma)u_i^{(a)}(\varsigma)dl(\varsigma) \tag{2.70}$$

where L is the boundary of the domain, $u_i^{(a)}$ and $t_i^{(a)}$ (and $u_i^{(b)}$ and $t_i^{(b)}$) are the displacements and tractions from the system (a) (and (b)).

The Somigliana's displacement identity follows from (2.70) and it expresses the displacements $u_i(z_F)$ at a point z_F within a domain D in terms of integrals of the tractions $t_i(\varsigma)$ and displacements $u_i(\varsigma)$ on the boundary L of the domain (Fig.2.8),

$$u_i(z_F) = \int_L t_j(\varsigma)U_{ij}(z_F,\varsigma)dl(\varsigma) - \int_L u_j(\varsigma)T_{ij}(z_F,\varsigma)dl(\varsigma), \quad \varsigma \in L,\ z \in D \tag{2.71}$$

where $i,j = x,y$ (the repeated index implies summation) and $\varsigma \neq z_F$; $U_{ij}(z_F,\varsigma)$ and $T_{ij}(z_F,\varsigma)$ are the tensor fields (test solutions) that give respectively the jth component of the displacements and tractions at the point ς due to a unit point force acting at the point z_F in the ith direction; $u_j(\varsigma)$ (and $t_j(\varsigma)$) are the components of displacement (traction) vector at the point ς. Equation (2.71) is valid for an infinite region provided the displacements and stresses decay at the infinity as $1/r$ and $1/r^2$, respectively, where $r = \sqrt{\varsigma_k\varsigma_k}$ is the distance from the origin [16]. In such case L may represent boundaries of one or more voids located in an infinite plane.

Combining the components of displacement at the point z in the complex displacement vector $u(z) = u_x(z) + iu_y(z)$ and following the procedure proposed in [100], one can obtain the complex analog of Somigliana's displacement identity. After that, Somigliana's stress and traction identities can be found by using the strain-displacement relations and Hooke's law in complex form (Eq.(2.66)).

The test solutions $U_{ij}(z_F,z)$ and $T_{ij}(z_F,z)$ that appear in (2.71) are usually associated with the fundamental solutions of an elastic problem under consideration. For example, the solution of Kelvin's problem (point force applied in the interior of an infinite elastic domain; zero body forces are assumed) can be obtained from potentials

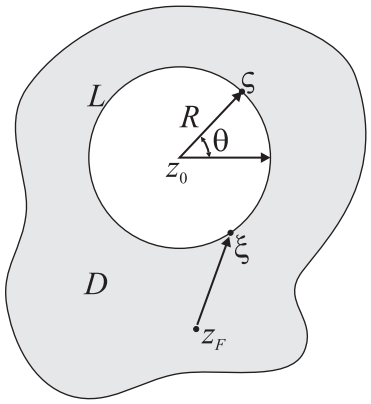

Figure 2.8: A circular hole in an infinite domain.

(2.69). Knowing the potentials, Kolosov-Muskhelishvili's formulae (2.65), (2.67) have to be used to obtain displacement and stresses, and $U_{ij}(z_F, z)$ and $T_{ij}(z_F, z)$ can be found from

$$\begin{aligned} u_i(z) &= U_{ij}(z_F, z)e_j \\ f_i(z) &= T_{ij}(z_F, z)e_j \end{aligned} \tag{2.72}$$

where e_j represents the unit vector in the direction of the unit concentrated force acting at point z_F. Here $f(z)$ is the resultant force function that is related to complex traction $t(z)$ as

$$t(z) = \frac{df(z)}{dz} \tag{2.73}$$

The expressions for $U_{ij}(z_F, z)$ and $T_{ij}(z_F, z)$ for Kelvin's problem [100] are

$$\begin{aligned} U_{ij}(z_F, z) &= \frac{1}{4\pi\mu(1+\kappa)}\left[-\kappa(i)^{r-1}\ln\left((z-z_F)\left(\overline{z}-\overline{z_F}\right)\right) + (-i)^{r-1}\frac{z-z_F}{\overline{z}-\overline{z_F}}\right] \\ T_{ij}(z_F, z) &= \frac{1}{2\pi(1+\kappa)}\left[-(i)^{r-1}\ln\left(z-z_F\right) + \kappa(i)^{r-1}\ln\left(\overline{z}-\overline{z_F}\right) - (-i)^{r-1}\frac{z-z_F}{\overline{z}-\overline{z_F}}\right] \end{aligned} \tag{2.74}$$

where $r = (1, 2)$ corresponds to $j = (x, y)$. References [12] and [32] provide the same

solution in real variables. The Kolosov-Muskhelishvili's potentials for other elastic problems and corresponding them fundamental solutions can be found elsewhere (e.g. [100], [101], [108]). In the case of elastic half-plane, the solution for $U_{ij}(z_F, z)$ and $T_{ij}(z_F, z)$ is called Melan's fundamental solution and it includes some additional terms that are responsible for providing zero tractions condition on the boundary of the half-plane [101].

The final step in the derivation of boundary integral equations adopted in the present work, is to take limit $z_F \rightarrow \xi \in L$ in the complex Somigliana's traction identity. This allows obtaining the equations that contain known and unknown physical parameters (e.g. displacements, displacement discontinuities, and tractions) on the boundaries of the domain only. Using superposition, multiple boundaries can be taken into account. The detailed derivation of such equations for the cases of full-plane and half-plane can be found in [100] and [101], respectively. The equations include singular and hyper-singular integrals (see Appendix A), and thus they are called complex hyper-singular boundary integral equations. Special treatment is required for the calculation of such integrals; for the case of circular boundaries these integrals were found in [102]. The latter reference also provides some information on the advantages of the obtained complex hyper-singular integral equations in comparison with other boundary integral equations.

2.2.2 Viscoelastic case

In viscoelastic case all material properties depend on time, and thus all the fundamental solutions for viscoelastic problem will be time-dependent. They can be obtained from the viscoelastic analog of Betti's reciprocal theorem, which in the absence of body forces is expressed in the time domain as ([8], [29])

$$\int_L \int_0^t t_i^{(a)}(\varsigma; t-\tau) \frac{\partial u_i^{(b)}(\varsigma;\tau)}{\partial \tau} d\tau dl(\varsigma) = \int_L \int_0^t u_i^{(b)}(\varsigma; t-\tau) \frac{\partial t_i^{(a)}(\varsigma;\tau)}{\partial \tau} d\tau dl(\varsigma) \qquad (2.75)$$

Note that t_i is referred to surface traction components, whereas t always signifies time. Similarly, the Somigliana's displacement identity can be expressed as ([8])

$$u_i(z;t) = \int_L \int_0^t \left[t_j(\varsigma;\tau) \frac{\partial U_{ij}(z,\varsigma;t-\tau)}{\partial \tau} - u_j(\varsigma;\tau) \frac{\partial T_{ij}(z,\varsigma;t-\tau)}{\partial \tau} \right] d\tau dl(\varsigma) \qquad (2.76)$$

The structure of the time-dependent Somigliana's traction identity is similar to (2.76), and it is provided in [64]. The solution of boundary integral equations in the time domain has been given by many authors (e.g. [8], [22], [62]), and it is usually based on time-stepping algorithms (time-scale discretization). In this work the boundary integral equations are formulated in the Laplace domain, and the solution of the corresponding elastic problem is sought.

Using the elastic-viscoelastic correspondence principle, the Laplace transformed analog of Betti's reciprocal theorem is found as ([116])

$$\int_L \hat{t}_i^{(a)}(\varsigma;s) \hat{u}_i^{(b)}(\varsigma;s) dl(\varsigma) = \int_L \hat{u}_i^{(b)}(\varsigma;s) \hat{t}_i^{(a)}(\varsigma;s) dl(\varsigma) \qquad (2.77)$$

The transformed Somigliana's displacement identity is as follows:

$$\hat{u}_i(z_F;s) = \int_L \hat{t}_j(\varsigma;s) \hat{U}_{ij}(z_F,\varsigma;s) dl(\varsigma) - \int_L \hat{u}_j(\varsigma;s) \hat{T}_{ij}(z_F,\varsigma;s) dl(\varsigma) \qquad (2.78)$$

Boundary integral equations that are originally obtained from (2.70)-(2.71) can be formulated in the Laplace domain, and the solution of the corresponding elastic problem found. After this, one has to use the analytical or numerical Laplace inversion to obtain the time-domain solution.

It is important to keep in mind that if physical material properties are used in the formulation of a problem (such as relaxation modulus or creep compliance, Eqs.(2.17)-(2.19)), their transformed counterparts has to be multiplied by the transform parameter s (cf. (2.42)). From the other hand, if one adopts differential formulation of viscoelastic constitutive equations, the transformed material properties should not be multiplied by the parameter s as they already include it (cf. (2.47)).

2.3 Fourier series

In the subsequent chapters the use of Fourier series expansions will be made, therefore some remarks about the Fourier series are provided. The advantages of using approximation of smooth functions by the Fourier series on circular or straight line segments have been shown elsewhere [33], [101], [108].

A real function $f(\theta)$ satisfying the Dirichlet smoothness condition [108] on the interval $[0, 2\pi]$ can be presented in the form of Fourier series,

$$f(\theta) = \frac{1}{2}\alpha_0 + \sum_{k=1}^{\infty} \left(\alpha_k \cos(k\theta) + \beta_k \sin(k\theta)\right) \tag{2.79}$$

where

$$\alpha_k = \frac{1}{\pi}\int_0^{2\pi} f(\theta)\cos(k\theta)\, d\theta$$

$$\beta_k = \frac{1}{\pi}\int_0^{2\pi} f(\theta)\sin(k\theta)\, d\theta, \quad k = 0, 1, 2, ... \tag{2.80}$$

Expression (2.79) can be converted to a complex form by using Euler's formulae for sin and cos functions,

$$f(\theta) = a_0 + \sum_{k=1}^{\infty} \left(a_k \mathrm{e}^{ik\theta} + a_{-k}\mathrm{e}^{-ik\theta}\right) = \sum_{-\infty}^{\infty} a_k \mathrm{e}^{ik\theta} \tag{2.81}$$

and a_n is found as

$$a_n = \frac{1}{2\pi}\int_0^{2\pi} f(\theta)\mathrm{e}^{in\theta} \tag{2.82}$$

For problems involving circular boundaries, it is convenient to use the complex Fourier series in slightly different form. For a circular hole presented in Fig.2.8 with the center at z_0 and the radius R the following function is introduced

$$g(\varsigma) = \frac{R}{\varsigma - z_0} \tag{2.83}$$

It is can be shown that for a circular segment

$$\frac{R}{\varsigma - z_0} = \exp(-i\theta) \tag{2.84}$$

where θ is the angle denoted in Fig.2.8. Thus, a Dirichlet smooth function $f(\varsigma)$, which may represent displacements or tractions on a circular boundary, can be expressed by infinite Fourier series as

$$f(\varsigma) = \sum_{-\infty}^{\infty} a_k g^{-k}(\varsigma) \tag{2.85}$$

Chapter 3

Linear viscoelastic analysis of a semi-infinite porous medium

3.1 Introduction

This chapter considers a problem of a semi-infinite, isotropic, linear viscoelastic half-plane containing multiple, non-overlapping circular voids. The problem is of practical importance in the area of mechanics of porous solids. It may also present interest in the area of fluid/gas related problems as time-dependent pore pressure induced by such substances can be directly taken into account by the method presented in the chapter. Besides, effects caused by the indentation processes can be studied due to the ability of the method to account for various loading conditions on the upper boundary of the semi-infinite medium.

Various numerical approaches are often used to solve the problems dealing with viscoelastic porous media. Among these approaches are the Finite Element and Boundary Element methods. The solution in the time domain can be obtained by adopting a time stepping algorithm or numerical Laplace transform. However, the accuracy of all such methods depend greatly on a number of parameters, such as quality of the mesh used for the discretization of a domain and its boundaries, size of a time step, etc. In addition, the Finite Element method cannot directly model an infinite or semi-infinite

domains. As a result, these methods are computationally intensive due to large number of degrees of freedom.

The review of different numerical approaches, used to solve time-dependent problems, can be found in [65]. The authors of the latter work considered the problem of an infinite viscoelastic plane containing multiple holes. A semi-analytical method used by Huang et al. [65] was initially proposed by Mogilevskaya and Crouch [102] for the problem of multiple elastic inhomogeneities located in an isotropic, elastic plane. The method is based on the solution of a system of complex hypersingular integral equations. As Huang et al. [65] considered the case of a viscoelastic solid, they employed the elastic-viscoelastic correspondence principle to obtain the solution for the corresponding elastic problem. Using the inverse Laplace transform, the authors were able to find the solution in the time domain.

In the present work, the method of Huang et al. [65] is extended to the problem of a semi-infinite, isotropic, linear viscoelastic half-plane containing multiple, non-overlapping circular holes. Constant or time dependent far-field stress acts parallel to the boundary of the half-plane and the boundaries of the holes are subjected to uniform pressure. Three types of loading conditions are assumed at the boundary of the half-plane: a point force, a force uniformly distributed over a segment, a force uniformly distributed over the whole boundary of the half-plane. The system of governing equations for the problem in the Laplace domain is more complicated than the system of equations from [65], as the current approach employs the corresponding Green's functions to simulate the conditions at the boundary of the half-plane. As a result this boundary is not involved in the system of governing equations. The method described in the chapter allows one to adopt a variety of viscoelastic models.

3.2 Problem formulation

Consider an isotropic linearly viscoelastic half-plane ($y \leq 0$) containing an arbitrary number N of non-overlapping, arbitrarily located circular holes, as shown in Fig.3.1. Three types of loading conditions are allowed at the surface $y = 0$ of the half-plane. These loads are: (i) a point force $F(t)$ applied at the point a, (ii) a force $F(t)$ uniformly distributed over the segment (a, b), (iii) a force $F(t)$ uniformly distributed over the whole boundary of the half-plane. Far-field stress $\sigma^{\infty}(t)$ acts parallel to the boundary of the half-plane. The boundary of each hole is assumed to be either traction free or subjected to uniform pressure $p_k(t)$, $k = 1, ..., N$. Let R_k, z_k, and L_k denote the radius, the center, and the boundary of the kth hole. The direction of travel is clockwise for all the boundaries L_k. The unit normal n points to the right of the direction of travel (i.e. inside the holes).

For practical applications it is sufficient to assume the following time-dependent behavior for the functions $p_k(t)$, $F(t)$ and $\sigma^{\infty}(t)$:

$$\begin{aligned} p_k(t) &= p_k \cdot f_p(t), \quad k = 1, ..., N \\ F(t) &= F \cdot f_F(t) \\ \sigma^{\infty}(t) &= \sigma^{\infty} \cdot f_{\infty}(t) \end{aligned} \tag{3.1}$$

where the constants p_k, σ^{∞} are real and the constant F is complex ($F = F_x + iF_y$, $i = \sqrt{-1}$). The first expression from (3.1) implies similar time-dependent behavior for all the functions $p_k(t)$, the second expression implies that the time-dependent behavior of the normal and tangential components of the surface loads is similar, and the third expression is added for the consistency.

The viscoelastic model is not specified at this point, as the method enables the adaptation of various models. The evolution of stresses, strains, and displacements in the viscoelastic half-plane is to be determined.

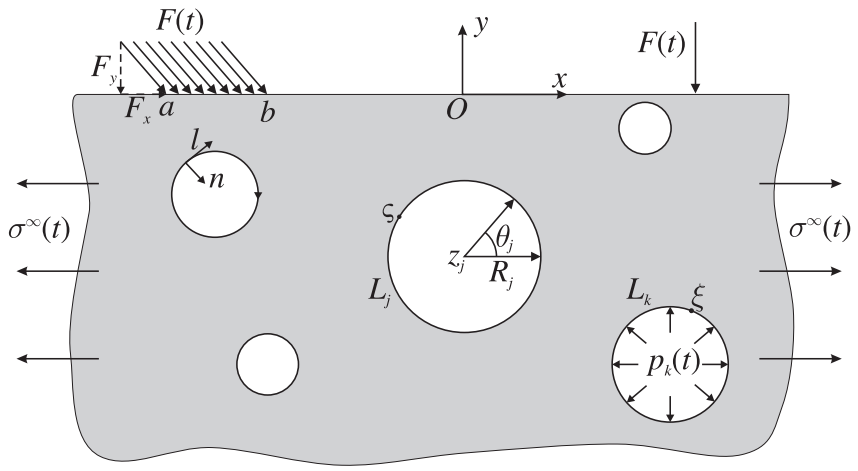

Figure 3.1: Problem formulation.

3.3 Basic equations

3.3.1 The system of boundary integral equations in the Laplace domain

The direct formulation of the complex boundary integral method for linear viscoelasticity [66] is employed for the treatment of the problem. The governing equations are obtained following the procedure outlined in Section 2.2. They represent the transformed Somigliana's traction identities written for each hole when the point z_F is allowed to approach its boundary (see Fig.2.8). In the case when the far-field stress and loads at the boundary of the half-plane are present, the superposition principle can be used to account for these loads. As the result the final system of N equations for the problem

in the Laplace domain can be written as

$$\sum_{j=1}^{N}\Bigg\{2\int_{L_j}\frac{\hat{u}_j(\varsigma;s)}{(\varsigma-\xi)^2}d\varsigma-\int_{L_j}\hat{u}_j(\varsigma;s)\frac{\partial^2}{\partial\varsigma\partial\xi}\left[K_1(\varsigma,\xi)+K_3(\varsigma,\xi)+K_4(\varsigma,\xi)\right]d\varsigma$$
$$-\int_{L_j}\overline{\hat{u}_j(\varsigma;s)}\frac{\partial^2}{\partial\bar{\varsigma}\partial\xi}\left[K_2(\varsigma,\xi)+K_5(\varsigma,\xi)+K_6(\varsigma,\xi)\right]d\bar{\varsigma}\Bigg\}=$$
$$-2\pi i\frac{\hat{\kappa}(s)+1}{4\hat{\mu}(s)}\left[\hat{p}_k(s)+\hat{\sigma}_k^{add}(\xi;s)\right]-\frac{1}{2\hat{\mu}(s)}\sum_{j=1}^{N}\hat{p}_j(s)\Bigg\{(\hat{\kappa}(s)-1)\int_{L_j}\frac{d\varsigma}{\varsigma-\xi} \tag{3.2}$$
$$+\int_{L_j}\frac{\partial}{\partial\xi}\left[\hat{\kappa}(s)K_1(\varsigma,\xi)+\hat{\kappa}(s)K_3(\varsigma,\xi)-K_4(\varsigma,\xi)\right]d\varsigma$$
$$-\int_{L_j}\frac{\partial}{\partial\xi}\left[K_2(\varsigma,\xi)+K_6(\varsigma,\xi)-\hat{\kappa}(s)K_5(\varsigma,\xi)\right]d\bar{\varsigma}\Bigg\},\qquad k=1,...,N$$

where $\xi=\xi_x+i\xi_y$ is the complex coordinate of a point $(\xi_x,\ \xi_y)$ on the contour L_k of the kth hole; $\varsigma=\varsigma_x+i\varsigma_y$ is the complex coordinate of a point $(\varsigma_x,\ \varsigma_y)$ on the contour L_j of the jth hole; $\hat{u}_j(\varsigma;s)=\hat{u}_{jx}(\varsigma;s)+i\hat{u}_{jy}(\varsigma;s)$ is the transformed complex displacement at the point ς; $\hat{\kappa}(s)$ is s-varying Kolosov-Muskhelishvili's parameter, $\hat{\kappa}(s)=3-4\hat{\nu}(s)$ for plane strain and $\hat{\kappa}(s)=(3-\hat{\nu}(s))/(1+\hat{\nu}(s))$ for plane stress ($\hat{\nu}(s)$ is the transformed Poisson's ratio); $\hat{\mu}(s)$ is s-varying analog of shear modulus[5] ; $\hat{p}_k(s)$ is the transformed pressure at the boundary of the kth hole; and a bar over a symbol denotes complex conjugation.

The kernels involved in system (3.2) are

$$\begin{aligned}
K_1(\varsigma,\xi)&=\ln\frac{\varsigma-\xi}{\bar{\varsigma}-\bar{\xi}} & K_2(\varsigma,\xi)&=\frac{\varsigma-\xi}{\bar{\varsigma}-\bar{\xi}}\\
K_3(\varsigma,\xi)&=\ln(\bar{\varsigma}-\xi) & K_4(\varsigma,\xi)&=\ln(\varsigma-\bar{\xi})+(\xi-\bar{\xi})\frac{\bar{\varsigma}-\varsigma}{(\varsigma-\bar{\xi})^2}\\
K_5(\varsigma,\xi)&=\frac{\xi-\bar{\xi}}{\varsigma-\bar{\xi}} & K_6(\varsigma,\xi)&=-\frac{\varsigma-\xi}{\bar{\varsigma}-\xi}
\end{aligned} \tag{3.3}$$

The function $\hat{\sigma}_k^{add}(\xi;s)$ in the right hand side of Eq.(3.2) is a complex function that represents the influence of transformed far-field stress $\hat{\sigma}^{\infty}(s)$ and transformed force

[5] It is assumed that the s-dependent elastic parameters (e.g. $\hat{\mu}(s)$, $\hat{\nu}(s)$) are known. They can be found by the application of the Laplace transform to the viscoelastic constitutive equations given in the differential or integral forms (see section 2.1.6).

$\hat{F}(s)$ applied at the boundary of the half-plane. Due to the superposition principle, the function $\hat{\sigma}_k^{add}(\xi;s)$ is expressed as follows:

$$\hat{\sigma}_k^{add}(\xi;s) = 2\hat{\sigma}_k^{\infty}(\xi;s) + \hat{\sigma}_k^{F}(\xi;s) \tag{3.4}$$

where $\hat{\sigma}_k^{\infty}(\xi;s)$ is the transformed traction on the trace of the boundary of the kth hole due to the far-field stress and $\hat{\sigma}_k^{F}(\xi;s)$ is the transformed traction at the same boundary due to the force at the boundary of the half-plane. Both terms in the right-hand side of Eq.(3.4) are obtained by using s-varying Kolosov-Muskhelishvili's potentials $\hat{\varphi}(s)$ and $\hat{\psi}(s)$, [108], and the transformed formula (2.68):

$$\hat{\sigma}(z;s) = \frac{\partial}{\partial z}\hat{\varphi}(z;s) + \overline{\frac{\partial}{\partial z}\hat{\varphi}(z;s)} + \frac{d\bar{z}}{dz}\left[z\overline{\frac{\partial^2}{\partial z^2}\hat{\varphi}(z;s)} + \overline{\frac{\partial}{\partial z}\hat{\psi}(z;s)}\right] \tag{3.5}$$

Kolosov-Muskhelishvili's potentials for the corresponding loadings are

i) For a far-field stress:

$$\begin{aligned}\hat{\Phi}^{\infty}(z;s) &= \frac{\partial}{\partial z}\hat{\varphi}^{\infty}(z;s) = \frac{\hat{\sigma}^{\infty}(s)}{4}\\ \hat{\Psi}^{\infty}(z;s) &= \frac{\partial}{\partial z}\hat{\psi}^{\infty}(z;s) = -\frac{\hat{\sigma}^{\infty}(s)}{2}\end{aligned} \tag{3.6}$$

ii) For a point force at the boundary of the half-plane (the Flamant's solution):

$$\begin{aligned}\hat{\Phi}^{F}(z;s) &= \frac{\partial}{\partial z}\hat{\varphi}^{F}(z;s) = -\frac{\hat{F}_x(s) + i\hat{F}_y(s)}{2\pi}\frac{1}{z-a}\\ \hat{\Psi}^{F}(z;s) &= \frac{\partial}{\partial z}\hat{\psi}^{F}(z;s) = \frac{\hat{F}_x(s) - i\hat{F}_y(s)}{2\pi}\frac{1}{z-a} - \frac{\hat{F}_x(s) + i\hat{F}_y(s)}{2\pi}\frac{\bar{a}}{(z-a)^2}\end{aligned} \tag{3.7}$$

where a is the point where the point force is applied, $\hat{F}_x(s)$ and $\hat{F}_y(s)$ are the transformed horizontal and vertical components of the point force, respectively.

iii) For a force uniformly distributed over the segment $(a,\ b)$:

$$\begin{aligned}\hat{\Phi}^{F}(z;s) &= \frac{\partial}{\partial z}\hat{\varphi}^{F}(z;s) = -\frac{\hat{F}_x(s) + i\hat{F}_y(s)}{2\pi}\int_a^b \frac{dw}{z-w}\\ \hat{\Psi}^{F}(z;s) &= \frac{\partial}{\partial z}\hat{\psi}^{F}(z;s) = \frac{\hat{F}_x(s) - i\hat{F}_y(s)}{2\pi}\int_a^b \frac{dw}{w-z} - \frac{\hat{F}_x(s) + i\hat{F}_y(s)}{2\pi}\int_a^b \frac{wdw}{(z-w)^2}\end{aligned} \tag{3.8}$$

where w is the dummy complex variable.

iv) For a uniform pressure over the whole boundary of the half-plane integrals in (3.8) have to be taken within the limits $(-\infty,\ \infty)$.

After the substitution of expressions (3.6) - (3.8) into formula (3.5), one obtains the expressions for the stress functions $\hat{\sigma}_k^{\infty}(\xi;s)$ and $\hat{\sigma}_k^{F}(\xi;s)$. As the results of this procedure expression (3.4) for $\hat{\sigma}_k^{add}(\xi;s)$ is found.

Note that due to the use of Melan's fundamental solution, the boundary of the half plane is not represented in governing system (3.2).

3.3.2 The viscoelastic analogs of Kolosov-Muskhelishvili's potentials

The transformed stress and displacement components at any point of the viscoelastic half-plane can be obtained using the following Kolosov-Muskhelishvili's formulae:

$$\begin{cases} 2\hat{\mu}(s)\hat{u}(z;s) = \hat{\kappa}(s)\hat{\varphi}(z;s) - z\overline{\dfrac{\partial}{\partial z}\hat{\varphi}(z;s)} - \overline{\hat{\psi}(z;s)} \\ \hat{\sigma}_{xx}(z;s) + \hat{\sigma}_{yy}(z;s) = 4\,\mathrm{Re}\left[\dfrac{\partial}{\partial z}\hat{\varphi}(z;s)\right] \\ \hat{\sigma}_{yy}(z;s) - \hat{\sigma}_{xx}(z;s) + 2i\hat{\sigma}_{xy}(z;s) = 2\left[\bar{z}\dfrac{\partial^2}{\partial z^2}\hat{\varphi}(z;s) + \dfrac{\partial}{\partial z}\hat{\psi}(z;s)\right] \end{cases} \tag{3.9}$$

The transformed strains are expressed through the transformed stresses as

$$\begin{cases} \hat{\varepsilon}_{xx}(s) + \hat{\varepsilon}_{yy}(s) = \dfrac{\hat{\kappa}(s)-1}{4\hat{\mu}(s)}\left(\hat{\sigma}_{xx}(s) + \hat{\sigma}_{yy}(s)\right) \\ \hat{\varepsilon}_{yy}(s) - \hat{\varepsilon}_{xx}(s) + 2i\hat{\varepsilon}_{xy}(s) = \dfrac{1}{2\hat{\mu}(s)}(\hat{\sigma}_{yy}(s) - \hat{\sigma}_{xx}(s) + 2i\hat{\sigma}_{xy}(s)) \end{cases} \tag{3.10}$$

These formulae represent the Laplace domain counterparts of expressions (2.65)-(2.67). Transformed potentials $\hat{\varphi}(z;s)$ and $\hat{\psi}(z;s)$ can be expressed as a superposition of solutions of Melan's and Flamant's problems. The solution for Melan's problem includes potentials for Kelvin's problem, and

$$\begin{aligned} \hat{\varphi}(z;s) &= \hat{\varphi}_{plane}(z;s) + \hat{\varphi}_{aux}(z;s) + \hat{\varphi}_F(z;s) \\ \hat{\psi}(z;s) &= \hat{\psi}_{plane}(z;s) + \hat{\psi}_{aux}(z;s) + \hat{\psi}_F(z;s) \end{aligned} \tag{3.11}$$

where $\hat{\varphi}_{plane}(z;s)$ and $\hat{\psi}_{plane}(z;s)$ are the potentials for the corresponding problem in a full plane (the Kelvin's solution) and $\hat{\varphi}_{aux}(z;s)$ and $\hat{\psi}_{aux}(z;s)$ are the additional potentials associated with the use of Green's functions specific for a half-plane problem (the Melan's solution). The latter can be obtained by the application of the Laplace transform to their elastic analogs given by Dejoie et al. [38]:

$$\begin{aligned}
\hat{\varphi}_{plane}(z;s) &= \frac{\hat{\mu}(s)}{\pi i(\hat{\kappa}(s)+1)}\sum_{j=1}^{N}\int_{L_j}\frac{\hat{u}_j(\varsigma;s)}{\varsigma-z}d\varsigma+\frac{\hat{\sigma}^{\infty}(s)}{4}z \\
\hat{\psi}_{plane}(z;s) &= -\frac{\hat{\mu}(s)}{\pi i(\hat{\kappa}(s)+1)}\sum_{j=1}^{N}\left\{-\frac{\hat{p}_j(s)}{2\hat{\mu}(s)}\left[\int_{L_j}\frac{\bar{\varsigma}d\varsigma}{\varsigma-z}+\hat{\kappa}(s)\int_{L_j}\ln(\varsigma-z)d\bar{\varsigma}\right]\right. \\
&\quad \left.+\int_{L_j}\frac{\overline{\hat{u}_j(\varsigma;s)}}{\varsigma-z}d\varsigma-\int_{L_j}\frac{\hat{u}_j(\varsigma;s)}{\varsigma-z}d\bar{\varsigma}+\int_{L_j}\frac{\hat{u}_j(\varsigma;s)\bar{\varsigma}}{(\varsigma-z)^2}d\varsigma\right\}-\frac{\hat{\sigma}^{\infty}(s)}{2}z
\end{aligned} \tag{3.12}$$

$$\begin{aligned}
\hat{\varphi}_{aux}(z;s) &= \frac{\hat{\mu}(s)}{\pi i(\hat{\kappa}(s)+1)}\sum_{j=1}^{N}\left\{\frac{\hat{p}_j(s)}{2\hat{\mu}(s)}\left[\hat{\kappa}(s)\int_{L_j}\ln(\bar{\varsigma}-z)d\varsigma+\int_{L_j}\frac{\varsigma-z}{\bar{\varsigma}-z}d\bar{\varsigma}\right]\right. \\
&\quad \left.-\int_{L_j}\frac{\hat{u}_j(\varsigma;s)}{\bar{\varsigma}-z}d\bar{\varsigma}+\int_{L_j}\overline{\hat{u}_j(\varsigma;s)}d\frac{\varsigma-z}{\bar{\varsigma}-z}\right\} \\
\hat{\psi}_{aux}(z;s) &= \frac{\hat{\mu}(s)}{\pi i(\hat{\kappa}(s)+1)}\sum_{j=1}^{N}\left\{-\frac{\hat{p}_j(s)}{2\hat{\mu}(s)}\left[-z\hat{\kappa}(s)\int_{L_j}\frac{d\varsigma}{\bar{\varsigma}-z}+z\int_{L_j}\frac{\varsigma-\bar{\varsigma}}{(\bar{\varsigma}-z)^2}d\bar{\varsigma}\right.\right. \\
&\quad \left.\left.-\int_{L_j}\ln(\bar{\varsigma}-z)d\bar{\varsigma}\right]-z\int_{L_j}\hat{u}_j(\varsigma;s)d\left(\frac{1}{\bar{\varsigma}-z}\right)\right. \\
&\quad \left.-z\int_{L_j}\overline{\hat{u}_j(\varsigma;s)}d\frac{\varsigma-\bar{\varsigma}}{(\bar{\varsigma}-z)^2}+\int_{L_j}\frac{\overline{\hat{u}_j(\varsigma;s)}}{\bar{\varsigma}-z}d\bar{\varsigma}\right\}
\end{aligned} \tag{3.13}$$

The expressions for the potentials $\hat{\varphi}_F(z;s)$ and $\hat{\psi}_F(z;s)$ are found by using the expressions (3.7) - (3.8). They are listed below for three types of loading at the boundary of the half-plane.

i) Point force:

$$\begin{aligned}
\hat{\varphi}_F(z;s) &= -\frac{\hat{F}(s)}{2\pi}\ln(z-a) \\
\hat{\psi}_F(z;s) &= \frac{\overline{\hat{F}(s)}}{2\pi}\ln(z-a)+\frac{\hat{F}(s)}{2\pi}\frac{\overline{a}}{z-a}
\end{aligned} \tag{3.14}$$

ii) Force uniformly distributed over the segment $(a,\ b)$ at the boundary:

$$\hat{\varphi}_F(z;s) = -\frac{\hat{F}(s)}{2\pi}\left[(b-z)\ln\frac{b-z}{a-z} - (b-a)\ln\frac{b-a}{a-z}\right] \tag{3.15}$$

$$\hat{\psi}_F(z;s) = \frac{\hat{F}(s)+\overline{\hat{F}(s)}}{2\pi}\left[(b-z)\ln\frac{b-z}{a-z} - (b-a)\ln\frac{b-a}{a-z}\right] + \frac{\hat{F}(s)}{2\pi}\left[a\ln(z-a) - b\ln(z-b)\right]$$

iii) Force uniformly distributed over the whole boundary:

$$\hat{\varphi}_F(z;s) = \frac{i}{2}z\overline{\hat{F}(s)} \tag{3.16}$$

$$\hat{\psi}_F(z;s) = \frac{i}{2}z\left(\hat{F}(s)+\overline{\hat{F}(s)}\right)$$

3.4 Numerical solution

3.4.1 Approximation of the transformed displacements

Upon the assumption that the unknown transformed displacements $\hat{u}_j(\varsigma;s)$ are smooth functions on each boundary L_j, they can be approximated by a truncated complex Fourier series as (see Section 2.3)

$$\hat{u}_j(\varsigma;s) = \sum_{m=-M_j}^{M_j}\hat{B}_{mj}(s)\exp(im\theta_j) = \sum_{m=-M_j}^{M_j}\hat{B}_{mj}(s)g_j^{-m}(\varsigma), \qquad \varsigma\in L_j,\ j=1,...,N \tag{3.17}$$

where θ_j is the angle between the axis Ox and the vector connecting the points z_j and ς (Fig.3.1); the function $g_j(\varsigma)$ is defined similarly to (2.83):

$$g_j(\varsigma) = \frac{R_j}{\varsigma - z_j} \tag{3.18}$$

Note that the number of Fourier coefficients is not necessarily the same for each hole and has to be determined in the process of numerical solution.

The unknown complex Fourier coefficients $\hat{B}_{mj}(s)$ are the functions of the Laplace transform parameter s only, and they do not depend on the space coordinates. After the

substitution of (3.17) into (3.2) the coefficients $\hat{B}_{mj}(s)$ can be taken outside of the space integrals. Thus, the integrals are the same as in the elastic case and, therefore, they can be evaluated analytically [38]. A similar procedure can be applied to the integrals involved in the expressions for the s-varying Kolosov-Muskhelishvili's potentials. For the sake of notational convenience, argument s is omitted in some lengthy expressions for the transformed quantities presented below.

3.4.2 Linear algebraic system

A system of linear algebraic equations can be obtained by using a Taylor series expansion method. According to this method all the functions $g_j^m(\xi)$ involved in the representations for the unknowns at the jth boundary can be re-expanded in terms of an infinite series of functions $g_k(\xi)$ as follows ([132]):

$$g_j^m(\xi) = g_j^m(z_k) \sum_{q=0}^{\infty} \begin{pmatrix} m+q-1 \\ q \end{pmatrix} g_k^q(z_j) g_k^{-q}(\xi), \quad \forall j \neq k \tag{3.19}$$

where the binomial coefficients $\binom{m}{n}$ are given by

$$\begin{pmatrix} m \\ n \end{pmatrix} = \frac{m!}{(m-n)!n!} \tag{3.20}$$

The functions $\overline{g_j(\xi)}$ can similarly be re-expanded in terms of functions $g_k(\xi)$ using the equation for a circle in the complex plane, from which it follows that

$$\overline{g_j(\xi)} = g_j^{-1}(\xi) \tag{3.21}$$

To reduce integral equations (3.2) to a linear system with the number of equations equal to the number of unknown coefficients $\hat{B}_{mk}$, one has to neglect the terms with powers $q > M_k$ and $q < -M_k$ in the Taylor series for every k, $k = 1, ..., N$. Using the resulting expressions for the functions $g_j(\xi)$ and $\overline{g_j(\xi)}$ and the orthogonality properties of the complex Fourier series, one can equate the coefficients in front of the terms with the

same powers of q in both sides of the final expressions. As a result one arrives at the system of $\sum_{k=1}^{N}(2M_k+1)$ complex linear equations in the Laplace domain:

$$\Upsilon_{kk,q}(\hat{B}_{mk}) + \sum_{\substack{j=1 \\ j\neq k}}^{N} \Upsilon_{kj,q}(\hat{B}_{mj}) =$$

$$= \begin{cases} -\dfrac{\hat{\kappa}+1}{4\hat{\mu}}\hat{\sigma}^{\infty} - \dfrac{1}{\hat{\mu}}\hat{p}_k - \dfrac{\hat{\kappa}+1}{4\hat{\mu}}\Omega_{k,0}(\hat{F}) + \dfrac{\hat{\kappa}-1}{2\hat{\mu}}\sum\limits_{j=1}^{N}\hat{p}_j\Xi_{kj,0} & \text{for } q=0 \\ -\dfrac{\hat{\kappa}+1}{4\hat{\mu}}\hat{\sigma}^{\infty} - \dfrac{\hat{\kappa}+1}{4\hat{\mu}}\Omega_{k,2}(\hat{F}) + \dfrac{\hat{\kappa}-1}{2\hat{\mu}}\sum\limits_{j=1}^{N}\hat{p}_j\Xi_{kj,2} & \text{for } q=2 \\ -\dfrac{\hat{\kappa}+1}{4\hat{\mu}}\Omega_{k,q}(\hat{F}) + \dfrac{\hat{\kappa}-1}{2\hat{\mu}}\sum\limits_{j=1}^{N}\hat{p}_j\Xi_{kj,q} & \forall\ q \text{ such that } -M_k \leq q \leq M_k,\ q\neq 1 \end{cases} \tag{3.22}$$

where $k = 1, ..., N$. The left-hand side (LHS) of (3.22) is the transformed analog of the LHS of the corresponding equations given in [38]. Due to some misprints in the referred paper, the corrected expressions for $\Upsilon_{kk,q}(\hat{B}_{mk})$ and $\Upsilon_{kj,q}(\hat{B}_{mj})$ are presented in Appendix B.1. The expressions for $\Xi_{kj,q}$ are given in Appendix B.2. The right-hand side (RHS) of (3.22) contains an additional term $\dfrac{\hat{\kappa}+1}{4\hat{\mu}}\Omega_{k,q}(\hat{F})$ as compared with the transformed RHS derived based on the expression given in [38]. This term is due to the influence of the force applied at the boundary of the half-plane, and it is given in Appendix B.3.

Separating the real and imaginary parts in the complex equations, one gets a system of linear real equations that can be written in a matrix form as

$$\underline{\underline{A}} \cdot \underline{\hat{B}}(s) = \underline{\hat{D}}_1(s) + \underline{\hat{D}}_2(s) + \underline{\hat{D}}_3(s) + \underline{\hat{D}}_4(s) \tag{3.23}$$

where the matrix of coefficients $\underline{\underline{A}}$, the vector of unknowns $\underline{\hat{B}}(s)$ and the vectors of RHS $\underline{\hat{D}}_i$ are

$$\underline{\underline{A}} = \begin{bmatrix} \underline{\underline{A}}_{11} & \underline{\underline{A}}_{12} & \cdots & \underline{\underline{A}}_{1N} \\ \underline{\underline{A}}_{21} & \underline{\underline{A}}_{22} & \cdots & \underline{\underline{A}}_{2N} \\ \vdots & \vdots & \ddots & \vdots \\ \underline{\underline{A}}_{N1} & \underline{\underline{A}}_{N2} & \cdots & \underline{\underline{A}}_{NN} \end{bmatrix} \tag{3.24}$$

$$\underline{\hat{B}}(s) = \begin{bmatrix} \underline{\hat{B}}_1(s) \\ \underline{\hat{B}}_2(s) \\ \vdots \\ \underline{\hat{B}}_N(s) \end{bmatrix}, \qquad \underline{\hat{D}}_i(s) = \begin{bmatrix} \underline{\hat{D}}_{i,1}(s) \\ \underline{\hat{D}}_{i,2}(s) \\ \vdots \\ \underline{\hat{D}}_{i,N}(s) \end{bmatrix}, \qquad i = 1, .., 4 \tag{3.25}$$

The submatrices $\underline{\underline{A}}_{kk}$ and $\underline{\underline{A}}_{kj}$ are deduced from the expressions given in Appendix B.1. As Eq.(3.22) degenerates when $q = 1$ (see App. B1-B3), and the equation for the term with $q = 0$ is real, the dimension of each submatrix $\underline{\underline{A}}_{kk}$ is $(4M_k - 1) \times (4M_k - 1)$, and the dimension of the submatrices $\underline{\underline{A}}_{kj}$ is $(4M_k - 1) \times (4M_j - 1)$. The submatrix $\underline{\underline{A}}_{kk}$ expresses the self-influence of the kth hole, and the submatrix $\underline{\underline{A}}_{kj}$ expresses the influence of the jth hole on the kth hole.

In Eq.(3.25), the subvectors $\underline{\hat{B}}_k$ are given by

$$\begin{aligned} \left[\underline{\hat{B}}_k\right] = \Big[&\mathrm{Re}\,\hat{B}_{-M_k k},\ \ \mathrm{Im}\,\hat{B}_{-M_k k}, ...,\ \ \mathrm{Re}\,\hat{B}_{-1k},\ \ \mathrm{Im}\,\hat{B}_{-1k}, \\ &\mathrm{Re}\,\hat{B}_{1k},\ \ \mathrm{Re}\,\hat{B}_{2k},\ \ \mathrm{Im}\,\hat{B}_{2k}, ...,\ \ \mathrm{Re}\,\hat{B}_{M_k k},\ \ \mathrm{Im}\,\hat{B}_{M_k k}\Big]^T \end{aligned} \tag{3.26}$$

The subvectors $\underline{\hat{D}}_{i,k}$ have similar structure. Note that the coefficients $\hat{B}_{0k}(s)$ and the imaginary part of $\hat{B}_{1k}(s)$ are not involved in (3.22), (3.26) as well as in the viscoelastic analogs of the Kolosov-Muskhelishvili's potentials (Eqs.(3.11-3.16)). These coefficients are responsible for the rigid body translation ($\hat{B}_{0k}$) and rotation ($\mathrm{Im}\,\hat{B}_{1k}$). They can be found from a procedure described in [132].

The number of Fourier coefficients $2M_k$ used to approximate the unknown displacements at the boundaries of the holes depend mostly on the geometry of the problem, but do not depend significantly on the material properties, which vary in time. This can be related to the fact that only small deformations are considered, and they do not cause changes in the geometry of the problem[6] . In the numerical simulations presented in Section 3.5, the number of Fourier coefficients $2M_k$ is found by solving system (3.22) for the parameter s corresponding to the time $t = 0$. Computations are performed initially for the number of terms $M_k = 2$, and then M_k is increased until a specified degree of

[6] Due to this assumption, the circular integration paths remain unchanged in time.

accuracy ϵ is achieved. In this work the degree of accuracy ϵ is defined as the maximum relative error between RHS and LHS of Eqs.(3.2). Details about the computation of the number of terms in the Fourier expansion are given in the works of Mogilevskaya and Crouch [102] and Dejoie et al. [38].

3.4.3 Solution in the Laplace domain

The transformed loads are obtained by applying the Laplace transform to expressions (3.1). They are as follows:

$$\begin{aligned} \hat{p}_k(s) &= p_k \cdot \hat{f}_p(s), \quad k = 1, ..., N \\ \hat{\sigma}^{\infty}(s) &= \sigma^{\infty} \cdot \hat{f}_{\infty}(s) \\ \hat{F}(s) &= F \cdot \hat{f}_F(s) \end{aligned} \tag{3.27}$$

Substitution of expressions (3.27) into system (3.22) allows one to represent the unknown coefficients $\hat{B}_{mk}$ ($m = -M_k, ..., M_k, \;\; k = 1, ..., N$) as the following combination (the underlining of vector and matrix quantities is omitted in the following expressions for notational convenience):

$$\begin{aligned} \hat{B}_{mk}(s) = \; & \underbrace{\frac{\hat{\kappa}(s)-1}{2\hat{\mu}(s)}\hat{f}_p(s)}_{\hat{\lambda}_1(s)} \cdot \underbrace{\left[A^{-1}\sum_{j=1}^{N} p_j \Xi_{kj,q}\right]}_{B^{(1)}_{mk}} + \underbrace{\frac{\hat{\kappa}(s)+1}{4\hat{\mu}(s)}\hat{f}_{\infty}(s)}_{\hat{\lambda}_2(s)} \cdot \underbrace{\left[-A^{-1}\sigma^{\infty}\right]}_{B^{(2)}_{mk}} + \\ & + \underbrace{\frac{\hat{f}_p(s)}{\hat{\mu}(s)}}_{\hat{\lambda}_3(s)} \cdot \underbrace{\left[-A^{-1}p_k\right]}_{B^{(3)}_{mk}} + \underbrace{\frac{\hat{\kappa}(s)+1}{4\hat{\mu}(s)}\hat{f}_F(s)}_{\hat{\lambda}_4(s)} \cdot \underbrace{\left[-A^{-1}\Omega_{k,q}(F)\right]}_{B^{(4)}_{mk}} = \sum_{l=1}^{4} \hat{\lambda}_l(s) B^{(l)}_{mk} \end{aligned} \tag{3.28}$$

where A^{-1} is the inverse of matrix A and $\Omega_{k,q}(F)$ depends on F in the same manner as $\Omega_{k,q}(\hat{F})$ depends on $\hat{F}$. Terms in the square brackets in Eq.(3.28) do not depend on the Laplace transform parameter s, and they can be found by solving the corresponding systems of linear equations. In this work the block Gauss-Seidel iterative algorithm is adopted to solve the systems of linear equations, as it provides good convergence rate

for the solution. Besides, matrix A can be calculated once only, as it depends only on geometric parameters of the problem.

After the substitution of expression (3.28) into the formulae for the s-varying Kolosov-Muskhelishvili's potentials (3.12)-(3.13) and using the latter to obtain the displacements and stresses from formula (3.9), one arrives at the following expressions:

$$\begin{aligned}\hat{u}(z;s) = {} & \frac{\hat{\kappa}}{2\hat{\mu}}\hat{f}_\infty \cdot \hat{H}_\infty(z) + \frac{\hat{\kappa}}{2\hat{\mu}}\frac{\hat{\kappa}-1}{\hat{\kappa}+1}\hat{f}_p \cdot H_p(z) + \frac{\hat{\kappa}}{\hat{\kappa}+1}\sum_{l=1}^{4}\hat{\lambda}_l H_l(z) + \frac{\hat{\kappa}}{2\hat{\mu}}\hat{f}_F \cdot H_F(z) \\ & - \frac{\hat{f}_\infty}{2\hat{\mu}} \cdot z\overline{H'_\infty(z)} - \frac{\hat{f}_p}{2\hat{\mu}}\frac{\hat{\kappa}-1}{\hat{\kappa}+1} \cdot z\overline{H'_p(z)} - \frac{1}{\hat{\kappa}+1}\sum_{l=1}^{4}\hat{\lambda}_l z\overline{H'_l(z)} - \frac{\hat{f}_F}{2\hat{\mu}} \cdot z\overline{H'_F(z)} \\ & - \frac{\hat{f}_\infty}{2\hat{\mu}} \cdot \overline{Q_\infty(z)} - \frac{\hat{f}_p}{2\hat{\mu}}\frac{\hat{\kappa}-1}{\hat{\kappa}+1} \cdot \overline{Q_p(z)} - \frac{1}{\hat{\kappa}+1}\sum_{l=1}^{4}\hat{\lambda}_l\overline{Q_l(z)} - \frac{\hat{f}_F}{2\hat{\mu}} \cdot \overline{Q_F(z)} \end{aligned} \tag{3.29}$$

The functions $H(z)$ and $Q(z)$ depend on the coordinates of the point z and the geometry of the problem only. Expressions for these functions are given in Appendix B.4. The derivatives in Eq.(3.29) are taken over the complex variable z.

Combinations of stress tensor components can be expressed as following:

$$\begin{aligned}\hat{\sigma}_{xx}(z;s) + \hat{\sigma}_{yy}(z;s) = {} & 4\,\mathrm{Re}\left\{\hat{f}_\infty \cdot H'_\infty(z) + \frac{\hat{\kappa}-1}{\hat{\kappa}+1}\hat{f}_p \cdot H'_p(z)\right. \\ & \left. + \frac{2\hat{\mu}}{\hat{\kappa}+1}\sum_{l=1}^{4}\hat{\lambda}_l H'_l(z) + \hat{f}_F \cdot H'_F(z)\right\} \end{aligned} \tag{3.30}$$

$$\begin{aligned}\hat{\sigma}_{yy}(z;s) - \hat{\sigma}_{xx}(z;s) + 2i\hat{\sigma}_{xy}(z;s) = {} & 2\left\{\frac{\hat{\kappa}-1}{\hat{\kappa}+1}\hat{f}_p \cdot \bar{z}H''_p(z) + \frac{2\hat{\mu}}{\hat{\kappa}+1}\sum_{l=1}^{4}\hat{\lambda}_l \bar{z}H''_l(z)\right. \\ & \left. + \hat{f}_F \cdot \bar{z}H''_F(z) + \hat{f}_\infty \cdot Q'_\infty(z) + \frac{\hat{\kappa}-1}{\hat{\kappa}+1}\hat{f}_p \cdot Q'_p(z) + \frac{2\hat{\mu}}{\hat{\kappa}+1}\sum_{l=1}^{4}\hat{\lambda}_l Q'_l(z) + \hat{f}_F \cdot Q'_F(z)\right\} \end{aligned}$$

In Eqs.(3.29) and (3.30) the terms dependent on the Laplace transform parameter s are separated from the terms that depend on the space coordinates. Therefore, it is possible to take the inverse Laplace transform of these expressions to obtain the solution

in the time domain. The s-dependent terms in Eqs.(3.29) and (3.30) are found as

$$\begin{aligned}
\hat{S}_1(s) &= \frac{\hat{\kappa}(s)}{2\hat{\mu}(s)}\hat{f}_\infty(s) & \hat{S}_2(s) &= \frac{\hat{\kappa}(s)}{2\hat{\mu}(s)}\frac{\hat{\kappa}(s)-1}{\hat{\kappa}(s)+1}\hat{f}_p(s)\\
\hat{S}_3(s) &= \frac{\hat{\kappa}(s)}{\hat{\mu}(s)}\frac{\hat{f}_p(s)}{\hat{\kappa}(s)+1} & \hat{S}_4(s) &= \frac{\hat{\kappa}(s)}{2\hat{\mu}(s)}\hat{f}_F(s)\\
\hat{S}_5(s) &= \frac{1}{2\hat{\mu}(s)}\hat{f}_\infty(s) & \hat{S}_6(s) &= \frac{1}{2\hat{\mu}(s)}\frac{\hat{\kappa}(s)-1}{\hat{\kappa}(s)+1}\hat{f}_p(s)\\
\hat{S}_7(s) &= \frac{1}{\hat{\mu}(s)}\frac{\hat{f}_p(s)}{\hat{\kappa}(s)+1} & \hat{S}_8(s) &= \frac{1}{2\hat{\mu}(s)}\hat{f}_F(s)\\
\hat{S}_9(s) &= \hat{f}_\infty(s) & \hat{S}_{10}(s) &= \frac{\hat{\kappa}(s)-1}{\hat{\kappa}(s)+1}\hat{f}_p(s)\\
\hat{S}_{11}(s) &= \frac{\hat{f}_p(s)}{\hat{\kappa}(s)+1} & \hat{S}_{12}(s) &= \hat{f}_F(s)
\end{aligned} \tag{3.31}$$

3.4.4 Solution in the time domain

The elastic fields in the time domain are found by the application of the analytical inverse Laplace transform to Eqs.(3.29) and (3.30). The final expressions are

$$\begin{aligned}
u(z;t) = {} & S_1(t)\left[H_\infty(z)+\frac{1}{2}H_2(z)\right] + S_2(t)\left[H_p(z)+H_1(z)\right] + S_3(t)H_3(z)\\
& + S_4(t)\left[\frac{1}{2}H_4(z)+H_F(z)\right] - S_5(t)\left[z\overline{H'_\infty(z)}+\frac{1}{2}z\overline{H'_2(z)}+\overline{Q_\infty(z)}+\frac{1}{2}\overline{Q_2(z)}\right]\\
& - S_6(t)\left[z\overline{H'_p(z)}+z\overline{H'_1(z)}+\overline{Q_p(z)}+\overline{Q_1(z)}\right] - S_7(t)\left[z\overline{H'_3(z)}+\overline{Q_3(z)}\right]\\
& - S_8(t)\left[\frac{1}{2}z\overline{H'_4(z)}+z\overline{H'_F(z)}+\frac{1}{2}\overline{Q_4(z)}+\overline{Q_F(z)}\right]
\end{aligned} \tag{3.32}$$

$$\begin{aligned}
\sigma_{xx}(z;s)+\sigma_{yy}(z;s) = {} & 4\,\mathrm{Re}\left\{S_9(t)\left[H'_\infty(z)+\frac{1}{2}H'_2(z)\right] + S_{10}(t)\left[H'_p(z)+H'_1(z)\right]\right.\\
& \left. +2S_{11}(t)H'_3(z) + S_{12}(t)\left[\frac{1}{2}H'_4(z)+H'_F(z)\right]\right\}\\
\sigma_{yy}(z;s)-\sigma_{xx}(z;s)+2i\sigma_{xy}(z;s) = {} & 2\left\{S_9(t)\left[\frac{1}{2}\bar{z}H''_2(z)+Q'_\infty(z)+\frac{1}{2}Q'_2(z)\right]\right.\\
& +S_{10}(t)\left[\bar{z}H''_p(z)+\bar{z}H''_1(z)+Q'_p(z)+Q'_1(z)\right] + 2S_{11}(t)\left[\bar{z}H''_3(z)+Q'_3(z)\right]\\
& \left. +S_{12}(t)\left[\frac{1}{2}\bar{z}H''_4(z)+\bar{z}H''_F(z)+\frac{1}{2}Q'_4(z)+Q'_F(z)\right]\right\}
\end{aligned} \tag{3.33}$$

where $S_n(t)$ $(n = 1, ..., 12)$ are the time domain counterparts of functions $\hat{S}_n(s)$. As the functions $H(z)$ and $Q(z)$ and their derivatives are independent of time, they are computed once only. After the calculation of the time-dependent functions $S_n(t)$ for every time instant one can compute the stresses and the displacements in the time domain. The expressions for time-varying strains can be obtained in similar manner using Eqs.(3.10).

An elaborate computer code was written in C++ programming language for conducting numerical simulations of viscoelastic fields in half- and full-plane containing multiple holes. For a brief overview of the code and the description of input data see Appendix E.

3.5 Examples

In the following numerical examples it is assumed that the viscoelastic material responds as a standard solid (Boltzmann model, Fig.2.4) in shear and elastically in bulk. This model is quite realistic as the shear modulus for many polymeric solids relaxes much more than the bulk modulus. As a result, the Poisson's ratio $\nu(t)$ is an increasing function of time for this material's behavior. The constitutive equations for the model in the Laplace domain are given by Eqs.(2.44)-(2.45), and s-dependent shear modulus and Kolosov-Muskhelishvili's parameter are expressed by Eqs.(2.47)-(2.50).

3.5.1 Examples for time-independent loading

This section considers a case of time-independent loading conditions. Far-field stress, pressure at the boundaries of the holes, and loads acting at the boundary of the half-plane are applied at the same time $t = 0$ and remain constant, such that

$$f_\infty(t) = H(t), \qquad f_p(t) = H(t), \qquad f_F(t) = H(t) \tag{3.34}$$

where $H(t)$ is Heaviside step function given by (2.3). The Laplace transform of functions (3.34) is

$$\hat{f}_\infty(s) = \frac{1}{s}, \qquad \hat{f}_p(s) = \frac{1}{s}, \qquad \hat{f}_F(s) = \frac{1}{s} \tag{3.35}$$

After the substitution of expressions (2.47), (2.50) and (3.35) into Eq.(3.31) and the application of the analytical inverse Laplace transform, the explicit expressions for the functions $S_n(t)$ are obtained (see Appendix B.5 for examples). Finally, the displacements and the stresses can be computed from expressions (3.32) and (3.33). However, as it was noticed by Huang et al. [65], stresses in any point of a viscoelastic porous medium do not depend on time if boundary tractions are constant in time (i.e. stresses do not depend on material properties). This means that stresses in viscoelastic case are exactly the same as the stresses in the corresponding "elastic" problem. For the case of a single hole in an infinite viscoelastic half-plane this can be shown explicitly, while for more complex geometries this fact can be ascertained numerically. This feature allows one to verify the results for the stresses obtained by the method developed here with the solutions for the corresponding elastic problems given elsewhere (e.g. [38]).

For the sake of simplicity, the following values for the material parameters are used for all the examples considered in the current chapter:

$$\begin{aligned} E_1 &= 8 \times 10^3 \sigma_0, \qquad & E_2 &= 2 \times 10^3 \sigma_0, \\ \eta &= 5 \times 10^3 \sigma_0 \cdot \sec, \qquad & K &= 17333.3 \sigma_0 \end{aligned} \tag{3.36}$$

The constant σ_0 serves to normalize all the loads and stresses. The definition of the constant σ_0 will be given for each numerical example.

It can be deduced from expressions (3.36) that the Poisson's ratio at zero time is $\nu(0) = 0.3$; the Poisson's ratio at infinite time is $\nu(\infty) \simeq 0.46$. These properties correlate well with the mechanical properties for polymethyl methacrylate [127].

Comparison with the results from the Finite Element (FE) method

Consider six holes of different sizes in a semi-infinite plane subjected to far-field stress $\sigma^{\infty} = \sigma_0$. The geometry of the problem and the boundary conditions are shown in Fig.3.2. A uniformly distributed load $F = -2\sigma_0$ is applied over the segment $(-0.2R_1,\ 2R_1)$ of the boundary of the half-plane. Note that the geometry of the problem does not posses any symmetry and all the boundary conditions are different (hole 1 is not pressurized).

The objective is to find displacements inside the half-plane by the presented method and compare them with the results obtained by the Finite Element method (FEM). For latter purpose, FEM software ANSYS® was used. Since ANSYS® can not directly model a semi-infinite area, all the calculations were performed using a large but finite rectangular domain of size $600R_1 \times 600R_1$. In order to achieve a relatively high degree of accuracy, 137676 quadrilateral 8-node elements were created with the ANSYS® mesh generator. The Prony series were adopted to approximate the relaxation of shear modulus, and a time stepping algorithm was applied to obtain the time domain solution. With 25 time steps the calculations took more than 6 hours on a standard PC (the configuration of used PC was: Intel® P4 3.6GHz/ 2Gb RAM).

The solution of the same problem was found by the present approach using the accuracy parameter $\epsilon = 10^{-4}$. Computations on the same PC took 70 seconds for several points of interest. The number of Fourier terms used for the approximations of the boundary displacements is given in Table 3.1.

To compare displacements and stresses obtained by both approaches it is necessary to introduce proper boundary conditions in the FE model. The vertical components of the displacements at all nodes of the lower boundary of the computational domain had to be constrained. In addition, both displacement components of the central node of the lower boundary of the domain were fixed. At the vertical boundaries of the domain tractions equal to those present at infinity were applied. This approach allows one to simulate the behavior of a semi-infinite plane subjected to a far field-stress and

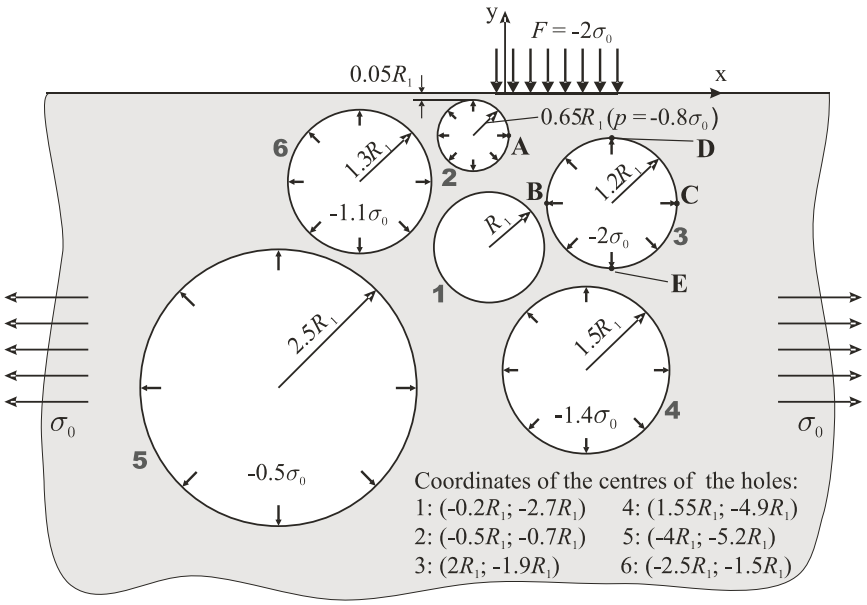

Figure 3.2: Geometry of the problem with 6 holes.

Table 3.1: Number of Fourier terms used in the approximation of displacements at the boundaries of the holes.

Hole	1	2	3	4	5	6
M_k	38	71	46	37	61	37

a variety of loadings at the boundary of the half-plane (one should expect that vertical displacement of any point located infinitely far from the boundary of the half-plane is zero).

In the present approach only the rigid body motion has to be constrained. This can be done if one assumes the displacements to be zero at one predefined point z_1, and the vertical component of the displacement to be zero at another predefined point z_2 located on the same horizontal line as the point z_1. To make sure that the procedures accounting for the rigid body motion in both methods are consistent, the following procedure was

conducted. The coordinates of the point z_1 were taken exactly the same as for the central node of the lower boundary of the domain used in the FE model. However, the point z_2 had to be located somewhere on the line, which represents the lower boundary of the domain in the FE model. The exact x-coordinate of this point was found by trial and error approach, so the best agreement between the results obtained by both methods was achieved.

By using these procedures, the displacements at several points in the half-plane have been compared. The horizontal and vertical components of the displacements at the point A (see Fig.3.2) are plotted in Fig.3.3. It can be seen that the results agree quite well.

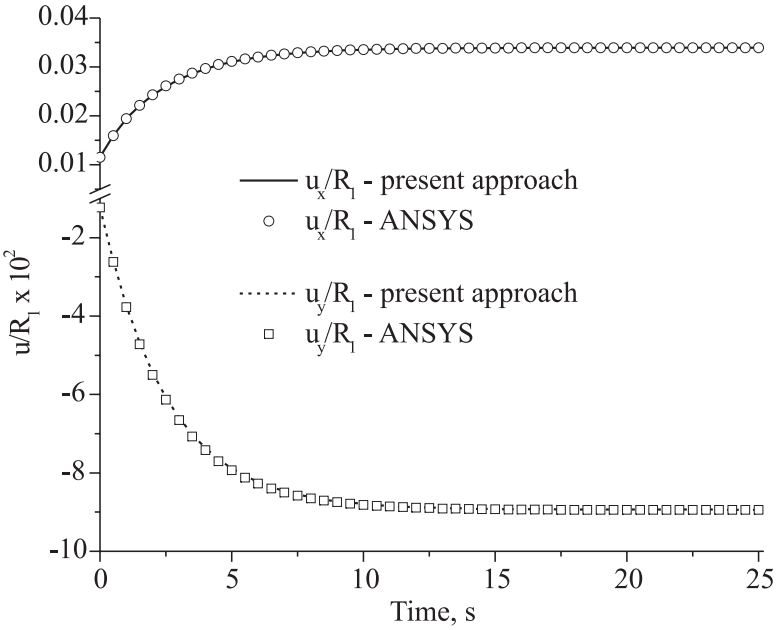

Figure 3.3: Evolution of displacement at the point A in Example 1.

Another way to compare the results is to consider the relative change of the length of a segment that connects two points in the half-plane. This approach does not require

fixing rigid body motion. For illustration purposes, the relative elongations of the diameter of hole 3 is presented below. The elongation in x and y directions is defined as follows:

$$\delta_x = \frac{u_x(C) - u_x(B)}{R_1}, \qquad \delta_y = \frac{u_y(E) - u_y(D)}{R_1} \tag{3.37}$$

The comparative results for δ_x and δ_y are given in Fig.3.4. The hole elongates in the x-direction more than in the y-direction, as should be expected. The results obtained by the presented method agree very well with the results obtained from the Finite Element method.

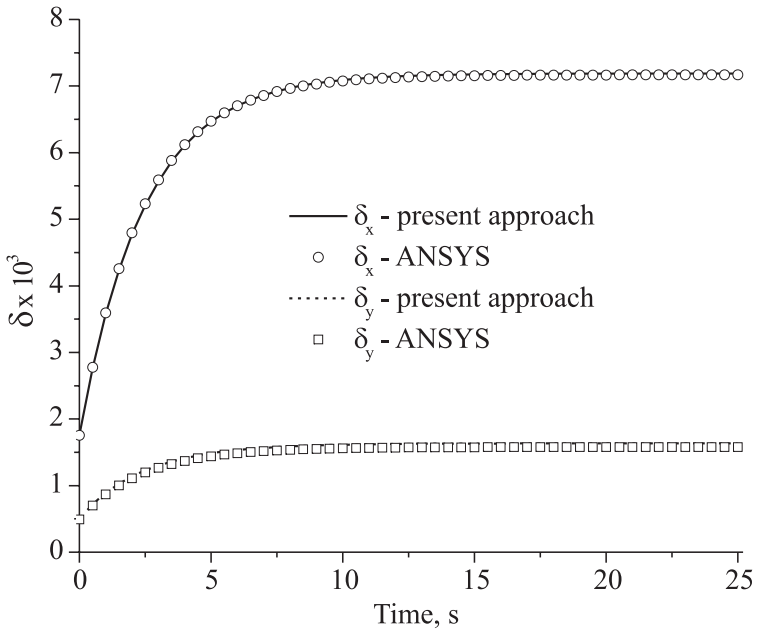

Figure 3.4: Evolution of the diameter of hole 3 in Example 1.

Examples with a single hole

This example considers a half-plane containing a single hole with traction free boundary. Four different loading conditions are assumed at the boundary of the half-plane, and a uniform far-field stress $\sigma^{\infty} = \sigma_0$ acts parallel to that boundary. The geometry of the problem and the loading conditions are shown in Fig.3.5(a,b) and Fig.3.6(a,b). The distribution of the hoop stress around the boundary of the hole is to be found as a function of the relative separation $\varepsilon = d/R$ between the hole and the boundary of the half-plane.

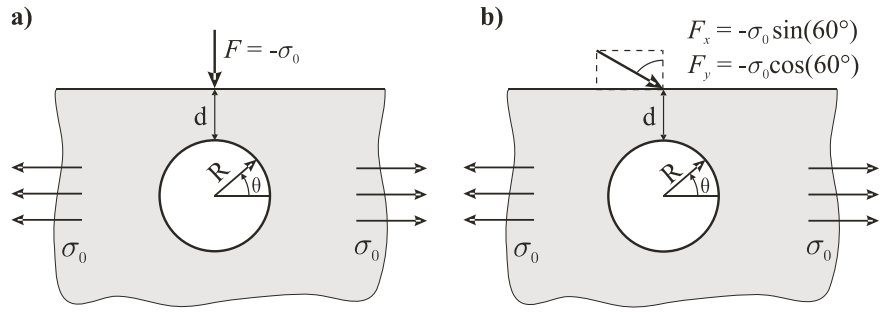

Figure 3.5: Geometry of the problem for Example 2: the case of a point force.

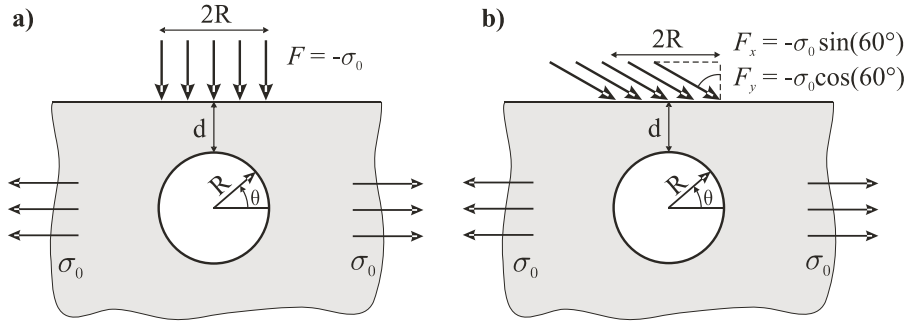

Figure 3.6: Geometry of the problem for Example 2: the case of a force distributed over a segment.

Table 3.2: Asymptotic behavior of the normalized hoop stresses for different geometries.

	Zero force (from [38])		a) Vertical Point Force			b) Inclined Point Force			
d/R	Max HS	M_1	Max HS	Min HS	M_1	Max HS	Min HS (left)	Min HS (right)	M_1
0.1	9.2270	39	49.9023	-22.147	133	31.195	-14.999	-7.113	150
0.05	12.8492	56	129.252	-60.297	277	75.209	-38.300	-21.273	299
0.01	28.3738	138	1355†	-657†	867	720‡	-372‡	-282‡	868
0.005	40.0633	200							
0.001	89.4708	403							

	c) Vertical Distributed Force			d) Inclined Distributed Force			
d/R	max HS	min HS	M_1	max HS	min HS (left)	min HS (right)	M_1
0.1	13.4306	-12.561	33	13.976	-10.517	-6.511	33
0.05	19.2663	-22.545	50	20.335	-18.797	-9.879	49
0.01	44.5445	-102.636	124	45.383	-72.683	-40.172	121
0.005	63.6442	-202.680	183	62.784	-132.997	-81.371	178
0.001	144.4630	-1002.76	440	131.609	-576.14	-440.506	430

† - to obtain these results the tolerance limit ϵ was relaxed to 0.03

‡ - to obtain these results the tolerance limit ϵ was relaxed to 0.09

Despite the fact the stresses in all four cases are exactly the same as for the corresponding elastic problems, the study is of interest as no results have been reported for the case when the upper boundary of a perforated half-plane is loaded with some tractions [7] . In the case of traction free boundary, Duan et al. [40] showed numerically that the asymptotic behavior of the maximum hoop stress is governed by $1/\sqrt{\varepsilon}$ singularity. This result was confirmed analytically by Callias and Markenscoff [21] and numerically by Dejoie et al. [38].

The number $2M_1$ of Fourier terms used in the present approach to achieve the solutions with the predefined accuracy $\epsilon = 10^{-4}$ is reported in Table 3.2. The notation "HS" in Table 3.2 stands for the hoop stress. Note that the tolerance limit had to be relaxed for the case of a point force for the relative separation $\varepsilon = 0.01$.

[7] Note that a concentrated force applied at the boundary of a half-plane containing no voids produces stresses that are singular at the point of application [9]. An inclined force distributed over a segment of the boundary of a half-plane produces locally infinite horizontal surface stresses at the end points of the segment [68], [121].

The plots of normalized hoop stresses for different values of ε are shown in Fig.3.7(a-d). One can notice the sharp increase in hoop stresses in the arc closer to the boundary of the half-plane. For all the cases, the hoop stress at the part of the boundary of the hole where $180^\circ \leq \theta \leq 360^\circ$ is virtually not affected by the change in the value of ε. For the case of a point force (Fig.3.7a,b), the amplitude of the minima of the hoop stress distribution are smaller than the amplitude of the main maximum. For the case of the distributed force (Fig.3.6), the amplitude of the minima are larger than the amplitude of the main maximum. For the cases of the inclined forces (Fig.3.5b and 3.6b), the amplitudes of the minima and main maximum become smaller than in all previous cases, and the distribution of the hoop stress becomes unsymmetrical relative to the angle 90°.

The results of numerical simulations has revealed that in the case of the point force shown in Fig.3.5a, the singularity $C/\varepsilon^{3/2}$, where $C \simeq 1.3577$, governs the asymptotic behavior of the maximum hoop stress. For the case of the force distributed over a segment (Fig.3.6a), the singularity $1/\varepsilon$ governs the asymptotic behavior of the minimum hoop stress. To obtain these results, numerical simulations were performed for the additional values of ε, however these results are not presented in Table 3.2.

Note that for the cases of inclined forces (Fig.3.5b and 3.6b), the singularities that govern the asymptotic behavior of the hoop stresses also depend on force inclination angle.

3.5.2 Time-dependent loading

Consider two examples with the same geometry but with different time-dependent loads applied at the boundary of the half-plane (Fig.3.8a and 3.8b). Both holes are subjected to uniform pressure (in expression (3.36) $\sigma_0 = -p_1$). Zero far-field stress is assumed. The time-dependent behavior of both loads is governed by the same harmonic law,

$$F = 5p_1 \left(1 + 0.9 \sin(\omega t)\right) \tag{3.38}$$

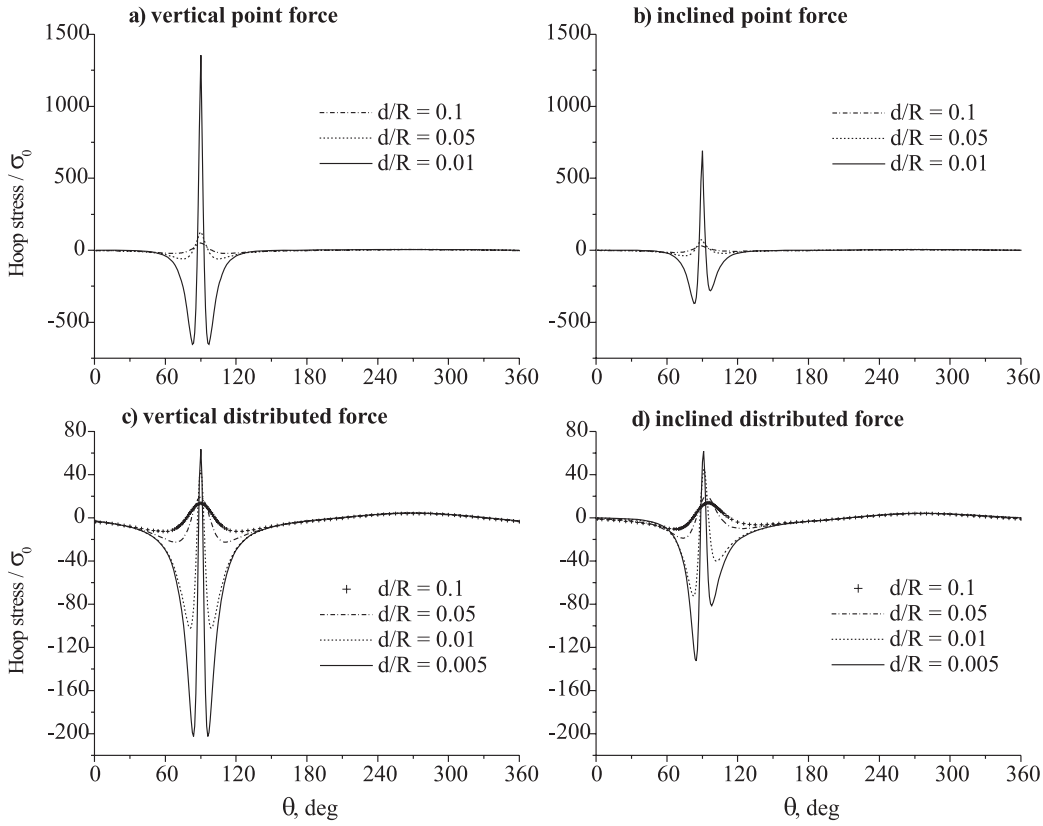

Figure 3.7: Normalized hoop stresses for different loads at the boundary of the half-plane.

where $\omega = 2\pi\nu$ is the circular frequency of the force variation, ν is the frequency, t is the time. Applying the Laplace transform to expression (3.38) one obtains three s-dependent functions $S_4(s)$, $S_8(s)$, $S_{12}(s)$. Their counterparts in the time domain are found according to the procedure described in Appendix B.5.

Both of the problems have been solved with the present approach. To achieve better accuracy the parameter ϵ was set to 10^{-5}. The number of terms in the Fourier series used to obtained the solutions with the predefined accuracy ϵ were $M_1 = 161$, $M_2 = 136$ (point force), $M_1 = 63$, $M_2 = 138$ (distributed force). It has been found

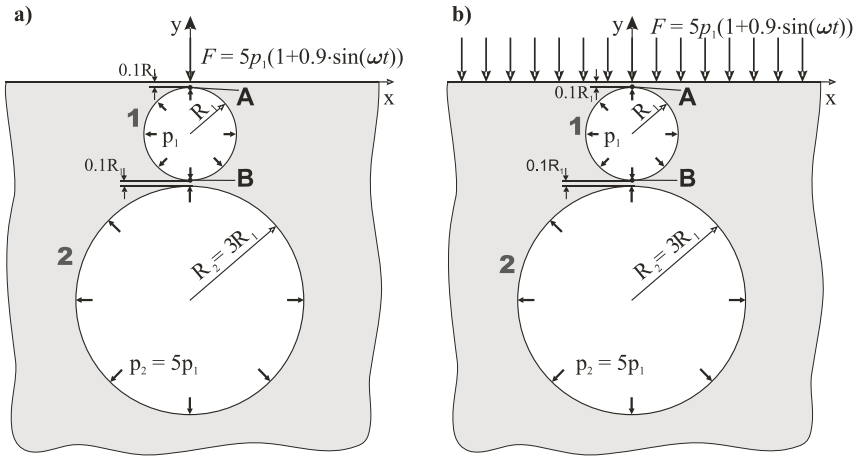

Figure 3.8: Geometry of the problem for example 3.

that the boundary stresses calculated by the present approach with $\epsilon = 10^{-5}$ agree with the prescribed boundary conditions for any moment of time. Next, the relative diameter elongation of the upper hole L_1 (Fig.3.8) was examined. The relative diameter elongation is given by

$$\delta_y = \frac{u_y(B) - u_y(A)}{R_1} \tag{3.39}$$

It is a well known fact that the amplitude of the steady-state vibrations of a point in a viscoelastic medium depends on the frequency of the force that excites the oscillations. The higher the frequency of the force, the lower the amplitude of the vibrations. This fact can be explained by that the viscous dashpot in the viscoelastic model does not respond instantaneously to the variation of the load. Therefore, the amplitude of the steady-state oscillations of the displacements depends on the ratio between the viscosity of the dashpot and the frequency of force variation.

The results presented in Fig.3.9 are in agreement with this conclusion. The plots shown in Fig.3.9 were obtained for the case of the point force applied at the boundary of the half-plane for two different frequencies: $\nu = 0.2$Hz and $\nu = 2$Hz. As it is expected,

the amplitude of the steady-state oscillations of δ_y is higher for the lower frequency. Similar results were obtained for other types of loads.

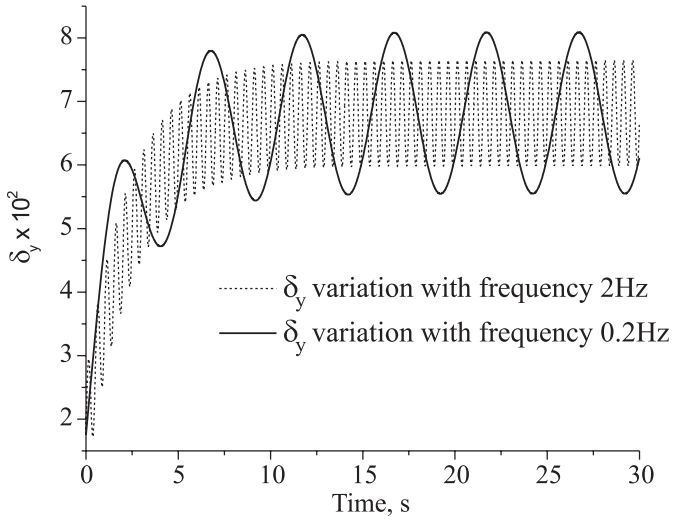

Figure 3.9: Variation of the diameter elongation of the upper hole for different frequencies of the point force applied at the boundary of the half-plane.

Figure 3.10 presents the results of simulations for the cases when a point force and a force distributed over the whole boundary of the half-plane are applied. Both forces vary in time by the same law given by Eq.(3.38), and the frequency of variations is $\nu = 0.2$Hz. However, it can be seen from Fig.3.10 that the steady-state oscillations of δ_y for these two cases are almost exactly in antiphase. As the amplitude of oscillations of δ_y for the case of the point force is larger than for the case of the force distributed over the whole boundary of the half-plane, the latter one is multiplied by 2.655 to make the visualization of the results easier.

In order to study this effect further, the size of the segment, undergoing uniform loading, was varied. It was found that when the size of the segment is smaller than two diameters of the bigger hole, the relative elongations δ_y due to the distributed force and due to the point force vary in phase. When the size of the segment is larger than

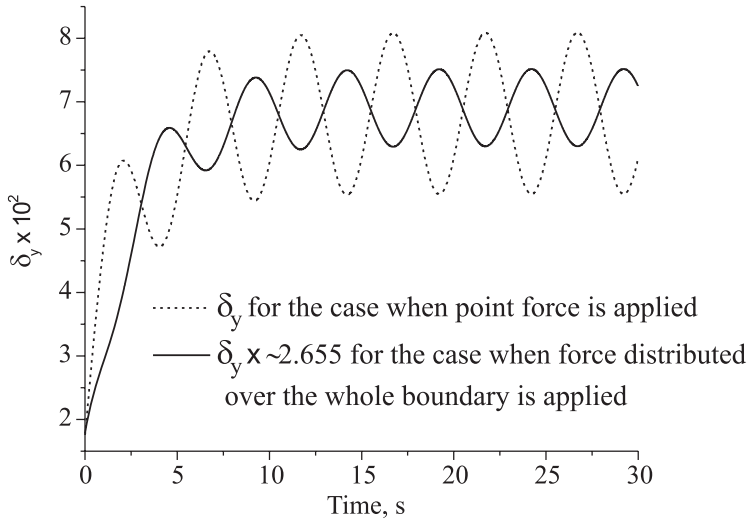

Figure 3.10: Variation of the diameter elongation of the upper hole for different types of forces applied at the boundary of the half-plane.

two diameters of the larger hole, the relative elongation δ_y corresponding to the case of the distributed force varies in antiphase in relation to the case of the point force. At the same time the amplitude of the steady-state oscillations of δ_y for the case of the distributed force is almost zero in the transition region. The results of numerical experiments for a single hole (the upper hole) show that there is no such effect for this case. Therefore, one can conclude that the effect is due to the interactions between the holes.

3.6 Summary

This chapter presents a semi-analytical method for solving the problem of a semi-infinite linear viscoelastic medium containing nonoverlapping circular holes. The semi-infinite medium is allowed to be subjected to different time-dependent loading conditions at its

boundary. Developed method is based on the use of the elastic-viscoelastic correspondence principle and the direct complex boundary integral approach.

The major advantage of the method is that all mathematical operations are performed analytically. Complex Fourier series provide very accurate approximations of boundary parameters, and the only error in the method comes from the truncation of these series. The method can adopt a variety of constitutive models, and it is capable of handling problems with a large number of holes. As a result, solutions for the various non-trivial problems of a porous linear viscoelastic media can be achieved with any desired degree of accuracy and with moderate computational cost. The present approach can provide a wide range of benchmark solutions.

A number of studies have revealed the capabilities of the method. For example, comparison with FEM results have showed that the present approach is more efficient for considered class of problems. The singularities that govern the asymptotic behavior of hoop stress have been found for the problem of a viscoelastic half-plane containing a single hole and subjected to different types of traction boundary conditions. An effect of antiphase oscillations of hole's size has been observed for the problem of a half-plane subjected to time dependent harmonic loads at its upper boundary.

Chapter 4

Viscoelastic state of a semi-infinite medium with multiple circular elastic inhomogeneities

4.1 Introduction

The problem of calculation of the detailed time-dependent fields in viscoelastic composite media is of practical importance in various engineering and scientific applications. A limited number of research works on this topic is available, which suggests that models describing the mechanical behavior of viscoelastic composites are still under the early development, and further study of such materials is needed.

Standard numerical methods, such as the Finite Element and the Boundary Element methods, can be used to solve the problems of viscoelastic media containing inhomogeneities. However, as denoted in the previous chapter, these methods are often computationally intensive and their accuracy depends on a number of parameters. There are few numerical methods custom designed to directly simulate the behavior of viscoelastic composite materials. The problem of an infinite, linear viscoelastic plane

containing multiple, non-overlapping, circular elastic inhomogeneities was considered by Huang et al. for the Kelvin [62] and Boltzmann viscoelastic models [63]. The numerical approach presented in these papers combines a direct boundary integral method, Fourier series approximations for the boundary unknowns, and a time-stepping algorithm. The method employed the assumption of time-independent viscoelastic Poisson's ratio. The same assumption was used by Zatula and Lavrenyuk [141] and Kaminskii et al. [70], who solved a system of boundary-temporal integral equations with the standard collocation Boundary Element method to model a viscoelastic half-plane containing elastic inhomogeneities of circular or rectangular shapes. The boundary conditions at the surface of the half-plane included a load distributed over a segment. Numerical results were presented for the case of two inhomogeneities only. Kaloerov and Mironenko [69] considered a linearly viscoelastic plate containing a row of aligned isotropic, elastic, elliptical inhomogeneities or cracks. The authors assumed that the bulk modulus of the plate is constant, while its Poisson's ratio at every moment in time t differs from the instantaneous value at $t = 0$ by a small parameter. Expanding the Kolosov-Muskhelishvili potentials for the problem in infinite series with respect to this parameter and equating the coefficients of the same powers of the parameter, the authors obtained a set of boundary conditions for the unknown functions. These functions themselves were represented by the infinite complex series. The coefficients in these series were determined by the least-squares method. The disadvantage of this technique is that the accuracy of this approach may depend on the choice of the small parameter.

The problem of an isotropic, linearly viscoelastic half-plane containing multiple, isotropic, circular elastic inhomogeneities is studied in the present chapter. Three types of loading conditions are allowed at the boundary of the half-plane; these loadings are the same as the ones considered in the previous chapter. The analysis employs the use of the elastic-viscoelastic correspondence principle based on the Laplace transform. The problem in the Laplace space is reduced to the complementary problems for (i) the bulk material of the perforated half-plane and (ii) the bulk material of each circular

disc. Each problem is described by the transformed complex Somigliana's traction identity. The transformed complex boundary parameters at each circular boundary are approximated by a truncated complex Fourier series. Numerical inversion of the Laplace transform is used to obtain the time domain solutions everywhere in the half-plane and inside the inhomogeneities. The method does not use the assumption of time-independent viscoelastic Poisson's ratio and allows one to adopt a variety of viscoelastic models. A method described in the present chapter is an extension of the previous work (see Chapter 3), where the problem of an isotropic, linearly viscoelastic half-plane containing multiple holes was considered. The inversion of the Laplace transform in the latter problem could be performed analytically, which is not the case for more general problem considered here.

4.2 Problem formulation

Consider an isotropic, linearly viscoelastic half-plane ($y \leq 0$) containing an arbitrary number N of non-overlapping, arbitrarily located, circular, isotropic elastic inhomogeneities, as shown in Fig.4.1a. The elastic properties of the inhomogeneities (shear moduli μ_k and Poisson's ratios ν_k, $k = 1, \ldots, N$) are assumed to be arbitrary. A hole is treated as a particular case of an inhomogeneity with zero elastic properties. Let R_k, z_k, and L_k denote the radius, the center, and the boundary of the kth inhomogeneity.

Three types of loading conditions are allowed at the surface $y = 0$ of the half-plane. These loads are: (i) a point force $F(t)$ applied at the point a, (ii) a force $F(t)$ uniformly distributed over the segment (a, b), (iii) a force $F(t)$ uniformly distributed over the whole boundary of the half-plane. Far-field stress $\sigma^{\infty}(t)$ acts parallel to the boundary of the half-plane. Perfect bond is assumed between each inhomogeneity and the bulk material of the half-plane. In case of a hole, its boundary is assumed to be either traction free or subjected to uniform pressure $p_k(t)$, $k = 1, ..., N_h$ (N_h is the number of holes). For practical applications it is sufficient to assume that the magnitude of loads $p_k(t)$, $F(t)$

and $\sigma^{\infty}(t)$ is constant and it can be separated from the time-dependent part as given by expressions (3.1).

The viscoelastic model is not specified at this point, as the method enables the adaptation of various models. The evolution of stresses, strains, and displacements in the viscoelastic half-plane and inside of the inhomogeneities are to be determined.

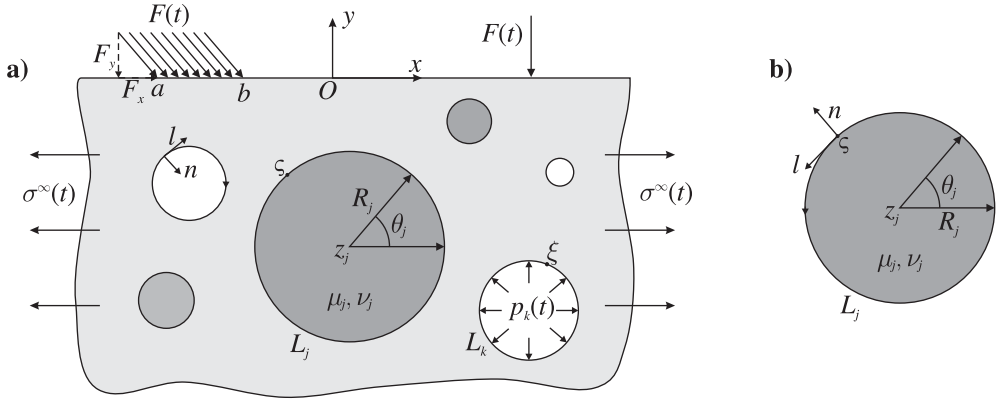

Figure 4.1: Geometry of the problem with multiple inhomogeneities.

4.3 Basic equations

The problem considered here can be decomposed into $N_d = N - N_h$ problems for each elastic disc and a complementary problem for the half-plane containing N cavities. The problems are interrelated by the condition of the perfect bond between the matrix and the discs. The analysis is based on the use of the elastic-viscoelastic correspondence principle (see Section 2.1.6).

4.3.1 The system of boundary integral equations in the Laplace domain

The system of governing equations is obtained by using the direct boundary integral method outlined in Section 2.2. The analysis uses the complex variable Somigliana's traction identities in the Laplace domain [66]. The system of governing equations includes the following equations:

I) The viscoelastic analog of Somigliana's traction identity at the boundary of the kth disc, $k = 1, ..., N_d$,

$$
\begin{aligned}
2\pi i \frac{\kappa_k + 1}{4\mu_k} \hat{\sigma}_k^d(\xi; s) = {} & \frac{1 - \kappa_k}{2\mu_k} \int_{L_k} \hat{\sigma}_k^d(\varsigma; s) \frac{d\varsigma}{\varsigma - \xi} - \frac{\kappa_k}{2\mu_k} \int_{L_k} \hat{\sigma}_k^d(\varsigma; s) \frac{\partial}{\partial \xi} K_1(\varsigma, \xi) d\varsigma \\
& + \frac{1}{2\mu_k} \int_{L_k} \overline{\hat{\sigma}_k^d(\varsigma; s)} \frac{\partial}{\partial \xi} K_2(\varsigma, \xi) d\overline{\varsigma} + 2 \int_{L_k} \frac{\hat{u}_k^d(\varsigma; s)}{(\varsigma - \xi)^2} d\varsigma \\
& - \int_{L_k} \hat{u}_k^d(\varsigma; s) \frac{\partial^2}{\partial \varsigma \partial \xi} K_1(\varsigma, \xi) d\varsigma - \int_{L_k} \overline{\hat{u}_k^d(\varsigma; s)} \frac{\partial^2}{\partial \overline{\varsigma} \partial \xi} K_2(\varsigma, \xi) d\overline{\varsigma}
\end{aligned}
\tag{4.1}
$$

where $\xi = \xi_x + i\xi_y$, $\varsigma = \varsigma_x + i\varsigma_y$ are complex coordinates of the points $(\xi_x,\ \xi_y) \in L_k$ and $(\varsigma_x,\ \varsigma_y) \in L_k$; $\hat{\sigma}_k^d(\varsigma; s) = \hat{\sigma}_{kn}^d(\varsigma; s) + i\hat{\sigma}_{kl}^d(\varsigma; s)$ is the unknown transformed complex traction at the point ς in a local coordinate system shown in Fig.4.1b; $\hat{u}_k^d(\varsigma; s) = \hat{u}_{kx}^d(\varsigma; s) + i\hat{u}_{ky}^d(\varsigma; s)$ is the unknown transformed complex displacement at the point ς in a global coordinate system; κ_k is the Kolosov-Muskhelishvili's parameter for kth disc, $\kappa_k = 3 - 4\nu_k$ for plane strain and $\kappa_k = (3 - \nu_k)/(1 + \nu_k)$ for plane stress. The direction of travel is counterclockwise for the boundary L_k.

The two kernels K_1 and K_2 in Eq.(4.1) corresponding to the Kelvin fundamental solution are given by expressions (3.3).

II) The viscoelastic analog of Somigliana's traction identity at the boundary of the kth cavity located in the viscoelastic half-plane, $k = 1, ..., N$,

$$\sum_{j=1}^{N}\left\{2\int_{L_j}\frac{\hat{u}_j^h(\varsigma;s)}{(\varsigma-\xi)^2}d\varsigma-\int_{L_j}\hat{u}_j^h(\varsigma;s)\frac{\partial^2}{\partial\varsigma\partial\xi}\left[K_1(\varsigma,\xi)+K_3(\varsigma,\xi)+K_4(\varsigma,\xi)\right]d\varsigma\right.$$
$$\left.-\int_{L_j}\overline{\hat{u}_j^h(\varsigma;s)}\frac{\partial^2}{\partial\overline{\varsigma}\partial\xi}\left[K_2(\varsigma,\xi)+K_5(\varsigma,\xi)+K_6(\varsigma,\xi)\right]d\overline{\varsigma}\right\}$$
$$-\pi i\frac{\hat{\kappa}(s)+1}{2\hat{\mu}(s)}\hat{\sigma}_k^h(\xi;s)-\frac{1}{2\hat{\mu}(s)}\sum_{j=1}^{N}\left\{(\hat{\kappa}(s)-1)\int_{L_j}\frac{\hat{\sigma}_j^h(\varsigma;s)}{\varsigma-\xi}d\varsigma\right. \tag{4.2}$$
$$+\int_{L_j}\hat{\sigma}_j^h(\varsigma;s)\frac{\partial}{\partial\xi}\left[\hat{\kappa}(s)K_1(\varsigma,\xi)+\hat{\kappa}(s)K_3(\varsigma,\xi)-K_4(\varsigma,\xi)\right]d\varsigma$$
$$\left.-\int_{L_j}\overline{\hat{\sigma}_j^h(\varsigma;s)}\frac{\partial}{\partial\xi}\left[K_2(\varsigma,\xi)+K_6(\varsigma,\xi)-\hat{\kappa}(s)K_5(\varsigma,\xi)\right]d\overline{\varsigma}\right\}$$
$$=-2\pi i\frac{\hat{\kappa}(s)+1}{4\hat{\mu}(s)}\hat{\sigma}_k^{add}(\xi;s)$$

where $\hat{u}_j^h(\varsigma;s)=\hat{u}_{jx}^h(\varsigma;s)+i\hat{u}_{jy}^h(\varsigma;s)$ is the unknown transformed complex displacement at the point $\varsigma\in L_j$; $\hat{\sigma}_j^h(\varsigma;s)=\hat{\sigma}_{jn}^h(\varsigma;s)+i\hat{\sigma}_{jl}^h(\varsigma;s)$ is the unknown transformed complex traction at the point $\varsigma\in L_j$ in a local coordinate system shown in Fig.4.1a; $\hat{\kappa}(s)$ and $\hat{\mu}(s)$ are the transformed Kolosov-Muskhelishvili's parameter and the shear modulus of the bulk material of the half-plane respectively. The direction of travel is clockwise for the boundary L_j.

In addition to the kernels K_1 and K_2, the kernels K_3 - K_6 (see Eqs.(3.3)) associated with the Melan's fundamental solution are involved in system (4.2). Due to the use of the Melan's fundamental solution, the boundary of the half-plane is not involved in governing system (4.2).

The function $\hat{\sigma}_k^{add}(\xi;s)$ in the right-hand side of Eq.(4.2) is a complex function that represents the combined influence of the transformed far-field stress $\hat{\sigma}^{\infty}(s)$ and transformed force $\hat{F}(s)$ applied at the boundary of the half-plane. It is given by expression (3.4), where $k=1,...,N$. Both terms in the right-hand side of Eq.(3.4) are obtained by using s-varying Kolosov-Muskhelishvili's potentials $\hat{\varphi}(\xi;s)$ and $\hat{\psi}(\xi;s)$, [108], and formula (3.5). The potentials $\hat{\varphi}$ and $\hat{\psi}$ for the far-field stress and the load applied at

the boundary of the half-plane are provided in Chapter 3.

Equations (4.1) and (4.2) are complemented by the following boundary conditions. For the case when the kth inhomogeneity is a hole, the traction $\hat{\sigma}_k^h(\xi;s)$ in Eq.(4.2) is

$$\hat{\sigma}_k^h(\xi;s) = \hat{p}_k(s), \quad \xi \in L_k \tag{4.3}$$

For the case when the kth inhomogeneity is an elastic disc, the conditions of the perfect bond are

$$\begin{aligned} \hat{u}_k^h(\xi;s) = \hat{u}_k^d(\xi;s) = \hat{u}_k(\xi;s), \quad \xi \in L_k \\ \hat{\sigma}_k^h(\xi;s) = \hat{\sigma}_k^d(\xi;s) = \hat{\sigma}_k(\xi;s), \quad \xi \in L_k \end{aligned} \tag{4.4}$$

4.3.2 Calculation of the s-dependent fields in the composite system

The transformed stresses and displacements at any point of the viscoelastic half-plane and inside of the elastic discs are obtained using the transformed analogs of Kolosov-Muskhelishvili's formulae given by Eqs.(3.9). The transformed strains can be found from (3.10). Corresponding sets of material properties for the inhomogeneities and the matrix should be used in these expressions for the evaluation of viscoelastic fields. Potentials involved in Eqs.(3.9) are as follows:

a) Potentials for the kth elastic disc ($\hat{\mu}(s) = \mu_k$ *and* $\hat{\kappa}(s) = \kappa_k$)

$$\begin{aligned} \hat{\varphi}_k(z;s) &= -\frac{1}{2\pi i(\kappa_k+1)}\left[\int_{L_k}\hat{\sigma}_k^d(\varsigma;s)\ln(\varsigma-z)d\varsigma - 2\mu_k\int_{L_k}\frac{\hat{u}_k(\varsigma;s)}{\varsigma-z}d\varsigma\right] \\ \hat{\psi}_k(z;s) &= -\frac{1}{2\pi i(\kappa_k+1)}\left\{\left[\int_{L_k}\hat{\sigma}_k^d(\varsigma;s)\frac{\overline{\varsigma}d\varsigma}{\varsigma-z} + \kappa_k\int_{L_k}\overline{\hat{\sigma}_k^d(\varsigma;s)}\ln(\varsigma-z)d\overline{\varsigma}\right]\right. \\ &\left. +2\mu_k\left[\int_{L_k}\frac{\overline{\hat{u}_k(\varsigma;s)}}{\varsigma-z}d\varsigma - \int_{L_k}\frac{\hat{u}_k(\varsigma;s)}{\varsigma-z}d\overline{\varsigma} + \int_{L_k}\frac{\hat{u}_k(\varsigma;s)\overline{\varsigma}}{(\varsigma-z)^2}d\varsigma\right]\right\} \end{aligned} \tag{4.5}$$

Expressions (4.5) were found by applying the Laplace transform to the corresponding elastic potentials given in [104].

b) Potentials for the bulk material of the viscoelastic half-plane

$$\hat{\varphi}(z;s) = \hat{\varphi}_{plane}(z;s) + \hat{\varphi}_{aux}(z;s) + \hat{\varphi}_F(z;s) \tag{4.6}$$
$$\hat{\psi}(z;s) = \hat{\psi}_{plane}(z;s) + \hat{\psi}_{aux}(z;s) + \hat{\psi}_F(z;s)$$

where $\hat{\varphi}_{plane}(z;s)$ and $\hat{\psi}_{plane}(z;s)$ are the potentials due to the Kelvin's fundamental solution and $\hat{\varphi}_{aux}(z;s)$ and $\hat{\psi}_{aux}(z;s)$ are additional potentials associated with the use of Green's functions specific for a half-plane problem. The potentials $\hat{\varphi}_F(z;s)$ and $\hat{\psi}_F(z;s)$ are given in Chapter 3, and the rest of the potentials are obtained by applying the Laplace transform to their elastic analogs given in [101]:

$$\begin{aligned}
\hat{\varphi}_{plane}(z;s) &= -\frac{1}{2\pi i(\hat{\kappa}+1)}\sum_{j=1}^{N}\left[\int_{L_j}\hat{\sigma}_j^h(\varsigma)\ln(\varsigma-z)d\varsigma - 2\hat{\mu}(s)\int_{L_j}\frac{\hat{u}_j(\varsigma)}{\varsigma-z}d\varsigma\right] + \frac{\hat{\sigma}^{\infty}}{4}z \\
\hat{\psi}_{plane}(z;s) &= -\frac{1}{2\pi i(\hat{\kappa}+1)}\sum_{j=1}^{N}\left\{\left[\int_{L_j}\hat{\sigma}_j^h(\varsigma)\frac{\overline{\varsigma}d\varsigma}{\varsigma-z} + \hat{\kappa}\int_{L_j}\overline{\hat{\sigma}_j^h(\varsigma)}\ln(\varsigma-z)d\overline{\varsigma}\right]\right. \\
&\quad \left. +2\hat{\mu}\left[\int_{L_j}\frac{\overline{\hat{u}_j(\varsigma)}}{\varsigma-z}d\varsigma - \int_{L_j}\frac{\hat{u}_j(\varsigma)}{\varsigma-z}d\overline{\varsigma} + \int_{L_j}\frac{\hat{u}_j(\varsigma)\overline{\varsigma}}{(\varsigma-z)^2}d\varsigma\right]\right\} - \frac{\hat{\sigma}^{\infty}}{2}z
\end{aligned} \tag{4.7}$$

$$\begin{aligned}
\hat{\varphi}_{aux}(z;s) &= -\frac{1}{2\pi i(\hat{\kappa}+1)}\sum_{j=1}^{N}\left\{\left[\hat{\kappa}\int_{L_j}\hat{\sigma}_j^h(\varsigma)\ln(\overline{\varsigma}-z)d\varsigma + \int_{L_j}\overline{\hat{\sigma}_j^h(\varsigma)}\frac{\varsigma-z}{\overline{\varsigma}-z}d\overline{\varsigma}\right]\right. \\
&\quad \left. +2\hat{\mu}\left[\int_{L_j}\frac{\hat{u}_j(\varsigma)}{\overline{\varsigma}-z}d\overline{\varsigma} - \int_{L_j}\overline{\hat{u}_j(\varsigma)}d\frac{\varsigma-z}{\overline{\varsigma}-z}\right]\right\} \\
\hat{\psi}_{aux}(z;s) &= -\frac{1}{2\pi i(\hat{\kappa}+1)}\sum_{j=1}^{N}\left\{z\left[\hat{\kappa}\int_{L_j}\hat{\sigma}_j^h(\varsigma)\frac{d\varsigma}{\overline{\varsigma}-z} - \int_{L_j}\overline{\hat{\sigma}_j^h(\varsigma)}\frac{\partial}{\partial z}\frac{\varsigma-z}{\overline{\varsigma}-z}d\overline{\varsigma}\right.\right. \\
&\quad \left. +2\hat{\mu}\left(\int_{L_j}\overline{\hat{u}_j(\varsigma)}d\frac{\partial}{\partial z}\frac{\varsigma-z}{\overline{\varsigma}-z} - \int_{L_j}\hat{u}_j(\varsigma)\frac{d\overline{\varsigma}}{(\overline{\varsigma}-z)^2}\right)\right] \\
&\quad \left. + \int_{L_j}\overline{\hat{\sigma}_j^h(\varsigma)}\ln(\overline{\varsigma}-z)d\overline{\varsigma} - 2\hat{\mu}\int_{L_j}\frac{\overline{\hat{u}_j(\varsigma)}}{\overline{\varsigma}-z}d\overline{\varsigma}\right\}
\end{aligned} \tag{4.8}$$

4.4 Numerical solution

4.4.1 Fourier series approximation of the unknowns at the boundaries

The unknown transformed stresses $\hat{\sigma}_k(\varsigma; s)$ at each boundary L_k are approximated by the following truncated complex Fourier series:

$$\hat{\sigma}_k(\varsigma; s) = \sum_{m=1}^{M_k} \hat{T}_{-mk}(s) g_k^m(\varsigma) + \hat{T}_{0k}(s) + \sum_{m=1}^{M_k} \hat{T}_{mk}(s) g_k^{-m}(\varsigma), \quad \varsigma \in L_k,\ k = 1, ..., N_d \tag{4.9}$$

where the function $g_k(\varsigma)$ is defined by (3.16).

The unknown transformed displacements $\hat{u}_k(\varsigma; s)$ at the boundary L_k are represented by the following series:

$$\hat{u}_k(\varsigma; s) = \sum_{m=1}^{M_k-1} \hat{B}_{-mk}(s) g_k^m(\varsigma) + \hat{B}_{0k}(s) + \sum_{m=1}^{M_k+1} \hat{B}_{mk}(s) g_k^{-m}(\varsigma), \quad \varsigma \in L_k,\ k = 1, ..., N \tag{4.10}$$

Note that the Fourier series in Eq.(4.10) are truncated differently from series representation (4.9) and (3.15). The reason for this is explained in [104].

4.4.2 System of complex algebraic equations

After substituting (4.9) and (4.10) into Somigliana's traction identity (4.1) and following the procedure similar to the one described in [104] for the elastic case, one arrives at the following expressions:

$$\begin{aligned} \hat{T}_{-1k}(s) &= 0 \\ \frac{\kappa_k - 1}{2\mu_k} \hat{T}_{0k}(s) &= \frac{2}{R_k} \operatorname{Re} \hat{B}_{1k}(s) \\ \frac{1}{2\mu_k} \hat{T}_{-mk}(s) &= \frac{m-1}{R_k} \hat{B}_{-(m-1)k}(s), \quad m \geq 2 \\ \frac{\kappa_k}{2\mu_k} \hat{T}_{mk}(s) &= \frac{m+1}{R_k} \hat{B}_{(m+1)k}(s), \quad m \geq 1 \end{aligned} \tag{4.11}$$

Expansion (4.9) with the use of (4.11) can now be rewritten as

$$\hat{\sigma}_k(\varsigma;s) = \frac{2\mu_k}{R_k}\left[\sum_{m=1}^{M_k-1} m\hat{B}_{-mk}(s)g_k^{m+1}(\varsigma)\right. \tag{4.12}$$
$$\left.+\frac{2}{\kappa_k-1}\,\mathrm{Re}\,\hat{B}_{1k}(s)+\frac{1}{\kappa_k}\sum_{m=2}^{M_k+1} m\hat{B}_{mk}(s)g_k^{1-m}(\varsigma)\right], \quad k=1,...,N_d$$

After the substitution of expressions (4.10) and (4.12) into Somigliana's traction identity (4.2), s-dependent Fourier coefficients $\hat{B}_{mk}(s)$ can be taken out from the integrals, and all the space integrals can be evaluated analytically. As a result, one arrives at the following system of complex algebraic equations:

$$\begin{cases} \hat{\Lambda}_{kk}(\xi;s)+\sum\limits_{\substack{j=1\\ j\neq k}}^{N_h}\hat{\Lambda}_{kj}(\xi;s)+\sum\limits_{r=N_h+1}^{N}\hat{\Pi}_{kr}(\xi;s)= \\ \quad =-\dfrac{\hat{\kappa}+1}{4\hat{\mu}}\left(\hat{p}_k+\hat{\sigma}_k^{add}(\xi;s)\right)+\sum\limits_{j=1}^{N_h}\hat{p}_j\hat{\Gamma}_j(\xi;s), \quad \xi\in L_k, \quad k=1,...,N_h \\ \sum\limits_{j=1}^{N_h}\hat{\Lambda}_{lj}(\xi;s)+\left[\hat{G}_{ll}(\xi;s)-\dfrac{\hat{\kappa}+1}{2\hat{\mu}}\hat{\sigma}_l(\xi;s)\right]+\sum\limits_{\substack{r=N_h+1\\ r\neq l}}^{N}\hat{\Pi}_{lr}(\xi;s)= \\ \quad =-\dfrac{\hat{\kappa}+1}{4\hat{\mu}}\hat{\sigma}_l^{add}(\xi;s)+\sum\limits_{j=1}^{N_h}\hat{p}_j\hat{\Gamma}_j(\xi;s), \quad \xi\in L_l, \quad l=N_h+1,...,N \end{cases} \tag{4.13}$$

The left-hand side of Eqs.(4.13) contains the unknown displacements at the boundaries of the cavities, while the right-hand side contains the known boundary tractions only. The following operators are involved in system (4.13):

- operators $\hat{\Lambda}_{kj}(\xi;s)$ $(k,j=1,...,N_h)$ obtained after the evaluation of the integrals in Eq.(4.2) containing the unknown Fourier coefficients over the boundaries of the holes;

- operators $\hat{\Pi}_{kj}(\xi;s)$ $(k,j=N_h,...,N)$ obtained after the evaluation of the integrals in Eq.(4.2) containing the unknown Fourier coefficients over the boundaries of those cavities that later are occupied by the elastic discs;

- operators $\hat{\Gamma}_j(\xi;s)$ $(j=1,...,N_h)$ obtained after the evaluation of the integrals in Eq.(4.2) containing the known tractions $\hat{p}_j$ over the boundaries of the holes ($\hat{p}_j$ is factored out in (4.13)).

Coefficients $\hat{B}_{0k}(s)$ and the imaginary part of $\hat{B}_{1k}(s)$ are not involved in the system of governing equations (4.13). These coefficients are responsible for the rigid body translation (B_{0k}) and rotation ($\mathrm{Im}\, B_{1k}$) and can be found from a procedure described in [132].

The expressions for the operators $\hat{\Lambda}_{\alpha\beta}$ and $\hat{\Gamma}_j$ can be obtained by applying the Laplace transform to the corresponding expressions used in [38]. Operators $\hat{\Pi}_{\alpha\beta}$ differ from the expressions for $\hat{\Lambda}_{\alpha\beta}$ by additional s-dependent multipliers in front of the unknown coefficients $\hat{B}_{-mk}(s)$, $\mathrm{Re}\,\hat{B}_{1k}(s)$, and $\hat{B}_{mk}(s)$ $(m=-(M_k-1),...,M_k+1,\ k=N_h+1,...,N$; see Appendix C.1). These multipliers are as follows:

$$\begin{aligned}
\hat{\alpha}_{1k} &= -\left(\frac{\mu_k}{\hat{\mu}}-1\right) && \text{in front of } \hat{B}_{-mk}(s)\\
\hat{\alpha}_{2k} &= -\left(\frac{\mu_k}{\kappa_k-1}\frac{\hat{\kappa}-1}{\hat{\mu}}-1\right) && \text{in front of } \ \mathrm{Re}\,\hat{B}_{1k}(s)\\
\hat{\alpha}_{3k} &= -\left(\frac{\mu_k}{\kappa_k}\frac{\hat{\kappa}}{\hat{\mu}}-1\right) && \text{in front of } \hat{B}_{mk}(s)
\end{aligned} \tag{4.14}$$

4.4.3 System of real linear algebraic equations

The Taylor series expansion method (the so-called addition theorem) described in [132] can be used to obtain a system of linear algebraic equations from expressions (4.13). According to this method all the functions $g_j^q(\xi)$ and $\overline{g_j^q(\xi)}$ involved in the representations for the unknowns at the jth boundary can be re-expanded in terms of an infinite series of functions $g_k(\xi)$ as given by expressions (3.19)-(3.21). As a result, all the operators $\hat{\Lambda}_{\alpha\beta}$ and $\hat{\Pi}_{\alpha\beta}$ at the left-hand side of (4.13) are expressed through the functions $g_k^q(\xi)$. Similarly, the operators $\hat{\Gamma}_j$ at the right-hand side of (4.13) can be expressed through the same functions. Using the orthogonality properties of the complex Fourier series, one can equate the coefficients in front of the terms $g_k^q(\xi)$ with the same powers in both

sides of the obtained expressions. A finite system of linear equations with the number of equations equal to the number of unknown coefficients $\hat{B}_{mk}$, $k = 1, ..., N$, is obtained if one neglects the terms with powers $q > M_k$ and $q < -M_k$ in the Taylor series for every k.

As a result, one arrives at the system of $\sum_{k=1}^{N}(2M_k + 1)$ complex linear equations in the Laplace domain ($k = 1, ..., N$):

$$\hat{\Upsilon}_{kk,q}(\hat{\mathbb{B}}_{mk}) + \sum_{\substack{j=1 \\ j\neq k}}^{N} \hat{\Upsilon}_{kj,q}(\hat{\mathbb{B}}_{mj}) + \Delta_k \cdot \hat{\Im}_k(\hat{\mathbb{B}}_{qk}) =$$

$$= \begin{cases} -\dfrac{\hat{\kappa}+1}{4\hat{\mu}}\hat{\sigma}^{\infty} - \dfrac{1-\Delta_k}{\hat{\mu}}\hat{p}_k - \dfrac{\hat{\kappa}+1}{4\hat{\mu}}\Omega_{k,0}(\hat{F}) + \dfrac{\hat{\kappa}-1}{2\hat{\mu}}\sum\limits_{j=1}^{N_h}\hat{p}_j\Xi_{kj,0} & \text{for } q = 0 \\ -\dfrac{\hat{\kappa}+1}{4\hat{\mu}}\hat{\sigma}^{\infty} - \dfrac{\hat{\kappa}+1}{4\hat{\mu}}\Omega_{k,2}(\hat{F}) + \dfrac{\hat{\kappa}-1}{2\hat{\mu}}\sum\limits_{j=1}^{N_h}\hat{p}_j\Xi_{kj,2} & \text{for } q = 2 \\ -\dfrac{\hat{\kappa}+1}{4\hat{\mu}}\Omega_{k,q}(\hat{F}) + \dfrac{\hat{\kappa}-1}{2\hat{\mu}}\sum\limits_{j=1}^{N_h}\hat{p}_j\Xi_{kj,q} & \forall\ q \text{ such that } -M_k \le q \le M_k,\ q \neq 1 \end{cases} \tag{4.15}$$

where

$$\hat{\Im}_k(\hat{\mathbb{B}}_{qk}) = \frac{\hat{\kappa}+1}{\hat{\mu}}\frac{\mu_k}{R_k} \cdot \begin{cases} \dfrac{1-q}{\hat{\alpha}_{3k}\kappa_k}\hat{\mathbb{B}}_{(1-q)k}\ , & \text{if } q \le -1 \\ \dfrac{2}{\hat{\alpha}_{2k}(\kappa_k - 1)}\operatorname{Re}\hat{\mathbb{B}}_{1k}\ , & \text{if } q = 0 \\ \dfrac{q-1}{\hat{\alpha}_{1k}}\hat{\mathbb{B}}_{(1-q)k}\ , & \text{if } q \ge 2 \end{cases} \tag{4.16}$$

and the function Δ_k is

$$\begin{aligned} &\Delta_k = 0 \text{ if } L_k \text{ is the boundary of a hole} \\ &\Delta_k = 1 \text{ if } L_k \text{ is the boundary of a cavity occupied by an elastic disc} \end{aligned} \tag{4.17}$$

In general, the coefficients $\hat{\mathbb{B}}_{mk}$ are different from the coefficients $\hat{B}_{mk}$ as they may include the multipliers given by Eq.(4.14). Operators $\hat{\Upsilon}_{kk,q}$, $\hat{\Upsilon}_{kj,q}$, $\Omega_{k,q}$, and $\Xi_{kj,q}$ can be found in Appendices B.1-B.3, where one should take into account the specific way of truncation of Fourier series in the present approach. One can see that (4.15) resembles the system (3.22) with the exception that additional terms Δ_k and $\hat{\Im}_k(\hat{\mathbb{B}}_{qk})$ are present.

Separating the real and imaginary parts in complex equations (4.15) and taking into account that Eq.(4.15) is real for $q = 0$, one arrives at a linear system of $\sum_{k=1}^{N}(4M_k - 1)$ equations. The resulting system of linear equations can be written in matrix form as follows:

$$\left[\underline{\underline{A}} + \underline{\underline{\hat{W}}}(s)\right] \cdot \hat{\mathbb{B}}(s) = \hat{\underline{D}}(s) \tag{4.18}$$

where s-independent matrix $\underline{\underline{A}}$ is

$$\underline{\underline{A}} = \left[\begin{array}{ccc|ccc} \overbrace{\quad\quad\quad}^{\text{block 1}} & & & \overbrace{\quad\quad\quad\quad\quad}^{\text{block 2}} & & \\ \underline{\underline{A}}_{11} & \cdots & \underline{\underline{A}}_{1N_h} & \underline{\underline{A}}_{1(N_h+1)} & \cdots & \underline{\underline{A}}_{1(N_h+N_d)} \\ \vdots & \ddots & \vdots & \vdots & \ddots & \vdots \\ \underline{\underline{A}}_{N_h1} & \cdots & \underline{\underline{A}}_{N_hN_h} & \underline{\underline{A}}_{N_h(N_h+1)} & \cdots & \underline{\underline{A}}_{N_h(N_h+N_d)} \\ \hline \underline{\underline{A}}_{(N_h+1)1} & \cdots & \underline{\underline{A}}_{1N_h} & \underline{\underline{A}}_{(N_h+1)(N_h+1)} & \cdots & \underline{\underline{A}}_{(N_h+1)(N_h+N_d)} \\ \vdots & \ddots & \vdots & \vdots & \ddots & \vdots \\ \underbrace{\underline{\underline{A}}_{(N_h+N_d)1}}_{\text{block 3}} & \cdots & \underline{\underline{A}}_{(N_h+N_d)N_h} & \underbrace{\underline{\underline{A}}_{(N_h+N_d)(N_h+N_d)}}_{\text{block 4}} & \cdots & \underline{\underline{A}}_{(N_h+N_d)(N_h+N_d)} \end{array}\right] \tag{4.19}$$

Matrix $\underline{\underline{A}}$ consists of the following blocks:

- block 1 represents the influence of a hole on another hole,
- block 2 - the influence of a hole on a cavity occupied by an elastic disc,
- block 3 - the influence of a cavity occupied by an elastic disc on a hole,
- block 4 - the influence of a cavity occupied by an elastic disc on another cavity occupied by an elastic disc.

The expressions for submatrices $\underline{\underline{A}}_{jk}$ are similar to those obtained in the previous chapter. The matrix $\underline{\underline{\hat{W}}}(s)$ is deduced from the expression for the operator $\hat{\Im}_k$. This

matrix is largely sparse and it has the following form

$$\underline{\underline{\hat{W}}}(s) = \left[\begin{array}{ccc|ccc} \mathbf{0} & ... & \mathbf{0} & \mathbf{0} & ... & \mathbf{0} \\ \vdots & \ddots & \vdots & \vdots & \ddots & \vdots \\ \mathbf{0} & ... & \mathbf{0} & \mathbf{0} & ... & \mathbf{0} \\ \hline \mathbf{0} & ... & \mathbf{0} & \underline{\underline{\hat{W}}}_{(N_h+1)(N_h+1)} & ... & \mathbf{0} \\ \vdots & \ddots & \vdots & \vdots & \ddots & \vdots \\ \mathbf{0} & ... & \mathbf{0} & \mathbf{0} & ... & \underline{\underline{\hat{W}}}_{NN} \end{array}\right] \tag{4.20}$$

where the only non-zero submatrices $\underline{\underline{\hat{W}}}_{kk}(s)$ are of the dimension $(4M_k-1)\times(4M_k-1)$, $k = N_h+1, ..., N$. They have the following form

$$\underline{\underline{\hat{W}}}_{kk}(s) = -\frac{\hat{\kappa}+1}{\hat{\mu}}\frac{\mu_k}{R_k}\cdot \overset{\overset{m=-(M_k-1)}{\longrightarrow} \qquad\qquad \overset{m=M_k+1}{}}{\left[\begin{array}{c|c|c} \frac{q-1}{\alpha_{1k}} & \mathbf{0} & \mathbf{0} \\ \hline \mathbf{0} & \frac{2}{\alpha_{2k}(\kappa_k-1)} & \mathbf{0} \\ \hline \mathbf{0} & \mathbf{0} & \frac{q+1}{\alpha_{3k}\kappa_k} \end{array}\right]} \begin{array}{l} q=M_k \\ \downarrow \\ q=-M_k \end{array} \tag{4.21}$$

The vector of unknowns $\underline{\hat{\mathbb{B}}}(s)$ is given by

$$\underline{\hat{\mathbb{B}}}(s) = \left[\begin{array}{c} \underline{\hat{\mathbb{B}}}_1(s) \\ \vdots \\ \underline{\hat{\mathbb{B}}}_{N_h}(s) \\ \underline{\hat{\mathbb{B}}}_{N_h+1}(s) \\ \vdots \\ \underline{\hat{\mathbb{B}}}_N(s) \end{array}\right] \tag{4.22}$$

and subvectors $\hat{\underline{\mathbb{B}}}_k(s)$ are defined as

$$\hat{\underline{\mathbb{B}}}_k(s) = \hat{\underline{B}}_k(s) = \begin{bmatrix} \operatorname{Re}\hat{B}_{-(M_k-1)k} \\ \operatorname{Im}\hat{B}_{-(M_k-1)k} \\ \vdots \\ \operatorname{Re}\hat{B}_{-1k} \\ \operatorname{Im}\hat{B}_{-1k} \\ \operatorname{Re}\hat{B}_{1k} \\ \operatorname{Re}\hat{B}_{2k} \\ \operatorname{Im}\hat{B}_{2k} \\ \vdots \\ \operatorname{Re}\hat{B}_{(M_k+1)k} \\ \operatorname{Im}\hat{B}_{(M_k+1)k} \end{bmatrix} \qquad \hat{\underline{\mathbb{B}}}_j(s) = \begin{bmatrix} \hat{\alpha}_{1j} \cdot \operatorname{Re}\hat{B}_{-(M_j-1)j} \\ \hat{\alpha}_{1j} \cdot \operatorname{Im}\hat{B}_{-(M_j-1)j} \\ \vdots \\ \hat{\alpha}_{1j} \cdot \operatorname{Re}\hat{B}_{-1j} \\ \hat{\alpha}_{1j} \cdot \operatorname{Im}\hat{B}_{-1j} \\ \hat{\alpha}_{2j} \cdot \operatorname{Re}\hat{B}_{1j} \\ \hat{\alpha}_{3j} \cdot \operatorname{Re}\hat{B}_{2j} \\ \hat{\alpha}_{3j} \cdot \operatorname{Im}\hat{B}_{2j} \\ \vdots \\ \hat{\alpha}_{3j} \cdot \operatorname{Re}\hat{B}_{(M_j+1)j} \\ \hat{\alpha}_{3j} \cdot \operatorname{Im}\hat{B}_{(M_j+1)j} \end{bmatrix} \tag{4.23}$$

$$k = 1, ..., N_h \qquad j = N_h + 1, ..., N$$

The vector of the right-hand side in Eq.(4.18) can be deduced from the expressions for operators $\Omega_{k,q}$ and $\Xi_{kj,q}$ given in Appendices B.2-B.3. It contains N subvectors consisting of $4M_k - 1,\ k = 1, ..., N$, elements and its transpose

$$\left[\hat{\underline{D}}(s)\right]^T = \left[\hat{\underline{D}}_1(s), \hat{\underline{D}}_2(s), ..., \hat{\underline{D}}_{N_h}(s), \hat{\underline{D}}_{N_h+1}(s), ..., \hat{\underline{D}}_N(s)\right] \tag{4.24}$$

4.4.4 Solution in the time domain

An algorithm of the numerical inversion of the Laplace transform

After the solution of system (4.18), the potentials involved in expressions (3.9) and (3.10) can be written in terms of s-dependent coefficients. Thus, the transformed fields can be expressed explicitly via the coefficients. To obtain the viscoelastic fields in the time domain, one needs to apply the inverse Laplace transform to s-dependent terms involved in the transformed fields.

In general case, system (4.18) can not be solved analytically as its both sides depend on the transform parameter s. This fact suggests that a procedure of the numerical inversion of the Laplace transform should be used. Most of the methods of the numerical Laplace inversion are based on the approximation of integral (2.41) by a sum of s-dependent function evaluated at certain points and multiplied by coefficients (weights) specific for a given point. For a detailed review of some popular methods the reader is referred to the papers of Davies and Martin [35] and Cheng et al. [25].

In the present work the method of the numerical Laplace inversion proposed by Stehfest [123] is employed. The series approximation for the Stehfest algorithm is given by

$$f(t) \approx \frac{\ln 2}{t} \sum_{n=1}^{N_{St}} C_n \hat{f}\left(n \frac{\ln 2}{t}\right) \tag{4.25}$$

where N_{St} is even and the coefficients C_n are

$$C_n = (-1)^{n+N_{St}/2} \sum_{k=(n+1)/2}^{\min(n,N_{St}/2)} \frac{k^{N_{St}/2}(2k)!}{(N_{St}/2-k)!k!(k-1)!(n-k)!(2k-n)!} \tag{4.26}$$

The detailed derivation of expressions (4.25) and (4.26) can be found in [123] and [76]. The number of terms N_{St} in the series is relatively small and usually varies in the range of $2 \leq N_{St} \leq 20$ that makes the calculation procedure fast in comparison with many other methods (see the comparison charts in [35]). Due to its simplicity, the algorithm can be easily implemented in various programming languages. Besides, the algorithm does not require the knowledge of the poles of the integrand (see Eq.(2.41)). For the case of monotonic smooth functions quite accurate results have been reported by Davies and Martin [35], Cheng et al. [25] and Stehfest [123]. However, no accurate results of the inversion should be expected for discontinuous functions or functions containing sharp peaks or rapid oscillations [123].

As the number of terms in approximation (4.25) does not change during the procedure of the calculation of viscoelastic fields, the coefficients C_n are evaluated only once and stored in the computer memory.

Calculation of viscoelastic fields in the time domain

In order to find the viscoelastic potentials in the time domain, one has to solve system (4.18) for each moment of time t and each point n in the Stehfest algorithm in accordance with expression (4.25). The Gauss-Seidel iterative algorithm combined with an algorithm based on LU decomposition are adopted to find the explicit solution of system (4.18). This technique provides good convergence rate even if the dimension of matrix $\underline{\underline{A}}$ is very large. After that all s-dependent terms involved in potentials (4.5)-(4.8) have to be evaluated at points $(n \ln 2/t)$. The expressions for the potentials in terms of the Fourier coefficients $\hat{\mathbb{B}}_{mk}(s)$ are given in Appendix C.2. The final step assumes the summation of expressions (3.9) and (3.10) for the viscoelastic fields over all points n in accordance with Eq.(4.25) for each moment of time t.

The stresses and strains in the time domain are uniquely expressed via potentials (4.5)-(4.8). However, the displacements in the time domain are defined up to some additional terms that could be found after the rigid body motion is fixed, similarly as explained in [104] (see also Example 1 in Chapter 3).

An efficient computer code was created for the simulation of viscoelastic fields at any moment of time and in any point of the viscoelastic matrix or elastic inhomogeneities. A brief outline of the code is provided in Appendix E.

Discussion of sources of errors

Three sources of errors can be identified in the present method: (**i**) error due to the use of the truncated series in approximations (4.10) and (4.12), (**ii**) error related to the iterative solution of system (4.18), and (**iii**) error due to the use of the numerical inversion of the Laplace transform.

Error (**i**) can be effectively controlled by using an appropriate number M_k of Fourier terms for the approximations of the displacements and tractions at kth circular boundary. The value of M_k for this boundary has to be determined in the process of the

numerical solution. This number depends mostly on the geometry of the problem, and a procedure similar to the one describe in the previous chapter is used to evaluate it. First, system (4.18) is solved for zero time moment to find the instantaneous, "elastic" Fourier coefficients. These coefficients are then substituted to original equation (4.2), and the normalized difference ϵ between the left-hand side and the right-hand side of the equation is compared with the predefined accuracy parameter ϵ_{spec}. In the case $\epsilon > \epsilon_{spec}$, the number of Fourier terms is increased. The iterations stop when the specified accuracy level is achieved for every circular boundary. The procedure is described in detail in [102].

Error (**ii**) can be easily controlled by comparing the solution obtained at a current step of iteration with the solution from the previous step. The iterations in Gauss-Seidel algorithm are proceeded until the desired degree of accuracy is achieved. In the majority of the cases considered in present work, no more than 30-50 iterations are required to achieve the degree of accuracy at the level of 10^{-8}.

Error (**iii**) for the Stehfest algorithm of the inversion can not be controlled automatically. Nevertheless, several indirect means to control it are available. They are the following:

1) The stresses at the boundary of the half-plane obtained numerically by using the present approach can be compared with the prescribed boundary conditions.

2) For several linear viscoelastic models (e.g. standard solid, Burgers models), the instantaneous ($t = 0$) or large time ($t \to \infty$) response is the same as for corresponding elastic medium. Thus, one can compare the solution obtained by the present approach with the solution of the corresponding elastic problem, which in certain cases can be found analytically.

3) For the problem of an infinite or semi-infinite perforated viscoelastic plane subjected to constant loading, the stresses in the matrix do not depend on time and are exactly the same as those for the corresponding elastic problem [65] (see also Chapter 3). Thus, one may consider a problem in which the inhomogeneities have very small shear moduli,

so they can simulate the holes in the numerical analysis. The stresses obtained from the solution of this problem should be the same or very close to the stresses obtained from the corresponding elastic problem.

4) The viscoelastic stresses, displacements and strains obtained with the use of the present approach should be consistent between each other. For example, the strains at any time moment can be obtained via transformed Kolosov-Muskhelishvili's potentials (see Eqs.(3.9)-(3.10)). At the same time, it is easy to find the horizontal strains along a horizontal path or vertical strains along a vertical path by numerically differentiating the corresponding displacements. In addition, the time-dependent strains inside the elastic inhomogeneities can be found from the stresses by using Hooke's law. The strains found by using both approaches should be in good agreement with each other.

5) The comparison of the selected examples with the Finite Element analysis can provide an estimate about the accuracy of the method and the accuracy of the inverse Laplace transform depending on the number of terms in Eq.(4.25).

An extensive study of the accuracy of the numerical inverse Laplace transform was conducted with the use of the means listed above. It was found that for the case of constant loading and for the constitutive models presented in the next section, the best accuracy is achieved when $N_{St} = 8 \div 10$. However, a smaller number of terms in the Stehfest algorithm should be used ($N_{St} = 4 \div 6$) for the calculation of the stresses near the singular points (where the stresses may be subjected to rapid variations). In such cases, the use of large number N_{St} may cause the sum in Eq.(4.25) to diverge [123], [25]. This effect is usually observed at small times only, and the error introduced by the reduction of the number of terms in Eq.(4.25) is relatively small (see Example 1 in this chapter for some details).

Time-depending loading is not considered in the present work. For this case the Stehfest algorithm does not provide accurate results. However, the method described in the present chapter is not restricted by the use of any particular procedure of the numerical inversion of the Laplace transform.

4.5 Examples

Two constitutive models for the material matrix are considered in the following numerical examples. The condition of plane strain is assumed hereafter.

Model I. For this model it is assumed that the material of the matrix responds as a standard solid (the Boltzmann viscoelastic model) in shear (see Fig.2.4), and elastically in bulk. Such behavior is quite realistic as the shear modulus for many polymeric solids relaxes much more than its bulk modulus. The constitutive equations for the model are given by expressions (2.43) and s-dependent shear modulus and Kolosov-Muskhelishvili's parameter are given by (2.47) and (2.50) respectively. Values of material parameters are taken the same as in the previous chapter (see Eq.(3.36)).

Model II. This model assumes that the bulk material of the viscoelastic matrix behaves according to the Burgers model (see Fig.2.5) in shear and elastically in bulk. With the use of Eq.(2.16), the constitutive equations for this model can be presented in the form

$$\ddot{\sigma}_{ij}(t) + \left(\frac{E_1}{\eta_1} + \frac{E_1}{\eta_2} + \frac{E_2}{\eta_2}\right)\dot{\sigma}_{ij}(t) + \frac{E_1 E_2}{\eta_1 \eta_2}\sigma_{ij}(t) = 2E_2\ddot{\varepsilon}_{ij}(t) + 2\frac{E_1 E_2}{\eta_2}\dot{\varepsilon}_{ij}(t), \quad i \neq j$$
$$\sigma_{kk}(t) = 3K\varepsilon_{kk}(t) \tag{4.27}$$

Figure 2.5 explains the meanings of the parameters involved in Eqs.(4.27). The expressions for s-varying shear modulus and Kolosov-Muskhelishvili's parameter can be obtained after applying the Laplace transform to (4.27). They are as follows:

$$\hat{\mu}(s) = \frac{E_1 s\left(s + \dfrac{E_2}{\eta_2}\right)}{s^2 + s\left(\dfrac{E_1}{\eta_1} + \dfrac{E_1}{\eta_2} + \dfrac{E_2}{\eta_2}\right) + \dfrac{E_1 E_2}{\eta_1 \eta_2}}$$
$$\hat{\kappa}(s) = 1 + \frac{6E_1 s\left(s + \dfrac{E_2}{\eta_2}\right)}{E_1 s^2 + \dfrac{E_1 E_2}{\eta_2}s + 3K\left[s^2 + s\left(\dfrac{E_1}{\eta_1} + \dfrac{E_1}{\eta_2} + \dfrac{E_2}{\eta_2}\right) + \dfrac{E_1 E_2}{\eta_1 \eta_2}\right]} \tag{4.28}$$

The parameters of the springs and the bulk modulus are taken the same as for the

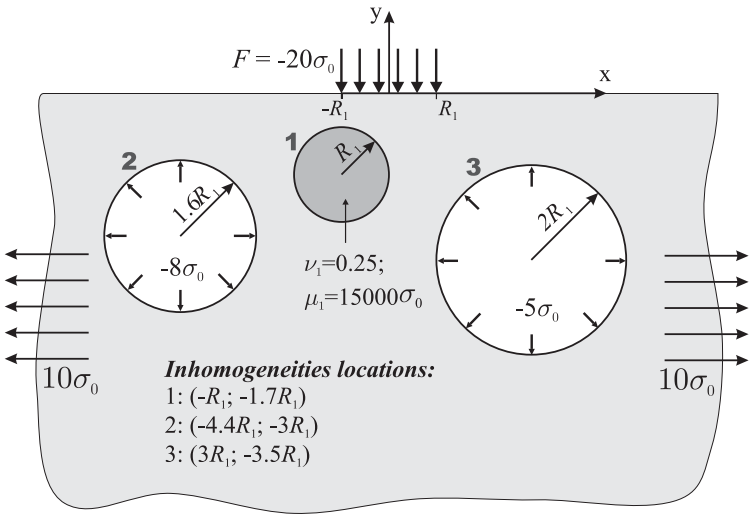

Figure 4.2: Problem geometry for Example 1.

first model, and the viscosity of the dashpots are

$$\eta_1 = 7 \times 10^3 \sigma_0 \cdot \text{sec}$$
$$\eta_2 = \eta \text{ (in Equation (3.36))} \tag{4.29}$$

It is worth to note that the Poisson's ratio $\nu(t)$ of the viscoelastic matrix is time-dependent for both constitutive models.

In all the examples presented below it is assumed that the loads applied to the boundaries of half-plane do not vary in time. Therefore, the time-dependent parts of the loads are the same as in expressions (3.34)-(3.35).

4.5.1 Comparison with the results from FEM (model I)

Consider the problem of a viscoelastic half-plane containing two holes and one rigid inhomogeneity as shown in Fig.4.2. The problem was solved by using the present approach and the Finite Element software ANSYS®.

Table 4.1: Number of Fourier terms M_k used in the approximation of the boundary displacements in Example 1 ($\epsilon_{spec} = 10^{-5}$).

	Left hole	Elastic disc	Right hole
M_k	18	23	20

A rectangular domain of size $600R_1 \times 500R_1$ (width x height) was used for the Finite Element analysis. In order to achieve a high degree of accuracy, the rigid disc was meshed with approximately 23100 quadrilateral 8-node elements, and 131400 elements of the same type were used for the viscoelastic matrix. The use of such large number of elements was not dictated by any factor; possibly a smaller number of elements could be used to achieve satisfactory accuracy of the results (however, it was found that the use of a mesh with about 35000 elements in total results in significantly less accurate solution). The Prony series were adopted to approximate the relaxation of the shear modulus of the matrix. Time stepping algorithm was applied to obtain the time domain solution from time $t = 0$ till time $t = 10\,\text{sec}$ with the time step $\delta t = 0.5\,\text{sec}$.

The stresses and strains obtained by both approaches can be compared directly. In order to compare the displacements it is necessary to introduce proper constraints in the finite element model and also constrain rigid body motion in the present approach. The procedure is described in details in Chapter 3.

In the present method, the accuracy parameter ϵ_{spec} was specified at the level $\epsilon_{spec} = 10^{-5}$. The number of Fourier terms M_k used in the approximation of the boundary displacements is given in Table 4.1. Using ten terms in sum (4.25) provided quite accurate results of the numerical Laplace inversion. The calculations with the present method took 8-10 seconds on a Dell$^{\text{TM}}$ computer workstation (Intel®P4 3.6GHz/ 2Gb RAM), while the finite element calculations required about 7 hours on the same computer workstation (no special optimization technique was used).

Some illustrative examples are given in Figs.4.3-4.6. Figures 4.3, 4.4 show very

good agreement between the results for the displacements and strains calculated with the use of both approaches. The graphs in Fig.4.3 and Fig.4.4 are plotted for several time instances only (0, 8 and 10 sec.), but good agreement has been found for all time moments for which the solution was obtained. The comparison of the time-dependent stresses, obtained by the present approach for two values of $N_{St} = 10$ and $N_{St} = 2$, with the results from the Finite Element analysis is illustrated in Fig.4.5 and Fig.4.6. One can see that for $N_{St} = 10$, the stresses exhibit very good agreement with those obtained by FEM (Fig.4.5). For the case of $N_{St} = 2$ some discrepancy in the results given in Fig.4.6 is observed at a small period of time only; at larger time the error diminishes. Similar behavior has been observed for all the examples considered in the present chapter. As the discrepancy is sufficiently small it seems reasonable to use smaller number of terms in Stehfest algorithm when large N_{St} causes the sum (4.25) to diverge.

The same procedure was performed to compare the viscoelastic fields for the case of a point force and a force distributed over the whole boundary of the half-plane. The results for these cases have revealed good agreement with the results from the Finite Element analysis.

4.5.2 Example with a single inhomogeneity (model I)

This example is concerned with a problem of a viscoelastic half-plane containing a single inhomogeneity. The material properties of the half-plane are described by constitutive model I. Four types of loading conditions are considered:

(i) far-field stress $\sigma^{\infty} = \sigma_0$ acting parallel to the boundary of the half-plane;

(ii) a point force $F = -\sigma_0$ acting perpendicular to the boundary of the half-plane along the axis of symmetry;

(iii) a force $F = -\sigma_0$ acting perpendicular to the boundary of the half-plane and distributed over a segment of length $2R$ whose center is located on the axis of symmetry;

(iv) a normal force $F = -\sigma_0$ uniformly distributed over the whole boundary of the half-plane.

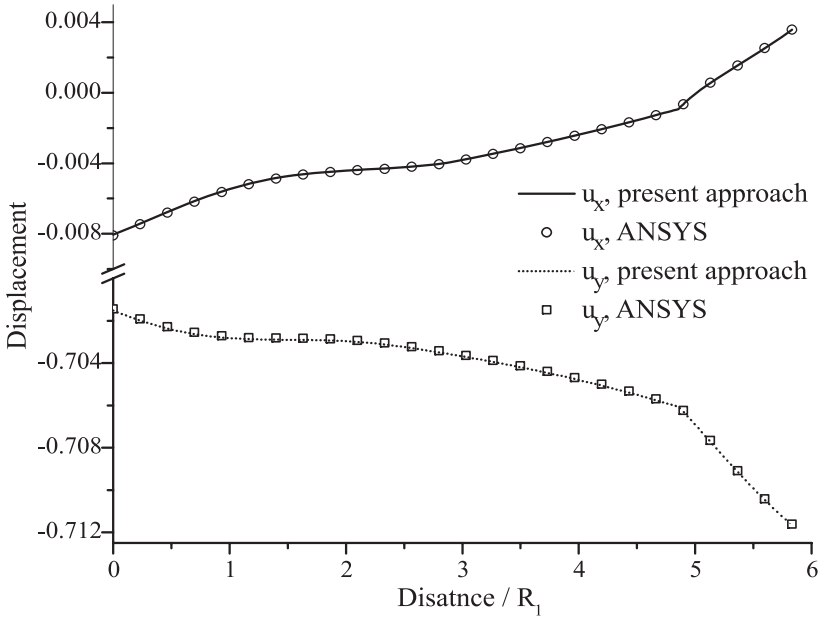

Figure 4.3: Variation of the displacements along the path $(-3R_1,\ -5R_1) \div (0,\ 0)$ at time $t = 8\,\text{sec}$.

This example studies the influence of the shear modulus of the inhomogeneity on the hoop stress at point A (the closest point to the boundary of the half-plane that is located on the intersection of the boundary of the inhomogeneity and the axis of symmetry).

The Poisson's ratio of the elastic inhomogeneity was set to $\nu = 0.35$, while its shear modulus was varied from $\mu_{inh} = 10^{-3}\sigma_0$ to $\mu_{inh} = 8{\cdot}10^5\sigma_0$. It is convenient to normalize μ_{inh} by the instantaneous shear modulus of the viscoelastic matrix $\mu(0) = 8000\sigma_0$. This value is equal to the elastic modulus E_1 in constitutive model I, as the dashpot does not exhibit instantaneous deformation (see Fig.2.4). Ten terms were used in the procedure of the numerical inversion of the Laplace transform (Equation (4.25)), and the number of Fourier terms M_k required to achieve the accuracy level $\epsilon_{spec} = 10^{-5}$ is reported in Table 4.2.

The fact that the hoop stress at point A is equal to the stress $\sigma_{xx}(t)$ allows for additional verification of the method and the computer code. Consider the case when

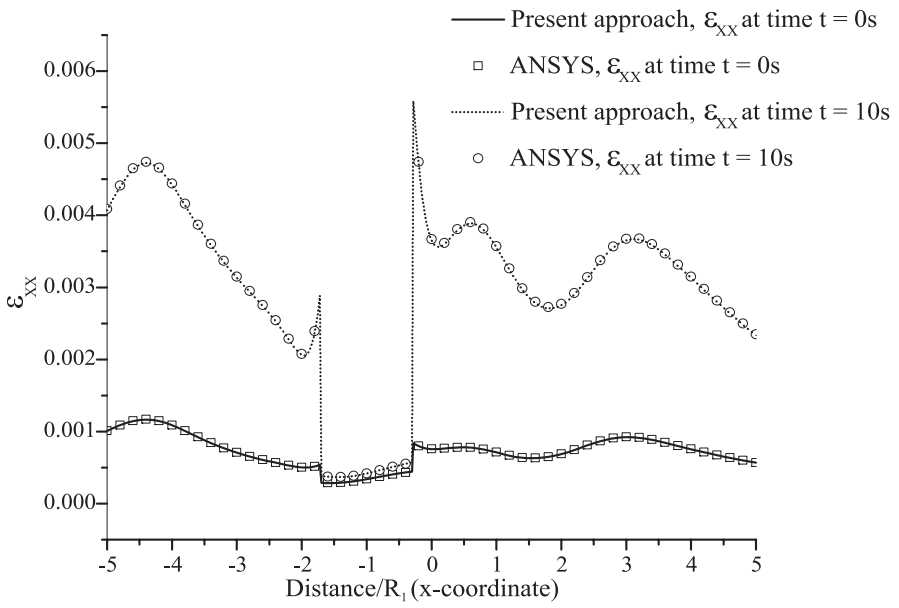

Figure 4.4: Variation of the horizontal strain along the path $(-5,-1) \div (5,-1)$.

Table 4.2: Number of Fourier terms M_k used in the approximation of the boundary displacements in Example 2 ($\epsilon_{spec} = 10^{-5}$).

Type of load	Far-field stress	Concentrated force	Force over a segment	Force over the boundary
M_k	37	209	34	22

the inhomogeneity is located far away from the boundary of the half-plane and its shear modulus is close to zero; far-field stress is applied parallel to the boundary of the half-plane. The stresses in the vicinity of the inhomogeneity will not be affected by that boundary and will be the same as in the case of a full plane. Besides, the stresses for this case do not depend on time, and they are exactly the same as the stresses in the corresponding "elastic" problem: $\sigma_{xx}/\sigma^{\infty} = 3$. The hoop stress found by the present method for $\mu_{inh} = 10^{-3}\sigma_0$ and $z_{center} = (0, -2000R)$ agrees with the elastic solution up to 6 significant digits for any moments of time.

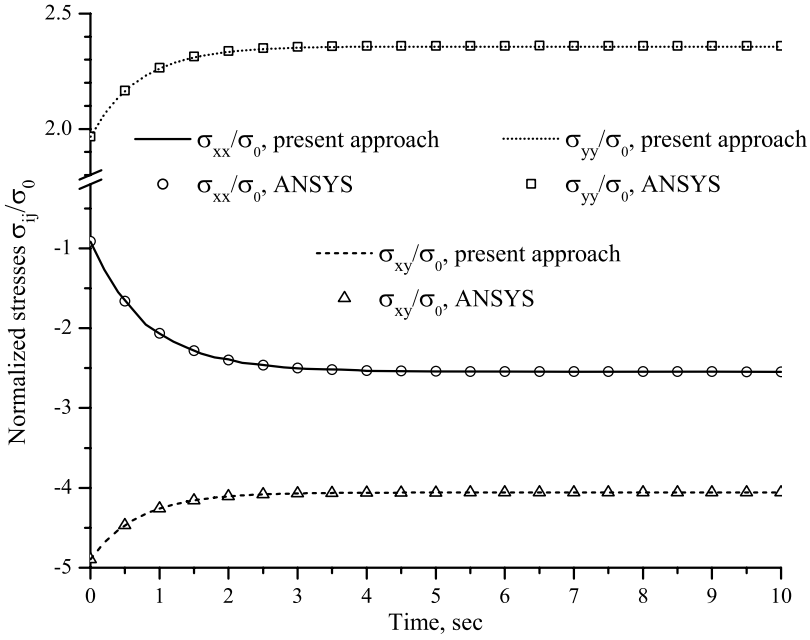

Figure 4.5: Variation of the normalized stresses at the point $(-2.28, \ -2.3)$ located inside the viscoelastic matrix ($N_{St} = 10$).

The variation of hoop stress at point A versus the shear modulus of the inhomogeneity is shown in Figs.4.7-4.10 for all types of loadings. The plots reveal that the hoop stress varies greatly with the variation of shear modulus of the inhomogeneity. However, in all four cases, the hoop stress exhibits an asymptotic behavior when $\mu_{inh}/\mu \to 0$ (the case of a hole) or $\mu_{inh}/\mu \to \infty$ (the case of a stiff inhomogeneity). In case (i), the hoop stress is tensile, see Fig.4.7, while it is compressive for case (iv), Fig.4.10. The hoop stress changes sign for two remaining cases of loadings, see Fig.4.8 and Fig.4.9.

The hoop stress at point A depends greatly on the separation distance between the inhomogeneity and the boundary of the half-plane. The investigation of this dependency for the case of a hole located in a viscoelastic half-plane is given in Chapter 3. It is interesting to compare the results obtained by the present approach with the results

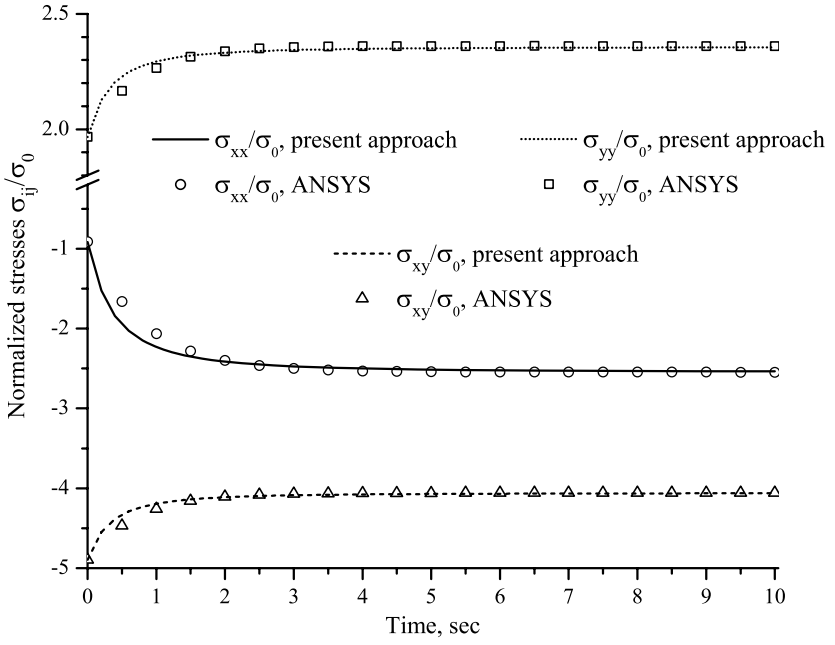

Figure 4.6: Variation of the normalized stresses at the point $(-2.28, \ -2.3)$ located in the viscoelastic matrix ($N_{St} = 2$).

obtained previously. It has been found that the hoop stresses obtained by the present method for $\mu_{inh} = 10^{-3}\sigma_0$ match with the results provided in Chapter 3 up to the third decimal number for any moment of time.

4.5.3 Example with two inhomogeneities (model II)

Two inhomogeneities with different elastic properties are considered in this example. The geometry of the problem is shown in Fig.4.11. Both inhomogeneities have the same radii R and their centers are located on the same horizontal line $y = -1.4R$. The separation distance between the inhomogeneities is $0.4R$. Far-field stress σ_0 acts parallel to the boundary of the half-plane. The bulk material of the half-plane behaves according to constitutive model II. The properties of the elastic inhomogeneities are as

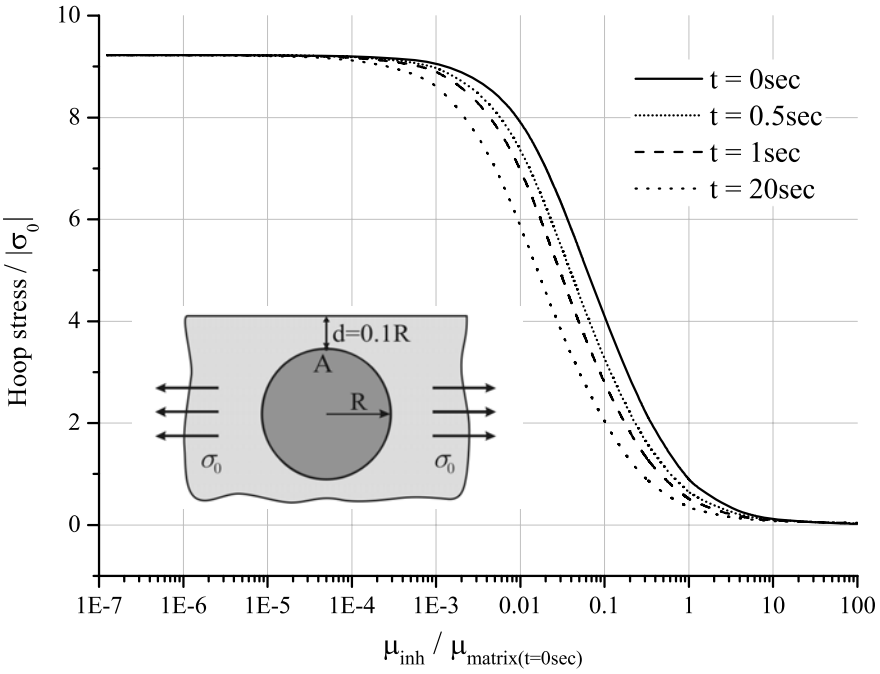

Figure 4.7: Variation of the normalized hoop stress at point A (loading i).

follows:

1. left inhomogeneity: $\nu = 0.35$, $\mu = 32000\sigma_0$ (rigid inhomogeneity),

2. right inhomogeneity: $\nu = 0.35$, $\mu = 400\sigma_0$ (soft inhomogeneity).

The distribution of maximum shear stress is to be found for different moments of time. The maximum shear stress at a point is given by the following expression:

$$\tau_{\max}(z,t) = \frac{\sigma_1(z,t) - \sigma_2(z,t)}{2} \tag{4.30}$$

where $\sigma_1(z,t)$ is the major in-plane principal stress and $\sigma_2(z,t)$ is the minor in-plane principal stress. The localization and the direction of the maximum shear stress can provide valuable information about the initiation and propagation of cracks.

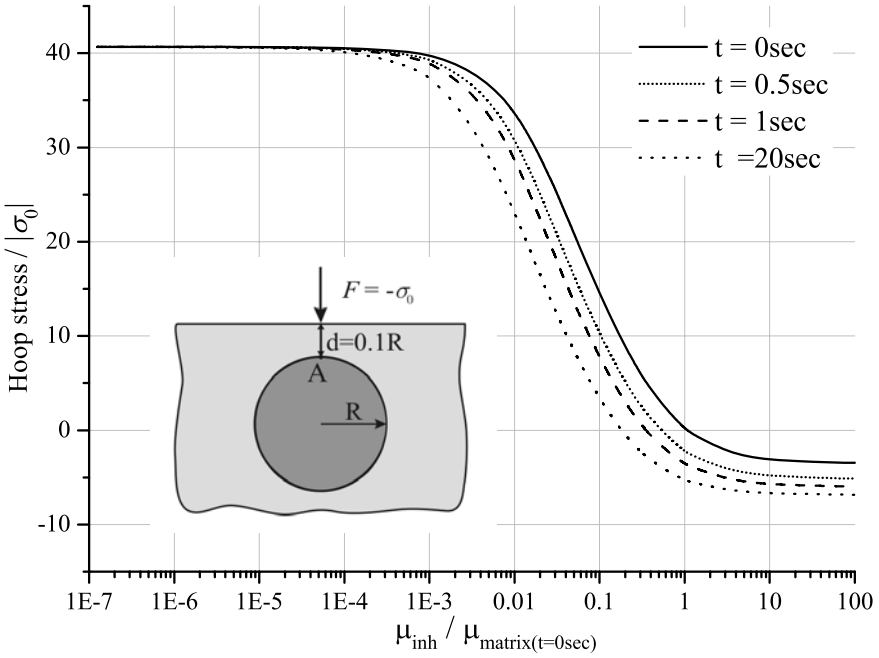

Figure 4.8: Variation of the normalized hoop stress at point A (loading ii).

The accuracy parameter ϵ_{spec} was specified at the level $\epsilon_{spec} = 10^{-5}$. To achieve this accuracy 51 terms in Fourier series ($M_k = 25$) were required for each inhomogeneity. The number of terms used in the algorithm of the numerical inverse Laplace transform was set to $N_{St} = 8$. It was found that using ten terms in approximation (4.25) causes the sum to diverge at certain points of the space domain. For additional verification of the results obtained in this example, a finite element model was built. The comparison of the solution found by using the present approach (for $N_{St} = 8$) and the one by the Finite Element approach has revealed very good agreement.

The contour plots of $\tau_{\max}(z,t)/\sigma_0$ are given in Figs.4.12-4.14 for three moments of time ($t = 0\,\text{sec},\ t = 5\,\text{sec}$ and $t = 300\,\text{sec}$). One can see that at the initial time $t = 0$, the highest shear stress concentration is localized between the soft inhomogeneity and the boundary of the half-plane. At the same time stress inside the inhomogeneity is

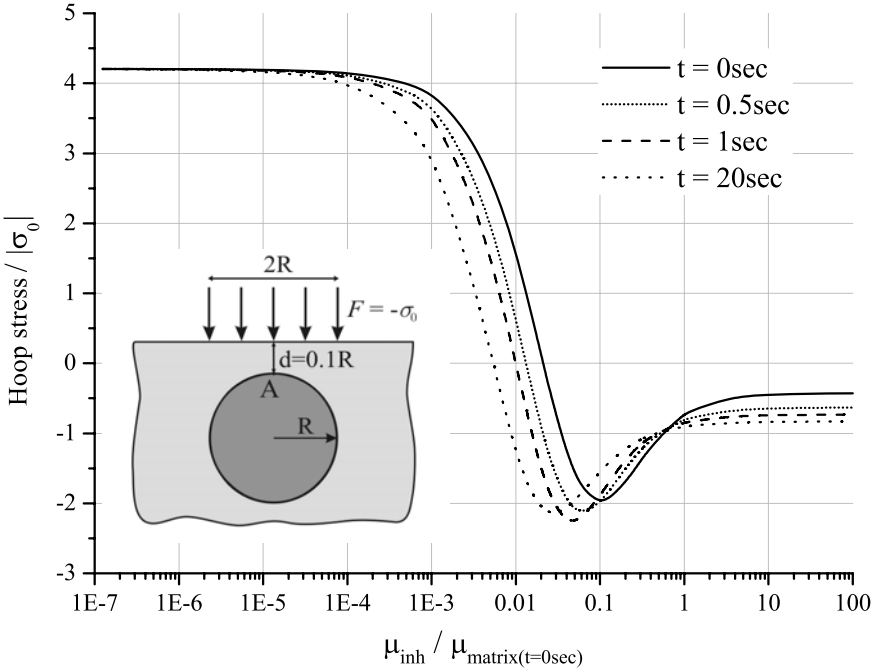

Figure 4.9: Variation of the normalized hoop stress at point A (loading iii).

much smaller than in the surrounding bulk material. These results are expected as the distribution of stress is similar to the one observed for a problem of a perforated half-plane. Stress inside the stiff inhomogeneity is about the same magnitude as in the surrounding matrix. Next figure (Fig.4.13) reveals that stress inside the inhomogeneities increases rapidly approaching the magnitude of the far-field stress σ_0 inside the stiff inhomogeneity. The distribution of the stress in the matrix also changes considerably, however, the maximum magnitude of $\tau_{\max}$ decreases from the level of $2\sigma_0$ to the level of σ_0. The distribution of stress at a large moment of time, (Fig.4.14), becomes symmetric relative to the line $x = 0$. At time $t = 300\,\text{sec}$ magnitude of the maximum shear stress almost reaches the level of $2\sigma_0$ again, but the maximum stress is localized inside the inhomogeneities.

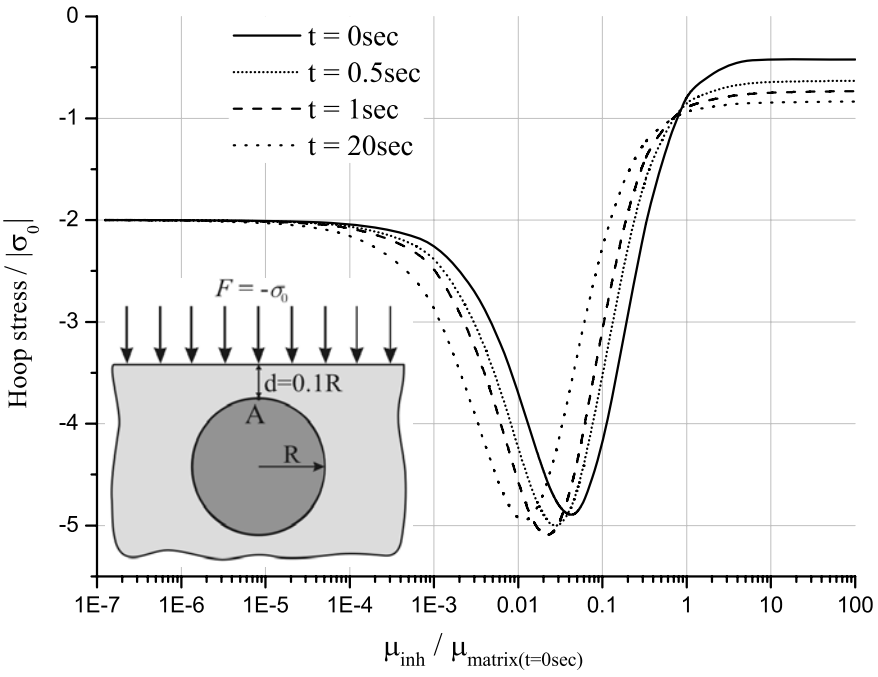

Figure 4.10: Variation of the normalized hoop stress at point A (loading iv).

The symmetric distribution of maximum shear stress allows one to suggest that for the case of constitutive model II and constant boundary loadings, stress anywhere in the medium does not depend on the material properties of its constituents at large moment of time. To support this conclusion, stress components have been found at a number of points inside the half-plane for several different sets of the material properties of the matrix and inhomogeneities. The illustrative results for the case of vertical stress σ_{yy} are presented in Figs.4.15 and 4.16. The first set of the material properties corresponds to that stated above in the current example. The second set is as follows:

$$E_1 = 1000\sigma_0,\ E_2 = 6000\sigma_0,\ \eta_1 = 3000\sigma_0 \cdot \sec,\ \eta_2 = 9000\sigma_0 \cdot \sec,\ K = 25000\sigma_0,$$

$$\text{Left inhomogeneity: } \nu = 0.4, \mu = 1200\sigma_0$$

$$\text{Right inhomogeneity: } \nu = 0.2, \mu = 16000\sigma_0$$

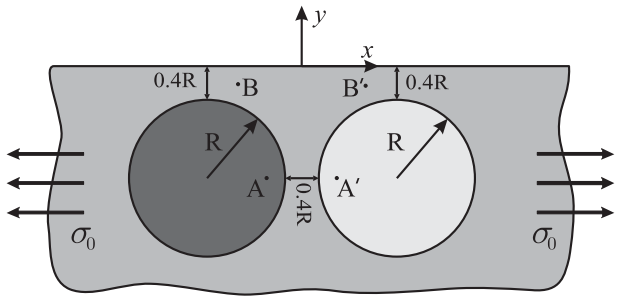

Figure 4.11: Problem geometry for Example 3.

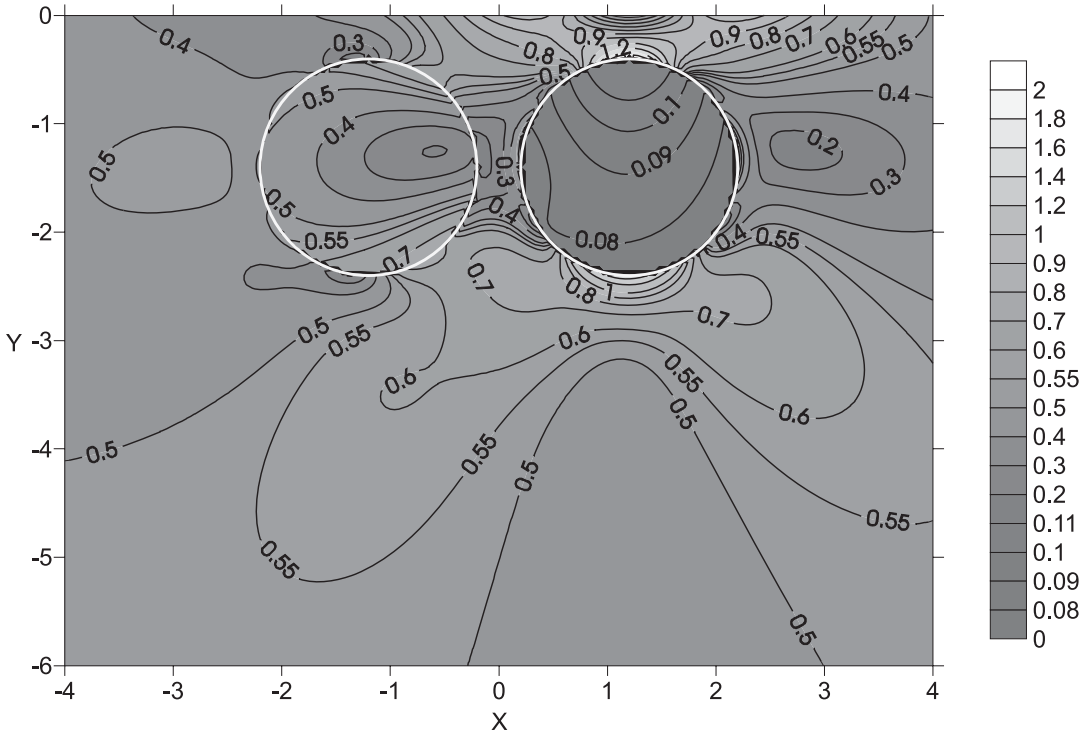

Figure 4.12: Contours of $\tau_{\max}(z,t)/\sigma_0$ at time $t = 0\,\text{sec}$.

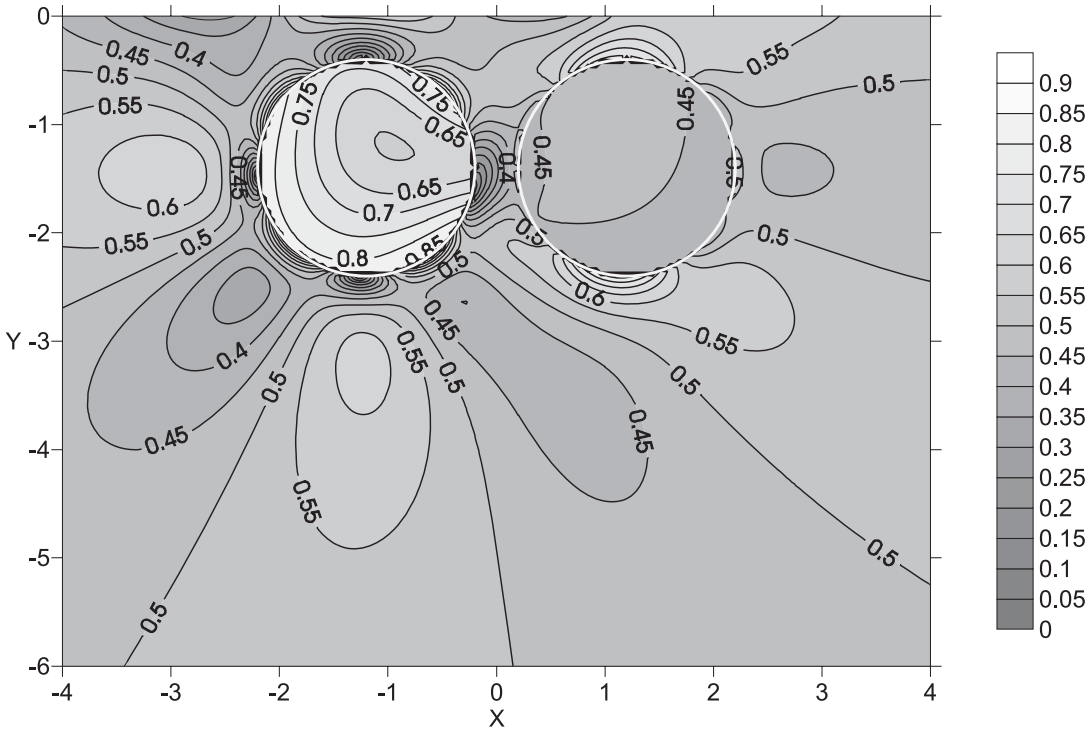

Figure 4.13: Contours of $\tau_{\max}(z,t)/\sigma_0$ at time $t = 5\,\text{sec}$.

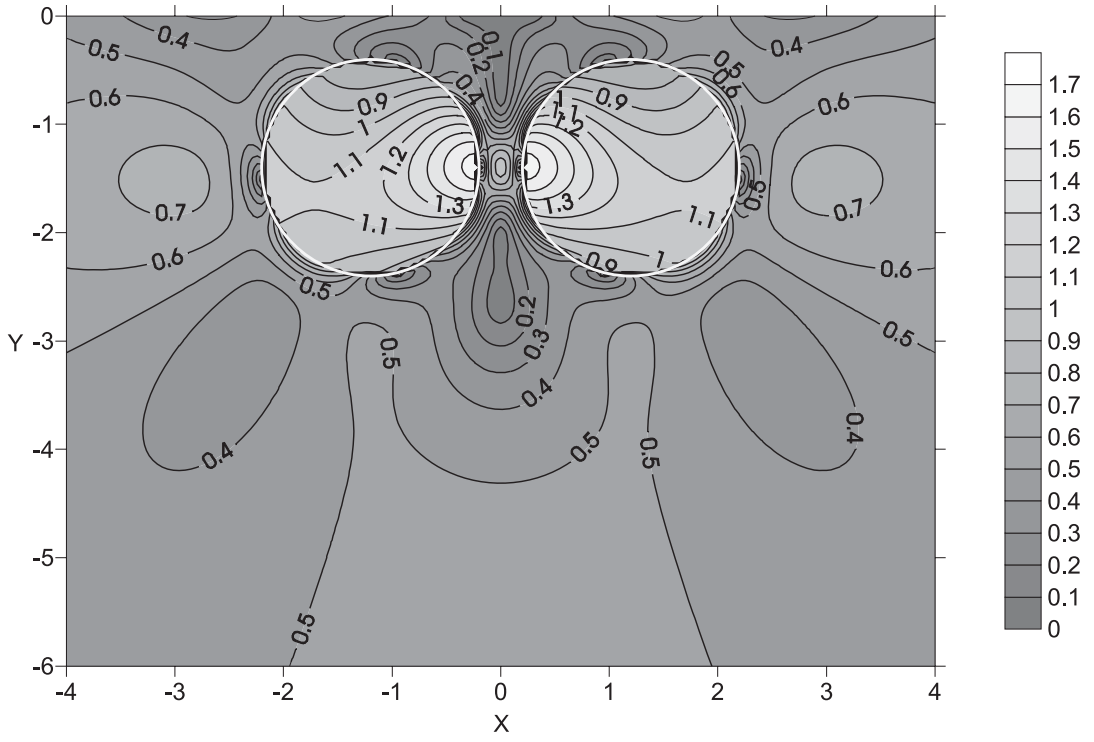

Figure 4.14: Contours of $\tau_{\max}(z,t)/\sigma_0$ at time $t = 300\,\text{sec}$.

The y component of stress was found at the points $A(-0.4R, \ -1.4R)$ and $A'(0.4R, \ -1.4R)$ located inside the left and right inhomogeneities correspondingly and points $B(-0.8R, \ -0.2R)$ and $B'(0.8R, \ -0.2R)$ located inside the matrix. The results presented in Figs.4.15 and 4.16 reveal that the stresses at large time, indeed, do not depend on the material properties, although they depend on the geometry of the problem and on the loading, i.e. stress in the medium is statically determined. Similar results has been obtained for other types of loadings. As a hole can be treated as inhomogeneity with zero elastic properties, the same conclusion can be made for the case of more complicated geometries including multiple holes and elastic inhomogeneities. It is important to note that the strains and displacements depend on material properties even when time is large. These results are supported by the results from the Finite Element analysis.

Numerical analysis for the case when viscoelastic matrix is described by constitutive model I has revealed that stresses do not exhibit asymptotic behavior at large times. It is the viscous flow introduced by the combination of dashpots in the Burgers model that is responsible for the steady solution at large times.

4.5.4 Large-time asymptotic behavior (model II)

Due to the fact that in certain cases it is possible to find the large-time asymptotic solution for time-dependent stresses, one can show analytically that stresses are statically determined for the case when matrix's behavior is described by the Burgers model. To illustrate this, consider a problem of a single elastic inhomogeneity located in a viscoelastic plane subjected to constant far-field stress $\hat{\sigma}^{\infty}$. For this problem system (4.2)

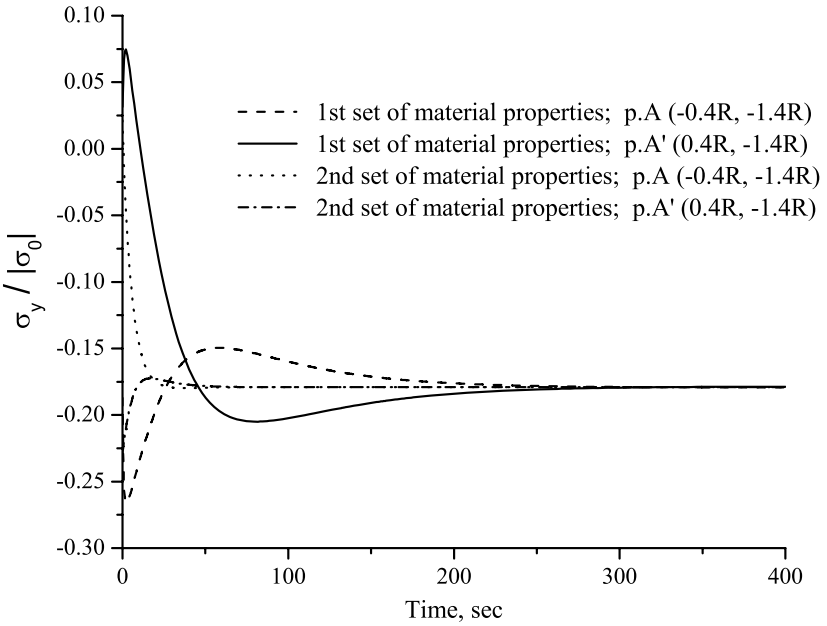

Figure 4.15: Variation of the normalized vertical stress at points A and A'.

reduces to the following single equation:

$$-2\int_L \frac{\hat{u}^h(\varsigma;s)}{(\varsigma-\xi)^2}d\varsigma + \int_L \hat{u}^h(\varsigma;s)\frac{\partial^2 K_1(\varsigma,\xi)}{\partial\varsigma\partial\xi}d\varsigma + \int_L \overline{\hat{u}^h(\varsigma;s)}\frac{\partial^2 K_2(\varsigma,\xi)}{\partial\overline{\varsigma}\partial\xi}d\overline{\varsigma}$$
$$+\frac{\hat{\kappa}(s)}{2\hat{\mu}(s)}\left[\int_L \hat{\sigma}^h(\varsigma;s)\frac{\partial K_1(\varsigma,\xi)}{\partial\xi}d\varsigma + \int_L \overline{\hat{\sigma}^h(\varsigma;s)}\frac{\partial K_2(\varsigma,\xi)}{\partial\xi}d\overline{\varsigma}\right] \qquad (4.31)$$
$$+\frac{\hat{\kappa}(s)-1}{2\hat{\mu}(s)}\int_L \frac{\hat{\sigma}^h(\varsigma;s)}{\varsigma-\xi}d\varsigma + \pi i\frac{\hat{\kappa}(s)+1}{2\hat{\mu}(s)}\hat{\sigma}^h(\xi;s) = 2\pi i\frac{\hat{\kappa}(s)+1}{4\hat{\mu}(s)}(1+g^2(\xi))\hat{\sigma}^\infty$$

where L is the boundary of the cavity occupied by the inhomogeneity. As there are only two terms $g^0(\xi)\equiv 1$ and $g^2(\xi)$ in the right-hand side of Eq.(4.31), the only non-zero Fourier coefficients $\hat{B}_m(s)$ present in approximations (4.10) are $\hat{B}_{-1}(s)$ and $\hat{B}_1(s)$. These coefficients are found from the solution of (4.31) and can be expressed as follows:

$$\hat{B}_{-1}(s) = \frac{\hat{\sigma}^\infty}{4}\frac{\hat{\kappa}(s)+1}{\hat{\mu}(s)+\hat{\kappa}(s)\mu_d}R$$
$$\mathrm{Re}\,\hat{B}_1(s) = \frac{\hat{\sigma}^\infty}{8}\frac{\hat{\kappa}(s)+1}{\hat{\mu}(s)+\dfrac{2\mu_d}{\kappa_d-1}}R \qquad (4.32)$$

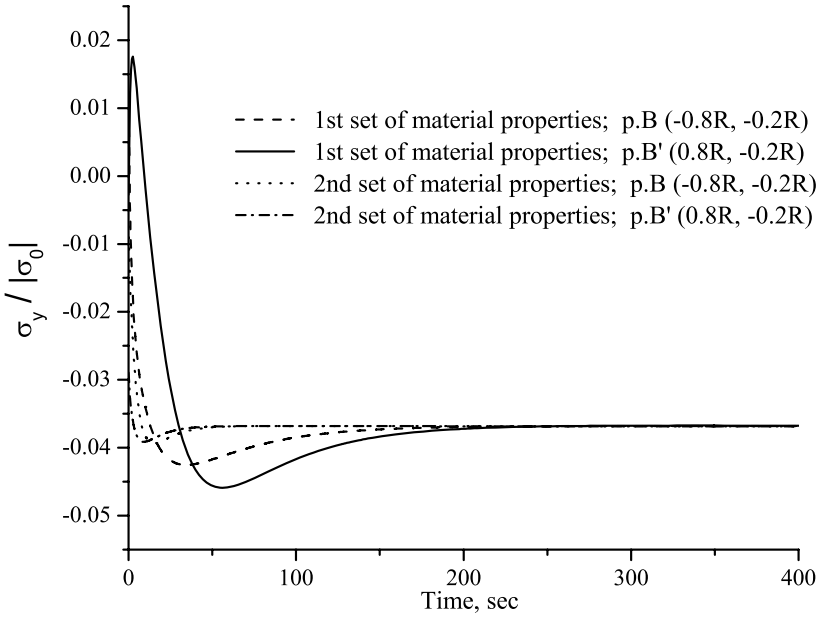

Figure 4.16: Variation of the normalized vertical stress at points B and B'.

where R is the radius of the inhomogeneity (elastic disc), μ_d and κ_d are its shear modulus and Kolosov-Muskhelishvili's parameter correspondingly.

As Kolosov-Muskhelishvili's potential $\varphi(z,t)$ is expressed through the sum of horizontal and vertical stress components (see Eq.(2.66)), its behavior is studied at $t \to \infty$. It follows from (4.7) that

$$\begin{aligned}
\hat{\varphi}(z,s) &= -\frac{\mu_d - \hat{\mu}(s)}{\hat{\mu}(s) + \hat{\kappa}(s)\mu_d} \frac{R^2}{z - z_c} \frac{\hat{\sigma}^{\infty}(s)}{2} + \frac{\hat{\sigma}^{\infty}(s)}{4} z, \qquad z \in \text{matrix} \\
\hat{\varphi}(z,s) &= \frac{\mu_d}{\kappa_d - 1} \frac{\hat{\kappa}(s) + 1}{\hat{\mu}(s) + \dfrac{2\mu_d}{\kappa_d - 1}} (z - z_c) \frac{\hat{\sigma}^{\infty}(s)}{4}, \qquad z \in \text{elastic disc}
\end{aligned} \tag{4.33}$$

where z_c is the complex coordinate of the center of the inhomogeneity.

The behavior of the potential in the time domain at $t \to \infty$ corresponds to the behavior of its Laplace transform at $s \to 0$. Expressions (4.28) give

$$\hat{\mu}(s) \to 0, \ \hat{\kappa}(s) \to 1 \text{ when } s \to 0 \tag{4.34}$$

Using Eqs.(4.33) and (4.34) and not accounting for the behavior of $\hat{\sigma}^{\infty}_{xx}(s)$ at $s \to 0$ (this quantity should be transformed back in the time domain), one gets

$$\hat{\varphi}(z,s) = \frac{\hat{\sigma}^{\infty}(s)}{4}\left[z - \frac{2R^2}{z - z_c}\right], \qquad z \in \text{matrix},\ s \to 0$$
$$\hat{\varphi}(z,s) = (z - z_c)\frac{\hat{\sigma}^{\infty}(s)}{4}, \qquad z \in \text{elastic disc},\ s \to 0 \tag{4.35}$$

Finally, using Eqs.(3.9) and (4.35) one arrives at

$$\sigma_{xx}(z) + \sigma_{yy}(z) = \sigma^{\infty}\left[1 + 2\,\mathrm{Re}\left(\frac{R}{z - z_c}\right)^2\right], \qquad z \in \text{matrix},\ t \to \infty$$
$$\sigma_{xx}(z) + \sigma_{yy}(z) = \sigma^{\infty}, \qquad \forall\ z \in \text{elastic disc},\ t \to \infty \tag{4.36}$$

It follows from expressions (4.36) that, at large times, the sum of the horizontal and vertical stresses found inside the inhomogeneity is constant and equal to the value of the far-field stress. The results given by Eqs.(4.36) can be used as the benchmark solution. Consider a single inhomogeneity located far from the boundary of the viscoelastic half-plane subjected to far-field stress σ^{∞}. Let $R = 1$ and $z_c = (5R,\ -2000R)$. It is assumed that the viscoelastic matrix obeys constitutive model II and $\nu_d = 0.2$, $\mu_d = 16000\sigma^{\infty}$. Table 4.3 shows the results for the combination $\sigma_{xx}(z) + \sigma_{yy}(z)$ calculated at several points located on two circular contours co-centrical with the boundary of the inhomogeneity. The first contour is located inside the inhomogeneity and its radius is $r = 0.8R$; the radius of the contour located outside the inhomogeneity is $r = 1.1R$. For both contours the angle is defined similarly as the angle shown in Fig.4.1b. Due to the symmetry of the problem the values of $\sigma_{xx}(z) + \sigma_{yy}(z)$ are given for the first quarter of the complex plane only. As one can see from Table 4.3, the combination $\sigma_{xx}(z) + \sigma_{yy}(z)$ tends to the results prescribed by Eqs.(4.36) when time is sufficiently large.

4.6 Summary

It has been shown that the proposed method of solution of the problem of a semi-infinite, isotropic, linear viscoelastic half-plane containing multiple elastic inhomogeneities is

Table 4.3: The values of $\sigma_{xx}(z) + \sigma_{yy}(z)$ found numerically and from Eq.(4.36).

Angle, deg	$t = 0\,\text{sec}$	$t = 5\,\text{sec}$	$t = 500\,\text{sec}$	Equation (4.36)
Circular contour located inside the matrix ($r = 1.1R$)				
0	1.359325	2.511734	2.652893	2.652893
15	1.311184	2.3092	2.431448	2.431447
30	1.179662	1.755867	1.826447	1.826446
45	0.99999999	1.00000011	1.00000012	1
60	0.820338	0.244133	0.173554	0.173554
75	0.688816	−0.3092	−0.431447	−0.431447
90	0.640676	−0.511733	−0.652893	−0.652893
Circular contour located inside the inhomogeneity ($r = 0.8R$)				
$0 \div 360$	1.076923	1.006881	1.00000006	1

efficient and accurate. As the upper boundary of the half-plane may be subjected to different loading conditions, the method can be successfully used in modeling of indentation processes.

An important feature of the algorithm is that most of the derivation including space integration, the Laplace transform, are performed analytically. In case of the perforated half-plane, when the method reduces to the one presented in Chapter 3, the inversion of the Laplace transform can be also performed analytically. However, in general case of the inhomogeneities, it has to be performed numerically.

An algorithm of the numerical inversion of the Laplace transform proposed by Stehfest [123] is used in the present work. It has been found that for the case of constant boundary conditions and for the constitutive models considered in the current work, the algorithm provides accurate results. The results of the numerical simulations indicate that the Stehfest algorithm does not provide accurate results for those problems, for which time-dependent boundary conditions are prescribed. However, the method described in the present chapter is not restricted to the use of any particular procedure of numerical inversion of the Laplace transform.

The major advantage of the algorithm is its time efficiency: the problems containing

large arrays of inhomogeneities (tens/hundreds) can be accurately solved in reasonable time on a standard single-processor PC. Calculations of viscoelastic fields can be effectively parallelized on multiprocessor/multicore machines, and multipole expansion method can be adopted [51], [133]. The present method allows one easily modify constitutive viscoelastic models in the computer code, if the expressions for the transformed shear modulus and Kolosov-Muskhelishvili's parameter are known.

Several numerical examples are considered in the chapter. New results have been obtained from the study of the hoop stress at a point on the boundary of a single inhomogeneity located in the vicinity of the boundary of the half-plane. The study has revealed that the hoop stress greatly depends on the material properties of the inhomogeneity and can be tensile or compressive depending on the time moment and shear modulus of the inhomogeneity. The results obtained for the case of constitutive model II have showed that the state of stress is statically determined at large moment of time. Stresses exhibit an asymptotic behavior that is defined only by the geometry of the problem when time tends to infinity. Nevertheless, the moment of time when the stresses approach the asymptotic behavior depends on the combination of the material parameters and can not be determined directly.

Chapter 5

Evaluation of effective transverse mechanical properties of isotropic viscoelastic composite materials

5.1 Introduction

The number and variety of engineering applications of viscoelastic porous media and fiber-reinforced viscoelastic composites have greatly increased in recent decades [48]. Rapid development and widespread use of composite materials requires new tools for simple and accurate evaluation of their effective mechanical properties.

Despite a number of micromechanical models and variational bounds available for the analysis of the elastic composites, accurate predictions of the effective properties of viscoelastic composite materials are still a subject of significant research [30], [58]. The most powerful tool in the analysis of viscoelastic media is the elastic-viscoelastic correspondence principle (see Section 2.1.6). However, as pointed out by Christensen [30] and Hashin [58], the application of the principle to obtaining the viscoelastic variational bounds is limited. In general, the minimum energy theorems that are so powerful for elastic composites, are applicable only in few highly restricted cases for viscoelastic

composites [30]. One of these cases includes a porous viscoelastic medium with constant Poisson's ratio. In this case, the viscoelastic analog of Hashin-Shtrikman bounds [52], [54] can be obtained based on use of the Laplace transform. To obtain the time-varying viscoelastic effective properties, one has to employ a procedure of analytical or numerical Laplace inversion. The latter is often a difficult task (see [83] for some techniques used for the numerical inversion of the Laplace transform in application to the homogenization processes).

A number of researchers applied the correspondence principle to specific micromechanical models to obtain the effective properties of viscoelastic composites. Wang and Weng [134] adopted the Mori-Tanaka scheme and numerical inversion of the Laplace transform. DeBotton and Tevet-Deree [37] used Composite Cylinder model and Hashin-Shtrikman bounds to estimate the effective transverse properties of viscoelastic fiber-reinforced composites. They inverted the transformed effective moduli analytically and compared their results with those from finite element simulations. As the calculation of the effective complex moduli does not require the Laplace inversion, many researchers have studied the dynamic properties of viscoelastic composites. For example, Brinson and Lin [19] adopted the Mori-Tanaka scheme and Hashin's approach [58] to obtain the effective complex moduli of multiphase viscoelastic composites.

Owing to the fact that the analysis of porous viscoelastic media is much simpler than the analysis of composites containing elastic phases, the behavior of porous materials is studied relatively well (see, for instance [67] and references therein). Torquato et al. [126] studied the effective mechanical properties of two-dimensional elastic and viscoelastic cellular solids. Based on the analysis of Hashin-Shtrikman bounds, the authors arrived at several important conclusions regarding the time-dependency of the effective moduli of viscoelastic porous solids. Particularly, they concluded that, for the case of very high porosity, the effective Poisson's ratio depends only on the structure of the composite and is independent on the viscoelastic properties of the matrix. Similar conclusions were made regarding ratios of the effective moduli to the corresponding

phase moduli (see details in [126]).

Some researchers adopted the so-called internal variables formulation approach. Lahellec and Suquet [78] used this approach together with a time-integration technique for the calculation of the effective viscoelastic properties. They reduced the original boundary-value problem to the problem of the minimization of an incremental energy function and obtained a system of non-linear equations at each time-step. Despite the fact that the method is free of disadvantages inherent to the inversion of the Laplace transform, its formulation and technical implementation are rather involved.

Among other methods that operate in the time domain are the Finite Element and the Boundary Element methods. These approaches employ the concept of Representative Unit Cell (RUC) or Representative Volume Element (RVE), for which proper time-dependent boundary conditions have to be specified. Time-stepping algorithms have to be used in combination with FEM or BEM to obtain the time-domain solution.

Finally, it should be noted that most of the authors who employ the concept of RUC limit themselves to the study of two-dimensional (2D) square-shaped RUCs (e.g. [17], [19], [90], [95], [139]). Such choice of the RUC appears to be the simplest one, but it leads to anisotropic overall behavior.

In this chapter, a new procedure is proposed for the evaluation of the effective transverse mechanical properties of viscoelastic composites. It is based on the use of the correspondence principle and employs the equivalent inhomogeneity technique [105]. The latter technique is based on the concept of a Representative Pattern (Fig.5.1a,b) that is used to represent the structure of a composite material. The basic idea of the technique is to construct a circular inhomogeneity in an infinite plane (Fig.5.1c,d) whose effects on the elastic fields at distant points are the same as those of a finite cluster of inhomogeneities (e.g. fibers of circular cross-section) arranged in a pattern that represents the composite material in question. The mechanical properties of the equivalent inhomogeneity correspond to the effective properties of the composite material. The problems presented in Figs.5.1c and 5.1d will be referred hereafter as Problem I and

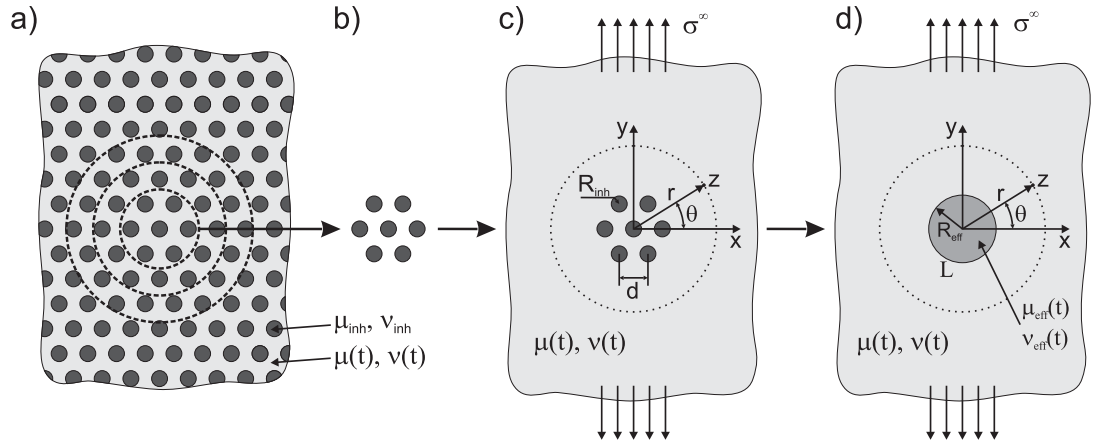

Figure 5.1: Problem formulation. a) A cross-section of a fiber-reinforced composite with hexagonal distribution of inhomogeneities. Several representative clusters of different size are shown by the dashed lines. b) An example of a representative cluster. c) The representative cluster in a plane with the same material properties as the composite's matrix (Problem I). d) The equivalent inhomogeneity (Problem II).

Problem II respectively.

The method of equivalent inhomogeneity has some common features with the approach of Maxwell [96], which was developed to analyze the effective electric conductivity of particulate composite materials. Maxwell assumed that spherical particles do not interact with each other and obtained a simple formula for the effective resistance, which is valid only for small volume fractions. Maxwell's approach was recently applied to the prediction of effective elastic properties of particulate composites by McCartney and Kelly [97]. However, as in the original Maxwell's approach, the interaction between particles was not considered. In the equivalent inhomogeneity technique, the interactions among the inhomogeneities are precisely accounted for.

Only hexagonal and random distributions of inhomogeneities are considered in the present work. This is due to the fact that only these patterns assure the overall isotropic transverse behavior of a composite material. For the case of the hexagonal arrangement,

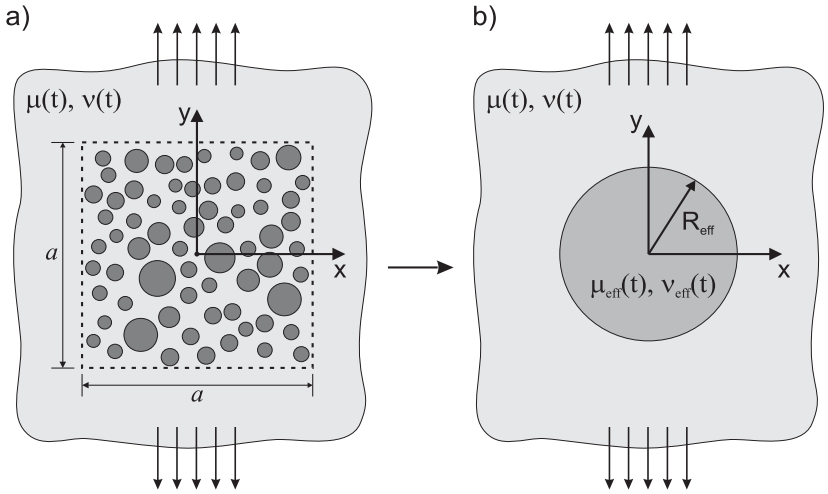

Figure 5.2: An example of the representative cluster of a composite with random arrangement of inhomogeneities (a) and the equivalent inhomogeneity (b).

the choice of the representative cluster is rather straightforward; several possible choices are depicted in Fig.5.1a. The origin of the coordinates can be placed at the center of the symmetry of the representative cluster (Fig.5.1c,d). For the case of the random arrangement of the inhomogeneities, the representative cluster can be generated in an area of square shape (Fig.5.2a). The origin of the coordinates can be placed at the center of the square.

5.2 Theoretical background

Several major modifications of the equivalent inhomogeneity technique are proposed to accommodate it for the evaluation of the effective transverse properties of viscoelastic composites. These modifications are outlined below.

i) As the present approach is designed for the composite materials with viscoelastic matrix, the equivalent inhomogeneity is also assumed to be viscoelastic.

ii) Even though the properties of the equivalent inhomogeneity vary in time, the radius of

the inhomogeneity is considered to be time-independent. This follows from the assumption that the area fractions of elastic constituents in the viscoelastic composite should not change with time. Thus, the radius of the equivalent viscoelastic inhomogeneity can be directly determined from the area fraction of the elastic phase as follows:

- for the case of a composite with hexagonal arrangement of identical elastic inhomogeneities

$$R_{eff} = \sqrt{\frac{S_f}{\pi f}} = \sqrt{\frac{N \cdot \pi R_{inh}^2}{\pi f}} = d\sqrt{\frac{3N}{2\pi}\tan(\pi/6)} \tag{5.1}$$

  where R_{eff} is the radius of the equivalent inhomogeneity, f is the area fraction of the elastic phase, S_f is the area occupied by this phase, N is the number of inhomogeneities in the representative cluster, R_{inh} is the radius of each inhomogeneity, and d is the distance between the neighboring inhomogeneities in the representative cluster (Fig.5.1c). It follows from Eq.(5.1) that the radius of the equivalent inhomogeneity does not depend on the area fraction f and it grows with the increase of the size of the representative cluster (increase of N).

- for the case of a composite with random arrangement of inhomogeneities

$$R_{eff} = \sqrt{\frac{S_k}{\pi f_k}} = \sqrt{\frac{S \cdot f_k}{\pi f_k}} = \sqrt{\frac{S}{\pi}} \tag{5.2}$$

  where S_k is the area occupied by the k-th elastic phase, f_k is its area fraction, and S is the area in which the representative cluster is generated. For the cluster given in Fig.5.2a, $S = a^2$. Note that the radius of the equivalent inhomogeneity in this case is defined only by the size of area S.

iii) The present approach employs the idea of matching viscoelastic stresses at some point z for problem I (Fig.5.1c) and for problem II (Fig.5.1d). The point z is located in the viscoelastic matrix, and its position can be varied. It is clear, however, that the location of the point should not be too close to the representative cluster, as the obtained stresses will be affected by the internal structure of the cluster. At the same

time, this location should not be too far away from the cluster, as the effect of the cluster diminishes at large distances where the stresses converge to the far-field stress. The results of numerical experiments show that reasonable distances to evaluate the stresses are in the range of $2-100$ sizes of the representative cluster; this finding agrees with the estimates of Mogilevskaya et al. [105]. As only two material properties are unknown, it is enough to find two components of the stress tensor at the point z.

iv) The stresses for the problem of the representative cluster (Problem I) and those for the problem of the viscoelastic equivalent inhomogeneity (Problem II) are matched in the Laplace domain, where the corresponding elastic problems are formulated and solved. Approaches presented in Chapter 3 and Chapter 4 are used for the calculation of stress fields in Problem I (Fig.5.1c). The Laplace domain solution of Problem II (Fig.5.1d) is outlined below.

5.2.1 Problem (II) of a single viscoelastic inhomogeneity in viscoelastic plane

Consider a problem of a single linearly viscoelastic isotropic inhomogeneity with shear modulus $\mu_{eff}(t)$, Poisson's ratio $\nu_{eff}(t)$, and radius R_{eff} embedded in an infinite linearly viscoelastic plane (matrix) with material parameters $\mu(t)$ and $\nu(t)$. Constant far-field stress is applied, and the distribution of stresses in the matrix is to be found. The solution employs the elastic-viscoelastic correspondence principle based on the Laplace transform.

The treatment of the problem is based on the standard superposition technique (see Chapter 4). The original problem (Fig.5.1d) is decomposed into two complementary ones: the problem of a single viscoelastic disc with unknown time-dependent displacements and tractions on its boundary and the problem of a viscoelastic plane subjected to a constant stress at infinity and containing a single circular hole with unknown tractions on the boundary. These two problems are interconnected by the condition of perfect bond. In the Laplace domain, the second problem (full plane with a hole) is described

by Eq.(4.31), and the problem of the single disc is described by Eq.(4.1), where all material properties are the functions of the transform parameter s. Due to the fact that both problems are solved independently in the Laplace domain, relations (4.11) hold, in which the material properties of the inhomogeneity have to be substituted by their Laplace counterparts. Thus, the solution for s-dependent Kolosov-Muskhelishvili's potentials at the point z located in the matrix can be obtained in the following form:

$$\begin{aligned}
\hat{\varphi}(z,s) &= -\frac{\hat{\mu}-\hat{\mu}_{eff}}{\hat{\mu}+\hat{\kappa}\hat{\mu}_{eff}}\frac{R_{eff}^2}{z}\frac{\hat{\sigma}_{yy}^{\infty}-\hat{\sigma}_{xx}^{\infty}-2i\hat{\sigma}_{xy}^{\infty}}{2}+\frac{\hat{\sigma}_{xx}^{\infty}+\hat{\sigma}_{yy}^{\infty}}{4}z \\
\hat{\psi}(z,s) &= -\frac{\hat{\mu}_{eff}\left(\hat{\kappa}-1\right)-\hat{\mu}\left(\hat{\kappa}_{eff}-1\right)}{2\hat{\mu}_{eff}+\hat{\mu}\left(\hat{\kappa}_{eff}-1\right)}\frac{R_{eff}^2}{z}\frac{\hat{\sigma}_{yy}^{\infty}+\hat{\sigma}_{xx}^{\infty}}{2} \\
&\quad -\frac{\hat{\mu}-\hat{\mu}_{eff}}{\hat{\mu}+\hat{\kappa}\hat{\mu}_{eff}}\frac{R_{eff}^4}{z^3}\frac{\hat{\sigma}_{yy}^{\infty}-\hat{\sigma}_{xx}^{\infty}-2i\hat{\sigma}_{xy}^{\infty}}{2}+z\frac{\hat{\sigma}_{yy}^{\infty}-\hat{\sigma}_{xx}^{\infty}+2i\hat{\sigma}_{xy}^{\infty}}{2}
\end{aligned} \tag{5.3}$$

It is assumed in the above expressions that the origin of the coordinate system coincides with the center of the inhomogeneity as shown in Fig.5.1d. Using Eq.(3.9), the combinations of the transformed stress components can be expressed as follows:

$$\begin{aligned}
\hat{\sigma}_{xx}+\hat{\sigma}_{yy} &= 2\frac{\hat{\mu}-\hat{\mu}_{eff}}{\hat{\mu}+\hat{\kappa}\hat{\mu}_{eff}}\left(\hat{\sigma}_{yy}^{\infty}-\hat{\sigma}_{xx}^{\infty}\right)\mathrm{Re}\,\frac{R_{eff}^2}{z^2}+\left(\hat{\sigma}_{xx}^{\infty}+\hat{\sigma}_{yy}^{\infty}\right) \\
\hat{\sigma}_{xx}-\hat{\sigma}_{yy}+2i\hat{\sigma}_{xy} &= -\frac{\hat{\mu}-\hat{\mu}_{eff}}{\hat{\mu}+\hat{\kappa}\hat{\mu}_{eff}}\left[2\frac{\overline{z}}{z}-3\frac{R_{eff}^2}{z^2}\right]\frac{R_{eff}^2}{z^2}\left(\hat{\sigma}_{yy}^{\infty}-\hat{\sigma}_{xx}^{\infty}-2i\hat{\sigma}_{xy}^{\infty}\right) \\
&\quad -\frac{\hat{\mu}_{eff}\left(\hat{\kappa}-1\right)-\hat{\mu}\left(\hat{\kappa}_{eff}-1\right)}{2\hat{\mu}_{eff}+\hat{\mu}\left(\hat{\kappa}_{eff}-1\right)}\frac{R_{eff}^2}{z^2}\left(\hat{\sigma}_{yy}^{\infty}+\hat{\sigma}_{xx}^{\infty}\right)+\left(\hat{\sigma}_{yy}^{\infty}-\hat{\sigma}_{xx}^{\infty}+2i\hat{\sigma}_{xy}^{\infty}\right)
\end{aligned} \tag{5.4}$$

5.2.2 Solution for the effective properties in the Laplace domain

Expressions (5.4) can be used to determine the transformed shear modulus $\hat{\mu}_{eff}$ and the Kolosov-Muskhelishvili's parameter $\hat{\kappa}_{eff}$ of the equivalent inhomogeneity (these parameters are, in fact, the s-dependent effective properties of the viscoelastic composite in question). While the right-hand side of Eqs.(5.4) contains two unknown parameters, the s-dependent stresses in the left-hand side are assumed to be known: they are found from the solution of Problem I (see Fig.5.1c). This solution is obtained based on the approaches described in Chapters 3 and 4.

In order to simplify the analysis, it is assumed hereafter that far-field stress is applied only in one direction, e.g. $\sigma_{xx}^{\infty} \neq 0,\ \sigma_{yy}^{\infty} = \sigma_{xy}^{\infty} = 0$. Using the first expression in (5.4), the effective shear modulus is obtained as

$$\hat{\mu}_{eff}(s) = \hat{\mu}(s)\frac{1 + \hat{D}_{xx}(z;s)}{1 - \hat{\kappa}(s)\hat{D}_{xx}(z;s)} \tag{5.5}$$

where

$$\hat{D}_{xx}(z;s) = \frac{1}{2R_{eff}^2 \operatorname{Re} z^{-2}}\left[\frac{\hat{\sigma}_{xx}(z;s) + \hat{\sigma}_{yy}(z;s)}{\hat{\sigma}_{xx}^{\infty}(s)} - 1\right] \tag{5.6}$$

It is seen from Eq.(5.5) that the effective shear modulus is proportional to the shear modulus of the matrix multiplied by another s-dependent function. The second expression in (5.4) can be used to find the effective Kolosov-Muskhelishvili's parameter $\hat{\kappa}_{eff}$. Taking the real part of this expression, one arrives at

$$\begin{aligned} &\frac{\hat{\mu}_{eff}\left(\hat{\kappa} - 1\right) - \hat{\mu}\left(\hat{\kappa}_{eff} - 1\right)}{2\hat{\mu}_{eff} + \hat{\mu}\left(\hat{\kappa}_{eff} - 1\right)} = \\ &= \frac{1}{R_{eff}^2 \operatorname{Re} z^{-2}}\left[\frac{\hat{\sigma}_{xx} - \hat{\sigma}_{yy}}{\hat{\sigma}_{xx}^{\infty}} - 1 - \frac{\hat{\mu} - \hat{\mu}_{eff}}{\hat{\mu} + \hat{\kappa}\hat{\mu}_{eff}} R_{eff}^2 \operatorname{Re}\frac{2\frac{\overline{z}}{z} - 3\frac{R_{eff}^2}{z^2}}{z^2}\right] \end{aligned} \tag{5.7}$$

The obtained expression can be significantly simplified if one can find such point z, for which the following conditions are satisfied:

$$\operatorname{Re}\frac{2z\overline{z} - 3R_{eff}^2}{z^4} = 0 \quad \text{and} \quad \operatorname{Re} z^{-2} \neq 0 \tag{5.8}$$

Two cases are possible: $2z\overline{z} - 3R_{eff}^2 = 2r^2 - 3R_{eff}^2 = 0$ or $\operatorname{Re} z^{-4} = 0$, while $\operatorname{Re} z^{-2} \neq 0$. Here $r = \sqrt{z\overline{z}}$ is the distance from the origin to the point z (see Fig.5.1c). It can be shown that for the first case, the distance at which the stresses have to be calculated is $r = \sqrt{3/2}R_{eff}$. This distance is not large enough in comparison with the size of the representative cluster. The stresses found at such distance are likely to be affected by the internal structure of the cluster. Therefore the second case is considered. The forth power of z is

$$z^4 = x^4 + y^4 - 6x^2y^2 + 4iyx\left(x^2 - y^2\right) \tag{5.9}$$

The expression $\operatorname{Re} z^{-4} = 0$ is satisfied if

$$x^4 + y^4 - 6x^2y^2 = 0 \quad \text{and} \quad x \neq y \tag{5.10}$$

Solving Eq.(5.10), one obtains the following conditions

$$y = \left(\sqrt{2} \pm 1\right) x \tag{5.11}$$

If $x \neq 0$ in Eq.(5.11), then $x \neq y$ and $\operatorname{Re} z^{-2} \neq 0$. Thus, if the stresses are found at the point z whose coordinates satisfy expressions (5.11), then the last term in Eq.(5.7) is zero. Conditions (5.11) are shown graphically in Fig.5.3.

Using the following notation

$$\hat{Q}_{xx}(z;s) = \frac{1}{R_{eff}^2 \operatorname{Re} z^{-2}} \left[\frac{\hat{\sigma}_{xx}(z;s) - \hat{\sigma}_{yy}(z;s)}{\hat{\sigma}_{xx}^{\infty}(s)} - 1 \right] \tag{5.12}$$

and Eq.(5.7), one arrives at the following expression for the transformed effective Kolosov-Muskhelishvili's parameter:

$$\hat{\kappa}_{eff}(s) = 1 + \frac{1 + \hat{D}_{xx}(z;s)}{1 - \hat{\kappa}(s)\hat{D}_{xx}(z;s)} \left[\frac{1 + \hat{\kappa}(s)}{1 + \hat{Q}_{xx}(z;s)} - 2 \right] \tag{5.13}$$

Expressions (5.5) and (5.13) can now be used to find the transverse effective properties of a viscoelastic composite in the Laplace domain.

It is convenient to use two-dimensional moduli for the case of plane problems. The relations between 2D and 3D moduli for plane strain and plane stress elasticity are provided in [42]. Using these relations together with Eqs.(5.5) and (5.13), one arrives at the following expressions for the effective two-dimensional shear and bulk moduli in the Laplace domain:

$$\begin{aligned} \hat{\mu}_{eff}^{2D} &= \hat{\mu} \frac{1 + \hat{D}_{xx}}{1 - \hat{\kappa}\hat{D}_{xx}} \\ \hat{K}_{eff}^{2D} &= 2\hat{\mu} \frac{1 + \hat{Q}_{xx}}{\hat{\kappa} - 1 - 2\hat{Q}_{xx}} \end{aligned} \tag{5.14}$$

Expressions (5.14) are the same for plane strain and plane stress problems if the corresponding plane strain or plane stress parameters ($\hat{\kappa}$, $\hat{D}_{xx}$, and $\hat{Q}_{xx}$) are used.

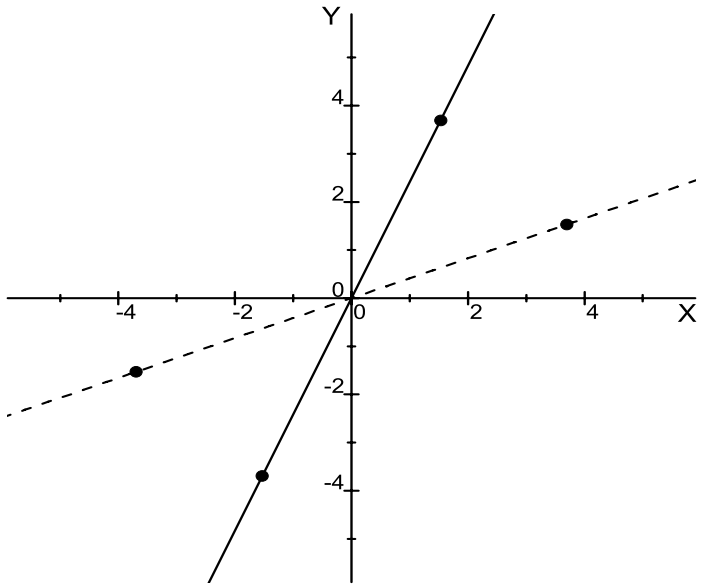

Figure 5.3: The plots of the lines described by Eqs.(5.11). Solid line corresponds to $y = \left(\sqrt{2}+1\right)x$, dashed line to $y = \left(\sqrt{2}-1\right)x$. Four points on the lines represent possible locations where stresses are found.

Note that expressions similar to those presented above can be obtained for other states of stress at infinity, e.g. for σ_{yy}^{∞} or σ_{xy}^{∞}. However, the analysis of these cases has revealed that they do not provide any advantages in comparison with the case presented above.

5.2.3 Solution for the effective properties in the time domain

In order to obtain the effective properties in the time domain, analytical or numerical inversion of the Laplace transform should be applied to the corresponding expressions in the Laplace domain. For the case of porous viscoelastic media, the effective properties can be obtained analytically in most cases (it depends on the complexity of a viscoelastic model that describes the behavior of the matrix). To arrive at the analytical solution, Eqs.(3.30) should be combined with expressions (5.5)-(5.6), (5.12)-(5.13), or (5.14) to

produce a sum of rational s-dependent functions. The rest of the procedure is similar to the calculation of time-dependent fields presented in Section 3.4.4.

In the case of a viscoelastic composite containing elastic inhomogeneities, a procedure of numerical inversion of the Laplace transform has to be adopted. In the present work the technique described in Section 4.4.4 is used.

The effective properties presented in the previous section correspond to the differential representation of viscoelastic constitutive equations. To obtain the integral representation (physical properties), an additional division by the transform parameter s is necessary when calculating the inverse Laplace transform.

Note that the notation for the three-dimensional material properties used hereafter does not include superscript $3D$, while the notation for the two-dimensional properties always includes superscript $2D$.

5.3 Dynamic (complex) effective properties

According to the Hashin's correspondence principle, the effective dynamic moduli of viscoelastic composites can be found directly from the corresponding "elastic" expressions in the Laplace domain (see section 2.2) by substituting the Laplace transform parameter s with the expression $i\omega$, where ω is the circular frequency. Then all transformed viscoelastic moduli of each phase (e.g. $\hat{\mu}(s)$ and $\hat{K}(s)$) and effective moduli are replaced with the corresponding complex moduli (e.g. $\hat{\mu}(s) \rightarrow \mu^*(\omega)$, $\hat{K}(s) \rightarrow K^*(\omega)$). The advantage of using complex moduli is that no Laplace inversion is required.

To illustrate the application of the Hashin's principle for obtaining the effective dynamic moduli, consider a problem of a composite viscoelastic medium under the condition of plane stress. Assume that the composite's matrix is described by the Boltzmann model (Fig.2.4) in shear, and its bulk modulus is constant. Using Eq.(2.47)

and Eq.(2.49), the following complex parameters for the matrix are obtained:

$$\mu^*(\omega) = \frac{E_1 E_2 + i E_1 \eta\omega}{E_1 + E_2 + i\eta\omega} = E_1 \frac{E_2 (E_1 + E_2) + \eta^2\omega^2}{(E_1 + E_2)^2 + \eta^2\omega^2} + i \frac{E_1^2 \eta\omega}{(E_1 + E_2)^2 + \eta^2\omega^2}$$
$$\kappa^*(\omega) = \frac{5}{3} + \frac{8}{9K}\mu^*(\omega) \tag{5.15}$$

These parameters should be used in the expressions for the effective moduli provided in the previous section and also for the calculation of stresses in problem I (Fig.5.1c). In the latter case each component of the stress tensor will be a complex-valued quantity. In order to calculate such stresses, the numerical implementation of the algorithms presented in Chapters 3 and 4 has to be significantly modified. This is due to the fact that one has to separate real and imaginary parts in all the expressions containing complex moduli (5.15) to be able to solve systems of linear equations with the standard methods (e.g. LU decomposition or Gauss-Seidel). Besides, it is important to avoid possible cases when the denominators of the expressions containing complex moduli become negligibly small (or identically zero) upon some combination of material properties and frequency ω. As the calculation of complex stress fields would require major changes in the developed computer codes, the evaluation of the effective dynamic moduli has been left as a subject for future study.

5.4 Error analysis

A few sources of numerical errors can be identified in the proposed methodology for the calculation of the effective properties of composite materials. These errors are related to the accuracy with which the stress components are found at the point z. For the case of porous viscoelastic media, the stresses are calculated semi-analytically, and the errors can be effectively controlled (see Chapter 3). For the case of fiber reinforced composites, the sources of errors are discussed in Chapter 4.

Inaccuracy in calculation of the effective properties may also arise from the following factors. As the proposed methodology for the evaluation of the effective properties

employs the stresses found at a single point, it is important that the representative cluster of a composite material in question possesses a high degree of isotropy. The stress field for an isotropic cluster is radially symmetric at distances far away from the cluster, and the effective properties are independent of the choice of a point at which stresses are found (as long as the coordinates of this point satisfy Eq.(5.11)). In practice however, it may be difficult to achieve a high degree of isotropy for the clusters with random arrangement of inhomogeneities. Due to this factor, it is proposed to calculate stresses in at least four points located symmetrically on the lines (5.11), as shown in Fig.5.3. Then the average between the effective properties corresponding to each of these points can be evaluated.

Expressions (5.1)-(5.2) used for the calculation of the radius of the equivalent inhomogeneity are based on pure geometrical considerations. An alternative way to calculate the radius of equivalent inhomogeneity R_{eff} is to generalize more rigorous procedure described in [105] for elastic composites. In this case, the radius found at zero time moment (when a composite can be treated as an elastic material) can be used for the evaluation of effective properties at all consequent moments of time. This is, however, much more elaborate procedure than the one presented above (cf. Eqs.(5.1)-(5.2)), and requires the knowledge of tractions in multiple points outside the representative cluster. Therefore, the procedure for the evaluation of R_{eff} developed by Mogilevskaya et al. [105] is used in the present work only in few cases, for the area fraction of elastic phase $f \geq 0.8$.

5.5 Results and discussion

5.5.1 Porous viscoelastic media

Several viscoelastic models will be used in this chapter to describe the time-dependent behavior of the matrix of porous media. These models are as follows:

Model A. The three-dimensional shear modulus of the matrix is time-dependent and given by the Boltzmann viscoelastic model (Fig.2.4). The three-dimensional bulk modulus of the matrix is constant. The constitutive equations in the Laplace domain are given by Eqs.(2.43)-(2.47), where

$$E_1 = 8 \times 10^3 \sigma_0, \qquad E_2 = 2 \times 10^3 \sigma_0, \tag{5.16}$$
$$\eta = 5 \times 10^3 \sigma_0 \cdot \sec, \qquad K = 17333.3 \sigma_0$$

and σ_0 serves to normalize all the loads and stresses, $[\sigma_0] = [Pa]$. At zero time, the 3D viscoelastic Poisson's ratio of the matrix $\nu(0) = 0.3$.

Model B. The three-dimensional Young's (relaxation) modulus of the matrix is time-dependent and given by the Boltzmann viscoelastic model (Fig.2.4). The Poisson's ratio of the matrix is assumed to be constant, $\nu = 0.2$. The Young's modulus in the Laplace domain is given by Eq.(2.47), where one should use $\hat{E}(s)$ instead of $\hat{\mu}(s)$. The parameters of the Boltzmann model are defined by Eq.(5.16).

Model C. The parameters for the constitutive model are the same as in model B, except that the Poisson's ratio of the matrix is $\nu = 0.4$.

Model D. The three-dimensional Young's modulus of the matrix is time-dependent and given by the Burgers model (Fig.2.5). The Poisson's ratio is assumed to be constant. The parameters of the Burger's model correspond to ED-6 resin; they were determined by Wang and Weng [134] based on the experimental data provided in [119]. These parameters are as follows:

$$E_1 = 3.27GPa, \qquad E_2 = 1.8GPa,$$
$$\eta_1 = 8000GPa \cdot hr, \qquad \eta_2 = 300GPa \cdot hr \tag{5.17}$$
$$\nu = 0.38$$

The condition of plane stress is assumed for the analysis of porous media.

Time-independent properties

Two important observations about the effective behavior of viscoelastic porous media can be made based on the direct analysis of expressions (5.5)-(5.6) and (5.12)-(5.13).

1) The parameters $\hat{D}_{xx}$ and $\hat{Q}_{xx}$ are time independent, and they are the same as for the corresponding elastic problem,

$$D_{xx}(z) = \frac{1}{2R_{eff}^2 \operatorname{Re} z^{-2}} \left[\frac{\sigma_{xx} + \sigma_{yy}}{\sigma_{xx}^{\infty}} - 1 \right] \tag{5.18}$$

$$Q_{xx}(z) = \frac{1}{R_{eff}^2 \operatorname{Re} z^{-2}} \left[\frac{\sigma_{xx} - \sigma_{yy}}{\sigma_{xx}^{\infty}} - 1 \right]$$

This follows from the fact that the stress in porous media does not depend on the material properties of the medium; the stress fields are statically determined for the case of constant tractions on the boundaries of the medium and at infinity (see Chapter 3).

2) If the Poisson's ratio of viscoelastic porous material is constant, then it follows from Eq.(5.13) and Eq.(2.53) that the effective Poisson's ratio is also constant. It depends only on the geometry of the problem and the Poisson's ratio of the matrix. Similar conclusions can be made regarding the values of ratios $\hat{\mu}_{eff}(s)/\hat{\mu}(s) = \hat{\mu}_{eff}^{2D}(s)/\hat{\mu}(s)$, $\hat{K}_{eff}^{2D}(s)/\hat{\mu}(s)$, and other similar ratios (cf. Eqs.(5.5), (5.14)).

Several other conclusions follow from the analysis of the results of numerical simulations and from their comparison with the results presented by Torquato et al. [126].

3) Torquato et al. [126] showed that, for the case of very high porosity, the effective Poisson's ratio depends only on the structure of the composite, and it is independent on the viscoelastic properties of the matrix. The results of numerical simulations conducted with the use of the present approach support this conclusion. To illustrate this, consider three distinct viscoelastic porous media described by models A-C. The effective 2D Poisson's ratios for these media are provided in Table 5.1 for the cases when porosity $f = 0.5$, $f = 0.7$, and $f = 0.8$. These results were obtained based on the analysis of a porous material with hexagonal arrangement of holes. The representative cluster in all

the cases included 19 holes, and the ratio of the radius of the equivalent inhomogeneity to the distance between the neighboring holes in the representative cluster found from (5.1) was $R_{eff}/d \simeq 2.289$. To achieve improved accuracy, the effective properties were calculated in four points satisfying Eqs.(5.11) and located on the same distance l from the origin of the coordinates, $l = 60d \simeq 26.217R_{eff}$. The average value for the effective moduli then was found.

It is seen from the Table 5.1 that the Poisson's ratio varies with time for model A only (as $K = const$), while it is a constant parameter for models B and C. As it was indicated above, the effective 2D Poisson's ratio does not depend on the properties of the matrix for high values of porosities. Indeed, data presented in Table 5.1 confirm that with the increase of the porosity of the material, the difference between ν_{eff}^{2D} found for models A-C decreases.

Table 5.1: The effective two-dimensional Poisson's ratio ν_{eff}^{2D} of viscoelastic porous media under the condition of plane stress. Capital letters A, B, and C indicate the viscoelastic model.

Time,	$f = 0.5$			$f = 0.7$			$f = 0.8$		
sec	A	B	C	A	B	C	A	B	C
0	0.405			0.61			0.721		
1	0.433			0.619			0.724		
2	0.438	0.384	0.427	0.62	0.604	0.617	0.725	0.718	0.724
3	0.439			0.62			0.725		
4	0.439			0.62			0.725		

Note that the physical limits for 2D plane stress Poisson's ratio of a homogeneous medium are the same as in 3D case, $-1 < \nu^{2D} < 0.5$. However, the upper limit for the effective 2D plane stress Poisson's ratio is 1 for the case of hexagonal arrangement of holes (see, for instance, [129] and references therein, and [42]).

4) Torquato et al. [126] found that for two-dimensional viscoelastic porous media with any porosity, $E_{eff}^{2D}(t)/E(t) = const$, and this ratio depends only on the composite's microstructure. The numerical results obtained with the present approach support this

conclusion. To illustrate this, consider the following example. Assume that the matrix of the first porous viscoelastic plate is described by model A, while the viscoelastic behavior of the matrix of the second plate is given by model B. Other parameters used for the numerical simulation are the same as in the previous example. The effective Young's moduli and the moduli of the matrices are shown in Fig.5.4 for the case $f = 0.25$. The analysis of the data graphically presented in Fig.5.4 reveals that the ratio of the relaxation moduli of the matrices $E_A(t)/E_B(t)$ varies with time. However, ratios $E^{2D}_{eff,A}(t)/E_A(t)$ and $E^{2D}_{eff,B}(t)/E_B(t)$ are virtually the same for all times, $E^{2D}_{eff,A}(t)/E_A(t) = E^{2D}_{eff,B}(t)/E_B(t) \simeq 0.495$. Analogous results have been obtained for other porosities.

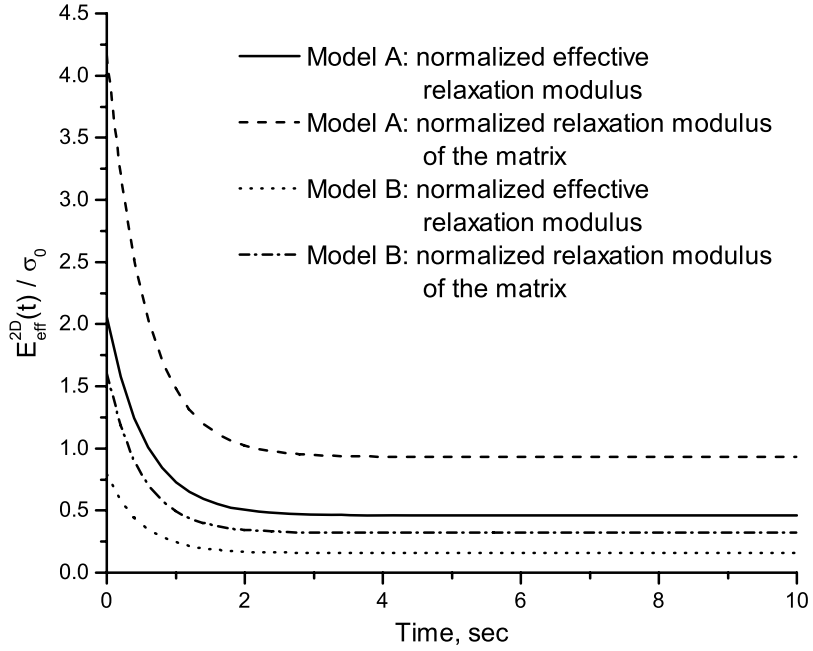

Figure 5.4: The plots of the normalized effective relaxation modulus and the relaxation modulus of the matrix when the matrix is described by models A and B ($f = 0.25$).

Comparison with micromechanical models and bounds

Two examples are considered in this section.

1) The first example studies viscoelastic porous media with time-dependent Poisson's ratio of the matrix. The number of the micromechanical models that can be used in this case to predict the effective viscoelastic moduli is rather limited. One of the most commonly used schemes is that due to Mori and Tanaka [19], [134].

It is assumed that the viscoelastic behavior of the matrix is described by model A. For this model, the expressions for the Mori-Tanaka scheme [134] can be inverted to the time domain analytically. In the present approach, it is assumed that the porous material has a hexagonal arrangement of holes, and the representative cluster consists of 19 holes. The rest of the parameters are the same as in the previous section.

The comparative results for two porosities $f = 0.4$ and $f = 0.8$ are presented in Figs.5.5 and 5.6 (the vertical axis on these figures is given in logarithmic scale). It is seen from the figures that the effective shear modulus obtained by the present approach for porosity $f = 0.4$ is very close to that predicted by the Mori-Tanaka scheme, and the results for the effective bulk modulus are virtually the same in both approaches. With the increase of the porosity to $f = 0.8$, the Mori-Tanaka scheme significantly overpredicts the effective shear modulus and slightly overpredicts the effective bulk modulus. This conclusion follows from the comparison with high-concentration asymptotic results that are obtained for zero time only. These asymptotic results were obtained by Day et al. [36] for the case of elastic sheets containing circular holes, and they are presented by filled circles in Figs.5.5 and 5.6. It follows from Figs.5.5 and 5.6 that the present approach provides the effective moduli that are much closer to the high concentration results. This can be explained by the fact that both of these approaches directly take into account the interaction between the holes, while the Mori-Tanaka scheme does it in an approximate manner.

2) The second example studies viscoelastic porous media with constant Poisson's ratio

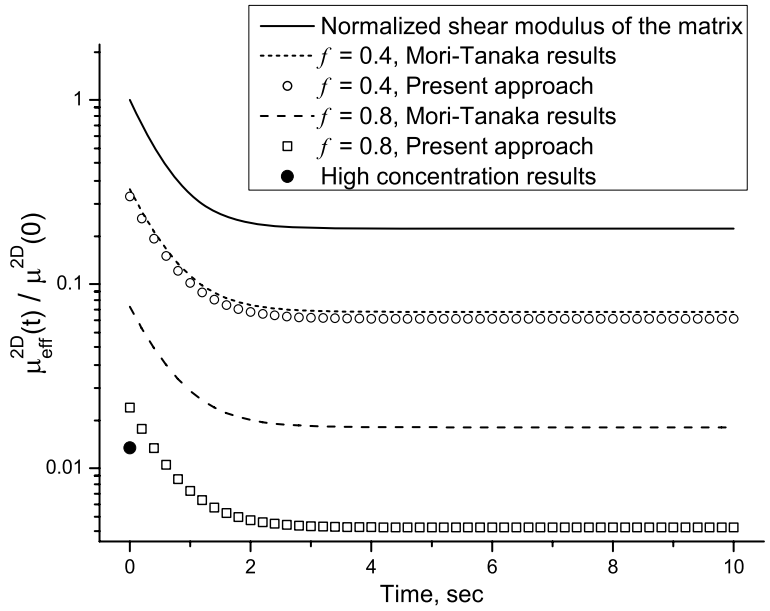

Figure 5.5: The plots of normalized effective plane stress shear moduli for the case when the viscoelastic matrix of is described by model A.

of the matrix. In this case a number of micromechanical models and bounds can be used to predict the effective properties of the porous medium. The Mori-Tanaka scheme, Generalized Self-Consistent method (GSCM), and Hashin-Shtrikman bounds are used in this example for the comparison of the results. Note that the lower Hashin-Shtrikman bound for porous media is trivially zero [54].

It is assumed that the viscoelastic behavior of the matrix is described by model D. The rest of the parameters are the same as in the previous example, except for the porosity, which is now $f = 0.7$. Figure 5.7 illustrates that the results obtained with the present approach lie between the bounds, though they do not coincide with the results from GSCM and the Mori-Tanaka scheme. GSCM underpredicts the effective shear modulus for the case of high porosity, and the results from the Mori-Tanaka scheme coincide with the Hashin-Shtrikman upper bound (this can be shown analytically).

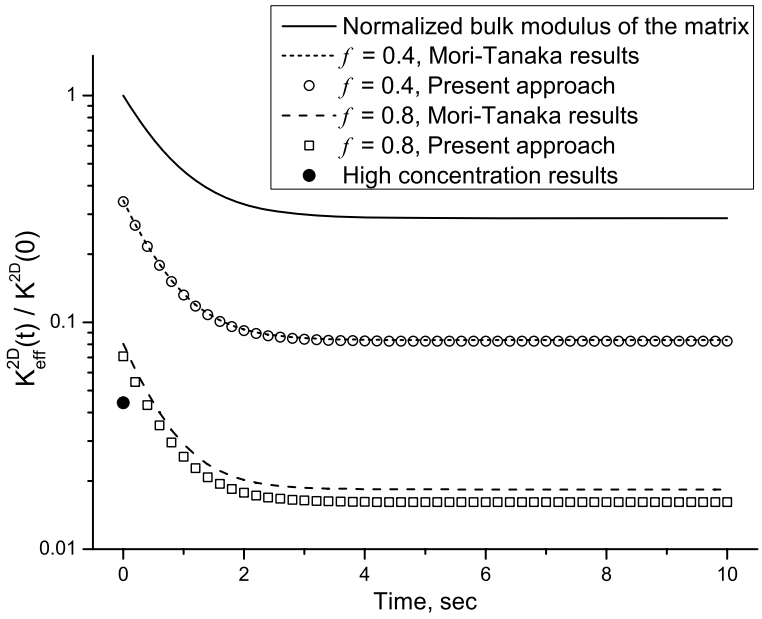

Figure 5.6: The plots of normalized effective plane stress bulk moduli for the case when viscoelastic matrix is described by model A.

Based on the fact that the present approach fully takes into account the interactions between the holes, the results for the time-dependent effective moduli are more accurate than those obtained from other approaches presented in Fig.5.7. Besides, the effective shear modulus found with the present approach is in excellent agreement with the rigorous results[8] presented by Eischen and Torquato[42] for $t = 0$. The results for the effective bulk are not provided as they are proportional to those for the shear modulus.

[8] Note that results in table IX presented in [42] were obtained for $\nu = 0.33$, while $\nu = 0.38$ is used in the present calculations. It was found, however, that this difference in the Poisson's ratios virtually does not affect the results for the effective shear modulus.

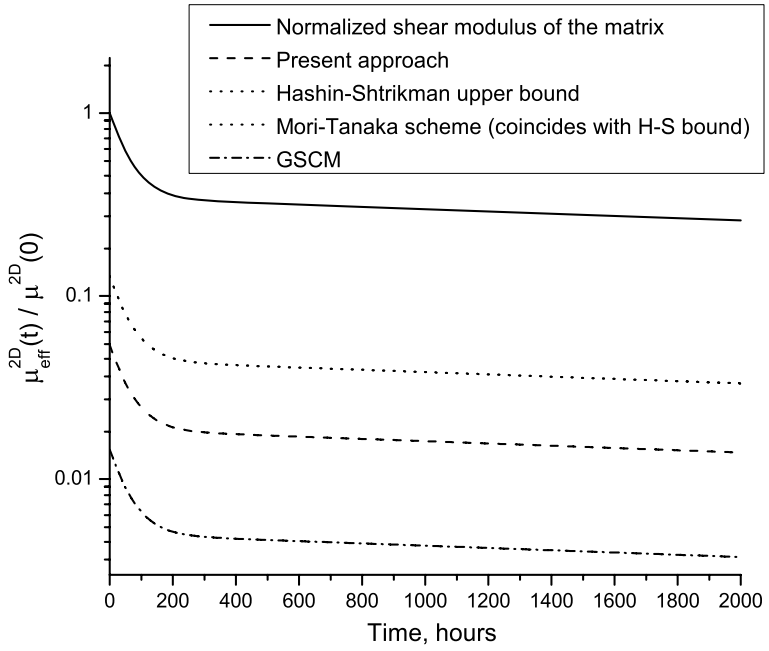

Figure 5.7: The plots of normalized effective plane stress shear moduli obtained from the present approach, GSCM, and Mori-Tanaka scheme, and the upper Hashin-Shtrikman bound (the last two coincide), $f = 0.7$.

Random distribution of holes

It is of interest to estimate the influence of the geometrical arrangement of inhomogeneities in the representative cluster on the effective moduli of a composite material. The concept of equivalent inhomogeneity suggests that the cluster and the arrangement of the inhomogeneities should not affect fields at large distances[9] , as long as the geometry assures overall isotropy.

To illustrate the above statements, consider a viscoelastic porous medium under the condition of plane stress. Two isotropic configurations of holes arrangement are studied: the hexagonal arrangement (Fig.5.8a) and the random one (Fig.5.8b). The

[9] See also discussion about the shape of the representative cluster in [113].

cluster with the hexagonal geometry contains 19 holes, and there are 60 holes in the cluster with random geometry. In order to study the influence of the geometry of the cluster on the effective properties, it is essential that the porosity and the size of the equivalent inhomogeneity are the same for both problems. First, the problem with the random arrangement of holes was solved. It was found that porosity in this problem $f \simeq 0.407$ and the radius of the equivalent inhomogeneity $R_{eff} \simeq 33.85$ (of units from Fig.5.8). Knowing f and R_{eff} and using Eq.(5.1), one can obtain geometric parameters for the problem with the hexagonal arrangement of holes, which in the present case are $R_{inh} \simeq 0.1462 R_{eff}$, $d \simeq 0.437 R_{eff}$. For the both problems presented in Fig.5.8, the material properties of the matrix obey model D.

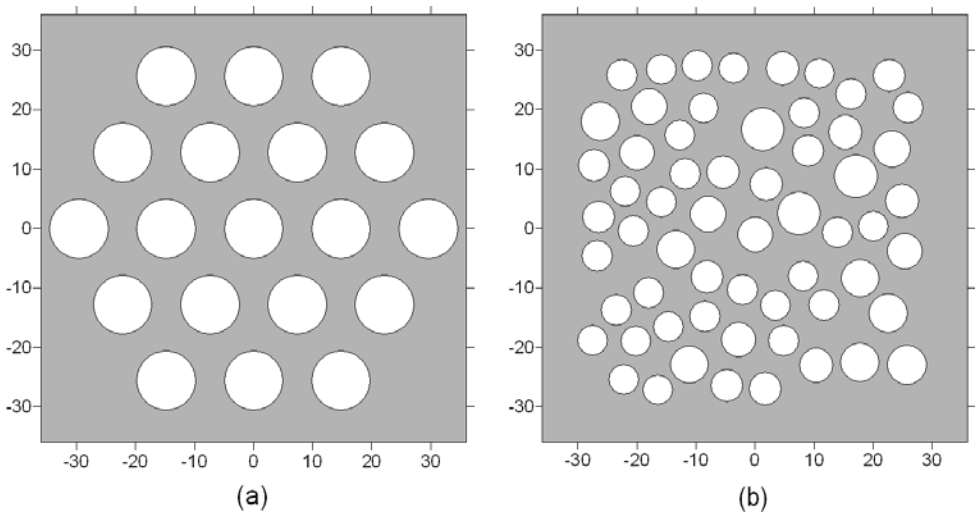

Figure 5.8: Hexagonal (a) and random (b) arrangement of holes in a representative cluster.

The viscoelastic fields were found at the distance of $\sim 50 R_{eff}$. The results for the effective plane stress shear modulus are presented in Fig.5.9. It is seen from the figure that the results from the present approach lie between the Hashin-Shtrikman bounds, though they differ from the predictions of GSCM and the Mori-Tanaka scheme (the

latter coincides with the upper Hashin-Shtrikman bound). However, the comparison of effective shear moduli from the present approach with the rigorous results obtained by Eischen and Torquato [42] for the time $t = 0$ has revealed very good agreement.

An important observation that follows from Fig.5.9 is that the results for the case of hexagonal and random distribution of holes are almost identical. The small difference between these results can be explained by the fact that the random distribution of holes (Fig.5.8b) is not fully isotropic (this may be due to the fact that the representative cluster has a square shape; see discussion in [113] on this topic).

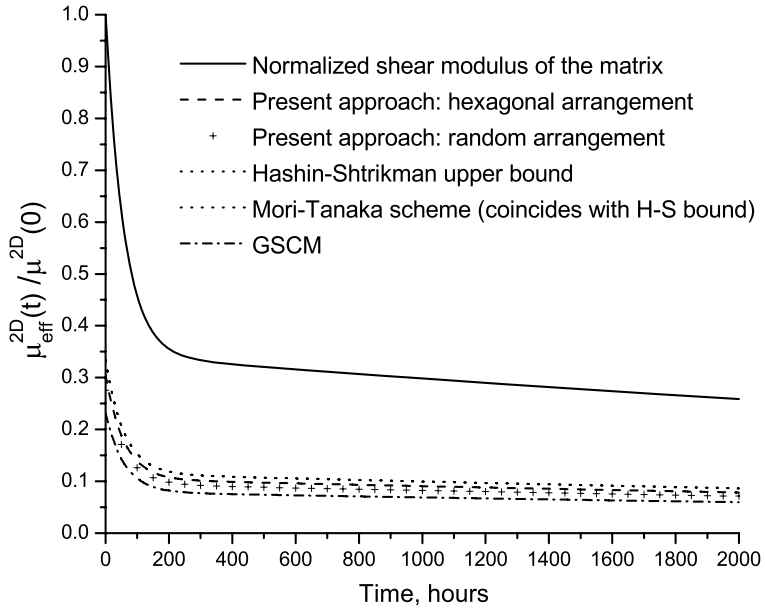

Figure 5.9: A comparison of the normalized 2D shear moduli obtained for the hexagonal and random arrangements of holes with the results from the micromechanical models and bounds ($f = 0.407$).

5.5.2 Fiber-reinforced composites

This section is devoted to the study of the transverse effective properties of viscoelastic composites reinforced by cylindrical elastic fibers, which are aligned in one (axial) direction. The latter fact allows using the assumption of the plane strain to treat the problem. The fibers are arranged in the hexagonal pattern (see Fig.5.1a) in the transverse direction. The matrix is assumed to behave according to the Boltzmann viscoelastic model (Fig.2.4) in shear, and the bulk modulus is considered to be time-independent.

This type of viscoelastic composite was thoroughly studied by DeBotton and Tevet-Deree [37], who reported the results for the longitudinal and transverse effective moduli for two volume fractions: $f = 0.2$ and $f = 0.45$. The authors used for the analysis of the transverse properties the Composite Cylinder model [53] and Hashin-Shtrikman bounds [54] formulated in the Laplace domain. They compared their results with the results from Finite Element simulations obtained with the use of the representative unit cell approach (e.g. [5]) and a time-stepping algorithm. In the present study, the Finite Element data from [37] are used as benchmark results for the estimation of the accuracy of the present approach. To make the comparison possible, the material properties in the following examples correspond to those used in [37]. Plane strain condition is assumed in all the examples. Two cases are considered; they are outlined below.

- **Case of stiff fibers.** The material properties for the Boltzmann model (Fig.2.4) used for characterization of the viscoelastic matrix in shear and the bulk modulus are as follows:

$$E_1 = 1.38GPa, \qquad E_2 = 9.82GPa, \tag{5.19}$$
$$\eta = 2.8MPa \cdot \sec, \qquad K = 5GPa$$

  The material properties of elastic fibers are

$$\mu_{inh} = 30.3GPa, \qquad K_{inh} = 40GPa \tag{5.20}$$

These properties correspond to E-glass fiber reinforced epoxy [37]. Note that the instantaneous shear modulus is $\mu(0) = 1.38GPa$ and the relaxed shear modulus $\mu(\infty) = 1.21GPa$. For the case of the Boltzmann model, the material possesses a single relaxation time, which is $\tau = 0.25 \cdot 10^{-3}$ sec in the present case. This time is used to normalize the time scale for all the results presented below. The area fractions of $f = 0.2$ and $f = 0.45$ are considered.

- **Case of soft fibers.** The parameters of the Boltzmann model (Fig.2.4) and the bulk modulus are as follows:

$$E_1 = 1.38GPa, \qquad E_2 = 3.22GPa, \tag{5.21}$$
$$\eta = 1.15MPa \cdot \text{sec}, \qquad K = 9GPa$$

The material properties of elastic fibers are

$$\mu_{inh} = 0.92GPa, \qquad K_{inh} = 2.25GPa \tag{5.22}$$

The instantaneous shear modulus is $\mu(0) = 1.38GPa$ and the relaxed shear modulus $\mu(\infty) = 0.97GPa$. The relaxation time is the same as in the previous case, $\tau = 0.25 \cdot 10^{-3}$ sec. Area fraction of $f = 0.45$ is considered only.

In the present approach the results were obtained with the use of the representative cluster containing 19 inhomogeneities distributed in hexagonal pattern (as in Fig.5.8a). For $f = 0.2$, the ratios $d/R_{inh} \simeq 4.259$ and $R_{eff}/d \simeq 2.289$. The distance at which the viscoelastic fields were evaluated in the Laplace domain was approximately $50R_{eff}$.

The results obtained by the present approach are compared with the the results of the FE simulations [37] and the Mori-Tanaka scheme predictions in Figs.5.10-5.12. The Mori-Tanaka scheme results are not shown in Fig.5.10 and Fig.5.12 as they coincide with those from the present approach and FE results. The figures show the time variation of the normalized effective shear and plane strain bulk moduli for the case of stiff (Figs.5.10-5.11) and soft (Fig.5.12) fibers. The variation of the shear and bulk moduli of the viscoelastic matrix are also provided on the plots.

One can notice rapid changes in the FE results for the initial moments of time, which can be explained by the fact that the load cannot be applied instantaneously in the viscoelastic finite element analysis; it has to be increased gradually over a number of very short time steps to reach some constant level. This is needed to satisfy the condition of stress and strain free material at $t \leq 0$. For all further moments of time, the plots in Figs.5.10-5.12 reveal remarkable agreement of the results from the present approach with those from the FE simulations. Note that the present results were obtained with the use of a numerical technique of the Laplace inversion (see Chapter 4 for details), and the results on Figs.5.10-5.12 prove that such an approach provides very accurate data for the effective properties.

The plots on Fig.5.13 present the time variation for the normalized effective 2D shear and bulk moduli for the case when area fraction of soft fibers is $f = 0.7$. The results from the present approach are compared with those from the Mori-Tanaka scheme only. No results of the finite element simulations are available for this area fractions. The FE simulations would require very large computational resources for high area fractions of fibers, as very fine meshes have to be used. The present approach does not possess such limitations.

5.6 Summary

This chapter presents the new approach for the calculation of the transverse effective mechanical properties of viscoelastic composite materials. Two types of composites are studied: viscoelastic porous media under the condition of plane stress and fiber reinforced composites under the condition of the plane strain. In the latter case, the fiber are assumed to be elastic. Only composites with isotropic transverse geometry are considered.

The approach is based on the use of the equivalent inhomogeneity technique [105], and it incorporates several major modifications of the technique to accommodate for the

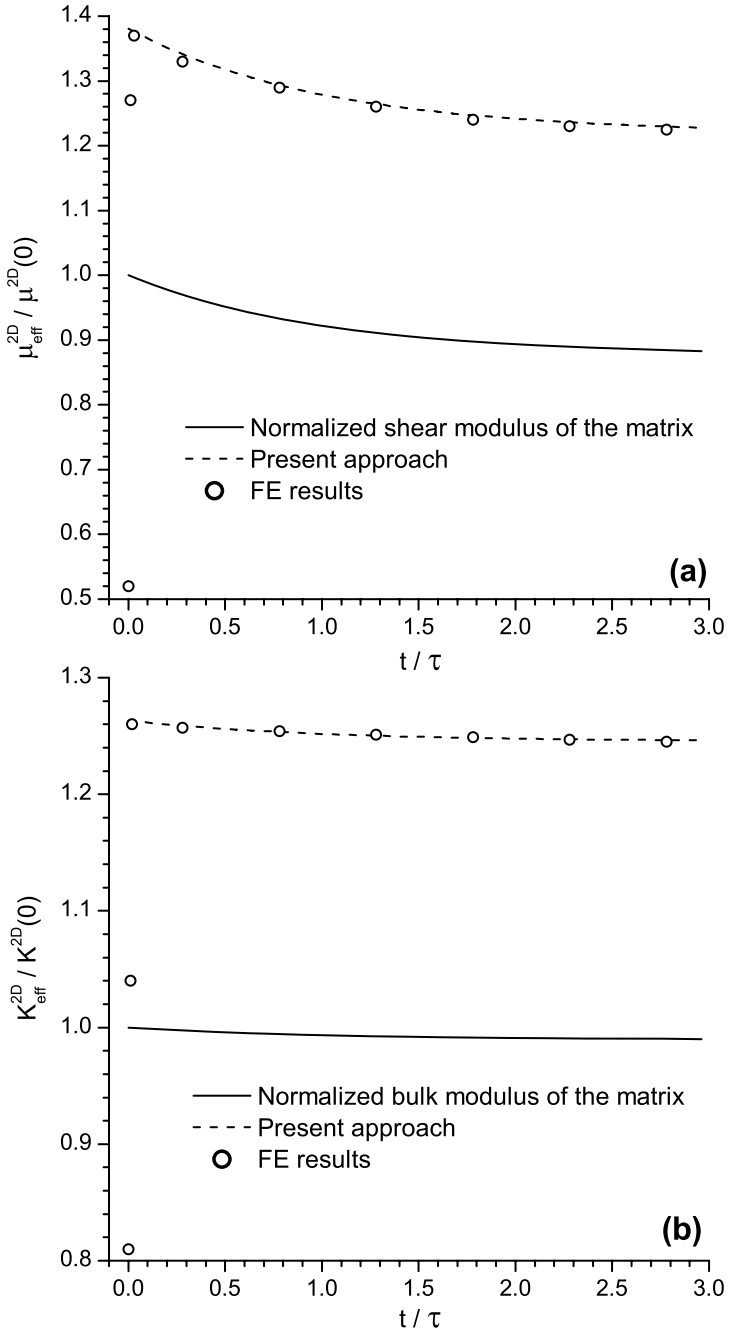

Figure 5.10: The effective plane strain transverse shear (a) and bulk (b) moduli. Finite element (FE) results are taken from [37]. Stiff fibers, $f = 0.2$.

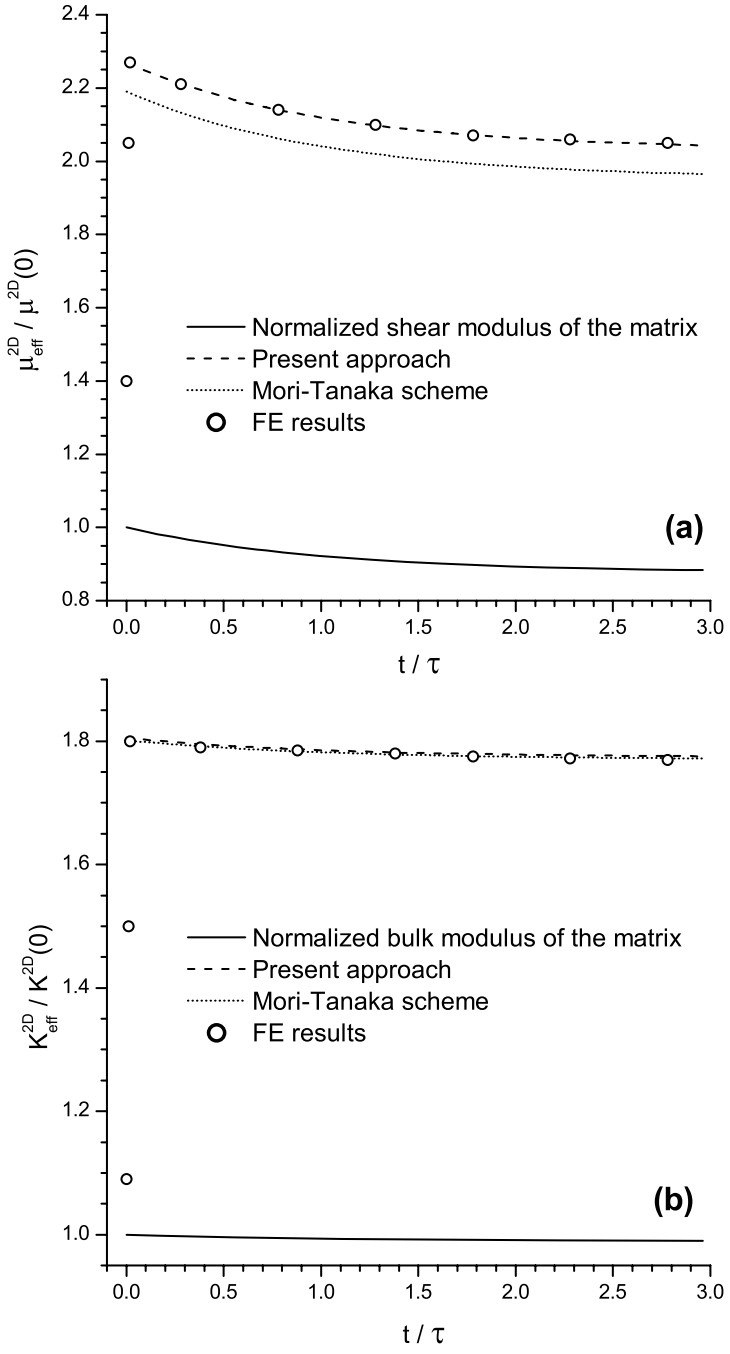

Figure 5.11: The effective plane strain transverse shear (a) and bulk (b) moduli. Finite element (FE) results are taken from [37]. Note that the results from the Mori-Tanaka scheme do not match those from the present approach and the FE results. Stiff fibers, $f = 0.45$.

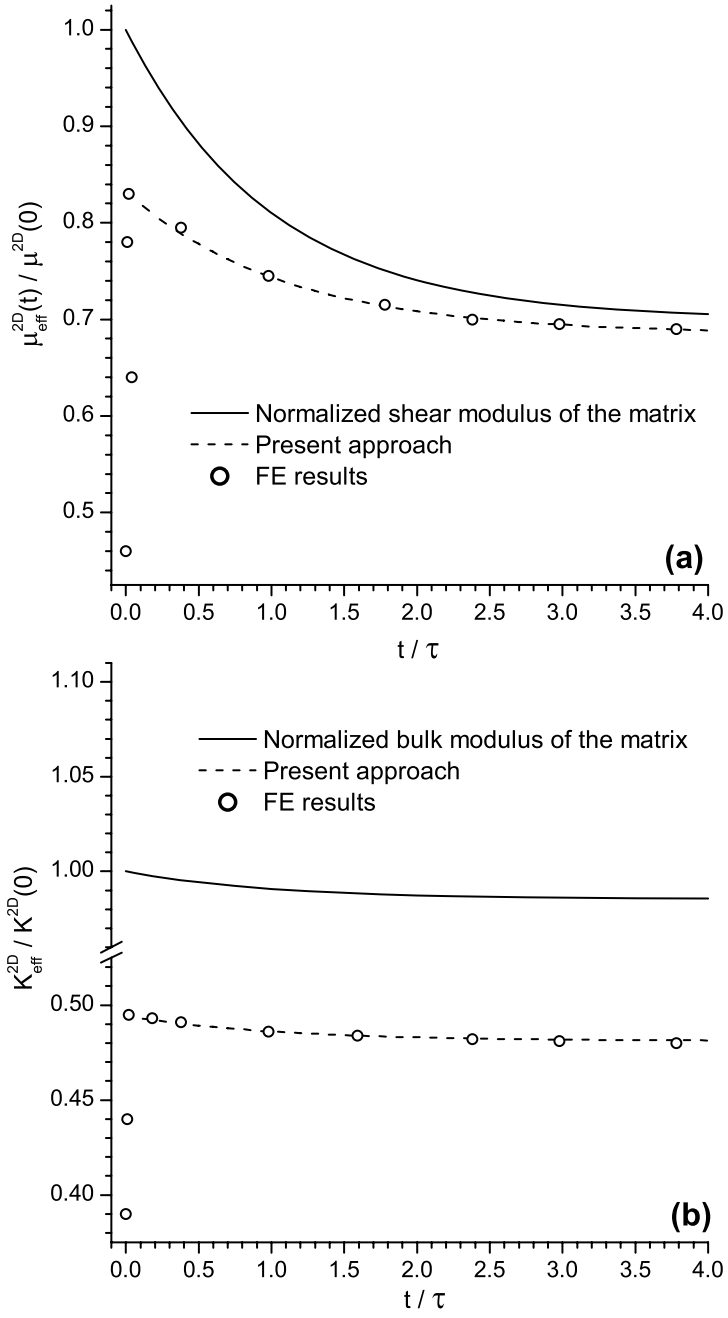

Figure 5.12: The effective plane strain transverse shear (a) and bulk (b) moduli. Finite element (FE) results are taken from [37]. Soft fibers, $f = 0.45$.

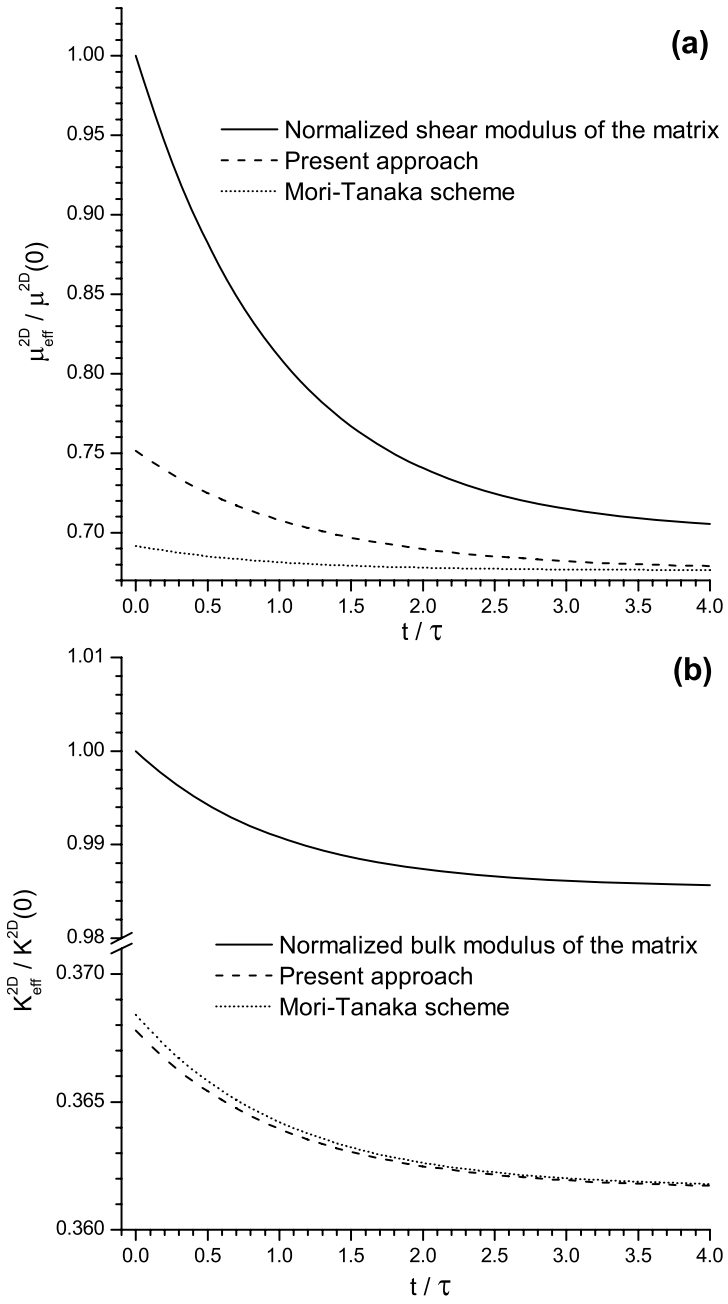

Figure 5.13: The effective plane strain transverse shear (a) and bulk (b) moduli. The comparison is provided with the results from the Mori-Tanaka scheme only. Soft fibers, $f = 0.7$.

viscoelastic behavior of the composite's matrix. The solution for the effective properties is found in the Laplace domain, where the stresses from the representative cluster are matched to the stresses from the single equivalent inhomogeneity. To obtain the effective properties in the time domain, analytical or numerical procedures of the Laplace inversion are used.

A number of numerical examples is considered. The first set of examples is designed to study porous viscoelastic media. Several important conclusions concerned with the time-independent properties of porous materials are presented. It is found that for the case when the viscoelastic matrix of a porous medium possesses constant Poisson's ratio, the effective Poisson's ratio and the ratios of other effective moduli to the corresponding phase moduli are time-independent. These ratios are determined only by the geometrical arrangement of the pores and by the Poisson's ratio of the matrix. This statement is valid for any porosity in the context of the presented approach. Comparison of the results with those from micromechanical models revealed good agreement for small porosities. It was found that for large porosities the present approach provides more accurate data than the Mori-Tanaka scheme and the GSCM.

For the case of fiber-reinforced composites, present results were compared with those from the Mori-Tanaka scheme and the finite element simulations. The latter were obtained with the use of the representative unit cell approach. Remarkable agreement has been found with the results from FE simulations, while a comparison with the results from the Mori-Tanaka scheme revealed some discrepancy in the examples with higher area fractions.

Analyzing the results of the Mori-Tanaka scheme presented in the current work, several conclusion can be made. (i) For the case when the bulk modulus of composite's matrix is constant, the Mori-Tanaka scheme predictions coincide with those from the present approach for area fractions $f \lesssim 0.6$ if material is weakened by holes or soft fibers; (ii) for the same case, the scheme underpredicts the effective moduli starting from the area fraction $f \simeq 0.3$ if material is reinforced by stiff fibers; (iii) for time-varying

bulk modulus (and constant Poisson's ratio) of the matrix, the scheme overpredicts the effective moduli starting from the area fraction $f \simeq 0.3$ if material is weakened by holes.

The results presented in the current work confirm that the developed methodology is simple and accurate; it fully takes into account the interactions between inhomogeneities. Despite the presented technique employs complex boundary integral equations (see Chapter 3 and 4) to obtain viscoelastic stresses in the problem with the representative cluster, it is expected that these stresses can be found by using any other analytical or numerical technique, for example, the Finite Element method. This makes the developed approach more versatile and applicable to larger variety of problems.

Chapter 6

Application of a matrix operator method for thermo-viscoelastic analysis of composite structures

6.1 Introduction

Composite structures consisting of elastic and viscoelastic materials play an important role in today's engineering applications. Such structures are used in various environmental conditions, often involving temperature variations. Due to the effects of thermal expansion and contraction of the materials, it is important to be able to predict the behavior of composite structures subjected to varying temperature. For the case of elastic media, temperature effects can be easily incorporated in the analysis, as material's elastic properties are time- and temperature independent. However, temperature change in viscoelastic media causes changes in material's rheological properties, which makes the analysis of thermo-viscoelastic problems more complex.

Time-temperature superposition (TTS) principle has been widely used to describe the effect of temperature on the mechanical response of thermorheologically simple viscoelastic materials. The principle is outlined in Chapter 2. Among the works based on the use of TTS are the following. Taylor et al. [124] proposed an integration scheme that

was used together with the Prony series approximation of viscoelastic properties to obtain a recursive expression for the solution of thermo-viscoelastic problems at each next time step. Chien and Tzeng [27] considered the problem of a thick laminated composite cylinder under elevated temperature change. The dependency of creep compliances from time was presented in a form of simple power functions that allowed obtaining closed form relations in the Laplace domain and using the analytical Laplace inversion. Ekel'chik et al. [43] studied a problem of a thick-walled orthotropic viscoelastic ring, and the authors applied a procedure of numerical inversion of the Laplace transform after the solution of the corresponding problem was obtained. Review of some other methods of solving quasi-static problems of linear thermo-viscoelasticity is provided in [20].

The aim of this work is to develop a simple and accurate approach for the calculation of thermal stresses and strains in the composite structures consisting from elastic and viscoelastic parts. The study of the time-depending behavior of such structures is of particular interest in the area of pavement engineering. The proposed approach is based on the application of the Volterra correspondence principle (see Section 2.1.6). While this principle is well known and has been applied to the solution of a number of viscoelastic problems (e.g. [11], [72], [114]), its application in the area of asphalt (pavement) engineering is rare. The proposed approach employs a discrete representation of time-varying functions, and the integral operator corresponding to the master relaxation modulus is presented in a matrix form. This technique is similar to the one used by Bažant [11]. However, application of such approach to the study of thermal deformations in viscoelastic asphalt binders is novel. Special attention is devoted to thermal stress development in the binders. If tensile stress in asphalt binders or mixtures exceeds their strength upon cooling, cracking occurs. The importance of the study of low-temperature cracking of asphalt pavements is dictated by the fact that this is one of the dominant distresses occurring in regions with cold climate where temperature variation can be significant over short periods of time.

6.2 Time-temperature superposition

A problem of deformation of viscoelastic media coupled with temperature variation can be treated with the use of a time-temperature superposition principle (see Section 2.1.5). It follows from the principle that real time t in (2.18) has to be substituted by reduced time ζ to account for the change in material's properties with temperature. Constitutive equation (2.18) is then written as

$$\sigma(\zeta) = \int_0^{\zeta} E(\zeta - \zeta') \frac{\partial \varepsilon(\zeta')}{\partial \zeta'} d\zeta' \tag{6.1}$$

where strain $\varepsilon(\zeta) = \varepsilon_{tot}(\zeta) - \varepsilon_{th}(\zeta)$, ε_{tot} results from a given displacement field, and ε_{th} is related to the effect of thermal expansion. For transient temperature conditions, the reduced time is given by (2.39).

Different functions can be adopted to fit the plot for the shift function. Shift function described by WLF equation [137] is often used to describe the behavior of polymers. In the present work, a linear function is adopted to describe the decimal logarithm of the shift factor a_T:

$$\log a_T = C_1 - C_2 T \tag{6.2}$$

where C_1 and C_2 are constants determined through the procedure of least squares fitting. It was found that expression (6.2) provides accurate fitting for the experimental data used in the current study.

Thermal strain ε_{th} is given by

$$\varepsilon_{th} = \alpha \Delta T \tag{6.3}$$

where α is the coefficient of thermal expansion (assumed to be constant) and ΔT is temperature change. For the sake of simplicity, the temperature variation is considered to be linear in time:

$$\Delta T(t) = C_0 t \tag{6.4}$$

where C_0 is the constant temperature rate. Cases of non-linear temperature change can be easily incorporated in the analysis. Temperature at any moment of time t is given

by

$$T = T_0 + \Delta T \tag{6.5}$$

where T_0 is the reference temperature.

Using Eq.(2.39) together with expressions (6.2)-(6.4), one obtains the relation between real time t and reduced time ζ, as well as relations between thermal strain ε_{th} and reduced time ζ. These relations are

$$\zeta(t) = A_1 \left[1 - 10^{C_0 C_2 t}\right], \quad A_1 = -\left[C_0 C_2 10^{(C_1 - C_2 T_0)} \ln 10\right]^{-1} \tag{6.6}$$

$$t(\zeta) = \frac{1}{C_0 C_2} \log(1 - \zeta/A_1) \tag{6.7}$$

$$\varepsilon_{th}(\zeta) = \frac{\alpha}{C_2} \log(1 - \zeta/A_1) \tag{6.8}$$

Due to the fact that the time shift is zero at the reference temperature, $10^{(C_1 - C_2 T_0)} = 1$ in (6.6).

For asphalt binders, the relaxation modulus master curve is obtained using CAM model [91] given by the following equation:

$$E(\zeta) = E_g \left[1 + \left(\frac{\zeta}{t_c}\right)^v\right]^{-w/v} \tag{6.9}$$

where E_g is the glassy modulus, t_c is the cross-over time, and v and w are the parameters of the model, which, in general, are some rational numbers. The CAM model is considered an effective phenomenological model for characterizing the linear viscoelastic behavior of asphalt binders.

6.3 Relaxation operator with varying temperature

The correspondence principles outlined in Section 2.1.6 can be used to solve a problem of thermal stress evolution in viscoelastic composite materials. However, for the case when the CAM model (6.9) is adopted to describe viscoelastic material behavior, its Laplace transform can not be found in a closed form. Another degree of complexity is introduced

by the fact that the Laplace transform of thermal strain described by (6.8) is a complex valued function of parameter s. Based on these observations, it seems impractical to use the elastic-viscoelastic correspondence principle based on the Laplace transform for the analysis of the problem. Therefore, the approach based on the integral operator representation (the Volterra correspondence principle) is adopted in the present work.

Due to the fact that for each value of reduced time ζ one can find the corresponding value of real time t (and vice versa), stress and strain in the reduced time domain can be substituted by their values found for the corresponding real time: $\sigma(\zeta) \equiv \sigma(\zeta(t)) \equiv \sigma(t),\ \varepsilon(\zeta) \equiv \varepsilon(\zeta(t)) \equiv \varepsilon(t)$. Therefore, it is possible to simplify expression (6.1) as follows:

$$\sigma(t) = \int_0^t E(\zeta(t) - \zeta'(\tau)) \cdot \frac{\partial \varepsilon(\tau(\zeta'))}{\partial \tau(\zeta')} \underbrace{\frac{\partial \tau(\zeta')}{\partial \zeta'} \cdot \frac{\partial \zeta'}{\partial \tau(\zeta')}}_{\equiv 1} d\tau(\zeta') =$$

$$= \int_0^t E\left[\zeta(t) - \zeta'(\tau)\right] \frac{\partial \varepsilon(\tau)}{\partial \tau} d\tau \tag{6.10}$$

It is seen that integral (6.10) is now similar to (2.18) with the only difference that the master relaxation modulus is still given in the reduced time domain. This allows using the stress-strain relation in the form

$$\sigma(t) = \tilde{E} \cdot \varepsilon(t) \tag{6.11}$$

where integral operator (relaxation operator) $\tilde{E}$ is defined as

$$\tilde{E} \cdot f(t) \equiv E(0) \cdot \left(f(t) - \frac{1}{E(0)} \int_0^t f(\tau) dE\left[\zeta(t) - \zeta'(\tau)\right] \right) \tag{6.12}$$

6.4 Matrix representation of the relaxation operator

For the analysis of viscoelastic problems considered in the present work, a procedure of numerical solution based on the representation of relaxation operator $\tilde{E}$ given by (6.12) as a matrix operator is adopted.

Consider a discrete set of time moments $t_0, t_1, ..., t_n$; $t_0 = 0$ and $t_n \equiv t$. Strain ε, as well as temperature variation $\Delta T(t)$ are presented as vector-columns $\underline{\varepsilon} \equiv \varepsilon_k = \varepsilon(t_k)$ and $\underline{\Delta T} \equiv \Delta T_k = T(t_k) - T(t_0)$. In order to obtain a matrix representation for integral operator $\tilde{E}$, the trapezoidal rule of numerical integration similar to the one used in [11] is employed. Thus, expression $\sigma = \tilde{E} \cdot \varepsilon$ for each moment of time k can be written as

$$\sigma_k \equiv \left(\tilde{E} \cdot \varepsilon\right)_k = E(0) \cdot \left(\varepsilon_k - \frac{1}{E(0)} \int_0^{t_k} \varepsilon(\tau) dE\left[\zeta(t) - \zeta'(\tau)\right]\right) =$$

$$= E_{k,k}\varepsilon_k - \frac{1}{2}\sum_{i=1}^{k} \left(\varepsilon_i + \varepsilon_{i-1}\right)\left(E_{k,i} - E_{k,i-1}\right) \tag{6.13}$$

where $E_{k,i} \equiv E\left[\zeta(t_k) - \zeta(t_i)\right]$ and $E_{k,k} \equiv E(0)$. Recalling that $\varepsilon_0 \equiv 0$ and rearranging terms in (6.13), the result is a vector-column $\underline{\sigma}$ consisting of terms

$$\sigma_k = \frac{1}{2}\left[\sum_{i=1}^{k-1} \left(E_{k,i-1} - E_{k,i+1}\right)\varepsilon_i + \left(E_{k,k-1} + E_{k,k}\right)\varepsilon_k\right], \; k = 1, ..., n \tag{6.14}$$

or in a matrix form

$$\underline{\sigma} = \underline{\underline{E}} \cdot \underline{\varepsilon} \tag{6.15}$$

Matrix $\underline{\underline{E}}$ is a lower-triangular matrix,

$$\underline{\underline{E}} = \begin{vmatrix} E_{1,0} + E_{1,1} & 0 & 0 & \dots & 0 \\ E_{2,0} - E_{2,2} & E_{2,1} + E_{2,2} & 0 & \dots & 0 \\ E_{3,0} - E_{3,2} & E_{3,1} - E_{3,3} & E_{3,2} + E_{3,3} & \dots & 0 \\ \vdots & \vdots & \vdots & \ddots & \vdots \\ E_{n,0} - E_{n,2} & E_{n,1} - E_{n,3} & E_{n,2} - E_{n,4} & \dots & E_{n,n-1} + E_{n,n} \end{vmatrix} \tag{6.16}$$

and

$$\underline{\varepsilon} = \begin{vmatrix} \varepsilon_1 \\ \varepsilon_2 \\ \vdots \\ \varepsilon_n \end{vmatrix} = \begin{vmatrix} \varepsilon_{tot\ 1} \\ \varepsilon_{tot\ 2} \\ \vdots \\ \varepsilon_{tot\ n} \end{vmatrix} - \alpha \begin{vmatrix} \Delta T_1 \\ \Delta T_2 \\ \vdots \\ \Delta T_n \end{vmatrix} \tag{6.17}$$

The lower-triangular structure of matrix $\underline{\underline{E}}$ represents the history-dependent nature of viscoelastic problems. Thus, it is obvious that for longer time histories the size of matrix

$\underline{\underline{E}}$ grows, which may reduce the efficiency of numerical computations. However, it has been found that for the problems considered in the present study, a relatively small number of subdivisions in the trapezoidal rule is necessary to obtain accurate solution in a large interval of temperatures (e.g. $T = +20°C \div -50°C$).

In general case of a boundary value problem describing an isotropic viscoelastic material, two integral operators are present in the solution. The problem can be simplified greatly, if one assumes that the Poisson's ratio is independent of time and temperature. This allows using only relaxation operator $\tilde{E}$ in the analysis of the problem. The assumption of constant Poisson's ratio is employed in the present work due to the following facts. Experimental data reveal that the Poisson's ratio of viscoelastic asphalt mixtures varies very little at low temperatures, and therefore it can be considered constant [61], [82]. The results of study of asphalt binders presented in [92] indicate that their Poisson's ratio can be reasonably assumed constant at low temperatures. In addition, the results of numerical simulations conducted in the present work also indicate that using constant but different values of the Poisson's ratio within a realistic range has very small effect on the final results. Therefore, the solution for viscoelastic problems can be represented in discrete form as a function of the only matrix operator $\underline{\underline{E}}$ multiplied by a vector of a known time function, e.g.

$$\underline{\sigma} = F\left[\underline{\underline{E}}\right] \cdot \underline{\varepsilon_{tot}} + G\left[\underline{\underline{E}}\right] \cdot \underline{\Delta T} \tag{6.18}$$

where F and G are some functions of matrices. In many cases it is much easier to calculate rational functions of matrices than functions of integral operators.

6.5 Analysis of a viscoelastic restrained bar

Consider a problem of thermal stress evolution in a restrained isotropic homogeneous viscoelastic bar (Fig.6.1). The total strain in this case is zero, and $\varepsilon = -\alpha\Delta T$. The

problem is described by expression (6.10), which is simplified to the following form:

$$\sigma(t) = -\alpha C_0 \int_0^t E(\zeta(t) - \zeta'(\tau))d\tau \tag{6.19}$$

Figure 6.1: Geometry for a problem of a restrained bar.

Due to a simple structure of the integrand in (6.19), it is possible to adopt various techniques of numerical integration to obtain thermal stress in the bar. Comparison of the results of integration with those obtained from (6.15)-(6.17) allows for the evaluation of the accuracy of the present approach.

In the present analysis, parameters corresponding to a modified asphalt binder[10] tested at temperatures $-24°C$, $-30°C$, $-36°C$ are used. These parameters were obtained following the procedure described in Appendix D.1, and they are given in Table 6.1. Tensile stress in the bar caused by temperature drop is determined by the present approach and by applying 24-points Gaussian quadrature technique of numerical integration. The latter technique provides highly accurate results. The application of the Gaussian quadrature for this problem was originally proposed by Voller (see [93]).

The comparative plots are presented in Fig.6.2. It is apparent from Fig.6.2 that both approaches produce virtually identical results. By testing the accuracy of the present method on various asphalt binders described by the CAM model (6.9), it was found that quite accurate results can be obtained for the number of integration points $n \gtrsim 1000$ used in the trapezoidal rule. Results presented in Fig.6.2 are obtained with $n = 2000$.

[10] This binder was modified with styrene-butadiene diblock copolymer (Black Max^{TM}) and produced by Husky Energy (Canada). Binder's performance grade (PG) is PG 64-34 [2]. This binder was tested in the Pavement Laboratory of the Department of Civil Engineering at the University of Minnesota. More information about the properties of this binder can be found in [94].

Table 6.1: Data used in the problem of a restrained bar.

Parameters for the CAM model	Other parameters
$E_g = 3\ GPa$,	$\alpha = 2 \times 10^{-4}\ ^\circ C^{-1}$,
$t_c = 1.04655 \cdot 10^{-6}$ sec,	$C_2 = 0.18562\ ^\circ C^{-1}$,
$v = 0.177585$,	$C_0 = -10\ ^\circ C/hour$,
$w = 0.359506$,	$T_0 = 20\ ^\circ C$.

Note that for longer time histories larger amount of segments in the trapezoidal rule has to be used to obtain accurate results. For the case when the properties of viscoelastic materials can not be described by the CAM model and/or linear shift function, the use of a more accurate integration rule (e.g. Simpson's rule) may be required.

6.6 Analysis of viscoelastic composite cylinder/ring

Consider a problem of a composite cylinder subjected to the uniform temperature variation. The geometry of the problem is given in Fig.6.3. The inner hollow cylinder (inclusion) is assumed to be elastic and the outer (binder) to be linearly viscoelastic. Plane-strain condition is assumed; plane stress solution can be easily obtained by an appropriate substitution of the elastic Young's moduli and Poisson's ratios [9] in the corresponding elastic problem. The assumption of perfect bond between the binder and inclusion is used, and the distribution of circumferential stresses and strains in each cylinder is of primary interest.

In order to obtain the solution of the corresponding elastic problem, it is assumed that the binder is an elastic material with Young's modulus E_b, Poisson's ratio ν_b, and the coefficient of thermal expansion α_b. Material properties of the inner cylinder (inclusion) are denoted as E_i, ν_i and α_i. The elastic solution for the circumferential stresses in the binder can be obtained in the form

$$\sigma_{\theta\theta}^{bind}(r) = \frac{a\,(r)\,E_i + b\,(r)\,E_b}{cE_i + E_b} E_b \Delta T \tag{6.20}$$

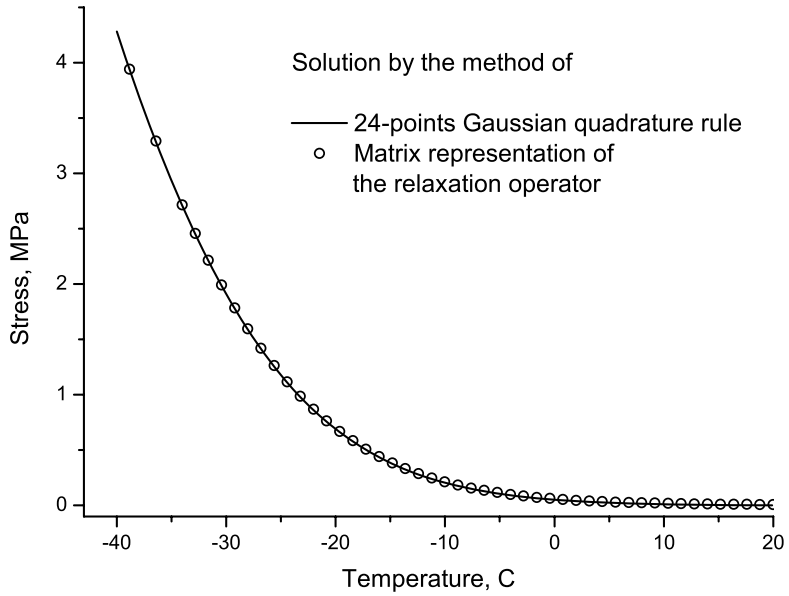

Figure 6.2: Comparison of stresses obtained from Eq.(6.19) with the use of highly-accurate 24-point Gaussian quadrature rule and by the method of matrix representation of the relaxation operator $\tilde{E}$.

where c is a constant and parameters $a(r)$ and $b(r)$ depend on the radius. Expressions for these parameters as well as an outline of the derivation of Eq.(6.20) are given in Appendix D.2.

Assuming that the Poisson's ratio of the binder does not vary with time and temperature, the solution for time-dependent circumferential stresses corresponding to the viscoelastic problem is

$$\underline{\sigma}_{\theta\theta}^{bind}(r;t) = \left[aE_i\underline{\underline{I}} + b\underline{\underline{E_b}}\right] \cdot \left[cE_i\underline{\underline{I}} + \underline{\underline{E_b}}\right]^{-1} \cdot \underline{\underline{E_b}}\ \underline{\Delta T} \tag{6.21}$$

where $\underline{\sigma}_{\theta\theta}^{bind}$ and $\underline{\Delta T}$ are vectors of size n, $\underline{\underline{I}}$ is identity $n \times n$ matrix, and $\underline{\underline{E_b}}$ is $n \times n$ matrix of relaxation functions given by (6.16). It is seen from Eq.(6.21) that the calculation of the inverse of matrix $\underline{\underline{M}} = \left(cE_i\underline{\underline{I}} + \underline{\underline{E_b}}\right)$ is required. This operation can be easily performed as $\underline{\underline{M}}$ is a lower-diagonal matrix.

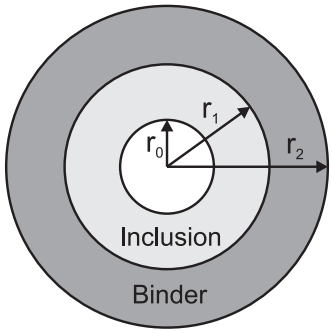

Figure 6.3: Geometry of an axisymmetric problem with a hollow inner part.

The solutions for circumferential strains in the binder and in the inclusion can be obtained in a form similar to (6.21). Particularly, total circumferential strain $\underline{\varepsilon}_{\theta\theta}^{inc}(r)$ in the inclusion is (subscript *tot* is omitted)

$$\underline{\varepsilon}_{\theta\theta}^{inc}(r;t) = \left[\alpha_i F_1\left(r, \underline{\underline{E_b}}\right) + \alpha_b F_2\left(r, \underline{\underline{E_b}}\right)\right] \cdot \underline{\Delta T} \tag{6.22}$$

where matrix functions $F_1\left(r, \underline{\underline{E_b}}\right)$ and $F_2\left(r, \underline{\underline{E_b}}\right)$ are

$$\begin{aligned} F_1\left(r, \underline{\underline{E_b}}\right) &= (1+\nu_i)\,\underline{\underline{I}} - 2\frac{r_1^2}{r^2}\left(1-\nu_i^2\right)\left[d\underline{\underline{I}} + gE_i\left(\underline{\underline{E_b}}\right)^{-1}\right]^{-1} \\ F_2\left(r, \underline{\underline{E_b}}\right) &= 2\frac{r_1^2}{r^2}\left(1-\nu_i\right)\left(1+\nu_b\right)\left[d\underline{\underline{I}} + gE_i\left(\underline{\underline{E_b}}\right)^{-1}\right]^{-1} \end{aligned} \tag{6.23}$$

and constants d and g are given in Appendix D.2.

6.6.1 Comparison with an analytical solution

Calculations presented in the analysis of the bar problem (Section 6.5) were rather simple and did not involve the evaluation of the inverse of operator $\tilde{E}$. To verify the accuracy of the method for more complex geometries, a problem of a composite cylinder presented in Fig.6.3 is considered. The plane strain viscoelastic solution for this problem is given by Eqs.(6.21)-(6.23). The results are compared with an analytical solution obtained by

the application of the Laplace transform. To be able to use the Laplace transform, the expression for the shift factor a_T given by Eq.(6.2) is replaced with the following linear function:

$$a_T^*(T) = C_1^* - C_2^* T \tag{6.24}$$

A superscript star at the quantities means that they have different interpretation than those used previously (cf.(6.2)). Using (6.24) and (6.3), the reduced time is expressed as

$$\zeta = -\frac{1}{C_0^* C_2^*} \ln \left| 1 + \frac{C_2^*(T_0 - T)}{C_1^* - C_2^* T_0} \right| \tag{6.25}$$

and

$$\begin{aligned} t^*(\zeta) &= \frac{C_1^* - C_2^* T_0}{C_0^* C_2^*} \left[1 - \exp(-C_0^* C_2^* \zeta)\right] \\ \Delta T^*(\zeta) &= \left(\frac{C_1^*}{C_2^*} - T_0\right) \left[1 - \exp(-C_0^* C_2^* \zeta)\right] \end{aligned} \tag{6.26}$$

Despite the fact that expressions (6.24)-(6.26) do not have physical interpretation (e.g., $C_1^* - C_2^* T_0 \neq 0$, which follows from Eq.(6.25)), the choice of a linear form for the shift factor (Eq.(6.24)) allows for determining the Laplace transform of $\Delta T^*(\zeta)$:

$$\Delta \hat{T}^*(s) = \left(\frac{C_1^*}{C_2^*} - T_0\right) \frac{C_0^* C_2^*}{s\left(s + C_0^* C_2^*\right)} \tag{6.27}$$

Similarly, the CAM model used for the description of the master relaxation modulus is substituted with a function, for which the Laplace transform can be easily found. A series of several exponents (Prony series) is used instead of representation (6.9):

$$E(\zeta) = \sum_i E_i^* \exp\left(\gamma_i^* \zeta\right) \tag{6.28}$$

$$\hat{E}^*(s) = \sum_i \frac{E_i^*}{s - \gamma_i^*} \tag{6.29}$$

For the illustration purposes it is enough to use only few terms in series (6.28); in the present analysis three terms are adopted.

Parameters C_1^*, C_2^*, E_i^*, and γ_i^* are presented in Table 6.2. Even though these parameters can be chosen arbitrarily for the purpose of comparative analysis, they were

obtained from the least squares fitting of actual functions $a_T(T)$ and $E(\zeta)$. The latter correspond to a modified asphalt binder with PG58-40. Note that it is not essential to have a perfect fitting of experimental data with new functions $a_T^*(T)$ and $E^*(\zeta)$, but rather use the same functions in the solution of the problem by the present approach and with the use of the correspondence principle based on the Laplace transform.

Data given in the second column of Table 6.2 correspond to the parameters of a composite cylinder, which properties and dimensions were taken accordingly to an ABCD specimen described in the details in the next subsection. The specimen consisted of an elastic ring with thickness $r_1 - r_0$, which was surrounded by a viscoelastic binder with thickness $r_2 - r_1$ (see Fig.6.3).

Table 6.2: Data used in the problem of a composite cylinder.

Parameters for $a_T^*(T)$ and $E^*(\zeta)$	Other parameters
$C_1^* = 41.156640$,	$T_0 = 18\ ^\circ C$,
$C_2^* = 2.276346\ ^\circ C^{-1}$,	$C_0 = -1\ ^\circ C/hour$,
$E_0^* = 38.598647\ MPa$,	$\alpha_1 = 1.4 \cdot 10^{-6}\ ^\circ C^{-1}$,
$\gamma_0^* = 0$,	$\alpha_2 = 2 \cdot 10^{-4}\ ^\circ C^{-1}$,
$E_1^* = 349.348243\ MPa$,	$E_1 = 141\ GPa$,
$\gamma_1^* = -0.517286 \cdot 10^9\ \sec^{-1}$,	$\nu_1 = 0.3$,
$E_2^* = 195.939985\ MPa$,	$\nu_2 = 0.33$,
$\gamma_2^* = -0.265315 \cdot 10^8\ \sec^{-1}$,	$r_0 = 23.75 \cdot 10^{-3}\ m$,
$E_3^* = 126.336051\ MPa$,	$r_1 = 25.4 \cdot 10^{-3}\ m$,
$\gamma_3^* = -0.137463 \cdot 10^7\ \sec^{-1}$,	$r_2 = 31.75 \cdot 10^{-3}\ m$.

Figure 6.4 compares the analytical plane strain solution for $\sigma_{\theta\theta}^{bind}(r_1)$ obtained using the Laplace transform with the numerical solution found by the present approach for $n = 2500$. As for the previous problem, the results from the both methods match very well. In this case, the stress rise linearly with the temperature decrease due to the use of the modified shift factor $a_T^*(T)$ that linearly depends on temperature.

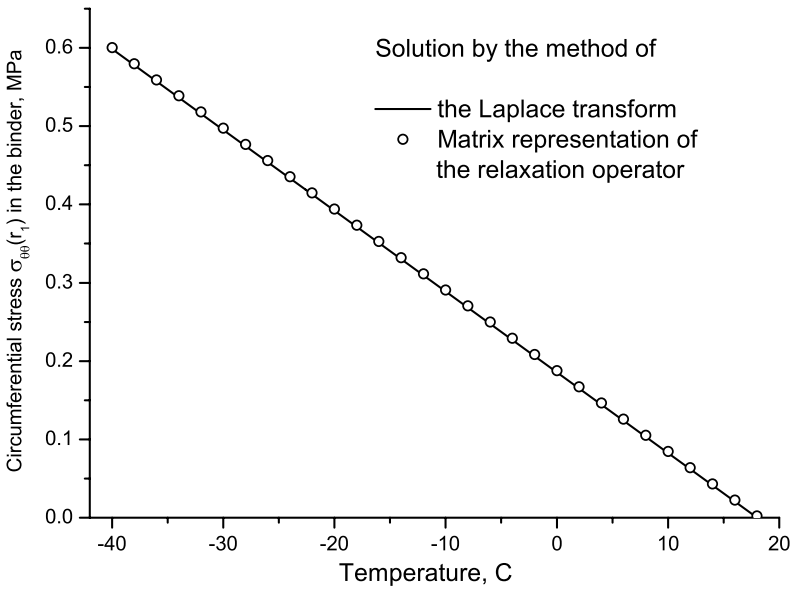

Figure 6.4: Comparison of circumferential stress $\sigma_{\theta\theta}^{bind}(r_1)$ in the composite cylinder problem obtained by using the Laplace transform (analytical solution) and by the method of matrix representation (Eqs.(6.15) - (6.17)) of the relaxation operator $\tilde{E}$ (numerical solution).

6.6.2 Simulation of thermal stresses in Asphalt Binder Cracking Device

This section is devoted to the study of viscoelastic fields evolution in specimens undergoing thermal loading in the Asphalt Binder Cracking Device (ABCD). ABCD was developed by Kim et al. [73], [74] for direct measurements of cracking temperature of asphalt binders. Based on the present approach, it is possible to relate measured strains to time-dependent thermal stresses that cause the cracking of the binder and determine its strength at the cracking temperature.

Schematic representation of the ABCD is given in Fig.6.5, and the description follows. The ABCD consists of a hollow invar (Ni-Fe alloy) ring with a uniform thickness surrounded by a layer of asphalt binder. A silicone mold (not shown in Fig.6.5) is used

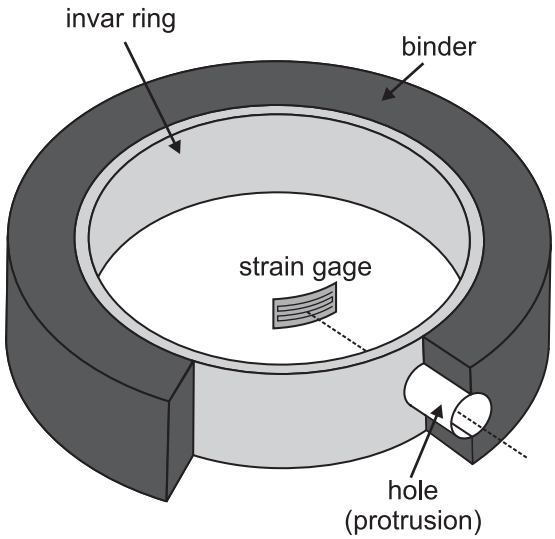

Figure 6.5: An ABCD specimen consisting of an elastic ring surrounded by a viscoelastic binder.

to form asphalt binder into a ring shape. The mold contains a cylindrical protrusion that extends through the thickness of the binder and touches the invar ring. The protrusion is shown as a hole in Fig.6.5. An electrical strain gage is glued on the inner surface of the invar ring across the protrusion. To determine the cracking temperature, a specimen is placed into a temperature chamber, where it is cooled down. Due to the fact that the coefficient of thermal expansion of asphalt binders ($\alpha \sim 2 \cdot 10^{-4}\ ^{\circ}C^{-1}$) is much larger than that for invar ($\alpha = 1.4 \cdot 10^{-6}\ ^{\circ}C^{-1}$), the contraction of the binder is constrained, which causes tensile circumferential stress development in the binder. As a result of cooling, the binder cracks around the hole, where the thickness (in axial direction) is the smallest. At the moment of cracking the accumulated stress is relieved, and this is expressed as a sudden drop in the strain readings by the strain gage. Thus, the cracking temperature of the asphalt binder can be determined as the temperature at which the sudden drop in measured strain occurs.

Despite the fact that the cracking temperature can be easily found from the strain

measurements, the magnitude of tensile stress in the binder that causes cracking, can not be directly determined from the strain gage readings. Using the present approach, it is possible to simulate both circumferential strain on the inner surface of the invar ring and circumferential stress in the binder. The knowledge of such strain-stress relations can provide a simple tool for the determination of the magnitude of tensile circumferential stress in the binder, which causes the cracking. This stress can be referred as the binder's strength at the cracking temperature.

In order to simulate thermal stresses and strains in an ABCD specimen, the model of composite cylinder (Fig.6.3) under the condition of plane stress is used. Circumferential strain at the inner side of the invar ring is given by (6.22), and expression (6.21) is used to calculate circumferential stress in the binder. Material properties corresponding to a modified asphalt binder [11] are used, and they are provided in Table 6.3. The rest of the parameters is given in the second column of Table 6.2. Stress-strain relations obtained for temperature rates $C_0 = -1$ °C/hour and $C_0 = -10$ °C/hour are shown in Fig.6.6. Circumferential stress is found at $r = r_1$ (inner surface of the binder ring) and $r = r_2$ (outer surface of the binder ring). Plots in Fig.6.6 reveal that the magnitude of circumferential stress is higher on the inner surface of the binder ring. Based on this, it is reasonable to conclude that cracking always starts from the inner side of the binder ring. Simulation results also show that at the same strain values, stresses in the binder are larger for the case when the magnitude of temperature rate is larger. This is related to the fact that stress in the binder is not able to fully relax when temperature drops faster. Plots similar to those given in Fig.6.6 can be obtained for any other binders.

The results presented in Fig.6.6 are obtained for the model that does not take into account the presence of the hole in the asphalt binder. To estimate the influence of the hole on the stress/strain fields around it, an elastic finite element (FE) model replicating

[11] This binder was modified with styrene-butadiene-styrene copolymer and produced by Flint Hills (USA). Binder's performance grade (PG) is PG 58-40 [2]. This binder was tested in the Pavement Laboratory of the Department of Civil Engineering at the University of Minnesota. More information about the properties of this binder can be found in [94].

Table 6.3: Data used in the ABCD problem.

Parameters for the CAM model	Other parameters
$E_g = 3\ GPa$,	$T_0 = 18\ ^\circ C$,
$t_c = 148.381583$ sec,	$C_1 = 3.03155$,
$v = 0.11346$,	$C_2 = 0.16842\ ^\circ C^{-1}$.
$w = 3.73643$,	

the geometry of an ABCD specimen was built. The effect of the influence of the hole in viscoelastic case would be qualitatively similar to that in the elastic problem. Full viscoelastic finite element analysis would be beyond the scope of this work, though it is possible to conduct such an analysis.

For the sake of simplicity, the Young's modulus of the binder in FE model was taken constant $E = 3GPa$ (this modulus corresponds to the initial value of the binder's relaxation modulus). Properties of the inner ring and the geometric parameters corresponded to those of actual ABCD specimen (see Table 6.2). The condition of the full bond between the binder and the invar ring was assumed. Due to the symmetry of the problem, only a quarter of the ABCD rings had to be modeled. Two models, one without a hole (Fig.6.7a) and another with a hole in the external ring (Fig.6.7b), were considered. Both models were subjected to temperature change of $\Delta T = -50^\circ C$, and circumferential strain along segment AB in Fig.6.7 was determined. The results of the FE simulations reveal (Fig.6.8) that the magnitude of circumferential strain in the model with a hole (Fig.6.7b) increases significantly at point A. At this location the difference reaches $\sim$55% in comparison with the case when no hole is present in the outer ring. Indeed, the presence of the hole causes stress concentration around it, and the additional stress causes local bending of the invar ring. This suggest that experimental strain measurements conducted across the hole can not be directly used for the calculation of thermal stresses in the binder with the use of the results presented in Fig.6.6. As follows from Fig.6.8, thermal stress may be estimated more accurately if

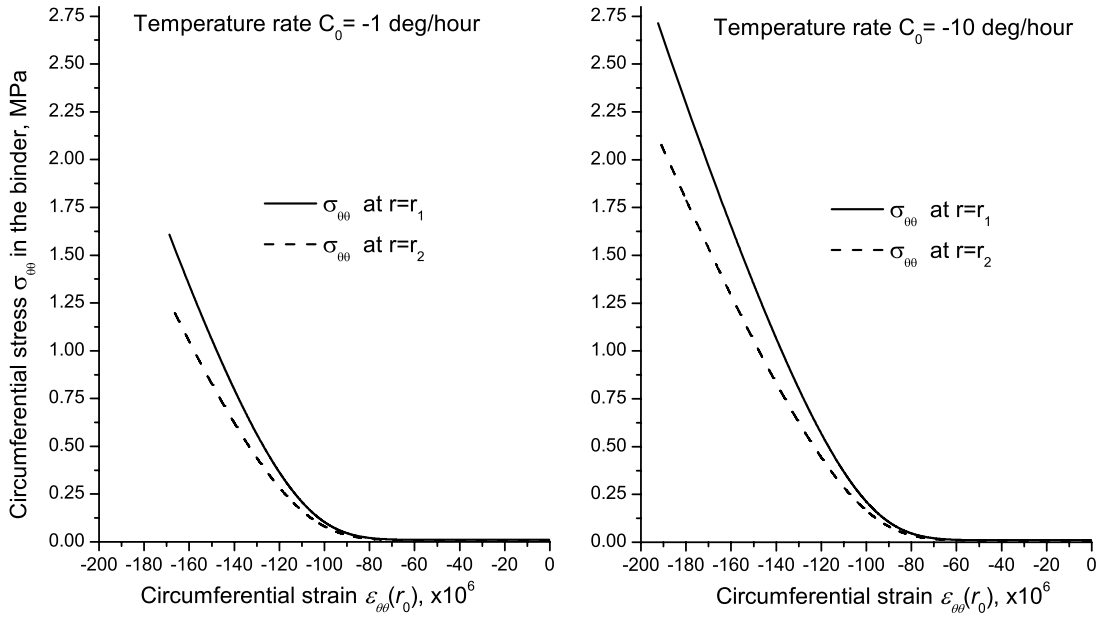

Figure 6.6: Stress-strain curves for strains on the inner surface of the invar ring and stresses in asphalt binder.

strain measurements are conducted at an angle different from 0°. Measurements taken at angles around 120° are likely to provide more accurate results.

In order to be able to fully incorporate the advantages of the present approach for the calculations of thermal stresses in ABCD specimens, a binder ring should be tested without a hole in it. In this case strain measurements can be conducted at any location. Based on this suggestion, it may be concluded that using ABCD (without a hole) together with the present approach may substitute two separate tests, the bending beam rheometer test and the indirect tensile test, which are currently used in asphalt industry for determining thermal stresses in binders, their strength and cracking temperature [3], [4].

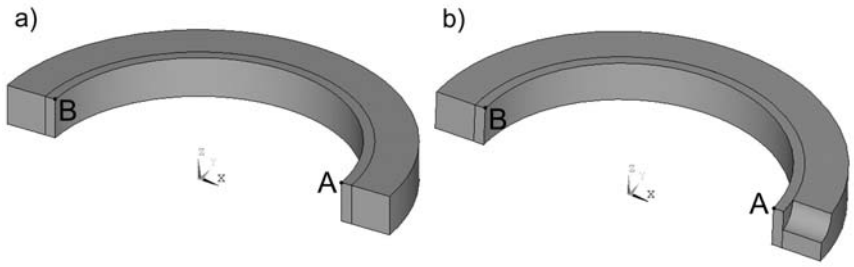

Figure 6.7: Finite element models used for simulations.

6.7 Summary

A problem of thermal stress development in composite structures containing one isotropic linearly viscoelastic phase is considered. The study is particularly devoted to the problems involving viscoelastic asphalt binders, which properties strongly depend on temperature. The ability to determine thermal stresses in asphalt binders and/or mixtures and the knowledge of their strength is critical for the proper design of road pavements. The approach presented in this chapter can be equally useful for the calculation of thermal stresses in other viscoelastic composite structures made of various polymers, resins, etc. for which time-temperature superposition principle is applicable.

The presented approach is based on the use of the Volterra correspondence principle. It is assumed that materials Poisson's ratio does not depend on time and temperature, which allows reducing the number of integral operators to one for the case of isotropic linear viscoelastic material. This assumption is valid for asphalt binders at low temperatures. Incorporating a numerical technique of solution, the integral operator corresponding to the master relaxation modulus is presented in a matrix form. The solution of a problem of viscoelastic composite structures is then reduced to the calculation of functions of matrices; the form of these functions is determined by the corresponding elastic solution.Application of such technique for the analysis of composite structures

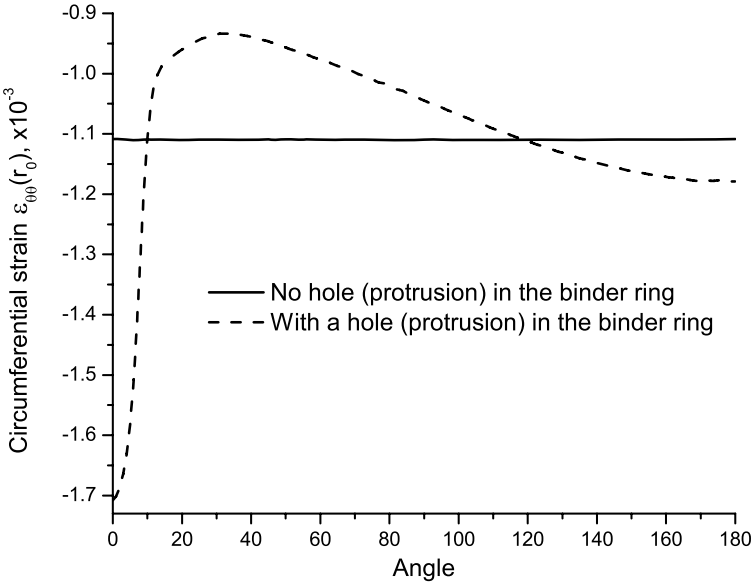

Figure 6.8: Circumferential strain $\varepsilon_{\theta\theta}(r_0)$ along segment AB of the finite element models (Fig.6.7). Angle of 0° corresponds to point A and angle of 180° to point B.

containing asphalt binders is novel.

Several examples are devoted to the estimation of the accuracy of the method. It is shown that for the case when viscoelastic asphalt binders are considered, the integration technique based on the use of the trapezoidal rule provides accurate results. For the case of other viscoelastic materials, it may be necessary to use more accurate integration schemes for the derivation of the matrix representation of the relaxation operator. The last example presents an approach that can be used for the calculation of thermal stresses and binder's strength in the Asphalt Binder Cracking Device. This can be done if proper values of circumferential strain are measured experimentally.

The method can be applied for isotropic viscoelastic problems in which all material properties (e.g. bulk and shear moduli) change with time and temperature. This is due to the fact that integral operators for the case of non-aging viscoelasticity are

commutative between each other (see Section 2.1.6). Composite materials with complex internal structures (e.g. asphalt mixtures) can be treated with the present method, if the effective mechanical and thermal properties are used. The method can also be extended to the problems involving non-uniform temperature distribution (temperature gradient) and heat transfer. However, the application may be limited in the following cases: the solution of the corresponding elastic problem is a transcendental function of elastic properties; viscoelastic media exhibit strong aging effects; time-temperature superposition principle is not applicable.

Chapter 7

Concluding remarks

This dissertation is concerned with the study of micro- and macro-mechanical behavior of viscoelastic composite materials and structures. Three important problems are considered. They are: i) the problem of calculation of time-varying fields in viscoelastic infinite and semi-infinite media containing inhomogeneities and voids, ii) the problem of evaluation of the effective properties of viscoelastic porous and composite materials, and iii) the problem of thermal deformation of viscoelastic composite structures. Several efficient mathematical and computational tools have been developed for the treatment of these problems.

To study the fiber-reinforced composites, a two-dimensional model that represents a cross-section of the composite along the plane perpendicular to the axes of the fibers is employed. It is assumed that this cross-section (an infinite plane) contains randomly distributed, non-overlapping circular holes (cavities) and/or elastic inclusions (fibers), which are perfectly bonded to the bulk material of the matrix. The inhomogeneities are of arbitrary size, and the properties of the elastic inclusions can be different. To extend the class of studied problems, the case of a half-plane is considered. The boundary of the half-plane can be subjected to various loading conditions and far-field stress can act parallel to this boundary. The analysis employs the correspondence principle based on the Laplace transform, and the problem is treated with the use of a direct boundary integral approach. The unknown boundary parameters are approximated by

truncated Fourier series, which allows reducing the original system of integral equations to a system of linear equations containing unknown Fourier coefficients. For the case of a viscoelastic porous medium, the inversion of all the transformed parameters (such as s-dependent stresses, strains, and displacements) to the time domain can be done analytically. The more general case of fiber-reinforced composites requires the use of numerical inversion of the Laplace transform. One of the major features of the developed method is that it can adopt a variety of viscoelastic models. Besides, all the operations of space integration are performed analytically, which enables the method to avoid any computational difficulties and errors inherent to the approaches based on the artificial discretization of a domain and its boundaries. Several numerical examples illustrate the efficiency and accuracy of the method. The comparison with the finite element simulations for some benchmark examples is provided.

One immediate application of the developed approach for the calculation of viscoelastic fields is the evaluation of the effective transverse properties of viscoelastic fiber-reinforced composites and porous materials. The information about the variation of stresses at certain points of the composite's matrix is used in combination with the equivalent inhomogeneity technique to provide the means for the solution of the problem. The latter technique is modified to adopt the case of viscoelastic matrix of a composite. The solution for the effective properties is obtained in the Laplace domain. To arrive at the time-dependent effective moduli, the analytical (in the case of porous media) or numerical (in the case of fiber-reinforced composites) inversion of the Laplace transform is used. The developed approach directly takes into account the interactions between the inhomogeneities enabling one to obtain accurate results in the whole range of area fractions or porosities. Due to the use of the equivalent inhomogeneity technique, the approach does not possess certain difficulties that are often encountered when using the Representative Volume Element or Repetitive Unit Cell techniques (e.g. the necessity to provide complex time-depending boundary conditions). The comparison of the results from the present approach with several benchmark solutions reveals the advantages of

the developed approach.

In various engineering applications it is important to be able to predict the variation of thermal stresses caused by the temperature change in viscoelastic composite materials and structures. These stresses are due to the mismatch between the coefficients of thermal expansion of the composite's constituents. The calculation of stresses, however, is complicated by the fact that the mechanical (and possibly thermal) properties of viscoelastic materials change with time and temperature. The work presented in the final research chapter of this dissertation is aimed to study the thermal stress and strain evolution in composite structures, whose viscoelastic component exhibits rather complex thermo-mechanical behavior. The proposed approach employs the Volterra correspondence principle and relies on the ability to obtain the analytical solution for the corresponding elastic problem. The approach adopts the discrete (matrix) representation of Volterra type operators (e.g. the relaxation operator). The particular attention is devoted to the analysis of thermal stress evolution in viscoelastic asphalt binders at low temperatures. To illustrate the application of the proposed approach, the problems of a composite ring and composite cylinder are analyzed. The approach, however, is not limited to these geometries, and the presented analysis sets the basis for further study of the materials with more complex structure.

References

[1] *Les 4 pages de la DGCIS*, 158(2002). ISSN: 1241-1515; http://www.insee.fr/sessi////4pages/pdf/4p158anglais.pdf

[2] American Association of State Highway and Transportation Officials (AASHTO) Designation M320-05, *Standard specification for performance graded asphalt binder*. Standard specifications for transportation materials and methods of sampling and testing, 29th Ed., Washington, D.C., 2008.

[3] American Association of State Highway and Transportation Officials (AASHTO) Designation T314-07, *Standard method of test for determining the fracture properties of asphalt binder in direct tension (DT)*. Standard specifications for transportation materials and methods of sampling and testing, 29th Ed., Washington, D.C., 2008.

[4] American Association of State Highway and Transportation Officials (AASHTO) Standard T 313-08, *Standard method of test for determining the flexural creep stiffness of asphalt binder using the bending beam rheometer (BBR)*. Standard specifications for transportation materials and methods of sampling and testing, 29th Ed., Washington, D.C., 2008.

[5] Achenbach JD, Zhu H, *Effect of interphases on micro and macromechanical behavior of hexagonal-array fiber composites*. Transactions of ASME 57:(1990), pp.956-963.

[6] Agarwal BD, Broutman LJ, Chandrashekhara K, *Analysis and performance of fiber composites*. 3d Ed. John Willey and Sons, New Jersey, 2006.

[7] Arutyunyan NK, Zevin AA, *Design of structures considering creep*. A.A. Balkema, Brookfield, VT, 1997.

[8] Banerjee PK, Butterfield R, *Boundary Element methods in engineering science*. McGraw-Hill, UK, 1981.

[9] Barber JR, *Elasticity*. Kluwer Academic Publishers, Dordrecht / Boston / London, 2002.

[10] Batchelor GK, *An Introduction to fluid dynamics*. Cambridge University Press, Cambridge, UK, 1967.

[11] Bažant ZP, *Numerical determination of long-range stress history from strain history in concrete*. Materials and Structures, 5:3(1972), pp.135-141.

[12] Becker AA, *The Boundary Element method in engineering: A complete course*. McGraw-Hill, UK, 1992.

[13] Beran MJ, *Statistical continuum theories*. Willey, New York, 1968.

[14] Bischoff JR, Catsiff E, Tobolsky AV, *Elastoviscous properties of amorphous polymers in the transition region - I*. Journal of American Chemical Society, 74(1952), pp.3378-3381

[15] Boltzmann L, *Zur theorie der elastischen nachwirkung*. Pogg. Ann. Phys. Chem., 7(1876), p.624.

[16] Brebia CA, Telles JCF, *Wrobel LC, Boundary element techniques: Theory and applications in engineering*. Springer, Berlin, 1984.

[17] Brinson LC, Knauss WG, *Thermorheologically complex behavior of multi-phase viscoelastic materials*. Journal of Mechanics and Physics of Solids, 39:7(1991), pp.859-880.

[18] Brinson LC, Knauss WG, *Finite element analysis of multiphase viscoelastic solids*. Journal of Applied Mechanics, 59:4(1992), pp.730-737.

[19] Brinson LC, Lin WS, *Comparison of micromechanics methods for effective properties of multiphase viscoelastic composites*. Composite Structures, 41(1998), pp.353-367.

[20] Bykov DL, Il'yushin AA, Ogibalov P.M, Pobedrya BE, *Some fundamental problems of the theory of thermoviscoelasticity*. Mechanics of Composite Materials, 7:1(1971), pp.36-49.

[21] Callias CJ, Markenscoff X, *Singular asymptotics analysis for the singularity at a hole near a boundary*. Quarterly of Applied Mathematics, XLVII:2(1989), pp.233-245.

[22] Carini A, Diligenti M, Maier G, *Boundary integral equation analysis in linear viscoelasticity: variational and saddle point formulations*. Computational Mechanics, 8:2(1991), pp.87-98.

[23] Catsiff E, Tobolsky AV, *Stress relaxation of polyisobutylene in the transition region (1,2)*. Journal of Colloid Science, 10(1955), pp.375-392.

[24] Chen CH, Chang YH, Cheng CH, *Micromechanics and creep behavior of fiber-reinforced polyether-ether-ketone composites*. Journal of Composite Materials, 29:3(1995), pp.359-371.

[25] Cheng A, Sidauruk P, Abousleiman Y, *Approximate inversion of the Laplace transform*. The Mathematical Journal, 4:2(1994), pp.76-82.

[26] Cheng AHD, Cheng DT, *Heritage and early history of the Boundary Element method*. Engineering Analysis with Boundary Elements, 29(2005), pp.268-302.

[27] Chien LS, Tzeng ZJ, *A thermal viscoelastic analysis for thick-walled composite cylinders*. Journal of Composite Materials, 29:4(1995), pp.525-548.

[28] Chou PC, Pagano NJ, *Elasticity: tensor, dyadic, and engineering approaches*. Dover, New York, 1992.

[29] Christensen RM, *Theory of viscoelasticity*. Academic Press, New York & London, 1971.

[30] Christensen RM, *Mechanics of Composite Materials*. New York:Wiley and Sons, Inc., 1979.

[31] Christensen RM, Lo KH, *Solution for effective shear properties in three-phase sphere and cylinder models*. Journal of Mechanics and Physics of Solids, 27(1979), pp.315-330. Erratum 34, p.639.

[32] Crouch SL, Starfield AM, *Boundary Element methods in solid mechanics*. George Allen & Unwin, London, 1983.

[33] Crouch SL, Mogilevskaya SG, *On the use of Somigliana's formula and Fourier series for elasticity problems with circular boundaries*. International Journal for Numerical Methods in Engineering, 58(2003), pp.537-578.

[34] Dally JW, Riley WF, *Experimental stress analysis*. College House Enterprises, LLC, Knoxville, TN, 2005.

[35] Davies B, Martin B, *Numerical inversion of the Laplace transform: a survey and comparison of methods*. Journal of Computational Physics, 33(1979), pp.1-32.

[36] Day AR, Snyder KA, Garboczi EJ, *The elastic moduli of a sheet containing circular holes*. Journal of Mechanics and Physics of Solids, 40:5(1992), pp.1031-1051.

[37] DeBotton G, Tevet-Deree L, *The response of a fiber reinforced composite with a viscoelastic matrix phase*. Journal of Composite Materials, 38:14(2004), pp.1255-1277.

[38] Dejoie A, Mogilevskaya SG, Crouch SL, *A boundary integral method for multiple circular holes in an elastic half-plane*. Engineering Analysis with Boundary Elements, 30(2006), pp.450-464.

[39] Doutres O, Dauchez N, *Characterisation of porous materials viscoelastic properties involving the vibroacoustical behaviour of coated panels*. Proceedings of the Symposium on the Acoustics of Poro-Elastic Materials (SAPEM), Lyon, France, 2005.

[40] Duan ZP, Kienzler R, Herrmann G, *An integral equation method and its application to defect mechanics*. Journal of the Mechanics and Physics of Solids, 34:6(1986), pp.539-561.

[41] Dub SN, Trunov ML, *Determination of viscoelastic material parameters by step-loading nanoindentation*. Journal of Physics D: Applied Physics, 41(2008), pp.1-6.

[42] Eischen JW, Torquato S, *Determining elastic behavior of composites by the Boundary Element method*. Journal of Applied Physics, 74:1(1993), pp.159-170.

[43] Ekel'chik VS, Konovalova LV, Ryabov VM, *Use of the Laplace transform to calculate temperature stresses in viscoelastic bodies during uniform cooling*. Mechanics of Composite Materials, 29:5(1994), pp.516-519.

[44] Eshelby JD, *The determination of the elastic field of an ellipsoidal inclusion and related problems*. Proceedings of the Royal Society of London A, 241(1957), pp.376-396.

[45] Eshelby JD, *The elastic field outside an ellipsoidal inclusion*. Proceedings of the Royal Society of London A, 252(1959), pp.561-569.

[46] Ferry JD, *Viscoelastic properties of polymers*. 2nd Ed., Willey, New York, 1961.

[47] Findley WN, Lai JS, Onaran K, *Creep and relaxation of nonlinear viscoelastic materials*. North-Holland Series in Applied Mathematics and Mechanics 18, North-Holland, Amsterdam, 1976. Reprinted: Dover, New York, 1989.

[48] Gay D, Hoa SV, Tsai SW, *Composite Materials: Design and Applications*. CRC press, Boca Raton, 2002.

[49] Golub GH, Van Loan CF, *Matrix computations*. 3d Ed., The John Hopkins University Press, Baltimore, MD, 1996.

[50] Göransson P, *Acoustic and vibrational damping in porous solids*. Philosophical Transactions of the Royal Society A, 364:1838(2006), pp.89-108.

[51] Greengard L, Rokhlin V, *A fast algortihm for particle simulations*. Journal of Computational Physics, 73(1987), pp.325-348.

[52] Hashin Z, Shtrikman S, *A variational approach to the theory of the elastic behavior of multiphase materials*. Journal of Mechanics and Physics of Solids, 11(1963), pp.127-140.

[53] Hashin Z, Rozen BW, *The elastic moduli of fibre-reinforced materials*. Journal of Applied Mechanics, 31(1964), pp.223-232.

[54] Hashin Z, *On elastic behavior of fibre reinforced materials of arbitrary transverse phase geometry*. Journal of Mechanics and Physics of Solids, 13(1965), pp.119-134.

[55] Hashin Z, *Viscoelastic behavior of heterogeneous media*. Journal of Applied Mechanics, 32(1965), pp.630-636.

[56] Hashin Z, *Viscoelastic fiber reinforced materials*. AIAA Journal, 4(1966), pp.1411-1417.

[57] Hashin Z, *Complex moduli of viscoelastic composites - I. General theory and application to particulate composites*. International Journal of Solids and Structures, 6(1970), pp.539-552.

[58] Hashin Z, *Analysis of composite materials*. Journal of Applied Mechanics, 50(1983), pp.481-505.

[59] Helsing J, Peters G, *Integral equation methods and numerical solutions of crack and inclusion problems in planar elastostatics*. SIAM Jounal on Applied Mathematics, 59(1999), pp.965-982.

[60] Hopkins IL, Hamming RW, *On creep and relaxation*. Journal of Applied Physics, 28:8(1957), pp.906-909.

[61] Huang YH, *Pavement analysis and design*. Englewood Cliffs, NJ: Prentice-Hall, 1993.

[62] Huang Y, Crouch SL, Mogilevskaya SG, *A time domain bounary integral method for a viscoelastic plane with circular holes and inclusions*. Engineering Analysis with Boundary Elements, 29:7(2005), pp.725-737.

[63] Huang Y, Crouch SL, Mogilevskaya SG, *Direct boundary integral procedure for a Boltzmann viscoelastic plane with circular holes and elastic inclusions*. Computational Mechanics 37(2005), pp.110-118.

[64] Huang Y, *Computational modeling of viscoelastic composite and porous materials*. PhD Thesis, University of Minnesota (Minneapolis, MN, USA), 2006

[65] Huang Y, Mogilevskaya SG, Crouch SL, *Semi-analytical solution for a viscoelastic plane containing multiple circular holes*. Journal of Mechanics of Materials and Structures, 1:3(2006), pp.101-131.

[66] Huang Y, Mogilevskaya SG, Crouch SL, *Complex variable boundary integral method for linear viscoelasticity. Part I - basic formulation*. Engineering Analysis with Boundary Elements, 30(2006), pp.1049-1056.

[67] Huang Y, Mogilevskaya SG, Crouch SL, *Numerical modeling of micro- and macro-behavior of viscoelastic porous materials*.Computational Mechanics, 41(2008), pp.797-816.

[68] Johnson KL, *Contact mechanics*. Cambridge University Press, Cambridge, UK, 1985.

[69] Kaloerov SA, Mironenko AB, *Analyzing the viscoelastic state of a plate with elliptic or linear elastic inclusions*. International Applied Mechanics, 43:2(2007), pp.198-208.

[70] Kaminskii AA, Zatula NI, Dyakon VN, *Investigation of the stress-strain state of viscoelastic piecewise-homogeneous bodies by the method of boundary integral equations*. Mechanics of Composite Materials, 38:3(2002), pp.209-214.

[71] Kaminskii AA, Selivanov MF, *A method for determining the viscoelastic characteristics of composites*. International Applied Mechanics, 41:5(2005), pp.469-480.

[72] Khazanovich L, *The elastic-viscoelastic correspondence principle for non-homogeneous materials with time translation non-invariant properties*. International Journal of Solids and Structures, 45:17(2008), pp.4739-4747.

[73] Kim SS, *Direct measurement of asphalt binder thermal cracking*. Journal of Materials in Civil Engineering, 17:6(2005), pp.632-639.

[74] Kim SS, Wysong ZD, Kovach J, *Low-temperature thermal cracking of asphalt binder by asphalt binder cracking device*. Transportation Research Record: Journal of the Transportation Research Board, 1962(2005), pp.28-35.

[75] Kolosov GV, *On an application of complex function theory to a plane problem of mathematical theory of elasticity*. Doctoral dissertation, University of Dorpat (Yur'ev), 1909 [In Russian].

[76] Kumar U, *Computer-aided numerical inversion of Laplace transform*. Active and Passive Electronic Components, 22(2000), pp.189-213.

[77] Kushch VI, Shmegera SV, Buryachenko VA, *Elastic equilibrium of a half plane containing a finite array of elliptic inclusions*. International Journal of Solids and Structures, 43(2006), pp.3459-3483.

[78] Lahellec N, Suquet P, *Effective behavior of linear viscoelastic composties: A time-integration approach*. International Journal of Solids and Structures, 44(2007), pp.507-529.

[79] Laws N, McLaughlin JR, *Self-consistent estimates for the viscoelastic creep compliences of composite materials*. Proceedings of the Royal Society, London, 39(1978), pp.627-649.

[80] Lee EH, *Viscoelasticity*. In Handbook of Engineering Mechanics (Editor: Flügge W), McGraw-Hill, New York, 1962.

[81] Legros B, Mogilevskaya SG, Crouch SL, *A boundary integral method for multiple circular inclusions in an elastic half-plane*. Engineering Analysis with Boundary Elements, 28(2004), pp.1083-1098.

[82] Levenberg E, Uzan J, *Uniqueness of the viscoelastic time-function for asphalt-aggregate mixes*. In: Proceedings of the International conference on advanced characterization of pavement and soil engineering (Editors: Loizos A, Scarpas T, Al-Quadi AL), Athens, Greece, 2007, pp.35-48.

[83] Lévesque M, Gilchrist MD, Bouleau N, Derrien K, Baptiste D, *Numerical inversion of the Laplace-Carson transform applied to homogenization of randomly reinforced linear viscoelastic media*. Computational Mechanics, 40(2007), pp.771-789.

[84] Levin V, Sevostianov I, *Micromechanical modeling of the effective viscoelastic properties of inhomogeneous materials using fraction-exponential operators*. International Journal of Fracture, 134(2005), pp.37-44.

[85] Linkov AM, *Plane problems of the static loading of a piecewise homogeneous linearly elastic medium*. Journal of Applied Mathematics and Mechanics, 47(1983), pp.527-532.

[86] Linkov AM, Mogilevskaya SG, *Complex hypersingular integrals and integral equations in plane elasticity*. Acta Mechanica, 105(1994), pp.189-205.

[87] Linkov AM, Mogilevskaya SG, *Complex hypersingular BEM in plane elasticity problems*. In: *Singular integrals in Boundary Element methods* (Editors: Sladek V, Sladek J), Chapter 9. Computational Mechanics Publications, Southhampton, 1998.

[88] Linz P, *Analytical and numerical methods for Volterra equations*. Siam, Philadelphia, 1985.

[89] Liu Y, You Z, *Determining Burger's model parameters of asphalt materials using creep-recovery testing data*. Proceedings of the Symposium on Pavement Mechanics and Materials at the Inaugural International Conference of the Engineering Mechanics Institute. May 18-21, 2008, Minneapolis, Minnesota. DOI: 10.1061/41008(334).

[90] Luciano R, Barbero EJ, *Analytical expressions for the relaxation moduli of linear viscoelastic composites with periodic microstructure*. Journal of Applied Mechanics, 62:3(1995), pp.786-793.

[91] Marasteanu MO, Anderson DA, *Improved model for bitumen rheological characterization*. In: Proceedings of the Eurobitume workshop on performance related properties for bituminous binders, Paper no. 133, Luxembourg, 1999.

[92] Marasteanu MO, Anderson DA, *Comparison of moduli for asphalt binders obtained from different test devices*. Journal of the Association of Asphalt Paving Technologists, 69(2000), pp.574-607.

[93] Marasteanu MO, Basu A, Hesp S, Voller V, *Time-temperature superposition and AASHTO MP1a critical temperature for low-temperature cracking.* International Journal of Pavement Engineering, 5:1(2004), pp.31-38.

[94] Marasteanu MO, Zofka A, Turos M, and other, *Investigation of Low Temperature Cracking in Asphalt Pavements.* National Pooled Fund Study 776, Minnesota Department of Transportation, 2007.

[95] Matzenmiller A, Gerlach S, *Micromechanical modeling of viscoelastic composites with compliant fiber-matrix bonding.* Computational Materials Science, 29(2004), pp.283-300.

[96] Maxwell JC, *A treatise on electricity and magnetism.* 3d Ed., Oxford, UK: Clarendon Press, 1892, pp.435-441.

[97] McCartney LN, Kelly A, *Maxwell's far-field methodology applied to the prediction of properties of multi-phase isotropic particulate composites.* Proceedings of the Royal Society A, 464:2090(2008), pp.423-446.

[98] McCrum NG, Buckley CP, *Principles of polymer engineering.* 2nd Ed., Oxford University Press, USA, 1997.

[99] Mesquita AD, Coda HB, Venturini WS, *Alternative time marching process for BEM and FEM viscoelastic analysis.* Internationa Journal for Numercal Methods in Engineering, 51(2001), pp.1157-1173.

[100] Mogilevskaya SG, Linkov AM, *Complex fundamental solution and complex variables Boundary Element method in elasticity.* Computational mechanics, 22(1998), pp.88-92.

[101] Mogilevskaya SG, *Complex hypersingular integral equation for the piece-wise homogeneous half-plane with cracks.* International Journal of Fracture, 102(2000), pp.177-204.

[102] Mogilevskaya SG, Crouch SL, *A Galerkin boundary integral method for multiple circular elastic inclusions*. International Journal for Numerical Mehods in Engineering, 52(2001), pp.1069-1106.

[103] Mogilevskaya SG, Crouch SL, *On the use of Somigliana's formula and Fourier series for elasticity with circular boundaries*. International Journal for Numerical Methods in Engineering, 58(2003), pp.537-578.

[104] Mogilevskaya SG, Crouch SL, Stolarski HK, *Multiple interacting circular nano-inhomogeneities with surface/interface effects*. Journal of mechanics and Physics of solids, 56:6(2008), pp.2298-2327.

[105] Mogilevskaya SG, Crouch SL, Stolarski HK, Benusiglio A, *Equivalent inhomogeneity method for evaluating the effective elastic properties of unidirectional multiphase composites with surface/interface effects.* International Journal of Solids and Structures, 47:3-4(2010), pp.407-418.

[106] Mori T, Tanaka K, *Average stress in matrix and average elastic energy of materials with mis-fitting inclusions*. Acta Mechanica, 21(1973), pp.571-583.

[107] Morland LW, Lee EH, *Stress analysis for linear viscoelastic materials with temperature variation*. Transactions of the Society of Rheology, 4(1960), p.223.

[108] Muskhelishvili NI, *Some basic problems of the mathematical theory of elasticity*. Noordhoff: Groningen, The Netherlands, 1963.

[109] Oliveira ERA, *Plane stress analysis by a general integral method*. ASCE Journal of Engineering Mechanics, 98(1968), pp.79-101.

[110] Pobedonostsev AI. *On the evaluation of the stresses in a half-plane with circular opening*. Journal of Applied Mathematics and Mechanics, 28(1964), pp.55-161. (Translation of Prikladnaya Matematika i Mekhanika).

[111] Polyanin AD, Manzhirov AV, *Handbook of integral equations*. CRC Press, Boca Raton, 1998.

[112] Pyatigorets AV, Mogilevskaya SG, Marasteanu MO, *Linear viscoelastic analysis of a semi-infinite porous medium*. International Journal of Solids and Structures, 45(2008), pp.1458-1482.

[113] Pyatigorets AV, Labuz JF, Mogilevskaya SG, Stolarski HK, *Novel approach for measuring the effective shear modulus of porous materials*. Journal of Material Science, 45(2010), pp.936-945.

[114] Rabotnov YuN, *Creep of construction elements*. Nauka, Moscow, 1966 [In Russian].

[115] Rabotnov YuN, *Mechanics of deformable bodies*. Nauka, Moscow, 1988 [in Russian].

[116] Rizzo FJ, Shippy DJ, *An application of the correspondence principle of linear viscoelastic theory*. Journal of Applied Mathematics, 21:2(1971), pp.321-330.

[117] Schwarzl F, Staverman AJ, *Time-temperature dependence of linear viscoelastic behavior*. Journal of Applied Physics, 23:8(1952), pp.838-843.

[118] Shafii-Mousavi M, *The essentials of Laplase transforms*. Research and Education Association, Piscataway, New Jersey, 1991.

[119] Skudra AM, Auzukalns YaV, *Creep and long-term strength of unidirectional reinforced plastics in compression*. Polymer Mechanics, 6:5(1973), pp.85-168.

[120] Somigliana C, *Sopra l'equilibrio di un corpo elastico isotropo*. Nuovo Cimento, 3(1885), pp.17-20.

[121] Soon S, Drescher A, Stolarski HK, *Tire-induced surface stresses in flexible pavements*. Transportation Research Record: Journal of the Transportation Research Board, 1896(2004), pp.170-176.

[122] Spencer SE, Sinclair GB, *Stress analysis of an elastic half-space perforated by twin circular holes and under gravitational loading*. International Journal of Mechanical Sciences, 24:1(1982), pp.27-35.

[123] Stehfest H, *Numerical inversion of Laplace transform*. Communications of the ACM, 13(1970), pp.47-49.

[124] Taylor RL, Pister KS, Goudreas GL, *Thermochemical Analysis of Viscoelastic Solids*. Internationa Journal for Numercal Methods in Engineering, 2(1970), pp.45-59.

[125] Tobolsky AV, *Structure and properties of polymers*. John Wiley, New York, 1960.

[126] Torquato S, Gibiansky LV, Silva MJ, Gibson LJ, *Effective mechanical and transport properties of cellular solids*. International Journal of Mechanical Sciences, 40:1(1998), pp.71-82.

[127] Tschoegl NW, Knauss WG, Emri I, *Poisson's ratio in linear viscoelasticity - a critical review*. Mechanics of Time-Dependent Materials, 6(2002), pp.3-51.

[128] Ugural AC, Fenster SK, *Advanced strength and applied elasticity*. 4th Ed., Prentice Hall, New Jersey, 2003.

[129] Vigdergauz S, *New results on the Poisson ratio behavior in matrix-inclusion planar composites*. Mathematics and Mechanics of Solids, 12(2006), pp.58-74.

[130] Volterra V, *Sulle equazioni integro-differenziali della teoria dell' elasticita*. Atti della Reale Academia dei Lencei, 18(1909), p.295.

[131] Volterra V, *Leçons sur les fonctions de lignes*. Gauthier-Villars, Paris, 1913.

[132] Wang J, Crouch SL, Mogilevskaya SG, *A complex boundary integral method for multiple circular holes in an infinite plane*. Engineering Analysis with Boundary Elements, 27(2003), pp.789-802.

[133] Wang J, Crouch SL, Mogilevskaya SG, *A fast and accurate algorithm for a Galerkin boundary integral method*. Computational Mechanics, 37(2005), pp.96-109.

[134] Wang YM, Weng GJ, *The influence of inclusion shape on the overall viscoelastic behavior of composites*. Transactions of ASME 59(1992), pp.510-518.

[135] Ward IM, *Mechanical properties of solid polymers*. 2nd Ed., John Willey and Sons, UK, 1983.

[136] Weeton JW, Peters DM, Thomas KL, *Engineers' guide to composite materials*. American Society for Materials, Ohio, 1986.

[137] Williams ML, Landel RF, Ferry JD, *The temperature dependence of relaxation mechanism in amorphous polymers and other glass-liquidis*. Journal of American Chemical Society, 77(1955), p.370.

[138] Wineman AS, Rajagopal KR, *Mechanical response of polymers: An introduction*. Cambridge University Press, 2000.

[139] Yi Y-M, Park S-H, Youn S-K, *Asymptotic homogenization of viscoelastic composites with periodic microstructures*. International Journal of Solids and Structures, 35:17(1998), pp.2039-2055.

[140] Zhang HH, Li LX, *Modeling inclusion problems in viscoelastic materials with the extended Finite Element method*. Finite Elements in Analysis and Design, 45(2009), pp.721-729.

[141] Zatula NI, Lavrenyuk VI, *Stressed-strained state of a viscous half-plane with circular inclusions*. International Applied Mechanics, 31:9(1995), pp.754-760.

Appendix A

A.1 Singular and hypersingular integrals

Singular integrals are the integral operators whose kernels are singular. That is they reach an infinite value at one or more points in the domain of integration.

Consider an integral of type

$$\int_L \frac{f(z)}{(z-z_0)^\gamma} dz \tag{A.1-1}$$

where $z \in L$ and $f(z)$ is some smooth function defined on contour L. In the case (i) $0 < \gamma < 1$ the integral is said to be weakly singular and it can be found in ordinary Riemann sense, (ii) $\gamma = 1$ the integral is called singular and it is integrable in the Cauchy principal value sense, (iii) $\gamma > 1$ the integral is called hypersingular and it can be determined only in Hadamard finite part sense. The function $f(z)$ is assumed to be smooth enough meaning that it has Holder's continuous derivative of $\gamma - 1$ order [87].

Particularly, for $\gamma = 1$ the integral (A.1-1) is defined in the following limiting sense (Cauchy principal value sense):

$$\mathcal{C}\int_a^b \frac{f(z)}{z-z_0} dz \stackrel{def}{=} \lim_{\epsilon \to 0^+} \left[\int_a^{z_0-\epsilon} \frac{f(z)}{z-z_0} dz + \int_{z_0+\epsilon}^b \frac{f(z)}{z-z_0} dz \right] \tag{A.1-2}$$

If $\gamma = 2$ the integral (A.1-1) is defined as Hadamard finite-part integral:

$$\mathcal{H}\int_a^b \frac{f(z)}{(z-z_0)^2} dz \stackrel{def}{=} \lim_{\epsilon \to 0^+} \left[\int_a^{z_0-\epsilon} \frac{f(z)}{(z-z_0)^2} dz + \int_{z_0+\epsilon}^b \frac{f(z)}{(z-z_0)^2} dz - \frac{2f(z_0)}{\epsilon} \right] \tag{A.1-3}$$

Aspects of the theory of complex hypersingular integrals and singular integral equations can be found in [86] and [87].

Appendix B

B.1 Coefficients obtained from space integrals for the half-plane problem

Let us define the following function:

$$h_j(\tau) = \overline{g_j(\bar{\tau})} = \frac{R_j}{\tau - \overline{z_j}} \tag{B.1-1}$$

The coefficients $\Upsilon_{kk,q}(\hat{B}_{mk})$ and $\Upsilon_{kj,q}(\hat{B}_{mk})$ involved in expression (3.22) are

a) for $j = k$

1. $(-q) \leq -1$

$$\Upsilon_{kk,-q} = \frac{1}{R_k} \left\{ \begin{array}{l} \sum\limits_{m=1}^{M_k} \overline{\hat{B}_{-mk}} m h_k^{m+1}(z_k) g_k^{q-1}(\bar{z}_k) \binom{m+q}{q} \times \\ \qquad \times \left[\begin{array}{l} -q h_k(z_k) + g_k(\bar{z}_k) \\ + \dfrac{(m+q+2)(m+q+1)}{m+1} h_k^2(z_k) g_k(\bar{z}_k) \end{array} \right. \\ -(1+q)\, \hat{B}_{(1+q)k} - (\hat{B}_{1k} + \overline{\hat{B}_{1k}})(q+1) h_k^2(z_k) g_k^q(\bar{z}_k) \\ -\sum\limits_{m=2}^{M_k} \hat{B}_{mk} m \binom{m+q}{q} h_k^{m+1}(z_k) g_k^q(\bar{z}_k) \end{array} \right. \tag{B.1-2}$$

2. $q = 0$

$$\begin{aligned} \Upsilon_{kk,0} = \frac{2}{R_k} \operatorname{Re} \Bigg\{ & \sum_{m=1}^{M_k} m \hat{B}_{-mk} g_k^{m+1}(\bar{z}_k) \left[1 + (m+2) g_k^2(\bar{z}_k) \right] \\ & - \hat{B}_{1k} \left[1 + 2 g_k^2(\bar{z}_k) \right] - \sum_{m=2}^{M_k} m \hat{B}_{mk} h_k^{m+1}(z_k) \Bigg\} \end{aligned} \tag{B.1-3}$$

3. $q = 1$

$$\Upsilon_{kk,1} = 0 \tag{B.1-4}$$

4. $q \geq 2$

$$\begin{aligned}
\Upsilon_{kk,q} \cdot R_k = & \sum_{m=1}^{M_k} \hat{B}_{-mk} m g_k^{m+1}(\bar{z}_k) h_k^{q-4}(z_k) \binom{m+q}{q} \times \\
& \times \left\{ \begin{array}{l}
h_k^4(z_k) \\
+\dfrac{1}{m+1} g_k^2(\bar{z}_k) h_k^2(z_k) \times \\
\times \left[(m+q+2)(m+q+1) h_k^2(z_k) + q(q-1) \right] \\
+\dfrac{q}{m+1} g_k^3(\bar{z}_k) h_k(z_k) \times \\
\times \left[(m+q+1)(m+q+2) h_k^2(z_k) + (q-1)(m+3) \right] \\
+ g_k(\bar{z}_k) h_k(z_k) q \left[h_k^2(z_k) + \dfrac{(q-1)(2m-q+4)}{(m+q)(m+q-1)} \right] \\
- g_k^2(\bar{z}_k) q(q-1) \left[h_k^2(z_k) + \dfrac{(q-2)(m+2)}{(m+q)(m+q-1)} \right]
\end{array} \right. \\
& - (q-1)\, \hat{B}_{(1-q)k} - (\hat{B}_{1k} + \overline{\hat{B}_{1k}}) g_k^2(\bar{z}_k) h_k^{q-3}(z_k) \times \left\{ \begin{array}{l}
(q+1) h_k^3(z_k) + (q-1) h_k(z_k) \\
+ g_k(\bar{z}_k) \left[(q+1) q h_k^2(z_k) + 2(q-1) \right]
\end{array} \right. \\
& - \sum_{m=2}^{M_k} \overline{\hat{B}_{mk}} m g_k^{m+1}(\bar{z}_k) \binom{m+q}{q} h_k^{q-3}(z_k) \times \left\{ \begin{array}{l}
h_k^3(z_k) + \dfrac{q(q-1)}{(m+q)(m+q-1)} h_k(z_k) \\
+ q g_k(\bar{z}_k) \left[h_k^2(z_k) + \dfrac{(m+1)(q-1)}{(m+q)(m+q-1)} \right]
\end{array} \right.
\end{aligned} \tag{B.1-5}$$

b) and for $j \neq k$

1. $(-q) \leq -1$

$$\Upsilon_{kj,-q} = \frac{1}{R_j} \left\{ \begin{array}{l} -\sum_{m=1}^{M_j} \hat{B}_{-mj} m \binom{m+q}{q} g_j^{m+1}(z_k) g_k^q(z_j) \\ +\sum_{m=1}^{M_j} \overline{\hat{B}_{-mj}} m \binom{m+q}{q} h_j^{m+1}(z_k) g_k^{q-1}(\bar{z}_j) \times \\ \quad \times \left\{ h_j^2(z_k) g_k(\bar{z}_j) \dfrac{(m+q+1)(m+q+2)}{m+1} + g_k(\bar{z}_j) + \right. \\ \qquad \left. h_j(z_k) \dfrac{R_k}{R_j} \left[-q + g_k^{-1}(z_j) g_k(\bar{z}_j)(m+q+1) \right] \right\} \\ -\sum_{m=2}^{M_j} \hat{B}_{mj} m \binom{m+q}{q} h_j^{m+1}(z_k) g_k^q(\bar{z}_j) \\ -(\hat{B}_{1j} + \overline{\hat{B}_{1j}})(q+1) h_j^2(z_k) g_k^q(\bar{z}_j) \end{array} \right. \tag{B.1-6}$$

2. $q = 0$

$$\begin{aligned} \Upsilon_{kj,0} = \frac{2}{R_j} \operatorname{Re} \Bigg\{ & -(\hat{B}_{1j} + \overline{\hat{B}_{1j}}) h_j^2(z_k) - \sum_{m=2}^{M_j} \hat{B}_{mj} m h_j^{m+1}(z_k) \\ & + \sum_{m=1}^{M_j} \hat{B}_{-mj} m \Big[-g_j^{m+1}(z_k) + g_j^{m+1}(\bar{z}_k) \\ & \left(1 + (m+2) g_j^2(\bar{z}_k) + (m+1) \frac{R_k}{R_j} g_j(\bar{z}_k) h_k^{-1}(\bar{z}_j) \right) \Big] \Bigg\} \end{aligned} \tag{B.1-7}$$

3. $q = 1$

$$\Upsilon_{kj,1} = 0 \tag{B.1-8}$$

4. $q \geq 2$

$$\Upsilon_{kj,q} \cdot R_j = \sum_{m=1}^{M_j} \hat{B}_{-mj} m \binom{m+q}{q} g_j^{m+1}(\bar{z}_k) h_k^{q-4}(z_j) \times$$

$$\times \left\{ \begin{array}{l} h_k^4(z_j) + \dfrac{(m+q+2)(m+q+1)}{m+1} g_j^2(\bar{z}_k) h_k^4(z_j) \\ + \dfrac{q(q-1)}{m+1} g_j^2(\bar{z}_k) h_k^2(z_j) + \dfrac{R_k}{R_j} g_j(\bar{z}_k) h_k(z_j) \times \\ \left[\begin{array}{l} (m+q+1) h_k^3(z_j) h_k^{-1}(\bar{z}_j) - q h_k^2(z_j) \\ + \dfrac{q(q-1)}{m+q} h_k^{-1}(\bar{z}_j) h_k(z_j) - \dfrac{q(q-1)(q-2)}{(m+q)(m+q-1)} \end{array} \right. \\ + \dfrac{R_k}{R_j} \dfrac{q(q-1)}{m+1} g_j^3(\bar{z}_k) h_k(z_j) \times \\ \left[\begin{array}{l} \dfrac{(m+q+2)(m+q+1)}{q-1} h_k^2(z_j) - (q-2) \\ + (m+q+1) h_k(z_j) h_k^{-1}(z_k) \end{array} \right. \\ + 2 \dfrac{R_k}{R_j} q g_j(\bar{z}_k) h_k(z_j) \times \\ \left[h_k^2(z_j) + \dfrac{q-1}{m+q} h_k(z_j) h_k^{-1}(z_k) - \dfrac{(q-1)(q-2)}{(m+q)(m+q-1)} \right] \\ + \left(\dfrac{R_k}{R_j} \right)^2 q(q-1) g_j^2(\bar{z}_k) \times \\ \left[\begin{array}{l} \dfrac{m+q+1}{q-1} h_k^3(z_j) h_k^{-1}(\bar{z}_j) + h_k^2(z_j) \left[h_k^{-1}(\bar{z}_j) h_k^{-1}(z_k) - 1 \right] \\ - \dfrac{q-2}{m+q} h_k(z_j) \left[h_k^{-1}(z_k) + h_k^{-1}(\bar{z}_j) \right] + \dfrac{(q-2)(q-3)}{(m+q-1)(m+q)} \end{array} \right. \end{array} \right. \tag{B.1-9}$$

$$+ \sum_{m=1}^{M_j} \overline{\hat{B}_{-mj}} m \binom{m+q}{q} h_j^{m+1}(\bar{z}_k) h_k^{q-2}(\bar{z}_j) \times \left\{ \begin{array}{l} \dfrac{q(q-1)}{m+1} h_j^2(\bar{z}_k) - h_k^2(\bar{z}_j) \\ + h_j(\bar{z}_k) \dfrac{R_k}{R_j} \left[-q h_k(\bar{z}_j) + \dfrac{q(q-1)}{m+q} g_k^{-1}(z_j) \right] \end{array} \right.$$

$$- (\hat{B}_{1j} + \overline{\hat{B}_{1j}}) \times \left\{ \begin{array}{l} (q-1) h_j^2(\bar{z}_k) h_k^{q-2}(\bar{z}_j) + g_j^2(\bar{z}_k) h_k^{q-2}(z_j) \left[(q+1) h_k^2(z_j) + (q-1) \right] + \\ \dfrac{R_k}{R_j} g_j^3(\bar{z}_k) h_k^{q-3}(z_j) \left[(q+1) q h_k^2(z_j) + q(q-1) h_k(z_j) h_k^{-1}(z_k) - (q-2)(q-1) \right] \end{array} \right.$$

$$- \sum_{m=2}^{M_j} \hat{B}_{mj} m \binom{m+q-2}{q-2} h_j^{m+1}(\bar{z}_k) h_k^{q-2}(\bar{z}_j)$$

$$+ \sum_{m=2}^{M_j} \overline{\hat{B}_{mj}} m g_j^{m+1}(\bar{z}_k) \binom{m+q}{q} h_k^{q-3}(z_j) \times \left\{ \begin{array}{l} -h_k^3(z_j) - \dfrac{q(q-1)}{(m+q-1)(m+q)} h_k(z_j) + \\ \dfrac{R_k}{R_j} q g_j(\bar{z}_k) \times \left[\begin{array}{l} -h_k^2(z_j) - \dfrac{q-1}{m+q} h_k(z_j) h_k^{-1}(z_k) \\ + \dfrac{(q-1)(q-2)}{(m+q-1)(m+q)} \end{array} \right. \end{array} \right.$$

B.2 Coefficients obtained from space integrals multiplied by pores pressure

The coefficients $\Xi_{kj,q}$ involved in expression (3.22) are

1. $(-q) \leq -1$

$$\Xi_{kj,-q} = (q+1)h_j^2(z_k)g_k^q(\bar{z}_j) \tag{B.2-1}$$

2. $q = 0$

$$\Xi_{kj,0} = 2\,\mathrm{Re}\, h_j^2(z_k) \tag{B.2-2}$$

3. $q = 1$

$$\Xi_{kj,1} = 0 \tag{B.2-3}$$

4. $q \geq 2$

$$\begin{aligned}\Xi_{kj,q} = &\underbrace{(q-1)h_j^2(\bar{z}_k)h_k^{q-2}(\bar{z}_j)}_{\text{no this term for } j=k} + (q+1)g_j^2(z_k)h_k^q(z_j) + (q-1)g_j^2(\bar{z}_k)h_k^{q-2}(z_j)\\ &+ 2\frac{R_k}{R_j}\binom{q+1}{q-1}g_j^3(\bar{z}_k)h_k^{q-1}(z_j) + 2\frac{R_k}{R_j}\binom{q}{q-2}g_j^3(\bar{z}_k)h_k^{-1}(z_k)h_k^{q-2}(z_j)\\ &\underbrace{-2\frac{R_k}{R_j}\binom{q-1}{q-3}g_j^3(\bar{z}_k)h_k^{q-3}(z_j)}_{\text{no this term for } q=2}\end{aligned} \tag{B.2-4}$$

B.3 Coefficients obtained from space integrals multiplied by external forces

Let us denote $\hat{F} = \hat{F}(s) = \hat{F}_x(s) + i\hat{F}_y(s)$.

a) For a point force at the point a:

1. $(-q) \leq -1$

$$\Omega_{k,-q} = \frac{\hat{F}}{2\pi R_k} g_k^{q+1}(a) \tag{B.3-1}$$

2. $q = 0$

$$\Omega_{k,0} = \frac{1}{2\pi R_k} \cdot 2\,\mathrm{Re}\left[\hat{F} \cdot g_k(a)\right] \tag{B.3-2}$$

3. $q = 1$

$$\Omega_{k,1} = 0 \tag{B.3-3}$$

4. $q \geq 2$

$$\Omega_{k,q} = \frac{1}{2\pi R_k} \left\{ \overline{\hat{F}}(1-q) h_k^q(\bar{a}) \left[h_k(\bar{a}) - g_k^{-1}(a) \right] + \hat{F} h_k^{q-1}(\bar{a}) \right\} \tag{B.3-4}$$

b) For a force uniformly distributed over a segment $(a,\ b)$ at the boundary:

1. $(-q) \leq -1$

$$\Omega_{k,-q} = -\frac{\hat{F}}{2\pi q} \left[g_k^q(b) - g_k^q(a) \right] \tag{B.3-5}$$

2. $q = 0$

$$\Omega_{k,0} = \frac{1}{2\pi} \cdot 2\,\mathrm{Re} \left(\hat{F} \ln \frac{b - z_k}{a - z_k} \right) \tag{B.3-6}$$

3. $q = 1$

$$\Omega_{k,1} = 0 \tag{B.3-7}$$

4. $q \geq 2$

$$\Omega_{k,q} = \frac{1}{2\pi} \left\{ \underbrace{\left(\overline{\hat{F}} + \hat{F} \right) \overline{\ln \frac{b - z_k}{a - z_k}}}_{\text{this term for } q=2 \text{ only}} + \overline{\hat{F}} \left(1 - \frac{1}{q} \right) \left[\overline{g_k^q(b)} - \overline{g_k^q(a)} \right] \right. \tag{B.3-8}$$

$$\left. + \overline{\hat{F}} h_k^{-1}(z_k) \left[\overline{g_k^{q-1}(b)} - \overline{g_k^{q-1}(a)} \right] - \underbrace{\frac{\hat{F} + (q-1)\overline{\hat{F}}}{q-2} \left[\overline{g_k^{q-2}(b)} - \overline{g_k^{q-2}(a)} \right]}_{\text{no this term for } q=2} \right\}$$

c) For a force uniformly distributed over the whole boundary:

1. $q = 0$

$$\Omega_{k,0} = \mathrm{Im}(\hat{F}) \tag{B.3-9}$$

2. $q = 2$

$$\Omega_{k,2} = i\,\mathrm{Re}(\hat{F}) \tag{B.3-10}$$

$\Omega_{k,q} = 0$ for all other q.

B.4 Time-independent functions involved in the solution for viscoelastic fields

The functions involved in Eq.(3.29) are

$$
\begin{aligned}
H_\infty(z) &= z\frac{\sigma^\infty}{4} \\
H_p(z) &= \sum_{j=1}^{N} p_j R_j h_j(z) \\
H_l(z) &= \sum_{j=1}^{N} \Bigg\{ \left[B_{1j}^{(l)} + \bar{B}_{1j}^{(l)}\right] h_j(z) + \sum_{m=2}^{M_j} B_{mj}^{(l)} h_j^m(z) + \\
&\quad + \sum_{m=1}^{M_j} \left[B_{-mj}^{(l)} g_j^m(z) + \bar{B}_{-mj}^{(l)} m h_j^{m+1}(z) \left(-h_j(z) + g_j^{-1}(z)\right)\right] \Bigg\} \\
H_F(z) &= \varphi_F(z), \text{ where one should use } F \text{ instead of } \hat{F}(s) \text{ in Eqs.(3.14)-(3.16)} \\
Q_\infty(z) &= -z\frac{\sigma^\infty}{2} \qquad \text{(B.4-1)} \\
Q_p(z) &= -\sum_{j=1}^{N} p_j \left[R_j g_j(z) - z h_j^2(z)\right] \\
Q_l(z) &= \sum_{j=1}^{N} \Bigg\{ \left(B_{1j}^{(l)} + \bar{B}_{1j}^{(l)}\right) \left[-g_j(z) + \frac{z}{R_j} h_j^2(z)\right] + \sum_{m=2}^{M_j} \left[B_{mj}^{(l)} \frac{z}{R_j} m h_j^{m+1}(z) - \bar{B}_{mj}^{(l)} g_j^m(z)\right] \\
&\quad + \sum_{m=1}^{M_j} \Bigg[B_{-mj}^{(l)} m g_j^{m+1}(z) \left(g_j(z) + \frac{\bar{z}_j}{R_j}\right) - \\
&\quad - \bar{B}_{-mj}^{(l)} \left(h_j(z) + \frac{z}{R_j} m h_j^{m+1}(z) \left((m+2)\, h_j^2(z) - (m+1)\frac{h_j(z)}{g_j(z)} + 1\right)\right)\Bigg] \Bigg\} \\
Q_F(z) &= \psi_F(z), \text{ where one should use } F \text{ instead of } \hat{F}(s) \text{ in Eqs.(3.14)-(3.16)}
\end{aligned}
$$

B.5 Time-dependent functions involved in the solution for viscoelastic fields

1. The inverse Laplace transform of functions $\hat{S}_n(s)$, $n = 1, ..., 12$ (see Eq.(3.31)) for $\hat{f}_\infty(s) = \dfrac{1}{s}$, $\hat{f}_p(s) = \dfrac{1}{s}$, $\hat{f}_F(s) = \dfrac{1}{s}$ can be found analytically. The final expressions can be quite lengthy and the use of symbolic calculations (e.g. in Maple$^{\text{TM}}$ or Mathematica®) is recommended. For the demonstration purposes few expressions are presented below.

$$
\begin{aligned}
S_1(t) &= -\frac{1}{6}\frac{2E_1^3E_2\exp\left(-\dfrac{\varkappa_1}{\varkappa_2}\dfrac{t}{\eta}\right) + 3\varkappa_2\left[\varkappa_1E_1\exp\left(-\dfrac{E_2t}{\eta}\right) - \varkappa_3\left(E_1+E_2\right)\right]}{\varkappa_1\varkappa_2E_1E_2} \\
S_2(t) &= \frac{1}{6}\frac{4\varkappa_1\varkappa_2E_1^2\exp\left(-\dfrac{\varkappa_4}{\varkappa_5}\dfrac{t}{\eta}\right) + \varkappa_5\left[3\varkappa_2\varkappa_3\left(E_1+E_2\right) - 2\varkappa_4E_1^2\exp\left(-\dfrac{\varkappa_1}{\varkappa_2}\dfrac{t}{\eta}\right)\right]}{\varkappa_1\varkappa_2\varkappa_4\varkappa_5} \\
&\vdots \\
S_{11}(t) &= \frac{\varkappa_1\varkappa_5 - E_1^2K\exp\left(-\dfrac{\varkappa_4}{\varkappa_5}\dfrac{t}{\eta}\right)}{2\varkappa_4\varkappa_5} \\
S_{12}(t) &= 1
\end{aligned}
\tag{B.5-1}
$$

where

$$
\begin{aligned}
\varkappa_1 &= \left(\frac{E_2}{3}+K\right)E_1 + KE_2, \qquad & \varkappa_2 &= \frac{E_1}{3}+K \\
\varkappa_3 &= \left(\frac{7E_2}{3}+K\right)E_1 + KE_2, \qquad & \varkappa_4 &= \left(\frac{4E_2}{3}+K\right)E_1 + KE_2 \\
\varkappa_5 &= \frac{4E_1}{3}+K
\end{aligned}
\tag{B.5-2}
$$

2. Consider the case when the force applied at the boundary of the half-plane depends on time as

$$
f_F(t) = \frac{F(t)}{F} = a_0 + b_0\cdot\sin(\omega t) \tag{B.5-3}
$$

where F is the complex amplitude of force variation, a_0 and b_0 are real constants. For the case considered in the last example of Chapter 3, $F = 5p_1$, $a_0 = 1$, $b_0 = 0.9$. The

Laplace transform of the normalized force $f_F(t)$ is

$$\hat{f}_F(s) = \frac{a_0}{s} + \frac{b_0\omega}{s^2+\omega^2} \tag{B.5-4}$$

The functions $S_4(t)$, $S_8(t)$, $S_{12}(t)$ can be found by using the analytical Laplace inversion of Eq.(3.31) and Eq.(B.5-4).

Appendix C

C.1 Operators involved in the system of governing equations

Operator $\hat{\Lambda}_{kk}$ is given by the Laplace transform of the corresponding operator presented in [38]:

$$\hat{\Lambda}_{kk}(\xi;s) = -\frac{1}{R_k}\left\{2\,\mathrm{Re}\,\hat{B}_{1k} + \sum_{m=1}^{M_k-1} m\hat{B}_{-mk}g_k^{m+1}(\xi) + \sum_{m=2}^{M_k+1}\hat{B}_{mk}g_k^{1-m}(\xi)\right\} \qquad \text{(C.1-1)}$$

Operator $\hat{\Pi}_{kk}$ is as follows:

$$\begin{aligned}\hat{\Pi}_{kk}(\xi;s) = \frac{1}{R_k}\Bigg\{&2\left(\frac{\mu_k}{\kappa_k-1}\frac{\hat{\kappa}-1}{\hat{\mu}}-1\right)\mathrm{Re}\,\hat{B}_{1k}+\\ &\left(\frac{\mu_k}{\hat{\mu}}-1\right)\sum_{m=1}^{M_k-1} m\hat{B}_{-mk}g_k^{m+1}(\xi)+\left(\frac{\mu_k}{\kappa_k}\frac{\hat{\kappa}}{\hat{\mu}}-1\right)\sum_{m=2}^{M_k+1}\hat{B}_{mk}g_k^{1-m}(\xi)\Bigg\} \qquad \text{(C.1-2)}\\ = -\frac{1}{R_k}\Bigg\{&2\hat{\alpha}_{2k}\,\mathrm{Re}\,\hat{B}_{1k}+\hat{\alpha}_{1k}\sum_{m=1}^{M_k-1} m\hat{B}_{-mk}g_k^{m+1}(\xi)+\hat{\alpha}_{3k}\sum_{m=2}^{M_k+1}\hat{B}_{mk}g_k^{1-m}(\xi)\Bigg\}\end{aligned}$$

Expression (C.1-2) differs from expression (C.1-1) by the presence of additional terms in front of unknown Fourier coefficients $\hat{B}_{-mk}$, $\mathrm{Re}\,\hat{B}_{1k}$, $\hat{B}_{mk}$ only. All other operators $\hat{\Pi}_{jk}$ can be obtained in a similar way from the corresponding expressions given in [38].

C.2 Potentials in the Laplace domain

a) Potentials for the kth elastic disc derived from Eq.(4.5) are

$$\hat{\varphi}(z,s) = \frac{2\mu_k}{\kappa_k - 1} \operatorname{Re} \hat{B}_{1k} g_k^{-1}(z) + \frac{2\mu_k}{\kappa_k} \sum_{m=2}^{M_k+1} \hat{B}_{mk} g_k^{-m}(z) \tag{C.2-1}$$
$$= \frac{2\mu_k}{\kappa_k - 1} \frac{1}{\hat{\alpha}_{2k}} \operatorname{Re} \hat{\mathbb{B}}_{1k} g_k^{-1}(z) + \frac{2\mu_k}{\kappa_k} \frac{1}{\hat{\alpha}_{3k}} \sum_{m=2}^{M_k+1} \hat{\mathbb{B}}_{mk} g_k^{-m}(z)$$

$$\hat{\psi}(z,s) = -\frac{2\mu_k}{\kappa_k - 1} \frac{\bar{z}_k}{R_k} \operatorname{Re} \hat{B}_{1k} - \frac{2\mu_k}{\kappa_k} \left[\frac{\bar{z}_k}{R_k} + g_k(z) \right] \sum_{m=2}^{M_k+1} m \hat{B}_{mk} g_k^{-(m-1)}(z)$$
$$- 2\mu_k \sum_{m=1}^{M_k-1} \overline{\hat{B}_{-mk}} g_k^{-m}(z) \tag{C.2-2}$$
$$= -\frac{2\mu_k}{\kappa_k - 1} \frac{\bar{z}_k}{\hat{\alpha}_{2k} R_k} \operatorname{Re} \hat{\mathbb{B}}_{1k} - \frac{2\mu_k}{\hat{\alpha}_{3k}\kappa_k} \left[\frac{\bar{z}_k}{R_k} + g_k(z) \right] \sum_{m=2}^{M_k+1} m \hat{\mathbb{B}}_{mk} g_k^{-(m-1)}(z)$$
$$- \frac{2\mu_k}{\hat{\alpha}_{1k}} \sum_{m=1}^{M_k-1} \overline{\hat{\mathbb{B}}_{-mk}} g_k^{-m}(z)$$

Similar expressions are used in [104] for the calculation of elastic potentials.

b) Potentials for the matrix derived from Eqs.(4.7) and (4.8) are

$$\hat{\varphi}_{plane}(z;s) = \frac{2\hat{\mu}}{\hat{\kappa}+1} \sum_{k=1}^{N} \sum_{m=1}^{M_k-1} \hat{\mathbb{B}}_{-mk} g_k^m(z) + \frac{\hat{\sigma}^\infty(s)}{4} z \tag{C.2-3}$$

$$\hat{\psi}_{plane}(z;s) = -\frac{\hat{\kappa}-1}{\hat{\kappa}+1} \sum_{k=1}^{N_h} \hat{p}_k R_k g_k(z) + \frac{2\hat{\mu}}{\hat{\kappa}+1} \sum_{k=1}^{N} \Big[-2 \operatorname{Re} \hat{\mathbb{B}}_{1k} g_k(z) \tag{C.2-4}$$
$$+ \sum_{m=1}^{M_k-1} m \hat{\mathbb{B}}_{-mk} g_k^{m+1}(z) \left(\frac{\overline{z_k}}{R_k} + g_k(z) \right) - \sum_{m=1}^{M_k+1} \overline{\hat{\mathbb{B}}_{mk}} g_k^m(z) \Big] - \frac{\hat{\sigma}^\infty(s)}{2} z$$

$$\hat{\varphi}_{aux}(z;s) = \frac{\hat{\kappa}-1}{\hat{\kappa}+1} \sum_{j=1}^{N_h} \hat{p}_j R_j h_j(z) + \frac{2\hat{\mu}}{\hat{\kappa}+1} \sum_{j=1}^{N} \Big[2 \operatorname{Re} \hat{\mathbb{B}}_{1j} h_j(z) \tag{C.2-5}$$
$$+ \sum_{m=1}^{M_j-1} m \overline{\hat{\mathbb{B}}_{-mj}} h_j^{m+1}(z) \left(g_j^{-1}(z) - h_j(z) \right) + \sum_{m=2}^{M_j+1} \hat{\mathbb{B}}_{mj} h_j^m(z) \Big]$$

$$\hat{\psi}_{aux}(z;s) = \frac{\hat{\kappa}-1}{\hat{\kappa}+1} z \sum_{j=1}^{N_h} \hat{p}_j h_j^2(z) + \frac{2\hat{\mu}}{\hat{\kappa}+1} \frac{z}{R_j} \sum_{j=1}^{N} \Big\{ 2\,\mathrm{Re}\,\hat{\mathbb{B}}_{1j} h_j^2(z) + \sum_{m=2}^{M_j+1} m \hat{\mathbb{B}}_{mj} h_j^{m+1}(z) - \sum_{m=1}^{M_j-1} m \overline{\hat{\mathbb{B}}_{-mj}} h_j^{m+1}(z) \times \times \left[1 - (m+1) g_j^{-1}(z) h_j(z) + (m+2) h_j^2(z) + \frac{1}{m} \frac{R_j}{z} h_j^{-1}(z) \right] \Big\} \tag{C.2-6}$$

where the function $h_j(z)$ is defined by (B.1-1).

The potentials $\hat{\varphi}_F(z;s)$ and $\hat{\psi}_F(z;s)$ are due to the use of the Flamant fundamental solution, and they do not depend on the displacements or stresses at the boundaries of the holes. The expressions for these potentials are given in Chapter 3.

Appendix D

D.1 Determination of master relaxation modulus from the BBR test

Master relaxation modulus $E(\zeta)$ of asphalt binders is determined from experimental data for creep compliances, which are obtained with the use of bending-beam rheometer (BBR) test. In this test [4], a small beam made of a asphalt binder or asphalt mix is subjected to three-point bending at different low temperatures (e.g. $-18°C$, $-24°C$, $-30°C$). The deflection and the applied load are measured in the real time. According to Euler-Bernoulli beam theory, the maximum elastic deflection at the mid-span of the beam is

$$\delta_{\max} = \frac{PL^3}{48EI} \tag{D.1-1}$$

where P is the concentrated load, L and I are the beam span and the moment of inertia, respectively, and E is Young's modulus of the material. Using (D.1-1), the creep compliance of the viscoelastic beam $D(t)$ can be determined as follows:

$$D(t) = \frac{48I}{PL^3}\delta(t) \tag{D.1-2}$$

where $\delta(t)$ is beam mid-span deflection history caused by load P applied at zero time moment.

Creep compliance $D(t)$ is converted to relaxation modulus $E(t)$ using the Hopkins-Hamming method [60] of numerical integration of convolution integral

$$\int_0^t E(t)D(t-\tau)d\tau = t \ . \tag{D.1-3}$$

After relaxation modulus $E(t)$ is obtained for each testing temperature, shift function $a_T(T)$ can be found by shifting each of the relaxation curves along time axis in such a way that they create a single smooth curve, which is called master relaxation curve. The direction of shifting is chosen in the correspondence with the reference temperature and current temperature. The master curve is fitted in the least square sense by the CAM model (6.9), and shift function is fitted by (6.2). Eventually, constants C_1 and C_2 and reduced time $\zeta(t)$ can be found.

D.2 Solution for an elastic axisymmetric problem

Solution of a problem of composite elastic cylinder (Fig.6.3) is outlined. The constitutive equations for total strains in each cylinder are written in polar coordinates (r, θ) as

$$\varepsilon_{rr} = \frac{1+\nu}{E}\left[(1-\nu)\,\sigma_{rr} - \nu\sigma_{\theta\theta} + \alpha E \Delta T\right] \qquad \text{(D.2-4)}$$
$$\varepsilon_{\theta\theta} = \frac{1+\nu}{E}\left[(1-\nu)\,\sigma_{\theta\theta} - \nu\sigma_{rr} + \alpha E \Delta T\right]$$

It is assumed that only radial displacement u exists, and strain components are expressed as (e.g. [128])

$$\varepsilon_{rr} = u_{,r}\ , \qquad \varepsilon_{\theta\theta} = u/r\ , \qquad \varepsilon_{r\theta} = 0 \qquad \text{(D.2-5)}$$

where comma means derivative. Substituting these expressions into (B1) and using the equilibrium equation

$$\frac{\partial \sigma_{rr}}{\partial r} + \frac{\sigma_{rr} - \sigma_{\theta\theta}}{r} = 0 \qquad \text{(D.2-6)}$$

it is straightforward to obtain the solution for the unknown radial displacement. Due to the cancelation of terms containing temperature, the result is

$$u = c_1 r + \frac{c_2}{r} \qquad \text{(D.2-7)}$$

where c_1 and c_2 are constants. The general solution for stresses in each elastic cylinder is

$$\sigma_{rr} = \frac{E}{1+\nu}\left[\frac{c_1}{1-2\nu} - \frac{c_2}{r^2}\right] - \frac{E}{1-2\nu}\alpha\Delta T \tag{D.2-8}$$
$$\sigma_{\theta\theta} = \sigma_{rr} + r\sigma_{r,r}$$

Using boundary conditions for the problem of composite cylinder (Fig.6.3)

$$\begin{aligned} \sigma_{rr}^{inc} &= 0 \quad at \quad r = r_0 \\ \sigma_{rr}^{inc} &= \sigma_{rr}^{bind} \quad at \quad r = r_1 \\ u_r^{inc} &= u_r^{bind} \quad at \quad r = r_1 \\ \sigma_{rr}^{bind} &= 0 \quad at \quad r = r_2 \end{aligned} \tag{D.2-9}$$

constants c_1 and c_2 are found for each cylindrical layer. As a result, the solution for the circumferential stresses in the binder is given by (6.20)-(6.21), in which

$$\begin{aligned} a(r) &= -\frac{r_1^2}{r^2}\frac{r_0^2 - r_1^2}{r_1^2 - r_2^2}\frac{r^2 + r_2^2}{r^2 - 2\nu_i r_1^2 + r_0^2}\frac{\alpha_b\left(\nu_b + 1\right) - \left(\nu_i + 1\right)}{\nu_i + 1} \\ b(r) &= -\frac{r_1^2}{r^2}\frac{r^2 + r_2^2}{r_1^2 - 2\nu_b r_1^2 + r_2^2}\frac{\left(\alpha_i - 1\right)\left(\nu_i + 1\right)}{\nu_b + 1} \\ c &= \frac{r_0^2 - r_1^2}{r_1^2 - r_2^2}\frac{r_1^2 - 2\nu_b r_1^2 + r_2^2}{r^2 - 2\nu_i r_1^2 + r_0^2}\frac{\nu_b + 1}{\nu_i + 1} \end{aligned} \tag{D.2-10}$$

The solution for total circumferential strains in the inclusion is given by (6.22)-(6.23), in which

$$\begin{aligned} d &= 1 + \left(1 - 2\nu_i\right)\frac{r_1^2}{r_0^2} \\ g &= \frac{r_1^2}{r_0^2}\frac{r_0^2 - r_1^2}{r_1^2 - r_2^2}\left[\left(1 - 2\nu_b\right) + \frac{r_2^2}{r_1^2}\right]\frac{1 + \nu_b}{1 + \nu_i} \end{aligned} \tag{D.2-11}$$

Appendix E

E.1 General information about the codes "PoreVeBI2D" and "VeBI2D"

Two computer codes were created for the simulation of the time-dependent fields in the problems of (i) viscoelastic half-plane containing holes and (ii) viscoelastic half-plane containing elastic inhomogeneities. The codes were implemented as Windows 32-bit console applications with the use of C++ programming language and Microsoft Visual Studio®. The names of the executable files created for the solution of problems (i) and (ii) are "PoreVeBI2D.exe" and "VeBI2D.exe" respectively. The codes share many common features, for example, the same structure of input data file, the same algorithms of the calculation of the number of Fourier terms, the same algorithms for the solution of systems of linear equations, etc. The major difference between the codes consists in the way the time-depending fields are calculated. The analytical inversion of the Laplace transform is implemented in the code "PoreVeBI2D"; all s-dependent expressions were analytically inverted with the use of packages for symbolic calculations, and the resulting time-dependent expressions were hard coded (see details in Chapter 3). Project "VeBI2D" is based on the Stehfest algorithm of numerical inversion of the Laplace transform (see Chapter 4), and thus, it does not use any precalculated expressions.

It would be out of scope of this appendix to describe the implementation details or to provide the source codes for the programs. Only major characteristics are outlined.

General features of both codes include the following:

- The ability to solve the problems of an infinite and semi-infinite elastic or viscoelastic medium containing elastic inclusions and/or pores.

  Stresses, strains, displacements, the principal and shear stresses, boundary displacements and tractions, and hoop stresses can be precisely calculated in any point of the domain in the Cartesian or polar coordinates.
- The ability to fix rigid body motion.
- Plane strain or plain stress problems can be considered.
- Two models describing the behavior of the matrix are implemented at the current stage. They are the Boltzmann and the Burgers viscoelastic models.
- New models can be introduced into the codes relatively easily. To do this, one has to modify *cpp*-file "modelParam.cpp" that contains all the information about the viscoelastic models and time-varying boundary conditions. The user has to change the expressions for the s-varying shear modulus and Kolosov-Muskhelishvili's parameter to those corresponding to a new model (these expressions can be obtained in a way similar to Eqs.(2.47), (2.50)).
- Both codes can be used for the calculation of the effective properties of viscoelastic composite and porous materials. The user has to type information about the representative cluster (the location and properties of the inhomogeneities) in the input data file. The programs automatically determine if the provided distribution of the inhomogeneities is isotropic and calculate values of 2D and 3D effective moduli for each moment of time.

Among some technical features of both codes are the following:

- Fully encapsulated class was created to store all input data, allowing sharing them between the files with the code and functions and protecting them from an accidental change.

- Most of the calculations are done with the use of complex variables. <complex> template class was used for this purpose.
- Most of the data arrays are stored with the use of dynamic memory allocation and STL template classes <vector> and <list>. Before storing very large arrays of data (hundreds of Megabytes or Gigabytes), the heap (part of physical and/or virtual memory of a computer) is tested for the amount of available memory. In the case this amount is insufficient, a warning message is displayed and an option to continue with the use of direct calculations is proposed. In the latter case the programs execute matrix calculations much slower, but they do not require storing large amounts of data in computer memory.
- Iterative block Gauss-Seidel algorithm [49] is adopted for the solution of systems of linear equations (SLE) of large size. Small size SLE are solved with the use of LU-decomposition method [49] implemented as a BLAS function (part of LAPACK library).
- Fast and simple algorithm was created for the calculation of large binomial coefficients (e.g. $\binom{700}{300}$).
- A fast iterative algorithm was created for the generation of randomly distributed inhomogeneities. The user is able to control a number of parameters, such as minimum and maximum sizes of the inhomogeneities, minimum distance between them, etc. (see the input file below). The programs try to generate random inhomogeneities within the given constraints.
- The program "VeBI2D" adopts the multithreaded architecture to speed up the calculations. If the number of field points multiplied by the number of time moments exceeds certain value, the program splits the space domain in several parts and assigns the calculations of the fields in each part to a single working thread (this is so-called parallel computing). The threads are not synchronized between each other except the major (executable) thread waits until all other threads return, and the code execution continues. The project "PoreVeBI2D" is implemented as

a single threaded application due to the use of hard-coded expressions for the calculations of time-varying fields.

- All information displayed on a monitor is also written into a log file that has the same name as the input data file (e.g. "_inp_StandSolid.log"). This helps the user to identify any possible problems during the execution and analyze the results.
- An option to include a unique identifier to the name of the files containing output information is implemented. This allows one to avoid an accidental overwriting of the files containing output data (if this option is not activated, the programs overwrite files with the same names automatically). For activation of this option see the syntax of the command lines below.

If the executable file is located in the same directory as an input data file, the syntax to run the program from a command line (run "cmd.exe" first) is the following:

- to produce output files without an identifier: "VeBI2D.exe input_data_file.inp"
- to produce output files with unique identifier added to their names: "VeBI2D.exe -t input_data_file.inp"

Similar syntax applies to the program "PoreVeBI2D.exe".

The codes produce the following output files:
"_BoundaryStresses.txt" – contains information about the values of the stress tensor components (Cartesian) at the boundaries of the inhomogeneities.
"_Circles.bna" – contains information about the boundaries of the inhomogeneities. It can be imported into Surfer® mapping software to create a base map. This map can be overlaid on a contour map to create nicely looking boundaries of the domain.
"_Coeficients_B.txt" – contains values of the Fourier coefficients at zero time moment. Usually they are needed to track errors or to debug the codes.

"_DisplacemntField.txt" – contains information about the values of displacements in the Cartesian coordinates.

"_DisplacemntFieldPolar.txt" – contains information about the values of displacements in the polar coordinates.

"_EffModuli.txt" – contains information about the 2D and 3D effective moduli.

"_HoopStresses.txt" – contains information about the values of the hoop stress at the boundaries of the inhomogeneities.

"_MaxShearStressField.txt" – contains information about the values of maximum shear stress in the Cartesian coordinates.

"_PrincipalStressField.txt" – contains information about the values of the major and minor principal stresses in the Cartesian coordinates and the angle between the major principal stress and Ox axis.

"_Name_of_input_file.log" – *log* file containing all the information displayed during the programs execution. "Name_of_input_file" will be substituted with the real name of the input file.

"_StrainField.txt" – contains information about the values of the strain tensor components at a point in the Cartesian coordinates.

"_StrainFieldPolar.txt" – contains information about the values of the strain tensor components at a point in the polar coordinates.

"_StressField.txt" – contains information about the values of the stress tensor components at a point in the Cartesian coordinates.

"_StressFieldPolar.txt" – contains information about the values of the stress tensor components at a point in the polar coordinates.

E.2 An example of input data file

Most of the information in the input data file is self explanatory. The parameters that can be varied by the user are typed in bold in the provided example. Few comments

about the input data are given below.

Block "Matrix Properties". Two models describing the viscoelastic behavior of the composite's matrix are accepted: (i) for time-dependent shear modulus and constant bulk modulus the user has to type "0" in the line "Type of moduli"; (ii) for time-dependent Young's modulus and constant Poisson's ratio the user should type "1".

Block "Geometry of the Problem". The user has to input the number of inhomogeneities and only then information about their locations and properties. Program "PoreVeBI2D.exe" ignores any information about the elastic inclusions if later is provided. To generate random array of the inhomogeneities, the user should type "yes" in the corresponding line. In this case, one has to be sure to comment out or delete any lines that contain information about the locations and properties of inhomogeneities. The necessary lines starting with the single symbol "#" should be uncommented to provide constraints for the generation of random inhomogeneities.

Block "Time Information". The user has to input information about the time moments at which the viscoelastic fields are going to be calculated. Calculation of elastic fields at $t = 0$ is separated from the rest of the time sequence, as it is not based on the use of the Laplace transform. One needs to be sure not to input 0 as the beginning of the time sequence (instead input "yes" to calculate the elastic fields).

Block "Calculation of the Fields and Results Output". Four different types of space grids are available (choose "PARAM" and uncomment the necessary lines).

PARAM=1 corresponds to a linear or circular segments. Several segments can be considered and each of them can be subdivided into a number of subsegments (or number of points). Circular segments represent the full circle.

Important! To calculate the effective properties, the user has to choose a circular segment and input the radius (R) of this segment. The center of the segment should be the same as the center of the representative cluster. The number of subsegments is irrelevant in this case.

PARAM=2 corresponds to a grid, which size is automatically determined based on the

analysis of the area occupied by the inhomogeneities plus some percentage of this area (provided by the user).

PARAM=3 corresponds to a grid, which size is automatically determined based on the analysis of the area occupied by the inhomogeneities plus some margin (provided by the user).

PARAM=4 corresponds to a general grid. All parameters of the grid are provided by the user.

Block "Fix rigid body motion". The user has to provide two points that are used to fix rigid body motion.

Block "Calculate hoop stresses". The user has to provide the inhomogeneity(s) number(s), range of angles and delta-angle (step) that will be used by the program to determine where to calculate the hoop stresses.

Block "Quantities to be calculated at a point". The user has to provide any combination of stresses, strains or displacements (e.g. "sxx srr exx err"). This option allows to reduce the working time of the programs by excluding the calculation of unnecessary parameters.

Block "Error level 1(smallest) - absolute value". The user has to input the absolute value of the error threshold used for determining the number of Fourier terms (value of 10^{-5} can be used for most of the problems). Errors for other levels are found by using the provided multipliers.

Block "Number of approximation points in the Stehfest algorithm". The user has to input the number of points used in the Stehfest algorithm of numerical inversion of the Laplace transform. Program "PoreVeBI2D.exe" ignores this option.

Block "Number of threads". The user has to input the maximum number of threads that will be used for the parallel computing of viscoelastic fields in program "VeBI2D.exe". Program "PoreVeBI2D.exe" ignores this option.

To run the program the following files must be present in the same directory as the program:
libacml_dll.dll, libacml_dll.lib, libifcoremd.dll, libmmd.dll

The current version of the program uses Burgers viscoelastic model
Boltzmann model can be obtained from Burgers model if the viscosity of the dashpot in Maxwell part of
the Burgers model is infinite
For this, enter Viscosity of Maxwell dashpot = -1

The file should be saved using WIN-1251 encoding
Lines that begin with symbol "#", empty lines and spaces are ignored; except...
No spaces are allowed after opening bracket (e.g. in coordinates). Follow this syntax: (X, Y)
The direction of travel for all angles is anti-clockwise. Starting point is the most right point

If problem of full-plane is solved, forces are ignored
Types of the forces: 0 - point force, 1 - force over a segment, 2 - force over the whole boundary
For half-plane problem YY, XY-stresses at infinity are ignored

################ General Information ###################################
Solve problem for half-plane (yes/no) : **yes**
Plane stress condition (yes/no; no - means plane strain) : **no**

################ Matrix Properties ######################################
Type of moduli (for G(t)-K type 0, for E(t)-nu type 1) : **0**
Stiffness of the Maxwell spring : **8e3**
Stiffness of the Kelvin spring : **2e3**
Viscosity of the Maxwell dashpot at time = 0 : **-1**
Viscosity of the Kelvin dashpot at time = 0 : **5e3**
Time-independent bulk modulus (K) or Poisson's ratio (nu) : **17333.33333333**

################ Loads ##
Constant part of stress (XX) at infinity (full/half-plane) : **10**
Constant part of stress (YY) at infinity (full-plane only) : **0**
Constant part of stress (XY) at infinity (full-plane only) : **0**

Type of force applied from the top (half-plane only) : **1**
Constant part of force (Tangential, Normal) : **(0, -20)**
Coordinates of the force applied (left) : **(-1, 0)**
Coordinates of the force applied (right) : **(1, 0)**

################ Geometry of the Problem ################################
Number of holes: **2**
Number of inclusions: **1**
Data for holes: (Coordinates of the center) Radius Internal_Pressure
(-4.4, -3) 1.6 -8
(3, -3.5) 2 -5
Data for inclusions: (Coordinates of the center) Radius Poisson's_Ratio Shear_Modulus
(-1, -1.7) 1 0.25 15000

Generate random inhomogeneities (yes/no; uncomment necessary lines!): **no**
Box where random holes will be generated
(upper left corner x,y) (lower right corner x,y) min_distance_between_inhomogeneities
(-10, 10) (10, -10) 0.2
Data for holes (min Radius, max Radius) (min, max Pressure)
(.2, 5) (0.5, 2)
Data for elastic discs (min, max Poisson's ratios) (min, max Shear moduli)
(0.2, 0.4) (1, 5)

################ Time Information #####################################
Calculate elastic fields at time = 0: **yes**
Time sequence (start time, end time, time step):
0.2 10 0.2

################ Calculation of the Fields and Results Output ##################
Type of the space mesh (PARAM): **4**
----
if PARAM=1
number of segments
begining_point(X, Y) end_point(X, Y) number_of_subsegments 1
....OR....
radius_of_an_arc(Rad, 0) center_of_an_arc(X, Y) number_of_subsegments 2
2
(10, -10) (3, 0) 500 1
(1500, 0) (0, 0) 1 2
----
if PARAM=2
number_of_points_in_grid(Ox) number_of_points_in_grid(Oy) margin(percent)
50 40 0
----
if PARAM=3
number_of_points_in_grid(Ox) number_of_points_in_grid(Oy) margin(absolute)
10 10 1
----
if PARAM=4
box: (Xmin, Ymin) (Xmax, Ymax) number_of_points_in_grid(Ox) number_of_points_in_grid(Oy)
(-10, 0) (10, 0) 200 100

Do you want to fix rigid body motion: **no**
If yes, then input two points which will be used to fix rigid body motion
#**(0, -50) (10, -50)**

Calculate hoop stress at the boundaries of the inhomogeneities: **no**
Range of angles used to calculate hoop stresses
inhomogeneity anle_min angle_max delta_angle
#**1 85 95 1**

Results output (0 - time in row, 1 - time in column): **1**
Quantities to be calculated at a point: **sxx syy sxy srr stt srt exx eyy exy err ett ert ux uy ur ut**

==========
= = = = = = = = = = = = = = ADVANCED OPTIONS = = = = = = = = = = = = = =
==========

Tolerance in Gauss-Sediel algorithm: **1e-10**

Error level 1(smallest) - absolute value: **1e-5**
Error level 2(medium) multiplier: **5**
Error level 3(largest) multiplier: **10**

Number of Fourier terms to add for error 1: **2**
Number of Fourier terms to add for error 2: **5**
Number of Fourier terms to add for error 3: **10**

Angle increment used for determination of max error (in deg): **1**

Number of approximation points in the Stehfest algorithm: **10**

Number of threads (applicable only if N_time_moments*N_mesh_points >= 1000): **2**
Recommended number of threads for single and double core/processor machines is 2,
for quad core/4 processors machines – 4